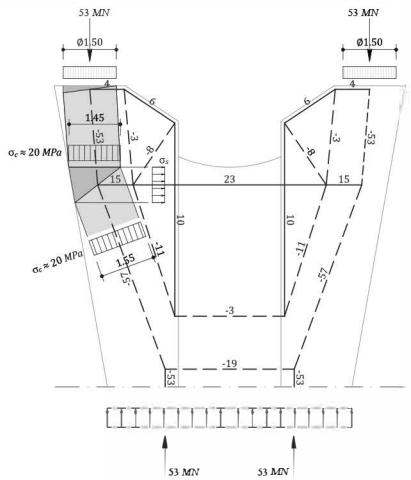
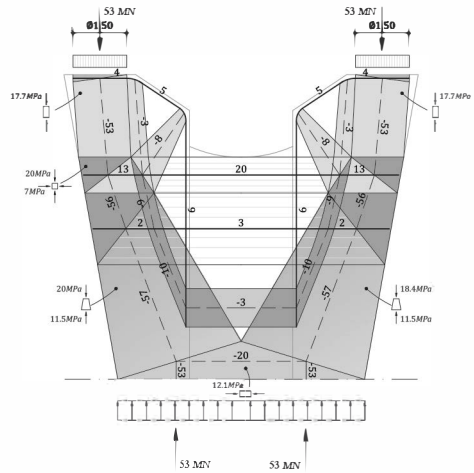
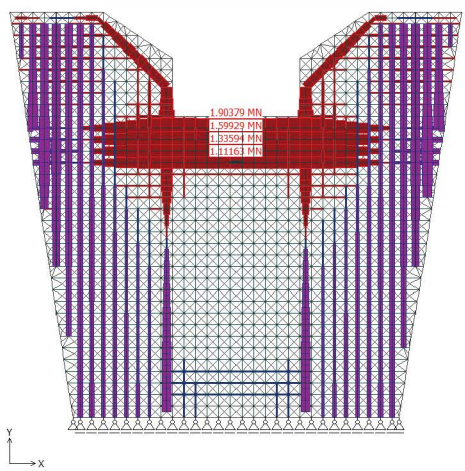
This document is the intellectual property of the fib – International Federation for Structural Concrete. All rights reserved.
This PDF of fib Bulletin 100 is intended for use and/or distribution solely within fib National Member Groups.

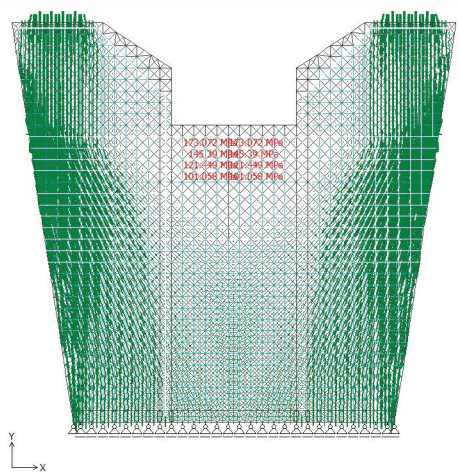
fib
CEB-FIP

Bulletin 100









Design and assessment with strut-and-tie models and stress fields: from simple calculations to detailed numerical analysis

State-of-the-art report

This document is the intellectual property of the fib – International Federation for Structural Concrete. All rights reserved.
This PDF of fib Bulletin 100 is intended for use and/or distribution solely within fib National Member Groups.

fib CEB-FIP Bulletin 100

Design and assessment with strut-and-tie models and stress fields: from simple calculations to detailed numerical analysis

State-of-the-art report

Working Party 2.2.4

September 2021

This document is the intellectual property of the fib – International Federation for Structural Concrete. All rights reserved.
This PDF of fib Bulletin 100 is intended for use and/or distribution solely within fib National Member Groups.

Approval for this bulletin

Subject to priorities defined by the Technical Council and the Presidium, the results of the *fib*'s work in commissions and task groups are published in a continuously numbered series of technical publications called *bulletins*. The following categories are used:

Category:	**Approval by**:
Technical report	Task group and chairpersons of the commission
State-of-the-art report	Commission
Manual / Guide to good practice / Recommendation	Technical Council
Model code	General Assembly

Any publication not having met the above requirements will be clearly identified as a preliminary draft.

fib Bulletin 100 was approved as a State-of-the-art report by Commission 2 *Analysis & Design* in 2021.

The *fib* Working Party 2.2.4 includes the following members:

Convener: Miguel Lourenco (Portugal, JSJ Consulting)

Members: João Almeida (Portugal, Instituto Superior Técnico Lisboa), Johan Blaauwendraad (Netherlands, Delft University of Technology), Stathis Bousias (Greece, University of Patras), Duarte Faria (Switzerland, Muttoni et Fernández, ingénieurs conseils SA), Miguel Fernández Ruiz (Switzerland, Ecole Polytechnique Fédérale de Lausanne & Spain, Universidad Politécnica de Madrid), Stein Atle Haugerud (Norway, Dr. techn. Olav Olsen a.s.), Linh Cao Hoang (Denmark, Technical University of Denmark), Kent Kempengren (Sweden, AFRY), Jaime Mata-Falcón (Switzerland, ETH Zürich), Carlos Meléndez (Spain, Esteyco SA), Boyan Mihaylov (Belgium, University of Liege), and Miguel Pedrosa Ferreira (Portugal).

Cover images: Figures 6-16a, 6-17, 6-18b, and 6-18d

© Fédération internationale du béton (*fib*) 2021.

Although the International Federation for Structural Concrete / Fédération internationale du béton (*fib*) does its best to ensure that all the information presented in this publication is accurate, no liability or responsibility of any kind, including liability for negligence, is accepted in this respect by the organisation, its members, employees or agents.

All rights reserved. No part of this publication may be reproduced, modified, translated, stored in a retrieval system or transmitted in any form or by any means – electronically, mechanically, through photocopying, recording or otherwise – without prior written permission from the *fib*.

ISSN 1562-3610
ISBN 978-2-88394-152-6
https://doi.org/10.35789/fib.BULL.0100
Layout by Marie Reymond (*fib*).
Printed by DCC Document Competence Center Siegmar Kästl e.K., Germany

This document is the intellectual property of the fib – International Federation for Structural Concrete. All rights reserved.
This PDF of fib Bulletin 100 is intended for use and/or distribution solely within fib National Member Groups.

Acknowledgements

This report was drafted by Working Party 2.24 "Strut-and-tie modelling" within the *fib* Commission 2.

Authors:

Miguel Filipe Passos Sério Lourenço (Convener/Editor)
JSJ,Lda, Portugal

Miguel Fernández Ruiz (Editor)
Ecole Polytechnique Fédérale de Lausanne, Switzerland
Universidad Politécnica de Madrid, Spain

Stein Atle Haugerud
Dr.techn. Olav Olsen, Norway

Johan Blaauwendraad
Netherlands

Stathis Bousias
University of Patras, Greece

Linh Cao Hoang
Technical University of Denmark, Denmark

Jaime Mata-Falcón
ETH Zurich, Swizerland

Carlos Meléndez Gimeno
Esteyco SA, Spain

Boyan Mihaylov
University of Liege, Belgium

Miguel Pedrosa Ferreira
Grupo NOV, Portugal

Quentin Roubaty
CFF, Switzerland

Contact details of Working Party members can be found in the members only section of the *fib* website, www.fib-international.org.

DOI by chapter

Chapters	DOI
1	https://doi.org/10.35789/fib.BULL.0100.Ch01
2	https://doi.org/10.35789/fib.BULL.0100.Ch02
3	https://doi.org/10.35789/fib.BULL.0100.Ch03
4	https://doi.org/10.35789/fib.BULL.0100.Ch04
5	https://doi.org/10.35789/fib.BULL.0100.Ch05
6	https://doi.org/10.35789/fib.BULL.0100.Ch06
7	https://doi.org/10.35789/fib.BULL.0100.Ch07
8	https://doi.org/10.35789/fib.BULL.0100.Ch08
9	https://doi.org/10.35789/fib.BULL.0100.Ch09
10	https://doi.org/10.35789/fib.BULL.0100.Ch10
11	https://doi.org/10.35789/fib.BULL.0100.Ch11

This document is the intellectual property of the fib – International Federation for Structural Concrete. All rights reserved.
This PDF of fib Bulletin 100 is intended for use and/or distribution solely within fib National Member Groups.

Foreword

Structural analysis has developed very quickly in recent years. Especially numerical methods based on finite elements and similar approaches promise very accurate results. However, checking these results seems to be almost impossible. The re-calculation using an independent method appears to be the only possibility of verification. Additionally, the application of numerical methods, especially the non-linear ones, requires the specification of many parameters, which are used as input data and need not be known with sufficient accuracy at the structural design stage. At the same time, they are crucial for the accuracy of the results. Although numerical methods provide a nice illustration of stress and displacement distribution in structural elements, it is reasonable to apply some transparent, simpler method for checking results obtained by numerical methods, which would clearly illustrate the flow of forces in structures. The strut and tie models are exactly that powerful tool that is suitable as an alternative method of analysis for structures and structural details, and that is able to serve also as a check of results obtained by numerical simulations. The strut and tie and stress fields models can provide the designer with a clear view showing the function of the structure and its reinforcement.

The bulletin you are just keeping in your hands is a comprehensive publication showing principles, development and application of strut and tie and stress fields models. The authors did an excellent job and, using a transparent explanation, they provided basic and also advanced information on how to create, apply and evaluate the strut and tie and compression fields models so that the designer could clearly understand the performance of structures, which make it possible for him to check the numerical results and also to optimize structural systems so that the forces could be more favourably transferred from loading points to supports. The bulletin shows not only the application of stress fields and strut and tie models for new structures but also their application for the assessment of existing structures, where the geometry and reinforcement are already fixed.

The concept of levels of approximation that is typical for the Model Code 2010 will also be applied in the Model Code 2020 and is also used in this bulletin. This concept allows for simple modelling in early design stages with lower effort up to refined models for specific structural elements subjected to complex loading situations. The refined models are then applicable for the evaluation of both ultimate and serviceability limit states.

A series of examples supplements a very valuable explanation of stress fields and strut and tie models. They illustrate the application of the methods on existing structures as well as on new structures. Different levels of approximation are used. Finally, also 3D models are briefly discussed and compared with 2D models.

The team of WG 2.2.4 produced an excellent work that will hopefully be appreciated by practitioners and will contribute to a wider application of the described models in the design of new structures and in the assessment of existing structures. It is a great pleasure for me to acknowledge this contribution of the team of WP 2.2.4. to the activities of *fib*.

Jan Vítek

Chair of Commission 2 *Analysis & Design*

This document is the intellectual property of the fib – International Federation for Structural Concrete. All rights reserved.
This PDF of fib Bulletin 100 is intended for use and/or distribution solely within fib National Member Groups.

Contents

Foreword i
Scope 1
1. Introduction 2
1.1 Past, Present and Future of strut-and-tie and stress field models 2
1.2 Application of stress fields and strut-and-tie models 5
1.2.1 Design and assessment of structures 5
1.2.2 Design for new structures 6
1.2.3 Assessment of existing structures 10
1.2.4 Considerations for retrofitting 12
2. General considerations on stress fields and strut-and-tie models 14
2.1 Stress fields as a lower-bound solution of limit analysis 14
2.2 Application of limit analysis to structural concrete 14
2.3 Idealization of material response 15
2.3.1 Concrete 15
2.3.2 2D Reinforced concrete 20
2.4 Constitutive relations 21
2.4.1 Concrete 22
2.4.2 Reinforcement 23
2.4.3 Tension stiffening 24
2.4.4 Anchorage of reinforcement 26
2.5 Limits of applicability 27
2.5.1 General considerations 27
2.5.2 Minimum reinforcement 27
2.5.3 Minimum inclination of the compression field 28
2.5.4 Deformation capacity 28
2.5.5 SLS response 29
2.6 Safety factor format 29
2.6.1 Partial safety factor 29
2.6.2 Use of other safety formats 30
3. Use of the Levels-of-Approximation approach to design with stress fields and strut-and-tie models 31
3.1 Introduction 31
3.2 Level-of-Approximation I 32
3.3 Level–of-Approximation II 32

This document is the intellectual property of the fib – International Federation for Structural Concrete. All rights reserved.
This PDF of fib Bulletin 100 is intended for use and/or distribution solely within fib National Member Groups.

3.4 Level-of-Approximation III 33
3.5 Level-of-Approximation IV 33
3.6 Summary 34
3.7 Example: Simply Supported Beam with Two Point Loads 35
3.7.1 Geometry, Loads and Bending Reinforcement 35
3.7.2 Level of Approximation I 36
3.7.3 Level of Approximation II 38
3.7.4 Level of Approximation III 41
3.7.5 Level of Approximation IV 42
3.7.6 Final considerations 43
4. Equilibrium-based models 44
4.1 Introduction 44
4.2 Complex strut-and-tie models as a combination of simple models 46
4.3 Basic strut-and-tie and stress field models 48
4.3.1 Introduction 48
4.3.2 Deep beam with uniform loading 48
4.3.3 Deep Beam with uniform suspended loading 52
4.3.4 Deep beam / corbels with suspended point loads 55
4.3.5 Continuous Deep Beam models 57
4.3.6 Dapped-end beam / re-entrant corners 63
4.3.7 Spreading of point loads / bottle effect 66
4.3.8 Point load near support 70
4.3.9 Final Remarks – Practical Rules 71
5. Principles of computer modelling 75
5.1 Introduction 75
5.2 Compatibility-based Stress field – Finite element method 75
5.2.1 Introduction 75
5.2.2 Finite elements 77
5.2.3 Mesh topology considerations 80
5.2.4 Additional considerations 82
5.2.5 Interpretation of results 84
5.2.6 Example 84
5.3 Finite Element Limit Analysis of Reinforced Concrete Structures 90
5.3.1 Introduction 90
5.3.2 Lower bound optimisation problem 91
5.3.3 Equilibrium finite elements for analysis of plane stress problems 93
5.3.4 Yield criterion for plane stress states 95
5.3.5 Examples 97
5.3.6 Discussion and concluding remarks 101

This document is the intellectual property of the fib – International Federation for Structural Concrete. All rights reserved.
This PDF of fib Bulletin 100 is intended for use and/or distribution solely within fib National Member Groups.

5.4 Adaptive Stress Field Method 103
5.4.1 Introduction 103
5.4.2 Formulation 103
5.4.3 Compression Stress Fields 105
5.4.4 Tension Stress Fields 107
5.4.5 Test Example 109
5.4.6 Application of the Adaptive Stress Field method to a deep beam test 111
5.5 Stringer-Panel Models 115
5.5.1 Introduction 115
5.5.2 Concept of the Stringer-Panel Model 116
5.5.3 Dimensioning the stringers, panels and nodes 120
5.5.4 Dapped beam end 121
5.5.5 Deviating columns in building 127
5.5.6 Building wall with opening 130
5.5.7 Outlook 141
6. Practical examples 144
6.1 Use of strut-and-tie models and stress fields for assessment of existing critical structures 144
6.2 Use of strut-and-tie models and stress fields for conceptual design of new structures 147
6.3 Applications to the assessment of a bridge 150
6.4 Padre Cruz Viaduct 153
6.4.1 Description of structure 153
6.4.2 LoA I Model 155
6.4.3 LoA II Model 157
6.4.4 LoA III Model 158
6.4.5 LoA IV Model 160
6.5 Assessment of a dapped-end beam at ultimate and serviceability limit states 160
6.5.1 Verification at ULS 162
6.5.2 Verification at SLS 163
6.6 Detailed assessment of an existing element 165
6.6.1 Context and motivation 165
6.6.2 Problem description 166
6.6.3 LoA I 168
6.6.4 LoA II 169
6.6.5 LoA III 170
6.6.6 In-situ beam test 171
6.6.7 Conclusion 173

This document is the intellectual property of the fib – International Federation for Structural Concrete. All rights reserved.
This PDF of fib Bulletin 100 is intended for use and/or distribution solely within fib National Member Groups.

7. Special topics 174
7.1 Effect of load reversals 174
7.1.1 Load reversals 174
7.1.2 Models for deep girders and short coupling beams 175
7.1.3 Shear failures at low ductility levels 180
7.1.4 Shear failures at high ductility levels 184
7.1.5 Comparisons with test database 186
7.1.6 Summary 188
7.2 3D models: general examples 189
7.2.1 Introduction 189
7.2.2 3D strut-and-tie models 190
7.2.3 Example of application of 3D strut-and-tie models: foundation of a wind tower turbine 193
7.2.4 3D stress field models 198
7.2.5 Design example of a four-pile cap 201
7.2.6 Conclusions 206
8. Conclusions and outlook 208
8.1 Conclusions 208
8.2 Outlook 209
9. References 210
Chapter 1 210
Chapter 2 212
Chapter 3 214
Chapter 4 215
Chapter 5 215
Chapter 6 219
Chapter 7 220
10. Notations 223
11. Definitions 226

This document is the intellectual property of the fib – International Federation for Structural Concrete. All rights reserved.
This PDF of fib Bulletin 100 is intended for use and/or distribution solely within fib National Member Groups.

Scope

Following the long-standing tradition of *fib* in promoting the use of consistent design methods, strut-and-tie models were formally incorporated in Model Code 1990 to serve as the design basis for discontinuity regions. This choice was largely acknowledged as a sound approach for design and was thereafter followed in many national standards. For Model Code 2010, some update and revision of the previous provisions was performed, but the scope of the method was particularly broadened by introducing its complementary use with the stress field method. Since Model Code 2010, significant new knowledge has been generated in this topic. Particularly, the use of software implementing the theoretical ground of the stress field method is becoming increasingly popular and efficient, allowing for design, optimisation and assessment of structures in a simple, transparent and accessible manner.

In this Bulletin, the current state-of-the-art of the strut-and-tie models (STM) and the stress field models (SFM) is presented. Reference is not only made to classical rigid-plastic solutions, but also to solutions considering compatibility of deformations, such as elastic-plastic approaches or models allowing investigation of serviceability behaviour and deformation capacity of concrete structures. It is shown in the Bulletin that all models share the same ground and fundamental hypotheses. Their results are presented in a unitary and consistent manner by means of compression fields in the concrete and stresses in the reinforcement. The consistency amongst these approaches and their potential use in practice is also explored by means of the Levels-of-Approximation (LoA) approach as described in Model Code 2010.

Another effort in this Bulletin has been devoted to provide comparisons of the solutions according to strut-and-tie and stress fields to tests, in order to discuss on their pertinence and limitations. This perspective is also completed with practical examples presented of structures actually designed with this technique and where the potential of these methods can be appreciated in a clear manner. Finally, a number of special topics are also covered in the Bulletin, related to numerical optimisation, verifications at serviceability states, minimum reinforcement or the applicability of the methods under cyclic or reversal actions.

This Bulletin not only aims to give state-of-the-art rules and methods to design according to these techniques, but also to provide an outlook of how these methods could be implemented in future standards. This material also serves as the background document for the revision of the current provisions of Model Code 2010 in the new Model Code 2020.

This document is the intellectual property of the fib – International Federation for Structural Concrete. All rights reserved.
This PDF of fib Bulletin 100 is intended for use and/or distribution solely within fib National Member Groups.

1. Introduction

1.1 Past, Present and Future of strut-and-tie and stress field models

Strut-and-tie models and stress fields have been widely used for decades in structural engineering for designing new structures and for assessing the structural capacity of existing ones. Traditionally, they have been considered as tools mostly addressed to regions where beam design theory does not apply, as for instance deep beams or discontinuities in geometry and loading. This scope was however widened when limit analysis design methods were introduced and generalised for beams with transverse reinforcement. This is for instance the case of the variable-angle truss model, where compression is carried by an inclined compression stress field developing in concrete and tension is only carried by the reinforcing steel (with no contribution to tension by concrete). Such an approach allows for a consistent design for structural concrete members, without any distinction between member type or regions. This approach is shown in Fig. 1-1, by presenting a beam subjected to four-point bending and a possible stress field as well as the corresponding strut-and-tie in equilibrium with the actions (which leads to a variable inclination of the struts in the fan regions and constant-angle compression fields). It can be noted that the same model can be consistently used for design of the flexural reinforcement in regions at a certain distance from the loads or right at their location, as well as for the design of the shear reinforcement (accounting for its inclination and properties) and verification of the concrete stresses.

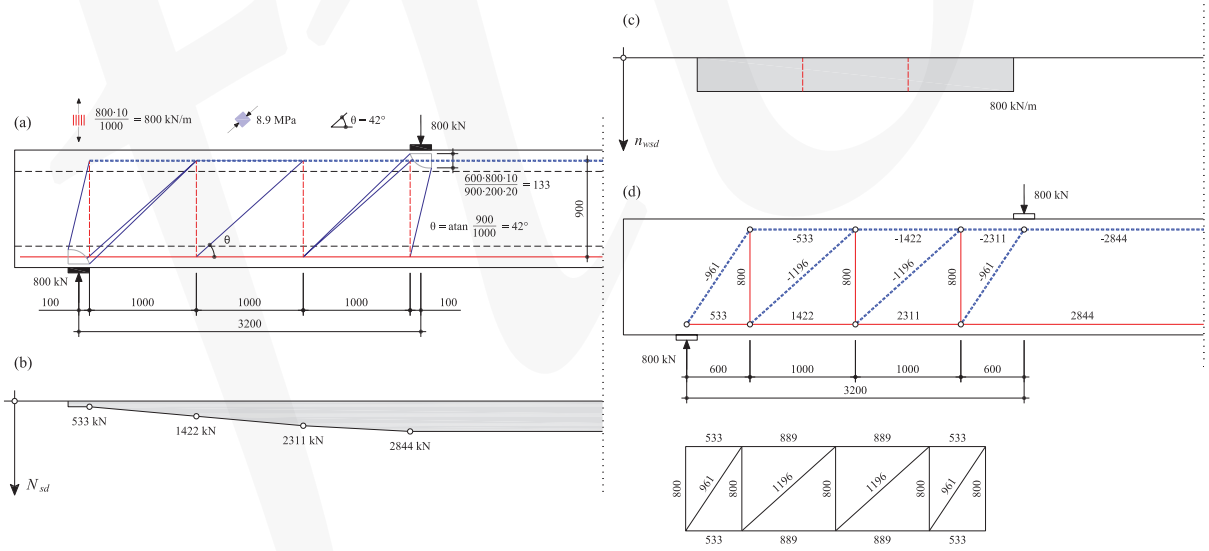


Fig. 1-1 Design for a linear member based on stress fields and strut-and-tie models: (a) actions and stress field; (b,c) corresponding forces in the flexural and shear reinforcement, respectively; and (d) corresponding strut-and-tie model

Also, in Fig. 1-1, it is interesting to note that such approach can be applied both with the development of a stress field (Fig. 1-1a), or the corresponding strut-and-tie model

https://doi.org/10.35789/fib.BULL.0100.Ch01

This document is the intellectual property of the fib – International Federation for Structural Concrete. All rights reserved.
This PDF of fib Bulletin 100 is intended for use and/or distribution solely within fib National Member Groups.

(Fig. 1-1d), referring the latter to the resultants (forces) of the compression fields (in the concrete) or tension fields (forces carried by the reinforcement). In fact, the use of both stress fields and strut-and-tie models is complementary and depends many times on the check or design to be performed (stresses in the compression field, tension in distributed reinforcement or tension in the chords).

Although, as previously explained, stress fields and strut-and-tie models are currently seen as consistent and alternative means to calculate the same physical model, their original development and application were however historically different.

With respect to strut-and-tie models, their origin can be traced to the truss models, originally developed on the basis of intuitions derived from the observation of beams. The first ideas were proposed by W. Ritter[1-1], refer to Fig. 1-2, where the main elements of the truss (strut and ties) were present (yet, there was no top compression chord drawn in the original figure and the vertical ties over the support were not statically necessary). These ideas were later developed more in detail by E. Mörsch[1-2]. Truss models allowed at that time calculating the internal forces of an idealised truss developing within a concrete structure and equilibrating the external actions. Compression forces were assumed to be carried by concrete and tension by reinforcement. In addition, the idealised truss was considered as an actual structure (normally statically-determinate). However, truss models were not widely used in the actual dimensioning of reinforced concrete structures until they were later developed in detail in Stuttgart[1-3], [1-4], [1-5] by inspiring the internal trusses on the elastic-uncracked response of concrete. Further evolutions actually showed that there was no actual need for the load-carrying model to be a truss, but that any model in equilibrium with the actions was suitable. Such equilibrium models were named as strut-and-tie models and largely generalised as a consistent tool for design of structural concrete[1-5]. Later works also showed that this approach was in fact consistent with the lower-bound theorem of limit analysis[1-5] and that it could be safely used for design of new structures. Eventually, automatic procedures were proposed for developing strut-and-tie models, providing guidelines to designer to suitably address strength and serviceability criteria.

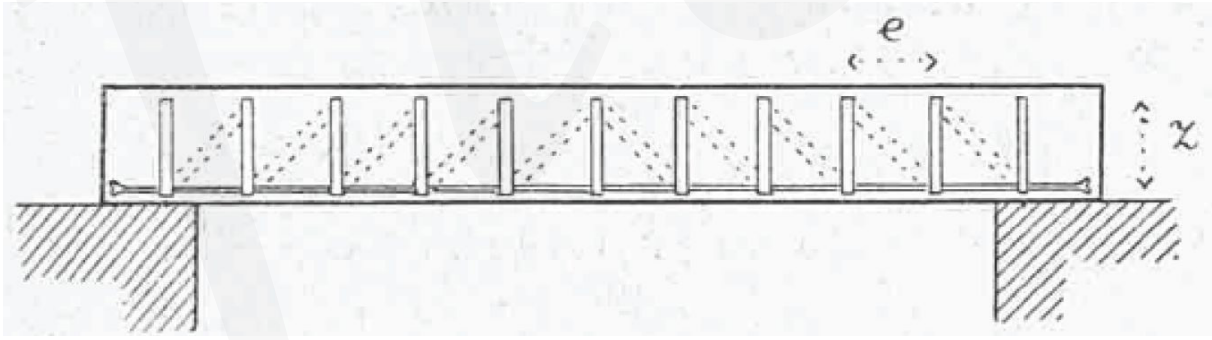


Fig. 1-2 Original truss model according to W. Ritter[1-1].

The origin of the stress field method is yet different to that of the strut-and-tie models. It was developed as application of the theory of plasticity to reinforced concrete design, with the aim of providing equilibrium-based solutions which were licit (respecting the yield criteria of the materials). The first comprehensive formulation of the theory of plasticity can be traced to Gvozdev in 1938[1-6] (published in English by R.M. Haythornthwaite in 1960[1-7]) who defined the concepts of the yield surface, upper- and lower-bound and exact solution. Similarly to the ideas developed by Wagner in 1929[1-8] for steel structures (named as the

This document is the intellectual property of the fib – International Federation for Structural Concrete. All rights reserved.
This PDF of fib Bulletin 100 is intended for use and/or distribution solely within fib National Member Groups.

tension field concept) and with the aid of the theory of plasticity, Drucker[1-9] developed the first rigid-plastic stress fields for a reinforced concrete member (with the development of the compression field concept). The first application by Drucker consisted of a stress field for a simply supported beam under a point load and a distributed load (Fig. 1-3). Drucker showed that such solutions respected equilibrium conditions and the stresses could be set below a plastic threshold (the influence of cracking on the strength of concrete was however neglected at that time) constituting thus lower-bound solutions to the strength. In addition, such stress fields could lead to kinematically admissible mechanisms and thus could yield to exact solutions according to the theory of plasticity. The stress field method was later intensively developed in Denmark[1-10] and in Switzerland[1-11], [1-12], [1-13] and their application was extended to different types of structural members.

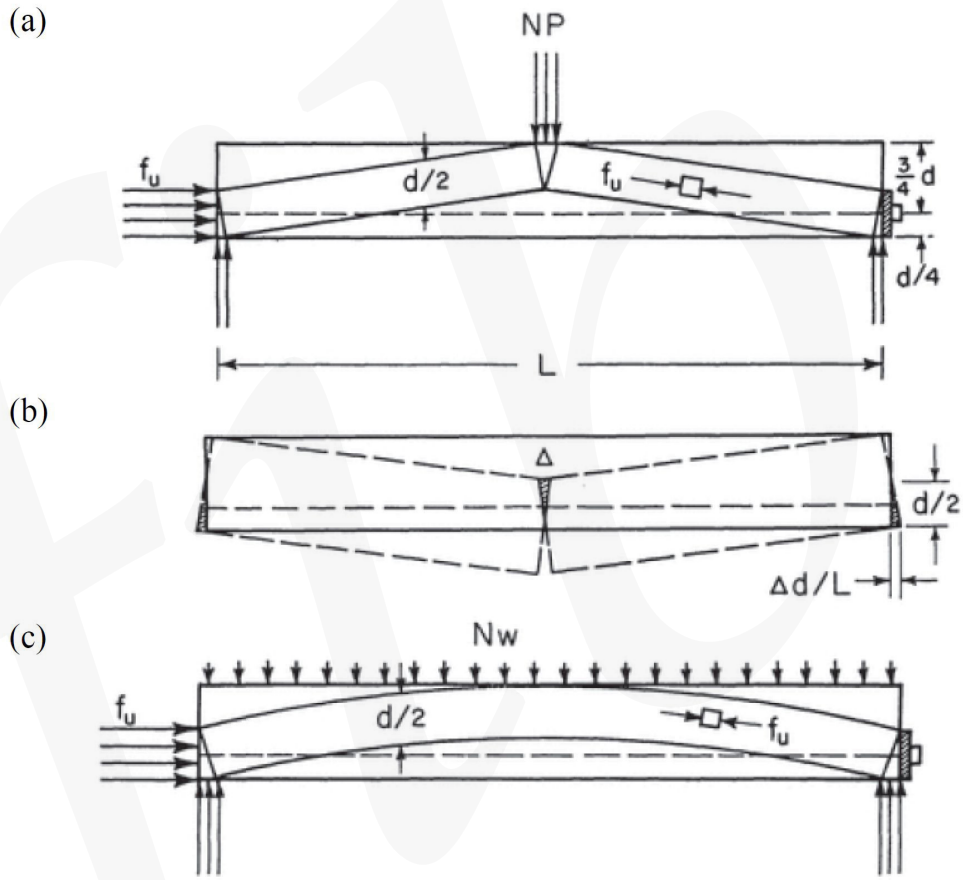


Fig. 1-3 First stress fields proposed for concrete structures according to Drucker[1-9]: (a) stress field under point load; (b) compatible mechanism; and (c)stress field for a beam subjected to uniform loading.

Based on the stress field method, special cases of stress fields were also developed based on a combination of panels (used in shear) and stringers at their boundaries (used to carry tension or compression forces). This approach has been termed as the stringer-panel method (SPM)[1-10], [1-13].

Currently, both stress fields and strut-and-ties are used taking advantage of their generality and consistency. Their scope has been enlarged with respect to the classical developments on rigid-plastic limit analysis[1-5], [1-10], [1-12], [1-13] by accounting for compatibility conditions in the development of suitable stress fields[1-15], [1-16], [1-17] or with numerical optimisation of yield conditions[1-18].

This document is the intellectual property of the fib – International Federation for Structural Concrete. All rights reserved.
This PDF of fib Bulletin 100 is intended for use and/or distribution solely within fib National Member Groups.

With respect to the introduction of compatibility conditions, this allows:

- investigating and optimising the behaviour for serviceability limit state, particularly with respect to cracking[1-17], [1-19]
- providing solutions where the resulting stress field is kinematically admissible at failure, thus yielding exact solutions according to limit analysis[1-20]
- calculating the strain state, thus allowing for a refined calculation of the concrete strength reduction factors and considering the potential increase of the force in the prestressing tendon. These aspects allow thus obtaining more refined estimates of member resistance
- automating the calculation and optimising the amount and location of the reinforcement[1-15], [1-21]
- accounting for the influence of tensile strength on members stiffness (i.e., tension stiffening) in order to cover load-deformation and deformation capacity aspects[1-17], [1-19]

With respect to the numerical optimisation of the yield conditions, it is aimed at the optimisation of the reinforcement layout with respect to the amount of reinforcement or the resistance of the member, yielding very fast computational techniques.

These advances have opened a wide range of new possibilities to the application of the stress field and strut-and-tie models and have allowed for the use of new tools. However, the correct use of these new techniques still requires a sound knowledge of the basic theoretical principles of limit analysis and of its limits of applicability. This will be shown within this document, as well as the possibilities offered by the combination of new and classical tools in the search for optimal solutions for design of new structures and for the assessment of existing ones.

1.2 Application of stress fields and strut-and-tie models

1.2.1 Design and assessment of structures

Currently, stress fields and strut-and-tie models are applied both for design of new structures as well as for the assessment of existing ones. It should be noted, however, that the approach followed for the two applications should in general be different as the scope of the tasks to be performed is also quite different:

- For new structures, the task of the engineer is to produce a safe design which respects economic criteria (dimensions, arrangement of reinforcement), is simple to build and has a satisfactory behaviour at serviceability limit state
- For assessment of existing structures, the task of the designer is rather to check if the strength is sufficient to carry the current actions. The engineer should not produce a reinforcement layout, but verify the strength of the existing one. Serviceability issues are not usually to be checked by analysis as this can be done in situ (unless a change in the actions is expected).

Due to the differences in the scope, the approach followed is thus different. For new structures, simple and safe load-carrying models are to be used. To that aim, the use of

This document is the intellectual property of the fib – International Federation for Structural Concrete. All rights reserved.
This PDF of fib Bulletin 100 is intended for use and/or distribution solely within fib National Member Groups.

strut-and-tie models with some local refinements by rigid-plastic stress fields is normally sufficient. This provides a lower-bound of the actual strength and yields sufficient freedom to the designer to decide on the location on the main reinforcement so as to allow for ease of construction. Only when repetitive or complex elements are to be designed, very refined analyses are justified (for instance by accounting for kinematic compatibility).

For the assessment of existing structures, simple models (lower-bound solutions) can be used at first to identify non-critical regions (where the strength is satisfied even for the simple load-carrying models). In the critical regions, where simple lower-bound solutions do not provide sufficient strength, the use of refined models is normally justified in order to avoid or to minimise strengthening (the savings in strengthening largely compensate for the cost of additional studies). Refined assessment models can be developed by accounting, for instance, for kinematic considerations. This allows fulfilling both the static theorem (lower-bound solution), as well as the kinematic theorem of the theory of plasticity (upper-bound solution), thus yielding the exact solution according to the theory of plasticity (highest lower-bound estimate of the strength). It should nevertheless be noted that the deformation capacity of the structure is to be verified so that plastic stress redistribution can effectively occur.

In this section, some strategies are discussed in order to approach the design and the assessment of a structure by means of strut-and-tie models or stress fields, highlighting their analogies but also their conceptual differences. In addition, some considerations regarding the application of strut-and-tie models and stress fields for the analysis and design of retrofitting interventions are also given.

1.2.2 Design for new structures

As previously stated, for the design of a new structure, the reinforcement layout should be determined in a simple and economic way. Working with lower-bound solutions, as strut-and-tie models or rigid-plastic stress fields, is thus an excellent methodology, as the designer can decide on the location and arrangement of the reinforcement. Detailed knowledge of the serviceability behaviour is, however, not explicit and some additional considerations, for instance deformation capacity, have to be taken into account. In this process, a number of approaches can be followed and will be presented hereafter.

1.2.2.1 Arrangement of the reinforcement based on the linear-elastic stress field of the member

A commonly followed approach to design new structures consists of the strut-and-tie model used for design on the elastic (uncracked) response of the member, refer to Fig. 1-4. This method was introduced early as a suitable way to identify the location of the struts and ties and was formulated in a consistent manner by Schlaich et al.[1-5].

This method has a number of advantages. It provides a clear methodology to produce the strut-and-tie model and leads to a reinforcement layout which in principle provides a satisfactory behaviour at serviceability limit states (as reinforcement is arranged in the regions where tensile stresses are expected). However, it also shows some drawbacks[1-15] as less freedom for the designer to choose the location of the reinforcement, the potential presence of TTT nodes (nodes where only tension ties are concurrent), the overestimation of the reinforcement for imposed strains and the underestimation of lever arms.

This document is the intellectual property of the fib – International Federation for Structural Concrete. All rights reserved.
This PDF of fib Bulletin 100 is intended for use and/or distribution solely within fib National Member Groups.

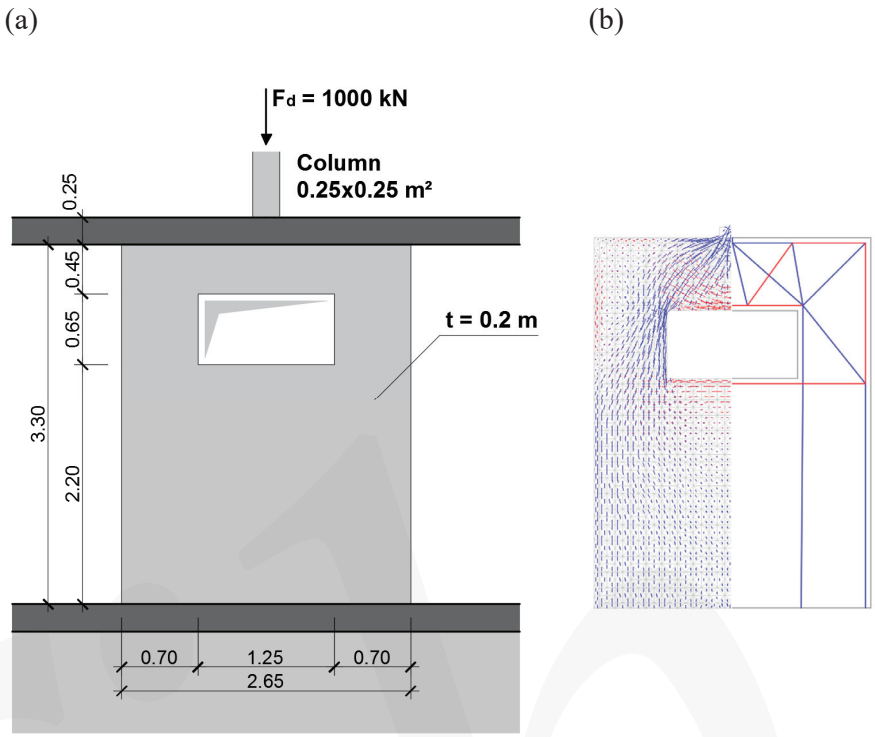


Fig. 1-4 Design inspired by the elastic uncracked stress field: (a) investigated case; and (b) elastic uncracked stress field (left) and assumed strut-and-tie model (right)

1.2.2.2 Arrangement of the reinforcement based on equilibrium considerations

- Generally, one can start on the basis of the resultants of forces to check the ideal location of the struts and ties and to resolve the conflicts of compression and tension resultants with respect to the geometry. For instance, one can see that the resultant in Fig. 1-5a is in conflict at the location of the opening
- As a second step, the struts and ties can be deviated to accommodate the load-carrying action to the actual geometry of the structure. This can be done by different means, usually adapting solutions valid from other cases[1-20]. For instance, in Fig. 1-5b one solution is shown. A detailed analysis of this solution shows however that the required thickness of the inclined struts is still in conflict with the opening and an indirect support condition is required. These enhancements in the model can be easily introduced by means of a strut-and-tie model (Fig. 1-5c) and its corresponding stress field (Fig. 1-5d).

This document is the intellectual property of the fib – International Federation for Structural Concrete. All rights reserved.
This PDF of fib Bulletin 100 is intended for use and/or distribution solely within fib National Member Groups.

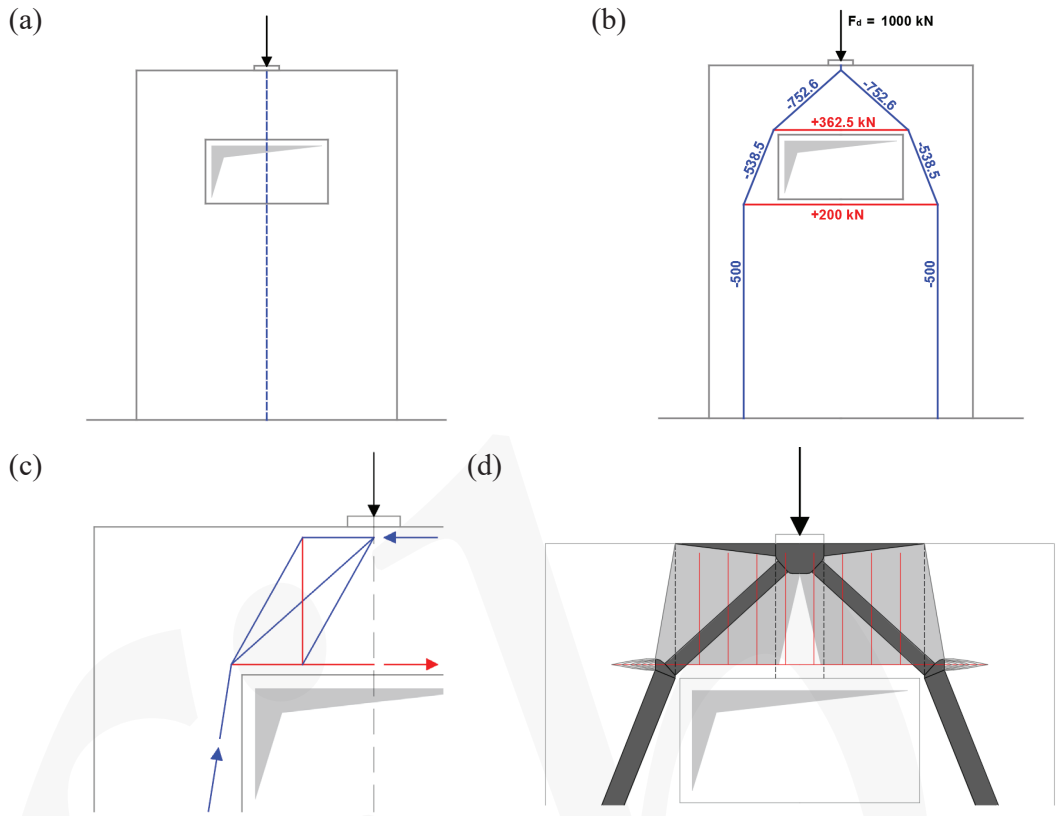
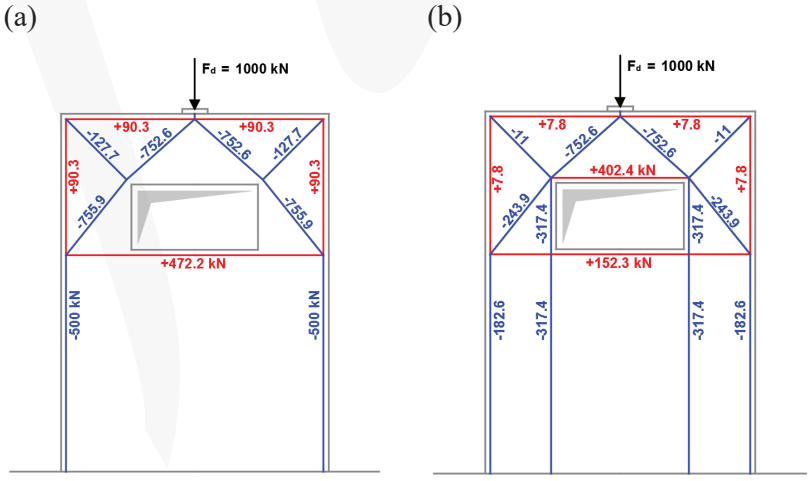


Fig. 1-5 Design based on equilibrium considerations: (a) resultant of forces; (b) possible equilibrium-based strut-and-tie model; (c) other alternative; and (d) combined model

Alternative strut-and-tie models can also be investigated. For instance, the one shown in Fig. 1-6a (frame-corner action). When different load-carrying actions can be combined (as for Fig. 1-6b, considerations of the cracking state[1-13] are normally useful, for instance by identifying the regions where cracking is prone to develop and arranging at least the minimum reinforcement. The resulting forces can then be used for designing the reinforcement layout (Fig. 1-6c, main reinforcement superimposed to the minimum amount).



This document is the intellectual property of the fib – International Federation for Structural Concrete. All rights reserved.
This PDF of fib Bulletin 100 is intended for use and/or distribution solely within fib National Member Groups.

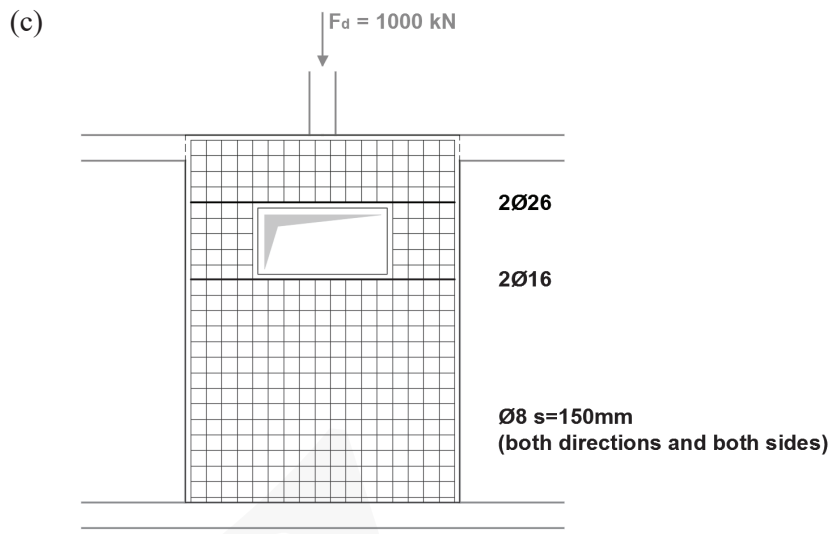


Fig. 1-6 Design based on equilibrium considerations: (a) resultant of forces; (b) combination of previous models; (c) reinforcement layout

It should be noted that following the formulation of the strut-and-tie model, its validity has to be confirmed and some local adjustments may be required (refer to Muttoni et al. [1-20]). For instance, it should be ensured that no TTT nodes are present, that the angle between the struts and the ties is not lower than a minimum value (usually adopted as 30°, refer to the detail in Fig. 1-5c-d) and that load spreading and zones in tension behind anchorages are suitably covered[1-20].

This method overcomes the difficulties related to the strut-and-tie models developed on the basis of elastic (uncracked) stress fields, mostly by providing complete freedom to the designer on the choice and arrangement of the reinforcement. Nevertheless, in some cases a certain level of experience is required as well as accounting (as previously stated) for potentially critical regions in terms of cracking.

1.2.2.3 Automated procedures

In some special cases, normally corresponding to structurally relevant members or for members that will be repeated (as for precasting), optimisation of the layout and the amount of reinforcement might be advisable. To that end, a number of automated procedures exist consistent with the strut-and-tie and stress field methods.

For instance, elastic-plastic stress fields can be used, as explained in (Fernández Ruiz et al.[1-15]. Accordingly, concrete can be assumed to be cracked, whereas the reinforcement is assumed to remain elastic. Starting from a basic mesh of reinforcement (minimum amount of reinforcement or higher homogeneous mesh), the area required in each tie can be adapted to satisfy the condition:

$$A_{s,i+1} = A_{s,i} \frac{\sigma_{s,i}}{f_{yd}} \geq A_{s,\min} \qquad 1\text{-}1$$

where $A_{s,i+1}$ refers to the required amount of reinforcement to be considered in the next iteration, $A_{s,i}$ to the amount of reinforcement in the present iteration, $\sigma_{s,i}$ to the calculated stress and f_{yd} to the design yield strength of the reinforcement. The aim of this procedure is to adapt the reinforcement in each iteration, in order to ensure that the yield strength is

This document is the intellectual property of the fib – International Federation for Structural Concrete. All rights reserved.
This PDF of fib Bulletin 100 is intended for use and/or distribution solely within fib National Member Groups.

respected. Compared to the previous approaches for design, it can be noted that this yields lower amounts of reinforcement, as the minimum reinforcement is taken into consideration in the calculation of the failure load. For the case of Fig. 1-4a-b, for instance, the optimisation procedure yields significantly lower concentrated reinforcement (compare Fig. 1-7a to Fig. 1-6c. On the other hand, this procedure can potentially lead to a large number of different reinforcement diameters and may require some adjustments to enhance constructability.

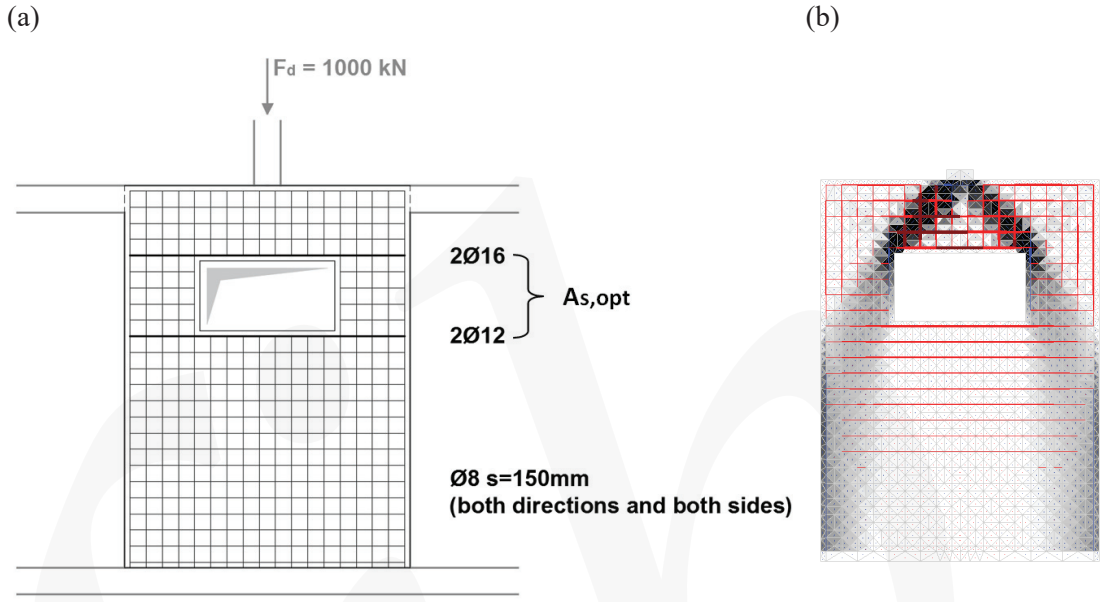


Fig. 1-7 Automated reinforcement optimisation by accounting for the presence of minimum reinforcement: (a) resulting reinforcement; and (b) elastic-plastic stress field at failure (design load)

1.2.3 Assessment of existing structures

For the assessment of existing structures, the geometry and reinforcement layout of the member is given and the engineer has to check whether the structural safety can be ensured with respect to the pertinent actions. In many cases, this is a complex task as many load-carrying mechanisms are possible. As previously stated, if simple lower-bound solutions do not yield sufficient strength, it is advisable to proceed to an optimisation of the lower-bounds in order to maximise the failure load. This allows avoiding, or at least minimising, the strengthening to be performed in the structure.

It can be noted, thus, that for the assessment of an existing structure, the engineer tries to find the exact solution according to the theory of plasticity, as this provides the lower-bound with largest resistance. Analytical and numerical approaches to this aim are discussed elsewhere[1-20]. In general, two approaches are possible:

- To consider an upper-bound and to check whether a lower-bound solution can be admissible for it. If this were not the case, the upper-bound solution has to be modified or adapted (a detailed discussion can be found in Muttoni et al.[1-20]). Two instances of this approach for the previous example are shown in Fig. 1-8a-b. Other mechanisms, such as the shear failure shown in Fig. 1-8c imply in addition dissipation of the concrete along the yield line[1-10]. The failure load can be obtained by equilibrium of the free-bodies, allowing derivation of the corresponding forces in the ties and struts[1-20]. If the strength of one element is not satisfied, the mechanism has to be modified in order to satisfy the yield criteria of

This document is the intellectual property of the fib – International Federation for Structural Concrete. All rights reserved.
This PDF of fib Bulletin 100 is intended for use and/or distribution solely within fib National Member Groups.

all elements. This approach has the advantage that it allows understanding which are the critical elements of the structure during the optimisation process. In addition, the exact solution (mechanism respecting the yield criterion of the struts and the ties) can be rapidly determined.

Alternatively, numerical approaches are also possible to optimise upper-bound solutions. This can be done for instance by means of non-linear optimisation techniques on the yield conditions.

- To optimise lower-bound solutions. This approach (complementary to the previous one) can be performed in a general way through numerical procedures that allow accounting for equilibrium, compatibility and yield conditions of the material. For instance, by using compatibility-based stress fields (see Section 5.2) such as the elastic-plastic stress field approach[1-15], see Fig. 1-8d. Optimisation by hand is also possible, yet it requires incorporating kinematic assumptions during the search of the optimal lower-bound (check of resulting mechanism), as per Muttoni et al.[1-13].

When assessing structures with limited ductility or very large amounts of plastic redistribution, stress fields can also be used to verify if the deformation capacity is sufficient (i.e. the materials do not fail before reaching the calculated plastic solution). This requires considering kinematic compatibility and assigning appropriate stiffness and failure criteria to the materials, refer to Kaufmann et al.[1-17].

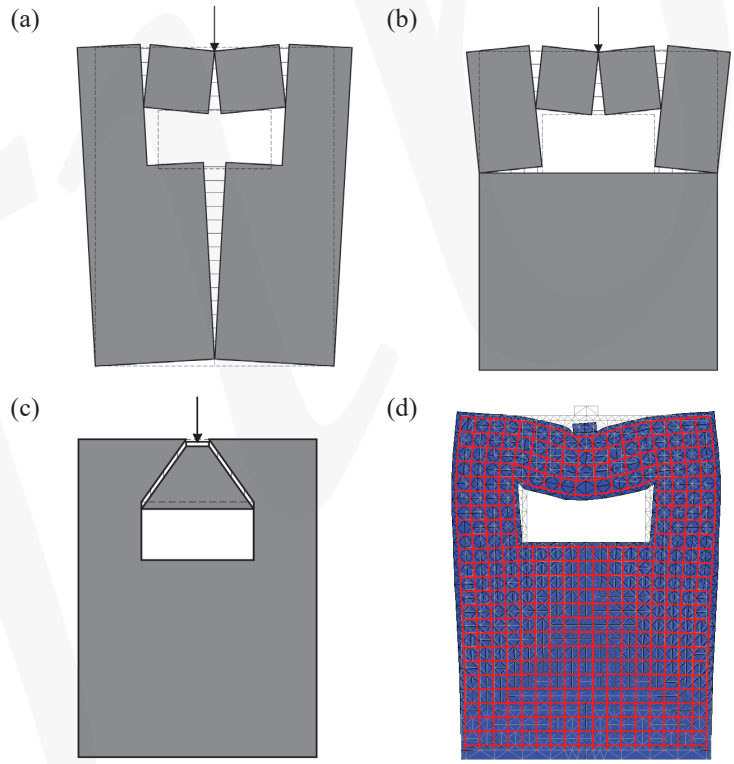


Fig. 1-8 Analysis of potential failure mechanisms: (a-b) rigid-plastic flexural mechanisms; (c) rigid-plastic shear mechanism; and (d) elastic-plastic stress field (Fig. 1-7) displacement field

It can be noted from the previous discussion that the stress field method is a suitable approach both for design and assessment of existing structures. This is due to the duality of the method of being both a tool for analysis and for design. For the design of new structures, it allows dimensioning of the required reinforcement and concrete areas by

This document is the intellectual property of the fib – International Federation for Structural Concrete. All rights reserved.
This PDF of fib Bulletin 100 is intended for use and/or distribution solely within fib National Member Groups.

checking the equilibrium and yield conditions for an assumed load-carrying mechanism. However, for the assessment of a given structure, the stress field and corresponding load-carrying mechanism may be adapted (as a nonlinear analysis tool) to maximise the failure load while respecting the deformation capacity of the materials.

1.2.4 Considerations for retrofitting

In some cases, following a refined assessment of the structural capacity, the need for strengthening of an existing structure is identified. This can be due to existing structural damage, or to the need for upgrading the load-carrying capacity. Strength, stiffness, deformation capacity and combinations thereof are the main structural characteristics modified through strengthening. Any structural property modification may be performed through an appreciable number of techniques (as for instance concrete jacketing, carbon/glass/basalt/aramid fibre-reinforced polymer jackets/strips, near-surface mounted reinforcement, steel jacketing, addition of diagonal bracing, bay infilling via reinforced concrete to form shear-walls) and their combinations. The application of strut-and-tie and stress field models is potentially a valuable tool to design consistently such intervention. The approach for so doing depends, however, on the ductility of the strengthened member. When a ductile behaviour can be expected (allowing for significant stress redistributions), strut-and-tie models or stress fields with rigid-perfectly plastic material behaviour can be applied with limited modifications. However, when the deformation capacity of the strengthened member is limited, then the required stress redistributions to fully activate the strengthening may not be possible. In this latter case, specific considerations of the strain field and of the development of cracking should be accounted for in the design of the strengthened member.

There is a handful of examples which regard assessment and the design of strengthening of existing structures by means of strut-and-tie models and stress fields. Among the early works was that by Chai et al.[1-22]: a strut-and-tie simple model was used to uncover the reasons of failure of a bridge pier footing specimen and to design a new configuration. The model was later modified for designing the retrofitting of existing bridge footings[1-23].

An extensive study using stress field models for designing the strengthening of existing foundations was performed by Fernandes[1-24]: strengthening involved use of micropiles, application of prestressing or footing enlargement, as well as combinations of the above (footing enlargement and prestressing, footing enlargement and micropiles), for both concentric and eccentric loading. Works in this field have also been performed by Menduiña et al.[1-25].

Another example of design of retrofitting employing strut-and-tie modelling is given by Voumard[1-26]. The case regarded the addition of corbels to existing columns to accommodate horizontal movement of beams supported on them. Simple models that were developed for two retrofitting approaches (precast-prestressed corbels or reinforced concrete ones) were sufficient to prove that transfer of forces across the column-new corbel interface could only be facilitated by one of the proposed solutions.

With respect to nonlinear cyclic truss models for reinforced concrete walls, Panagiotou et al.[1-27] developed first approaches successively updated by Lu et al.[1-28] and Lu et al. [1-29]. The model is of intermediate complexity and can successfully predict the post-

This document is the intellectual property of the fib – International Federation for Structural Concrete. All rights reserved.
This PDF of fib Bulletin 100 is intended for use and/or distribution solely within fib National Member Groups.

cracking cyclic response in global force-displacement terms as well as regarding concrete softening or crushing. Within this field, nonlinear truss modelling was also developed by Qazi et al.[1-30] to assess the capacity of a reinforced concrete wall strengthened with carbon fibre-reinforced polymers and subjected to lateral deformation.

Recent developments in the field of strengthening of deep beams include a strut-and-tie model by Dhahir[1-31], reinforced in shear via FRP sheets or strips. This approach has been successfully compared to 46 deep beams with different amounts of FRP. Suitable approaches in this field have been also proposed by Mihaylov et al.[1-32].

Far from being exhaustive, the above aims to demonstrate that strut-and-tie and stress field models can be extended to cover the assessment of existing structures and, if proved necessary, the design of the appropriate in each case retrofitting intervention in each case. Nevertheless, more research is necessary before being satisfactorily introduced in modern codes and application guidelines are developed to attract the attention of engineering practice.

This document is the intellectual property of the fib – International Federation for Structural Concrete. All rights reserved.
This PDF of fib Bulletin 100 is intended for use and/or distribution solely within fib National Member Groups.

2. General considerations on stress fields and strut-and-tie models

2.1 Stress fields as a lower-bound solution of limit analysis

Limit analysis (theory of plasticity) is a powerful tool to estimate the failure load of a structure considering a perfect plastic behaviour of materials. In particular, limit analysis has shown to be a suitable tool for design and assessment of reinforced concrete (an extensive review of this theory can be consulted in Chen and Han[2-1]). Stress field models are based on the lower-bound theorem (or static principle) of limit analysis, defined by Drucker[2-2] (previous contributions to this theorem by Gvozdev can be consulted in Nielsen and Hoang[2-3]):

> If an equilibrium distribution of stress can be found in the concrete and the steel which is nowhere tensile in the concrete and is everywhere at or below yield, the structure will not collapse or will just be at the point of collapse.

Strut-and-tie or stress field models consider concrete and reinforcement as different elements, whose internal forces equilibrate the external actions and shall fulfil the yield conditions of the materials (the definition of the yield conditions is made for each material individually and not for reinforced concrete, as heterogeneous material).

For the design of a new structure, selecting a suitable lower-bound is sufficient. For assessment of existing members where the geometry and reinforcement are given, the best lower-bound to be selected is that corresponding to the exact solution, both fulfilling the conditions of lower-bound theorem (an equilibrated distribution of stresses that respects the yield condition) and of upper-bound theorem, or kinematic principle (a valid mechanism that respects the flow rule of yield surface).

2.2 Application of limit analysis to structural concrete

Limit analysis assumes that materials behave in a rigid-perfectly plastic manner (i.e., the materials require sufficient deformation capacity to develop the plastic stress redistributions required in the element). However, it shall be noted that the deformation capacity of concrete is limited and this can also be the case for the reinforcement (due to material response or slip at laps and anchorages). This may consequently compromise the applicability of limit analysis to structural concrete. This topic was initially researched by M.P. Nielsen in Denmark and B. Thürlimann in Switzerland, followed by extensive investigations on the deformation capacity of structural concrete by other researchers[2-3], [2-4], [2-5], [2-6], [2-7], [2-8]. The results of these and similar investigations are reflected in the following provisions of current design codes:

- The enhanced brittleness (strain softening) of concrete in compression for high material resistances is accounted for by reducing the equivalent plastic strength by a brittleness factor. This is considered as a material effect.
- Concrete cracking (considered as a structural effect) reduces the capacity of concrete to transfer compression forces. This is accounted for by means of a strength reduction factor considering the state of transversal strains (or crack widths).

https://doi.org/10.35789/fib.BULL.0100.Ch02

This document is the intellectual property of the fib – International Federation for Structural Concrete. All rights reserved.
This PDF of fib Bulletin 100 is intended for use and/or distribution solely within fib National Member Groups.

- The tensile strength of concrete is neglected for equilibrium. Its effect is only considered with respect to its influence on member stiffness and deformation capacity (tension-stiffening effect of embedded reinforcement).
- Minimum reinforcement should be provided to avoid brittle failures (crack localisation) and to provide the required deformation capacity of the elements.
- Rules addressed to ensure that the deformation capacity is not exceeded. These rules depend on the modelling technique, but might include limits to the following values: inclination of the compression field; rotation of the compression field with respect to the uncracked state; amount of moment redistribution in redundant girders; and compression zone depth.
- Detailing rules shall be considered consistently (e.g. location of anchorage regions and reinforcement arrangement, minimum and maximum rebar spacing and confining reinforcement).

The specific provisions highly depend on the structural element and may vary depending on the design code or recommendations (partly justified by the different ductility properties of the reinforcement among countries[2-9]). For the particular case of stress fields and strut-and-tie models, concrete tensile strength is also neglected for equilibrium, while the effect of transversal strains and the increasing brittleness of higher strength concretes should be taken into account using a reduced effective compressive strength. Moreover, for rigid-plastic design, it is a standard practice to choose a solution not differing excessively from the uncracked stress state[2-10], [2-11], [2-12] with a minimum inclination of the compression field with respect to the ties; this ensures that the deformation capacity demand of the proposed solution is not excessive. When following these rules, as well as when using minimum reinforcement and suitable effective compressive strength values, stress fields and strut-and-tie models can be applied without significant restrictions. Further information on the limits of applicability of strut-and-tie models and stress fields will be provided in Section 2.5.

2.3 Idealization of material response

2.3.1 Concrete

In strut-and-tie and stress field models, the concrete carries compression stresses (no tensile capacity due to its brittle response). Yet, even in compression, the actual uniaxial response of concrete is not perfectly plastic and thus an equivalent plastic strength needs to be defined, see Fig. 2-1.

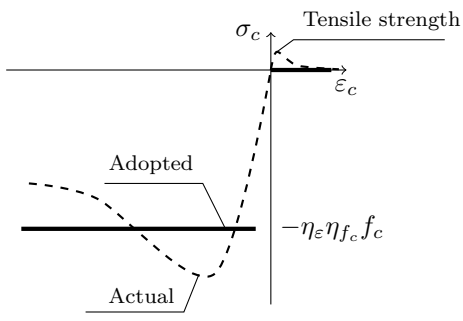


Fig. 2-1 Uniaxial concrete stress-strain relationship and assumed plastic concrete resistances

This document is the intellectual property of the fib – International Federation for Structural Concrete. All rights reserved.
This PDF of fib Bulletin 100 is intended for use and/or distribution solely within fib National Member Groups.

The main factors considered for defining the equivalent plastic strength derive from:

- Material effects, to account the properties of the material. The most important is the brittleness factor, due to strain softening after peak strength η_{f_c};
- Structural effects, to account the response of the structure under biaxial loading and its effects on the material response. This is typically the influence of transverse cracking considered by the factor η_ε.

2.3.1.1 Uniaxial compression

When idealised as a uniform compression field, concrete strength shall be reduced with respect to its uniaxial peak stress value. This is justified by the strain softening response of concrete, see Fig. 2-2. For plastic redistributions to develop, it is assumed that the material develops strain levels above that corresponding to the peak strength. Thus, to keep the deformation energy unaltered, the plastic strength shall be diminished. A strength reduction factor is typically used, which is usually refered to as the brittleness factor (η_{f_c}[2-13]). The brittleness factor depends on the uniaxial compressive material strength (increased brittleness for higher concrete strengths) and is usually considered by the following factor that covers most typical redistribution levels in structural concrete:

$$\eta_{f_c} = \left(\frac{30}{f_c \left[MPa \right]} \right)^{\frac{1}{3}} \leq 1 \qquad 2\text{-}1$$

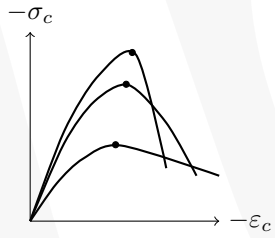


Fig. 2-2 Concrete stress-strain relationship for different compression strength

Consequently, the plastic strength of concrete, f_{cp}, results:

$$f_{cp} = \eta_{fc} \cdot f_c \qquad 2\text{-}2$$

For those cases in which stress fields and strut-and-tie models are formulated ensuring kinematic compatibility, an alternative in considering the concrete brittleness is to limit maximum concrete deformation, as typically done in design based on cross-sectional analysis. The decrease of concrete strain limit provided by standards allows accounting for the enhanced brittleness for high material resistances. This approach allows a direct verification of the deformation capacity and will be discussed in Section 2.4.

This document is the intellectual property of the fib – International Federation for Structural Concrete. All rights reserved.
This PDF of fib Bulletin 100 is intended for use and/or distribution solely within fib National Member Groups.

Other material phenomena may also modify compression strength and/or maximum deformation and can be included, if pertinent and relevant, for example[2-14]:

- Confinement
- Sustained loading
- Low-cycle fatigue

2.3.1.2 Biaxial loading

Although the application of stress fields and strut-and-tie models can be performed in a general manner following a 3D approach[2-15] (see Chapter 7.2), these tools are in many cases applied assuming plane stress conditions (e.g. walls and shells).

Several authors have evaluated the concrete strength based on the results of experimental tests with panels subjected to different stress states. Their studies conclude that the yield criterion for plain concrete can be represented in a simplified manner, as shown in Fig. 2-3, for plane strain and plane stress.

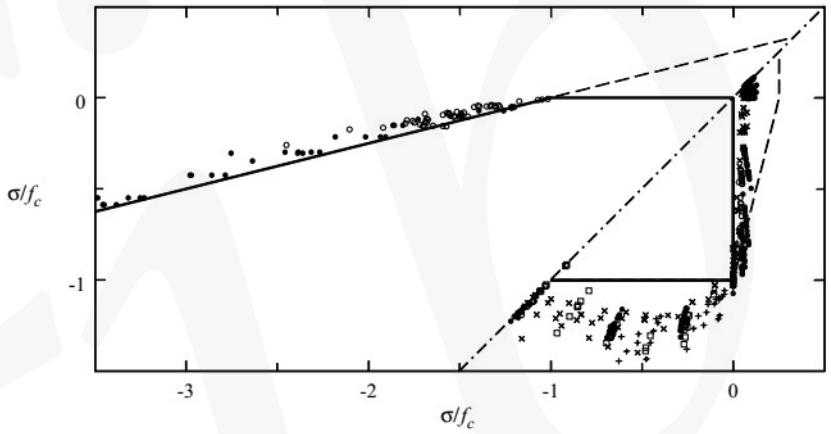


Fig. 2-3 Yield conditions of plain concrete for plane strain (upper left) and for plane stress (lower right) compared with experimental results[2-7]

The presented yield conditions (thick lines in Fig. 2-3) are based on a Mohr-Coulomb law with a cut-off for tensile strength, see Fig. 2-4. The corresponding parameters, cohesion and friction angle are related to the compressive strength[2-4].

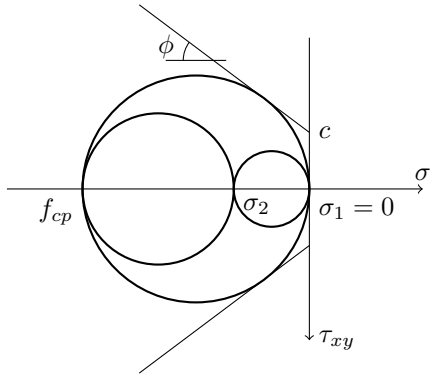


Fig. 2-4 Mohr-Coulomb criteria applied to uncracked concrete[2-3]

This document is the intellectual property of the fib – International Federation for Structural Concrete. All rights reserved.
This PDF of fib Bulletin 100 is intended for use and/or distribution solely within fib National Member Groups.

It should be noted that the presence of confinement under plane strain conditions allows increasing the compressive strength above the uniaxial concrete compressive strength. A plane stress field with compression along the two principal directions does not increase concrete resistance above the uniaxial compressive strength, because the third principal stress is null.

The behaviour of cracked concrete differs from that of uncracked concrete since existing cracks disturb the transmission of the compression field, soften the response and reduce the capacity. To ensure the ability of the compression field to cross existing cracks, a minimum smeared reinforcement allowing for internal redistributions after cracking should always be provided. Most existing models predicting the behaviour of cracked concrete rely on a reduction of the plastic uniaxial concrete compressive strength to account for the structural effect of cracking (factor η_ε), as will be discussed in the following. The resulting concrete yield criteria for cracked concrete under plane stress conditions can be regarded as a modification of the uncracked behaviour, where the maximum strength reduces for the case of a principal compression stress field together with a positive transverse strain, see Fig. 2-5. Such modification could alternatively be seen as a shrinkage of the yield surface (keeping its squared shape), in order to respect the convexity condition (refer to dotted red line in Fig. 2-5). This does not modify any governing condition as the only possible stress state when cracking develops implies $\sigma_{c,3} = 0$.

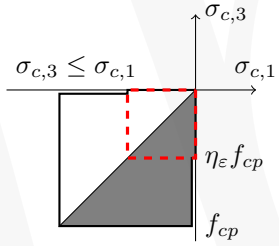


Fig. 2-5 2D yield condition for plain cracked concrete

As experimentally observed, the presence of reinforcement[2-16] and particularly when it is in tension leading to cracking in a compression field[2-16], [2-17] reduces its compressive strength. This effect, known as compression softening, is considered in Fig. 2-5 by the strength reduction factor η_ε, that accounts for the influence of existing cracking generally relying on the transverse strain, ε_1.

Several proposals for this compression softening factor can be found in the literature (Vecchio, Kaufmann, Sigrist…), which were empirically derived in the context of compression field approaches and cover different physical mechanisms. A mechanical approach to the contribution of these different mechanisms has also been developed and can be consulted elsewhere[2-18]. One important observation is that all relationships found in the literature have not been directly developed from experimental measurements, but using calculated data based on certain hypotheses. Hence, compression softening relationships are highly dependent on the specific assumptions considered in the models from which they were derived, and using these relationships for models with different assumptions may lead to significant inconsistencies[2-9]. Some compression softening relationships derived on the basis of fictitious rotating cracks, as stress fields assume, are presented in the following (see Fig. 2-8d).

This document is the intellectual property of the fib – International Federation for Structural Concrete. All rights reserved.
This PDF of fib Bulletin 100 is intended for use and/or distribution solely within fib National Member Groups.

Vecchio and Collins[2-17] proposed the first expression usable in this manner. The formula for compression softening was derived on the basis of the results of thirty plane stress panels with different reinforcement ratios and compressive strength and subjected to shear forces:

$$\eta_\varepsilon = \frac{1}{0.8 + 0.34\dfrac{\varepsilon_1}{-\varepsilon_c}} \not> 1 \qquad 2\text{-}3$$

The value of ε_c is the compressive strain value at peak strength (negative quantity). This formula was derived formulating the equilibrium on average stresses (i.e. considering an average tensile strength) and assuming interlock resistance at the cracks. The model assumes a softer strength, but not softening of the peak strain. The constitutive relationship used for concrete was a simple parabola (Hognestad parabola[2-19]). Vecchio and Collins[2-20] proposed the following coefficient that was derived with softened strength and peak strain, from a database of 116 panel and shell element tests (the Popovics[2-21] constitutive relationship was used to model concrete):

$$\eta_\varepsilon = \frac{1}{1 + 0.35\left(\dfrac{-\varepsilon_1}{\varepsilon_2} - 0.28\right)^{0.80}} \not> 1 \qquad 2\text{-}4$$

Zhang[2-22], based on fifty-five full size concrete panels subjected to various types of membrane stress, proposed the following factor derived from a softening strength and softening strain in concrete response:

$$\eta_\varepsilon = \frac{1}{\sqrt{1 + 400\,\varepsilon_1}} \qquad 2\text{-}5$$

Kaufmann[2-7] proposed a compression softening relationship, which depends on concrete compressive strength in order to cover the brittleness material effect as well. This relationship, derived from a database of more than 200 panel tests, after eliminating those specimens in which both reinforcements yielded at the ultimate, reads, for the case of 27 MPa compressive strength, reads as:

$$\eta_\varepsilon = \frac{1}{1.2 + 90\,\varepsilon_1} \qquad 2\text{-}6$$

This relationship is derived based on a model establishing equilibrium at the cracks, considering tension stiffening by means of the Tension Chord Model[2-8] and using a parabolic constitutive relationship for concrete. Sigrist[2-23] modified this relationship in the context of a stress field approach for beams including compatibility, as follows:

$$\eta_\varepsilon = \frac{1}{1.2 + 55\,\varepsilon_1} \qquad 2\text{-}7$$

which was adopted (with an upper-bound value of 0.65) for the shear verifications in *fib* Model Code 2010[2-24] (LoA II §7.3.3.3). Another expression is proposed in this code (§7.3.9.1) to be used in the design of the reinforcement in 3D solid elements:

$$\eta_\varepsilon = 0.6 \not< \frac{1.18}{1.14 + 3.40\,\max\left(\varepsilon_x, \varepsilon_y\right)} \not> 1 \qquad 2\text{-}8$$

This document is the intellectual property of the fib – International Federation for Structural Concrete. All rights reserved.
This PDF of fib Bulletin 100 is intended for use and/or distribution solely within fib National Member Groups.

The latter formulation also requires the rotation of compression field between uncracked and cracked states to be below 15º.

The different proposals are shown in Fig. 2-6, where reduced differences can be observed, for small principal tensile strains. In fact, most formulations coincide in the point $\eta_\varepsilon = 0.55$, which is typically considered in hand-calculations for the case of tension oblique to the direction of compression (see Fig. 2-7c). Therefore, analysis of stress fields shows in general little sensitivity to the compression softening formula used for the case of principal tensile strains below 10‰. Extensive validations by using the original formulation from Vecchio and Collins can be consulted elsewhere (using 150 experimental results with good results in the prediction of ultimate load capacity[2-13]).

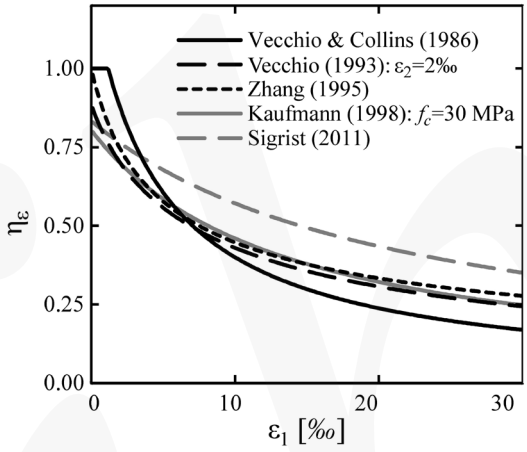


Fig. 2-6 Comparison of strain-based compression softening formulations

In hand-made analysis based on rigid-plastic models, designers typically define this softening factor for each region of the member based on the expected potential cracking state and angle of the compression field. Fig. 2-7 depicts the relevant provisions of *fib* Model Code 2010[2-24]. Other provisions (e.g. ACI 318-14 [2-245]) propose a more complex classification for evaluating the level of softening including the amount of transverse reinforcement. Application of these code provisions to complex structures is time-consuming and even challenging, as some regions do not clearly fit the existing classifications.

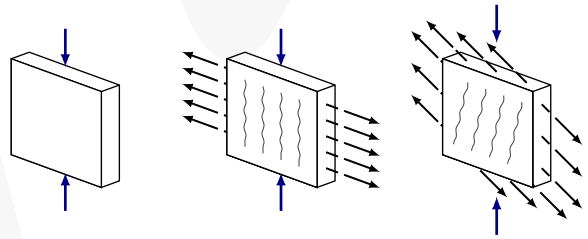


Fig. 2-7 Softening factor for different conditions (MC2010)

2.3.2 2D Reinforced concrete

Whenever stress fields are formulated ensuring kinematic compatibility, a refined method to determine softening due to concrete cracking can be used. This approach was originally proposed by Fernández Ruiz and Muttoni[2-26] and consists of determining the effective concrete compressive strength from the principal strain, ε_1, perpendicular to the principal compression direction, similar as in compression field analyses accounting for compression softening.

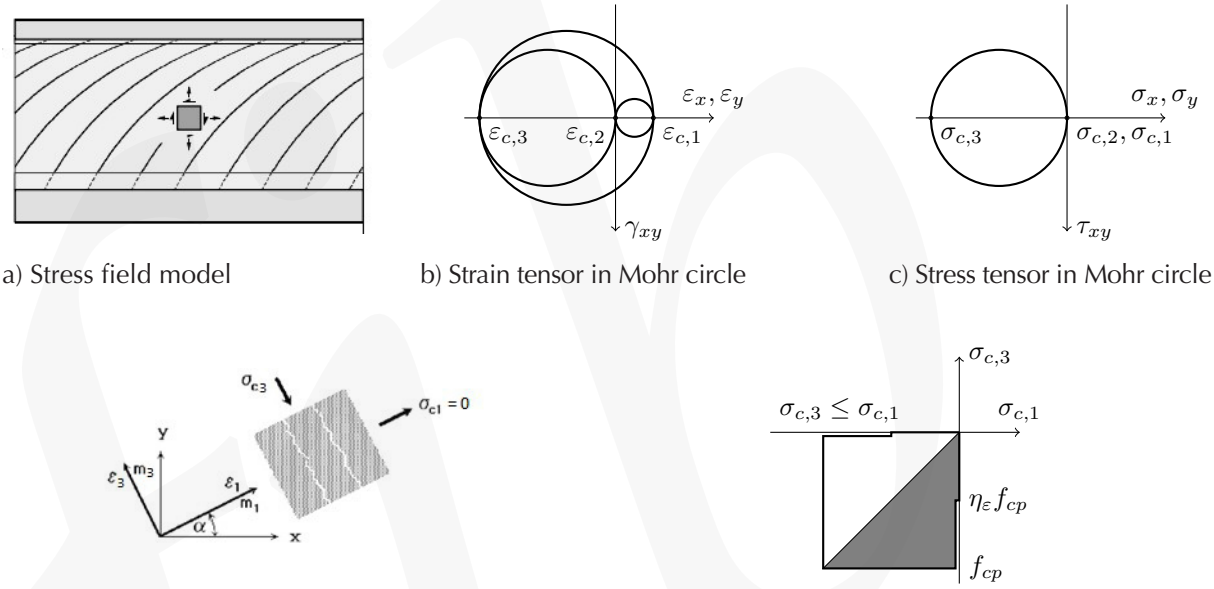
This document is the intellectual property of the fib – International Federation for Structural Concrete. All rights reserved.
This PDF of fib Bulletin 100 is intended for use and/or distribution solely within fib National Member Groups.

A licit stress field for concrete can be derived in a simple and consistent manner as shown in Fig. 2-8[2-27] by adopting plane stress conditions. At each point (Fig. 2-8a), the strain tensor is determined from the displacement field (Fig. 2-8b). A rotating crack model (ensuring a stress-free state at the cracks, with cracks perpendicular to the principal strain direction) with parallel principal directions of strains and stresses tensors (Fig. 2-8c,d), is then assumed. The corresponding stress tensor is represented in Fig. 2-8c. The yield criterion is shown in Fig. 2-8 e with the respective equations reading:

$$\text{if } \varepsilon_{c,3} \le \varepsilon_{c,1} < 0 \Rightarrow -f_{cp} \le \sigma_{c,3} \le \sigma_{c,1} < 0 \qquad 2\text{-}9$$

$$\text{if } \varepsilon_{c,3} < 0 \le \varepsilon_{c,1} \Rightarrow -\eta_{\varepsilon} \cdot f_{cp} \le \sigma_{c,3} < 0 \text{ and } \sigma_{c1} = 0 \qquad 2\text{-}10$$

$$\text{if } 0 \le \varepsilon_{c,3} \le \varepsilon_{c,1} \Rightarrow \sigma_{c,3} = \sigma_{c,1} = 0 \qquad 2\text{-}11$$



a) Stress field model b) Strain tensor in Mohr circle c) Stress tensor in Mohr circle

d) Stress free crack -Rotating crack model e) 2D yield condition for cracked concrete

Fig. 2-8 Concrete response

2.4 Constitutive relations

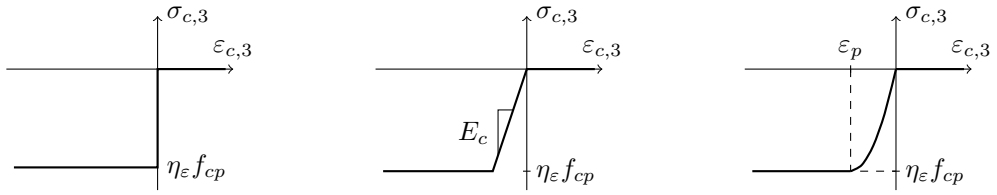
The stress-strain laws to be used for stress field analyses can be tailored depending on the degree of refinement of the analysis, ranging from simple hand-made calculations based only on equilibrium, to refined analyses accounting for compatibility conditions. In general, it is possible to define three levels of refinement:

- Rigid-perfectly plastic
- Linear elastic-perfectly plastic
- Nonlinear elastic-perfectly plastic

This document is the intellectual property of the fib – International Federation for Structural Concrete. All rights reserved.
This PDF of fib Bulletin 100 is intended for use and/or distribution solely within fib National Member Groups.

2.4.1 Concrete

Strain limits might be considered whenever an estimate of the deformation capacity is required (see section 2.5).



a) Rigid-perfectly plastic

b) Linear elastic-perfectly plastic

c) Nonlinear elastic -perfectly plastic

Fig. 2-9 Different concrete stress-strain functions

The nonlinear constitutive function can be expressed, for instance, by using the formulation presented in the *fib* Model Code[2-24] §5.1.8.1:

$$\sigma_{c3} = \eta_\varepsilon \cdot f_{cp} \frac{k\left(\frac{\varepsilon_{c3}}{\varepsilon_p}\right) - \left(\frac{\varepsilon_{c3}}{\varepsilon_p}\right)^2}{1 + \left(k - 2\left(\frac{\varepsilon_{c3}}{\varepsilon_p}\right)\right)}, \varepsilon_p \le \varepsilon_{c3} \le 0 \qquad 2\text{-}12$$

$$\sigma_{c3} = \eta_\varepsilon \cdot f_{cp}, \varepsilon_{c3} \le \varepsilon_p \qquad 2\text{-}13$$

where the strain peak value, ε_p, depends whether the model for η_ε factor is associated to a type I curve (strength and strain softening), or to a type II function (strength softening only), see Fig. 2-10. For the first case, $\varepsilon_p = \eta_\varepsilon \varepsilon_c$ should be used; otherwise $\varepsilon_p = \varepsilon_c$. The constant parameters, depending on the concrete grade, are presented in Table 2-1.

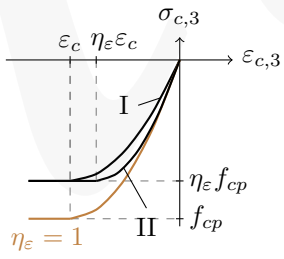


Fig. 2-10 Stress-strain functions for concrete, with strain softening (I) and without strain softening (II)

Table 2-1 Plastic concrete strength, tangent modulus of elasticity, peak strain and plasticity number

Concrete Grade	C20	C30	C40	C50	C60	C70	C80	C90	C100
f_{cp} [MPa]	20.0	30.0	36.3	42.2	47.6	52.8	57.7	62.4	66.9
E_c [GPa]	26.2	29.7	33.0	36.0	38.9	41.7	44.4	46.0	47.5
ε_c [‰]	-2.1	-2.3	-2.4	-2.5	-2.6	-2.7	-2.8	-2.9	-3.0
k	2.28	2.04	1.82	1.66	1.55	1.47	1.41	1.36	1.32

This document is the intellectual property of the fib – International Federation for Structural Concrete. All rights reserved.
This PDF of fib Bulletin 100 is intended for use and/or distribution solely within fib National Member Groups.

For other cases, it may be necessary to refine the stress-strain relationship. For instance, for proper evaluation of SLS – Service Limit state, as cracking or deformation, a model that accounts for the long-term effects should be used.

2.4.2 Reinforcement

Steel behaves initially as a linear elastic material. The response of hot rolled, quenched and self-tempered reinforcement (see Fig. 2-11) shows a distinct plastic plateau after this linear elastic phase (which defines the yield strength, f_y), followed by a strain-hardening range. Hot rolled and stretched reinforcement shows a smooth transition from the initial elastic phase to the strain-hardening branch, without a distinct yield plateau (as during stretching the material already reaches the strain-hardening range). In this case, the yield strength of the material is often defined as the stress at which a permanent strain of 0.2% remains after unloading (see Fig. 2-11).

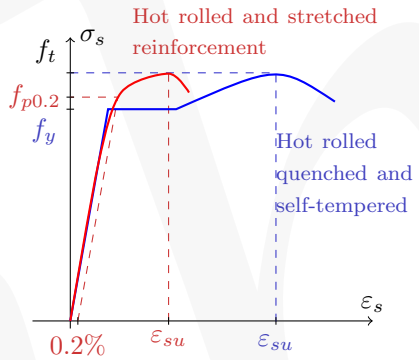
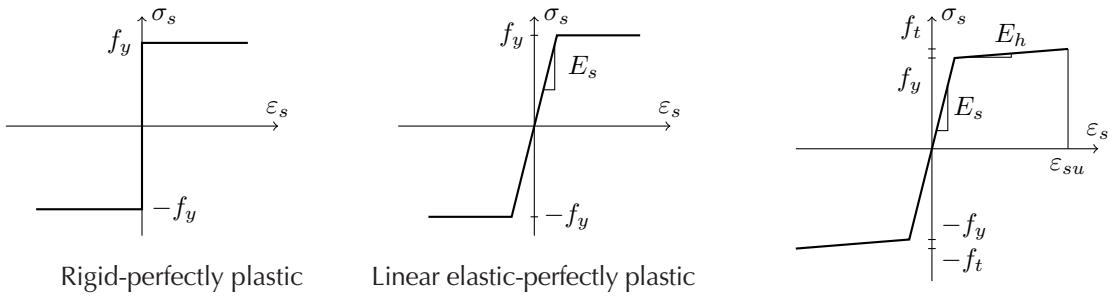


Fig. 2-11 Stress-strain characteristics of reinforcement in uniaxial tension.

In strut-and-tie and stress field models, reinforcing bars are essentially used to carry the tensile forces. However, they can also be used as compression reinforcement, if the reinforcing bars are properly braced (avoiding buckling). The yield criteria in limit analysis is defined simply as $|\sigma_s| \leq f_y$. The stress-strain laws reproduced in Fig. 2-12 are the most common idealizations of the material response. More refined idealizations[2-28], [2-29], [2-30] might be used for assessment purposes, if the actual stress-strain characteristics of the reinforcement are known.

For the case of prestressing tendons, its behaviour can be assumed as rigid-perfectly plastic. Its effect can be modelled either by an equivalent load or by an initial strain. Using the second alternative is necessary to account the initial strains to assess stresses correctly in the tendons.

This document is the intellectual property of the fib – International Federation for Structural Concrete. All rights reserved.
This PDF of fib Bulletin 100 is intended for use and/or distribution solely within fib National Member Groups.



Rigid-perfectly plastic

Parameters:
f_y – yield strength

Linear elastic-perfectly plastic

Parameters:
E_s – modulus of elasticity
f_y – yield strength

Linear elastic with hardening

Parameters:
E_s – modulus of elasticity
f_y – yield strength
f_t – tensile strength
ε_{su} – Elongation at maximum stress

Fig. 2-12 Reinforcement stress-strain idealizations

2.4.3 Tension stiffening

The structural response of the reinforcing steel embedded in concrete differs from the material response of the bare reinforcement previously described. Even though concrete tensile strength is neglected in stress fields in terms of equilibrium (i.e. formulating equilibrium at stress free cracks), the concrete tensile stresses between cracks are not null. These stresses reduce the reinforcement deformations between cracks, leading to a stiffer average response of the reinforcement, as seen in Fig. 2-13. The deformation capacity of the member is also reduced, particularly for low amounts of reinforcement. This effect, known as tension stiffening, influences the load-deformation behaviour of the analysed structure; therefore, it should be considered when assessing the serviceability behaviour (namely deformations and cracking) and/or the deformation capacity.

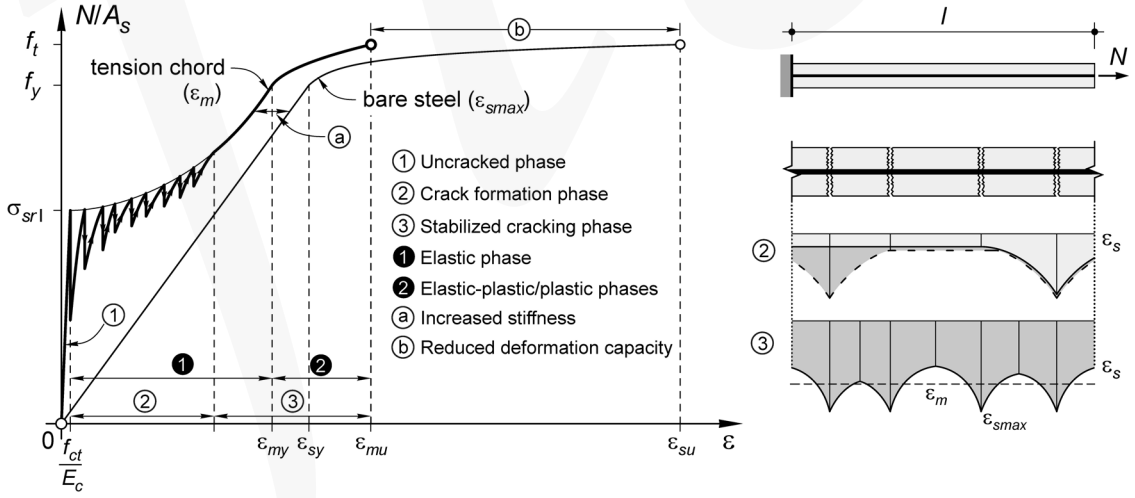


Fig. 2-13 General behaviour of a reinforced concrete element under tension, considering non-homogeneous concrete tensile strength (adapted from Alvarez[2-31]).

Tension stiffening is a structural effect as its magnitude depends on the (effective) reinforcement ratio. A straightforward and effective technique to account for this phenomenon within stress field modelling consists of modelling the reinforcement in terms of average

This document is the intellectual property of the fib – International Federation for Structural Concrete. All rights reserved.
This PDF of fib Bulletin 100 is intended for use and/or distribution solely within fib National Member Groups.

strains rather than maximum strains at the cracks (Fig. 2-13). In this way, the stiffness of each reinforcement can be increased to consider the effect of the surrounding concrete (depending on the reinforcement ratio). This is, for instance, the approach followed by Marti et al.[2-8] in the Tension Chord Model, in which simplified bond shear stress-slip relationships ($\tau_b = \tau_{b0} = 2\ f_{ctm}$ for $\sigma_s \leq f_y; \tau_b = \tau_{b1} = f_{ctm}$ for $\sigma_s > f_y$) were assumed (Fig. 2-14a). The maximum spacing between cracks (s_{r0}) results from the condition that the tensile stresses in the concrete cannot exceed the concrete tensile strength fct. It should be noted that the minimum theoretical crack spacing is half the maximum crack spacing, because at the limit, a new crack may form when f_{ct} is attained at the centre between two cracks. Hence, the crack spacing can only be determined by an upper and a lower bound, that is, $s_r = \lambda\, s_{r0}$ with $0.5 \leq \lambda \leq 1.0$. Designers should assume a certain value of λ to consider tension stiffening. Considering maximum crack spacing ($\lambda = 1.0$) might lead to the worst ultimate behaviour, but to a better serviceability response. Therefore, it is generally recommended to assume an average crack spacing ($\lambda = 0.67$) when computing tension stiffening for stress fields and strut-and-tie models. While experiments might show an uncracked initial behaviour, for design purposes it is more practical to assume that structural elements might be pre-cracked (e.g. cracked due to previous loading or because of existence of non-mechanical cracks). An extension of the Tension Chord Model for considering initial cracking can be found elsewhere[2-32].

The resulting behaviour provided by the Tension Chord Model is highly dependent on the reinforcement ratio (Fig. 2-14c-d). Hence, assigning an appropriate concrete area acting in tension between the cracks to each reinforcing bar is crucial. Provisions to assign this effective concrete area depending on the concrete cover and spacing between bars are given in design codes for specific cases. To solve the lack of generality of these provisions, Mata-Falcón et al.[2-33] proposed a numerical procedure to calculate this effective reinforcement ratio for any configuration of reinforcement.

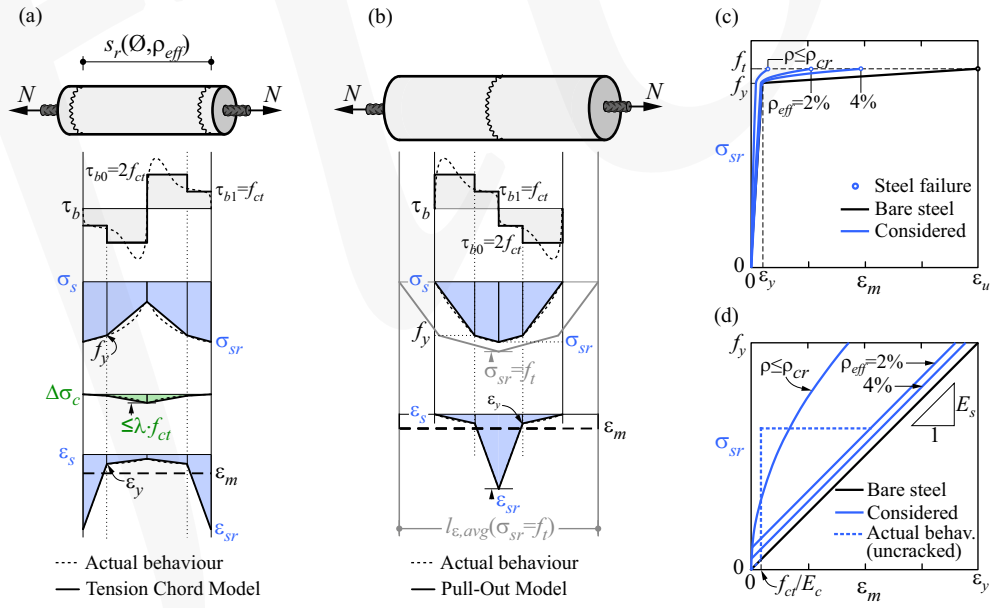


Fig. 2-14 Modelling of tension stiffening: (a) Tension Chord Model[2-8] for stabilised cracking with distribution of bond shear, steel and concrete stresses, and steel strains between cracks; (b) pull-out assumption[2-33] for non-stabilised cracking with distribution of bond shear and steel stresses and strains around the crack; (c) resulting tension stiffening behaviour in terms of reinforcement stresses at the cracks and average strains for European B500B steel and λ=0.67; (d) detail of the initial branches of the tension chord response.

This document is the intellectual property of the fib – International Federation for Structural Concrete. All rights reserved.
This PDF of fib Bulletin 100 is intended for use and/or distribution solely within fib National Member Groups.

It should be noted that the Tension Chord Model is not applicable for reinforcement ratios lower than ρ_{cr}, i.e., the minimum reinforcement ratio for which the reinforcement is able to carry the cracking load without yielding. The value of this minimum reinforcement is obtained as follows:

$$\rho_{cr} = \frac{f_{ct}}{f_y - (n-1)f_{ct}} \qquad 2\text{-}14$$

where $n = E_s / E_c$ = modular ratio. For conventional concrete and reinforcing steel, ρ_{cr} amounts to approximately 0.6%.

Application of the Tension Chord Model for $\rho<\rho_{cr}$ might underestimate crack spacing and the tension stiffening effect, resulting in significant overestimation of the deformation capacity. A consistent quantification of crack spacing in these low reinforced regions (generally corresponding to stirrups) is challenging, as cracks are generated by either non-mechanical actions (e.g. shrinkage) or the progression of cracks controlled by other reinforcement. In such situations, Mata-Falcón et al.[2-33] proposed considering the simplified bond shear stress-slip relationships of the Tension Chord Model, but assuming a crack spacing equal to the distance between points with zero slip when the reinforcing bar reaches its tensile strength (f_t) at the crack ($l_{\varepsilon,avg}$ in Fig. 2-14b). In this way, the behaviour of the bonded reinforcement is independent from the effective reinforcement ratio and the exact concrete tensile stresses remain unknown. In spite of its simplicity, this pull-out assumption provides good strength predictions for failures due to insufficient ductility of the reinforcement[2-33], [2-34], [2-35]. Further research is still required to validate the best approach to model low reinforced regions and to determine whether other effects (such as aggregate interlock or size effect) could play a significant role in such cases.

Approaches other than those in which tension-stiffening effects are implicitly accounted for by means of a modified reinforcement behaviour may also be followed, considering numerical models for the reinforcement in tension and its interaction with the surrounding concrete. Such approaches are computationally more demanding, but have a series of advantages, such as the possibility to account for variable crack spacing according to the stress profile in the reinforcement[2-36].

2.4.4 Anchorage of reinforcement

The transfer of forces between steel and concrete is performed by bond, inside or outside of the nodal regions. This is done for simplification purposes, as stress fields considering the interaction of bond in the compression fields is possible[2-26]. In simple cases, as anchorage of tie occurs outside of the nodal region, this verification only influences the detailing of the reinforcement, by extending the reinforcement length or evaluating the maximum force that reinforcement can support in case of assessment. To calculate the anchorage length, a simple rigid-plastic bond model can be used (as that used by the Tension Chord Model). Alternatively, more refined bond models can be used. The transverse pressure influences the anchorage capacity and can be used to reduce the anchorage length or to increment the bond strength. It should be noted that the design values of bond imply a much higher degree of conservatism than other failure modes. This conservatism should be kept when modelling bond in stress fields or strut-and-tie models.

In the case of compatibility-based stress fields (as elastic-plastic stress fields), the usual formulation is to consider a perfect bond between the two materials. The resultant

This document is the intellectual property of the fib – International Federation for Structural Concrete. All rights reserved.
This PDF of fib Bulletin 100 is intended for use and/or distribution solely within fib National Member Groups.

anchorage/lap capacities are checked as an a posteriori procedure. In case of violation of the yield condition a simple procedure to satisfy the yield conditions of bond is to reduce the area of the reinforcement for limiting the axial force below the maximum force that is possible to transfer due to bond. An explicit model for bond stress-slip can alternatively be used to evaluate correctly the stiffness and the load-carrying capacity of a structure. The transverse pressure also influences the response and can be explicitly incorporated with a finite element (0D) with 3 nodes, two for surrounding concrete and one for steel, in case of using FE models[2-37].

2.5 Limits of applicability

2.5.1 General considerations

The use of limit analysis requires a certain level of deformation capacity in the response of the materials. In general, reinforced concrete members fulfilling the conditions discussed in Section 2.2 present sufficiently large deformation capacities to allow for the use of limit analysis[2-7]. However, these conditions (implemented in codes of practice) might not be respected in some cases (as for instance structures built following older design codes or for some cases of strengthening or retrofitting, see section 1.2.4). This section discusses the circumstances under which stress fields and strut-and-tie models are still applicable, despite not fulfilling all the provisions presented in Section 2.2.

For the case of plain concrete members or members with less than minimum reinforcement, stress fields and strut-and-tie models are not applicable and a theory accounting for crack localisation must be used. A specific formulation must also be used in the case of failure due to concrete crushing occurring before yielding of reinforcement (see Nielsen and Hoang[2-3], elements usually called “over-reinforced”).

For special cases, where concerns exist over the conditions ensuring sufficient deformation capacity (for example low ductility of the reinforcement, very low available amount of transverse reinforcement, very large amounts of plastic redistribution…), stress fields and strut-and-tie models still remain applicable provided that: (i) the deformation capacity is explicitly verified (as shown in Section 2.5.4) or, (ii) there is sufficient experimental validation proving the applicability of the methodology for the specific structural case under analysis.

2.5.2 Minimum reinforcement

As previously introduced, stress field analysis requires in general the provision of a minimum amount of reinforcement, to:

- avoid brittle failure after cracking, and,
- ensure sufficiently deformation capacity with distributed reinforcement.

This reinforcement may also be used for other purposes, although not related to stress field design, such as:

- To satisfy serviceability requirements (crack control)
- To ensure robustness or integrity
- To avoid explicit checks of undesirable failure modes

This document is the intellectual property of the fib – International Federation for Structural Concrete. All rights reserved.
This PDF of fib Bulletin 100 is intended for use and/or distribution solely within fib National Member Groups.

With respect to the amount of minimum reinforcement required to ensure the necessary deformation capacity of a member, there is still no general consensus about it and current recommendations are mostly based on experience and empirical observations. In the absence of more refined recommendations, the value provided by *fib* Model Code 2010[2-24] for shear reinforcement should be considered as the minimum amount of transverse reinforcement for stress fields and strut-and-tie models. This value $\rho_{\min} = \frac{0.08\sqrt{f_{ck}}}{f_{yk}}$, leads to an amount of transverse reinforcement of 0.09% for conventional concrete and reinforcement (f_{yk} = 500 MPa; f_{ck} = 30 MPa). A refinement of this value will attract research efforts in the future by clarifying the role of bond, material ductility[2-9], [2-34] size effect and energy balance at the moment of cracking.

2.5.3 Minimum inclination of the compression field

The use of a refined calculation for the effective compressive strength accounting for concrete softening allows formulation of stress fields with inclinations of the compression field flatter than the minimum inclinations provided by design codes (derived for the case of manually calculated compression softening, as in Fig. 2-7).

2.5.4 Deformation capacity

Compatibility-based stress fields account for strain compatibility and can be used to explicitly check material strain limits. For other cases, the prescribed rules defined in codes or in literature should be used.

Concrete failure in compression might be defined by the ultimate strain limit for cross section analysis (ε_{cu}). This can provide, in certain cases, a better estimation of the deformation capacity than when a rigid-perfectly plastic behaviour is considered. However, the resulting strains when using e.g. a finite element based method, might be locally unrealistic and mesh size dependent (unless the softening behaviour of concrete is modelled, which is out of the scope of stress field and strut-and-tie modelling). To avoid issues of local mesh size dependency, the strain limit in compression should be imposed to the strain averaged over a certain length. A good estimate of the averaging length is the characteristic crushing band length (l_{cb}) of concrete in compression. While there is no consensus on the value of l_{cb} for any situation, twice the thickness of the structure at the compression zone might be a reasonable estimate.

Consideration of a yield plateau and neglecting the reinforcement hardening, $\sigma_s \leq f_y$, do not provide any strain limitation. Therefore, neither the rigid-perfectly plastic idealization, nor the linear elastic-perfectly plastic idealization of the reinforcement (Fig. 2-12) are suited to verify the deformation capacity. When an explicit verification of the deformation capacity is required, a bilinear idealization (linear elastic with hardening) that considers the tensile strength of the material (maximum allowable stress) and the elongation at maximum force (maximum allowable strain) should be considered. Moreover, the tension stiffening effect should also be included (Section 2.4.3), as it has a significant impact on the deformation capacity even for large reinforcement amounts (e.g. the deformation capacity for bonded reinforcement with ρ = 2% is approximately 25% of that of the bare reinforcing steel, see Fig. 2-14c).

This topic should not govern the load bearing capacity of the structures when the minimum amount of transverse reinforcement is provided, but may be relevant for reinforcements

This document is the intellectual property of the fib – International Federation for Structural Concrete. All rights reserved.
This PDF of fib Bulletin 100 is intended for use and/or distribution solely within fib National Member Groups.

with low ductility or for amounts of transverse reinforcement lower than the minimum defined by Model Code 2010 which can be found in some existing structures. Recent studies[2-35] state that, in particular cases, brittle failures due to insufficient ductility of the transverse reinforcement might also occur even when typical minimum amount of transverse reinforcement is provided.

2.5.5 SLS response

Other than for verifying the Ultimate Limit State, stress fields can be used to assess the serviceability response of structures. This topic requires accounting for compatibility conditions, tension-stiffening and long-term effects. Crack widths (w) can be generally calculated as outlined in Fig. 2-15 based on crack spacing (s_r), average reinforcement strain (ε_m) and relative angle between the crack (θ_r, as defined by the principal directions of stresses and strains) and the reinforcement direction (θ_b):

$$w = \frac{w_b}{\cos\left(\theta_r + \theta_b - \pi/2\right)} = \frac{\varepsilon_m \cdot s_r}{\cos\left(\theta_r + \theta_b - \pi/2\right)} \qquad 2\text{-}15$$

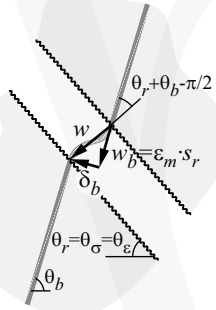


Fig. 2-15 Crack width calculation from reinforcement average strains.

The calculation of crack widths in non-stabilised crack patterns is, for the particular case of dapped-ended beams, addressed in Section 6.5. Other examples discussing the serviceability behaviour can be found in Sections 3.7.5, 4.3 and 5.2 of this document.

2.6 Safety factor format

2.6.1 Partial safety factor

The MC 2010 §7.11.3.4 proposes different approaches for the combination of safety factors of the loads and the materials. The simplest one is to assume the partial coefficient factors. In this approach, the material strength is reduced by partial safety factors accounting for material uncertainties, geometrical uncertainties and model uncertainties. In typical design of concrete structures, the design strength ($f_d = f_k/\gamma_c$) is obtained by considering the following partial safety factors[2-24]:

Concrete $\gamma_c = 1.5$

Steel $\gamma_c = 1.15$

This document is the intellectual property of the fib – International Federation for Structural Concrete. All rights reserved.
This PDF of fib Bulletin 100 is intended for use and/or distribution solely within fib National Member Groups.

The partial safety factor method can be used in a simple manner in hand-made calculations and rigid-plastic stress fields or strut-and-tie models, by modifying the material strengths. Also, it can be consistently used for compatibility-based stress fields (as elastic-plastic stress fields) by reducing only the plastic plateau of the materials. The consistency and reliability of this approach has been investigated and verified elsewhere [2-38].

2.6.2 Use of other safety formats

Alternative approaches to the partial safety factor can also be used. They can be based on performing a high number of simulations varying the geometric and material values according to their scatter and also considering the epistemic error of the method (as performing Monte Carlo analyses). Also, approaches based on a global safety factor or the Estimation of Coefficient of Variation are also possible.

This document is the intellectual property of the fib – International Federation for Structural Concrete. All rights reserved.
This PDF of fib Bulletin 100 is intended for use and/or distribution solely within fib National Member Groups.

3. Use of the Levels-of-Approximation approach to design with stress-fields and strut-and-tie models

3.1 Introduction

Strut-and-tie and stress field models are acknowledged as powerful tools for design of structural concrete members. They allow a rational understanding of the structural behaviour by relying on the idea of following the internal flow of forces. Despite its advantages, the method has also found some difficulties for its use in practice. Some aspects frequently mentioned are: the non-uniqueness of the solution (which yields to discussion on the suitability of the models, mainly concerning ductility and serviceability behaviour); the need for engineering judgment to develop a suitable model; and the calculation process (which may, sometimes, be time-consuming, especially for complex geometry and load state).

The main goal of this chapter is to provide guidelines to develop suitable strut-and-tie and stress fields models following the Levels-of-Approximation (LoA) approach, i.e. the level of accuracy of strength and / or behaviour prediction, is progressively refined by successively increasing the model refinement. This is normally accompanied by an increase on the expected failure load when more refined analyses are performed (but may not hold true for cases not complying with the hypotheses to derive lower-level LoAs). The selection of the LoA must be adequately defined and may depend on several aspects: design phases of the project (preliminary design, detailed design…), complexity of the region or structure, regions that can influence global structural behaviour, assessment or design of a structure, etc. The suitable design strategy and the adequate LoA for a specific case should be defined employing the necessary accuracy and the time devoted to the analysis.

The LoA approach for the application of stress fields and strut-and-tie models may be very useful in practical applications, since it is very common that the designer decides the time to be dedicated to the analysis, according to the complexity of the case and required accuracy of the prediction. In fact, most designers use the LoA concept in several design processes in a natural manner. However, unlike other applications of the LoA concept (such as in shear or punching), the strut-and-tie model does not have one complete equation involving all the relevant parameters, and the lower LoA are obtained by neglecting or simplifying some aspects.

The application of the LoA concept in stress fields and strut-and-tie models must be applied by progressively refining the design model. To that aim, it is advised to start with simple load-carrying models, but general enough to incorporate thereafter any relevant parameter, such as material behaviour, secondary load actions, etc. Thereafter, the model is refined as needed. The objective for higher-order LoA is to have a more precise simulation of the actual structural behaviour of the element. The designer must be clearly aware of the simplifications in the model for the lower-order LoA and must be sure that those assumptions lead to a safe-side estimate of the actual failure load.

https://doi.org/10.35789/fib.BULL.0100.Ch03

This document is the intellectual property of the fib – International Federation for Structural Concrete. All rights reserved.
This PDF of fib Bulletin 100 is intended for use and/or distribution solely within fib National Member Groups.

3.2 Level-of-Approximation I

In general, this level of approximation may be used for the conception or the design of a new structure (the *fib* Model Code for Concrete Structures 2010[3-1]).

It is the simplest and least time-consuming LoA, and presumably the one yielding the safest estimation of the ultimate load. Thus, this level must rely on a simple (safe-sided) design model, that essentially follows a simple load-carrying action. A simple strut-and-tie model shall be established and calculated accounting only for equilibrium conditions. Compatibility conditions may be indirectly considered by means of design rules to provide suitable behaviour (no explicit calculation required).

Typically, the design model should follow the main load path to calculate the main reinforcement, avoiding less important or alternative load-carrying actions that may increase the complexity of the model. Other reinforcement required may be calculated by local refinements and other calculations, avoiding again this procedure in the simple initial model.

The check of relevant nodes, struts and bars anchorage length, should be performed according to the initial simple model (i.e. the design process should be consistent with the initial model) and using simplified rules for compression softening.

In general, the following steps may be implemented to apply the LoA I to strut-and-tie models:

Step 1: Develop a basic strut-and-tie model and use it to calculate the location and area of the main reinforcement. The designer must include suitable assumptions to ensure that the simplified model provides a safe solution.

Step 2: Refine the model (with more detailed models for specific regions) whenever necessary and follow code provisions or specific bibliography to calculate the remaining required reinforcement. There is no need to include the refinements within the simple initial model if these refinements do not contradict or significantly modify the global initial model.

Step 3: Check the nodes, struts (or compression fields) as well as anchorage lengths that may be critical.

Step 4: Besides the main reinforcement, provide minimum reinforcement for the region to provide for robustness, ductility and suitable serviceability behaviour.

3.3 Level–of-Approximation II

This level of approximation is appropriate for the design of a new structure as well as for a general or brief assessment of an existing member (the *fib* Model Code for Concrete Structures 2010[3-1]).

For the LoA II, an equilibrium-based model should also be developed such as in LoA I. However, most of the local refinements and alternative load-carrying models, must be explicitly included within the design model. The model should include not only the resultants but also the stress field model, showing the widths of the main struts and the distribution widths of the reinforcement, whenever it is necessary.

In general, the following steps may be followed to apply the LoA II:

Step 1: Define a full strut-and-tie model that takes into consideration the main load-carrying model and the appropriate local refinements. If necessary or relevant for

This document is the intellectual property of the fib – International Federation for Structural Concrete. All rights reserved.
This PDF of fib Bulletin 100 is intended for use and/or distribution solely within fib National Member Groups.

the analysis, include alternative load-carrying actions within the design model. Calculate the width of the critical struts and develop a full stress field model, or only partially at the relevant regions.

Step 2: Check the nodes and any compression strength within the model that may be critical using simplified rules for compression softening. Follow the geometry and forces calculated for the initial model (i.e. be consistent along all the calculation process).

Step 3: Provide main reinforcement, minimum reinforcement and a proper detailing for the region to ensure robustness, ductility and suitable serviceability behaviour.

3.4 Level-of-Approximation III

A level III (or higher) approximation may be used for the design of a member in a complex loading state or a more elaborate assessment of a structure (the *fib* Model Code for Concrete Structures 2010[3-1]).

For the LoA III, equilibrium, compatibility and constitutive relationships must be properly computed, and a non-linear analysis based on strain compatibility should be performed. The designer may use a nonlinear finite element method or any other nonlinear technique providing a licit stress field (nonlinear optimisation techniques are also possible). It is very important to apply proper simplifications and assumptions, consistent with the theoretical bases of the stress field method, so that the interpretation of results may be clear and lead to appropriate conclusions on the structural behaviour.

The main goal of the analysis is predicting the behaviour at ultimate load. Hence, simplified elastic-plastic constitutive relationships may be implemented for concrete and reinforcement (refer to Section 2.4 for details). The compression softening effect on the compressive strength should be automatically quantified based on the state of transversal strain computed in the analysis. SLS may not be explicitly calculated, but adequate provisions must be provided to ensure adequate service behaviour.

In general, the following steps may be followed to apply the LoA III:

Step 1: For this kind of analysis, region detailing (i.e. reinforcement) must have been previously defined. This may be performed by applying the lower LoA.

Step 2: Develop a nonlinear analysis and check the steel stresses and concrete compression stresses at all load levels and validate the previously defined reinforcement layout. Serviceability behaviour and ductility aspects may be analysed in a simplified manner whenever tension stiffening effects are not relevant for calculation of reinforcement forces (see detailed considerations in Section 6.5). Secondary reinforcement may also be considered if it enhances the structural behaviour (such as: clear increase of strength, enhanced ductility or better serviceability behaviour).

This LoA may be time-consuming and requires knowledge of some additional parameters. Its need should thus be carefully analysed and may be reserved for special cases or developed by more experienced designers using specialised software.

3.5 Level-of-Approximation IV

For the LoA IV, the same principles as for LoA III are applied. The main improvement is that the analysis must provide output for service behaviour and deformation capacity. This

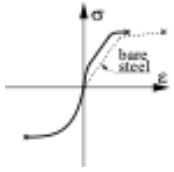
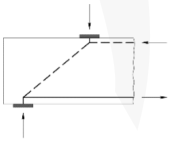
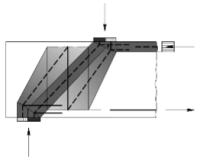
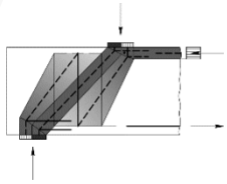
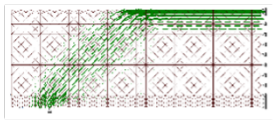
This document is the intellectual property of the fib – International Federation for Structural Concrete. All rights reserved.
This PDF of fib Bulletin 100 is intended for use and/or distribution solely within fib National Member Groups.

means that a proper constitutive relationship for the materials should be considered (refer to Section 2.4). While the concrete tensile strength should be neglected in terms of strength (as in the other LoA), its influence on the member stiffness (i.e., tension-stiffening) should be considered. Unless there is certainty that the structural elements are not pre-cracked due to previous load stages or non-mechanical actions, the initial uncracked stiffness should be neglected (i.e. assuming fully cracked behaviour). Bond laws for anchorage verifications may be included in the analysis.

3.6 Summary

The applicability of the levels-of-approximation for strut-and-tie and stress field models is summarized in the following table.

Table 3-1 Appilcability of the levels-of-approximation for strut-and-tie and stress field models

	LoA I	**LoA II**	**LoA III**	**LoA IV**
Main use	**Design (ULS)**	**Design (ULS)**	**Assessment (ULS)**	**Assessment (ULS)** **Design (SLS)**
Conditions	Equilibrium	Equilibrium	Equilibrium + Compatibility	Equilibrium + Compatibility
Constitutive relationships	Rigid-plastic 	Rigid-plastic 	Elastic-plastic 	Nonlinear with tension stiffening 
Model	Simple resultant model. Refinements and definition of strut widths whenever necessary (e.g. at nodes). 	Stress field model including alternative load-carrying mechanisms (if relevant)[1]. 	 Compatibility-based stress field model including all relevant load-carrying mechanisms and predicting internal stress redistribution.  FEM with reinforcement modelled with 1D elements.	

This document is the intellectual property of the fib – International Federation for Structural Concrete. All rights reserved.
This PDF of fib Bulletin 100 is intended for use and/or distribution solely within fib National Member Groups.

<table>
<tr><th></th><th>LoA I</th><th>LoA II</th><th>LoA III</th><th>LoA IV</th></tr>
<tr><td>Main use</td><td>Design (ULS)</td><td>Design (ULS)</td><td>Assessment (ULS)</td><td>Assessment (ULS)
Design (SLS)</td></tr>
<tr><td>Output</td><td>Strut and tie forces (ULS)</td><td>Concrete stresses in stress fields; tie forces (ULS)</td><td>Concrete stresses in stress fields; tie stresses (ULS)(2)</td><td>Concrete and reinforcement stresses and strains (ULS+SLS)</td></tr>
<tr><td>Additional verifications</td><td colspan="2">Relevant nodes and struts.
Ties.
Anchorage length.
Service behaviour.</td><td>Anchorage length.
Service behaviour.
Ultimate strain for concrete and for reinforcement.</td><td>If not direct output:
Anchorage length.
Ultimate strain for concrete and for reinforcement.</td></tr>
<tr><td rowspan="3">Requirements</td><td colspan="4">Minimum reinforcement
Detailing rules (e.g. maximum rebar spacing and confining reinforcement)</td></tr>
<tr><td colspan="2">Rules to limit stress redistributions to ensure adequate service behaviour and ductility.</td><td rowspan="2"></td><td rowspan="2"></td></tr>
<tr><td>Rules to account for alternative load-carrying mechanisms.</td><td></td></tr>
</table>

(1) The load distribution between statically indeterminate or redundant models may be estimated in the LoA II based on specific prescribed rules for the structural element or linear-elastic analysis.

(2) SLS and ductility aspects may be analysed in a simplified manner whenever tension stiffening effects are not relevant for calculation of reinforcement forces

3.7 Example: Simply Supported Beam with Two Point Loads

3.7.1 Geometry, Loads and Bending Reinforcement

Consider the simply supported beam with point loads shown in Fig. 3-1 to be designed for a shear force V_d = 1'000 kN using a concrete grade C35 (f_{ck} = 35 MPa) and ordinary reinforcing steel S500 (f_{yk} = 500 MPa). The objective is to illustrate the application of the LoA's I and II to strut-and-tie and stress field models, for the design of a new structure. A very simple example is presented to clarify the application of the methodology. All checks and calculations will be based on *fib*'s Model Code for Concrete Structures 2010 (MC2010)[3-1] provisions.

This document is the intellectual property of the fib – International Federation for Structural Concrete. All rights reserved.
This PDF of fib Bulletin 100 is intended for use and/or distribution solely within fib National Member Groups.

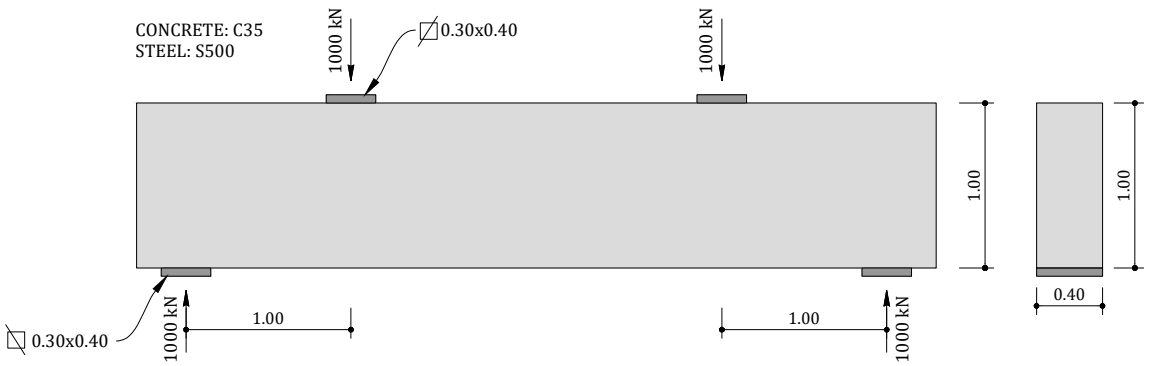


Fig. 3-1 Beam loads and geometry

Define the inner lever arm z, the bottom tension and the top compression at the mid span by applying the usual sectional method (to that aim, the concrete strength of the adjacent CCC node can be used to calculate the thickness of the compression chord). Calculate the longitudinal bottom reinforcement for the beam, provide minimum longitudinal web reinforcement and skin reinforcement (see Fig. 3-2).

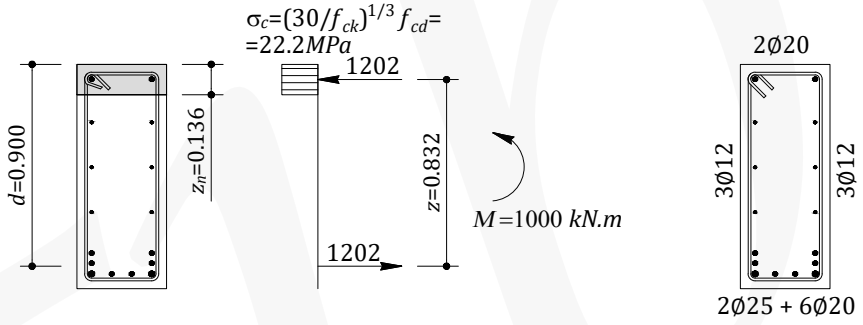


Fig. 3-2 Sectional method and calculation of the bending reinforcement

$$T = 1.202 \text{ MN} \Rightarrow A_{s,req} = 2'763 \text{ mm}^2 \Rightarrow 2\varnothing 25 + 6\varnothing 20; A_{s,prov} = 2'866 \text{ mm}^2 \qquad 3\text{-}1$$

3.7.2 Level of Approximation I

Step 1: Define a simple and safe-side strut-and-tie model. In this case a simple model consisting of a diagonal strut, from the point load to the support, is enough to calculate the main reinforcement and to check the nodal region. If necessary, a simple stress field model can be drafted to check any compression strength within the region. In most cases, however, the definition of the widths at the nodal region is sufficient to check compression and anchorage length (see Fig. 3-3).

This document is the intellectual property of the fib – International Federation for Structural Concrete. All rights reserved.
This PDF of fib Bulletin 100 is intended for use and/or distribution solely within fib National Member Groups.

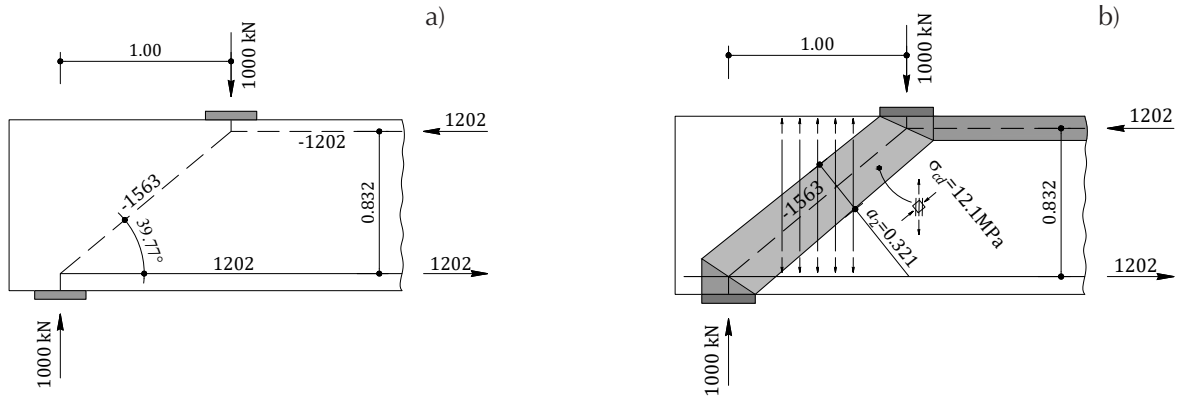


Fig. 3-3 a) Simple strut-and-tie model; b) Simple stress-field-model

Step 2: Since the point load is at a distance of the support $0.5<a/z<2.0$, part of the load must be transferred by stirrups to ensure an adequate service behaviour[3-2], [3-3], [3-4]. Stirrups' force may be calculated per $F_w = \frac{F}{3}(2\frac{a}{z}-1)$ and should be distributed over a width of approximately $0.75(a-0.3) \approx 0.5$m.

$$F_w = \frac{F}{3}\left(2\frac{a}{z}-1\right) = \frac{1'000}{3}\left(2\frac{1.0}{0.832}-1\right) = 468 \text{ kN} \qquad 3\text{-}2$$

$$f_w = 936 \text{ kN/m} \Rightarrow \left(A_s/s\right)_{req} = 2'152 \text{ mm}^2/\text{m} \Rightarrow \text{Stirrups } \varnothing 12 \,/\, /0.10;$$
$$\left(A_s/s\right)_{prov} = 2'262 \text{ mm}^2/\text{m} \qquad 3\text{-}3$$

Step 3: Check diagonal compression field. The diagonal strut develops in a region with vertical tension strains due to force at the stirrups. It is thus relevant to check the compression field with the reduced concrete compression strength for the considered concrete grade C35 (see Fig. 3-3, cracked concrete conditions). In the middle of the strut, it results: Eq. 3-4. Also check node stresses and anchorage length of the bars. Be consistent with the simple initial design model.

$$\sigma_c = 12.1 \text{ MPa} < \sigma_{c,Rd} = 0.55\left(\frac{30}{f_{ck}}\right)^{\frac{1}{3}} f_{cd} = 12.2 \text{ MPa} \qquad 3\text{-}4$$

In the simple model in Fig. 3-3 the bottom tension must be extended up to the support, thus the force to be anchored at nodal region shall be calculated accordingly. For the CCC node, the maximum compression is equal to the maximum allowable one (see Fig. 3-4b).

$$\sigma_c = 22.2 \text{ MPa} < \sigma_{c,Rd} = \left(\frac{30}{f_{ck}}\right)^{\frac{1}{3}} f_{cd} = 22.2 \text{ MPa} \qquad 3\text{-}5$$

For the CCT node, the bars are partially anchored over the support and the remaining force develops by bond behind the support. The design bond stresses ($f_{bd,p}$) in the support region may be increased due to the favourable effect of transverse pressure and outside support region bond stresses are given by f_{bd}. Furthermore, the contribution of the bends and hooks were considered by dividing the bond strength for straight bars by 0.7. According to MC2010: $f_{bd,p} = 3.94$ MPa for the length over the plate and $f_{bd} = 2.76$ MPa for the outside length, providing the following bond forces.

This document is the intellectual property of the fib – International Federation for Structural Concrete. All rights reserved.
This PDF of fib Bulletin 100 is intended for use and/or distribution solely within fib National Member Groups.

$$F_b^{\varnothing 25} = n_{bars}\pi \varnothing \cdot l_{b1} \cdot f_{bd,p} = 2 \cdot \pi \cdot 25 \cdot 300 \cdot 3.94 \cdot 10^{-3} = 186 \text{ kN}$$
$$F_b^{\varnothing 25} = n_{bars}\pi \varnothing \cdot l_{b2} \cdot f_{bd} = 2 \cdot \pi \cdot 25 \cdot 150 \cdot 2.76 \cdot 10^{-3} = 65 \text{ kN}$$
$$F_b^{\varnothing 20} = n_{bars}\pi \varnothing \cdot l_{b1} \cdot f_{bd,p} = 6 \cdot \pi \cdot 20 \cdot 300 \cdot 3.94 \cdot 10^{-3} = 446 \text{ kN} \qquad 3\text{-}6$$
$$F_b^{\varnothing 20} = n_{bars}\pi \varnothing \cdot l_{b2} \cdot f_{bd} = 6 \cdot \pi \cdot 20 \cdot 150 \cdot 2.76 \cdot 10^{-3} = 156 \text{ kN}$$
$$F_b^{total} = \frac{853}{0.7} = 1'219 \text{ kN} < T_y = 435 \cdot 2'866 \cdot 10^{-3} = 1'246 \text{ kN} > 1'202 \text{ kN}$$

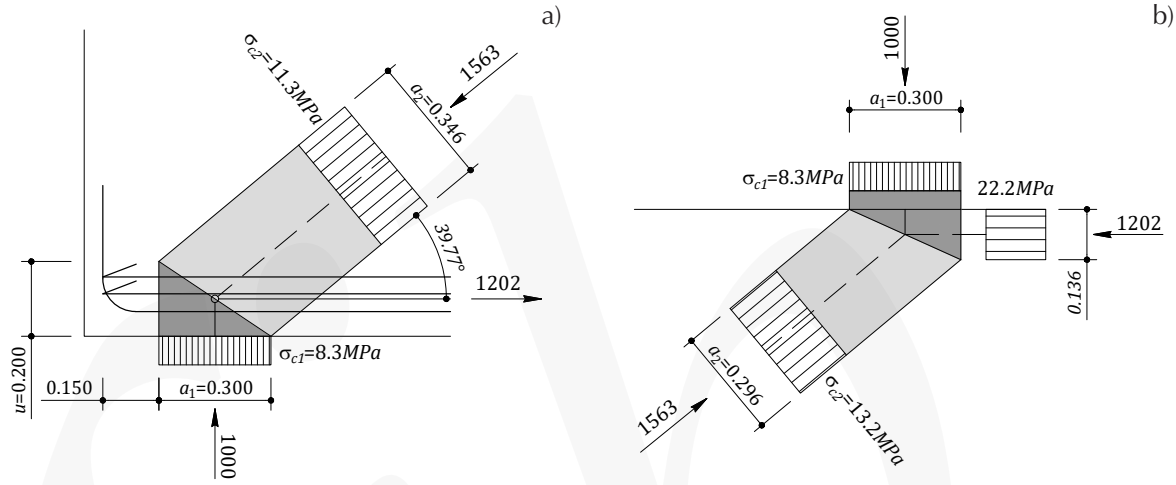


Fig. 3-4 a) CCT node; b) CCC node

Step 4: Full detailing for the beam, following the simple model, of transverse reinforcement and check of the nodal region. Note, that the calculated stirrups must be extended beyond the supports to provide confinement and to equilibrate the out-of-plane tension at node region. In the remaining region shear is zero and minimum shear reinforcement is provided.

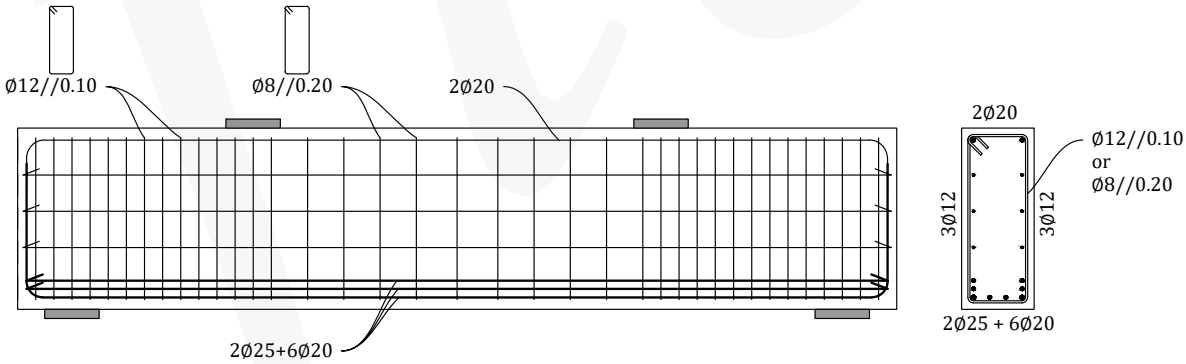


Fig. 3-5 Beam Detailing

3.7.3 Level of Approximation II

Step 1: Define the strut-and-tie model and include the necessary and relevant refinements within the model. In this case, include the required stirrups in the design model (see two possible models in Fig. 3-6a and Fig. 3-6b). Note that in this case, the

This document is the intellectual property of the fib – International Federation for Structural Concrete. All rights reserved.
This PDF of fib Bulletin 100 is intended for use and/or distribution solely within fib National Member Groups.

required force to be anchored at the support is less than in LoA I (920 kN vs 1202 kN). For assessment of existing structures, one can also refine the model considering the horizontal reinforcement (see Fig. 3-6c or Fig. 3-6d), which leads to a further reduction of the bottom tension to be anchored at the support. Following these strut-and-tie models, the force to be anchored at the support is less than in LoA I, leading to a less critical situation than previously. A partial or full stress field model (see Fig. 3-7a or Fig. 3-7b) can be developed and all the necessary checks be performed. The diagonal compression stresses, the width of the distribution of stirrup and nodal widths and stresses, are clearly defined in the design model and all calculations and checks should be developed according to the design model.

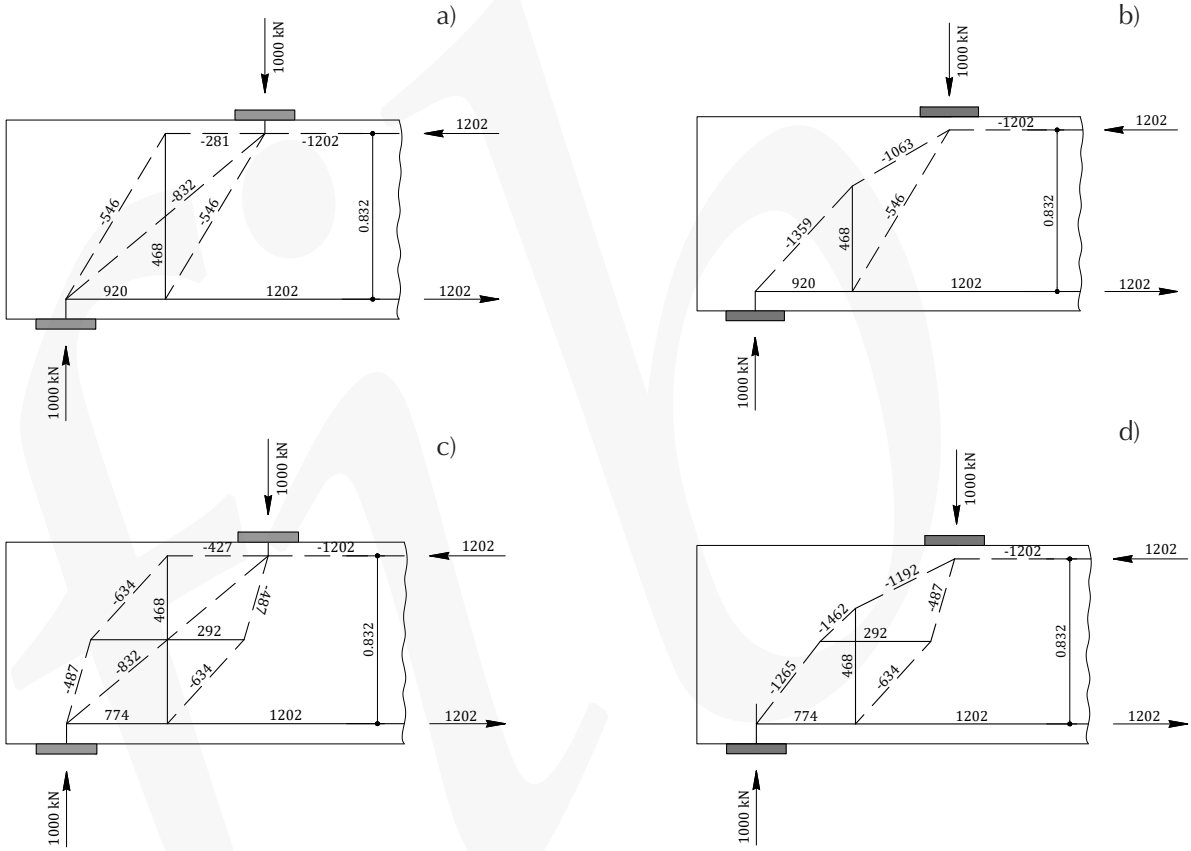


Fig. 3-6 a) Strut-and-tie model including load path carried by stirrups; b) Alternative strut-and-tie model; c) Strut-and-tie model including vertical and horizontal reinforcement; d) Alternative strut-and-tie model

Step 2: Check all compression strength within the model that may be critical (spreading of the strut leading to lower concrete stresses than LoA I). Follow the geometry and forces calculated for the stress field model. Check the bars anchorage length following the same procedure, as in LoA I.

This document is the intellectual property of the fib – International Federation for Structural Concrete. All rights reserved.
This PDF of fib Bulletin 100 is intended for use and/or distribution solely within fib National Member Groups.

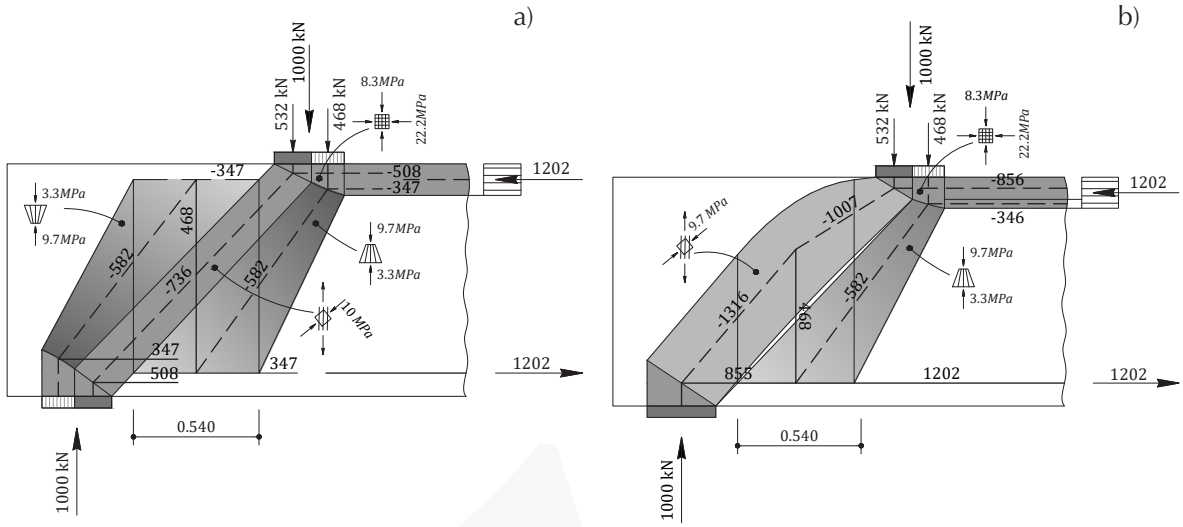


Fig. 3-7 a) Stress field model; b) Alternative stress field model

Diagonal strut stresses:

$$f_w = 468/0.54 = 867 \text{ kN/m} \Rightarrow \left(A_s/s\right)_{req} = 1'992 \text{ mm}^2/\text{m} \Rightarrow \text{Stirrups } \varnothing 12//0.10;$$
$$\left(A_s/s\right)_{prov} = 2'262 \text{ mm}^2/\text{m} \qquad 3\text{-}7$$

$$F_b^{total} = \frac{853}{0.7} = 1'219 \text{ kN} < Ty = 435 \cdot 2'866 \cdot 10^{-3} = 1'246 > 855 \text{ kM} \qquad 3\text{-}8$$

$$\sigma_c = 10 \text{ MPa} < \sigma_{c,Rd} = 0.55\left(\frac{30}{f_{ck}}\right)^{\frac{1}{3}} f_{cd} = 12.2 \text{ MPa} \qquad 3\text{-}9$$

$$\text{CCC node: } \sigma_c = 22.2 \text{ MPa} = \sigma_{c,Rd} = \left(\frac{30}{f_{ck}}\right)^{\frac{1}{3}} f_{cd} = 22.2 \text{ MPa} \qquad 3\text{-}10$$

$$\text{CCT node: } \sigma_c = 9.7 \text{ MPa} < \sigma_{c,Rd} = 0.75\left(\frac{30}{f_{ck}}\right)^{\frac{1}{3}} f_{cd} = 16.6 \text{ MPa} \qquad 3\text{-}11$$

Step 3: Full detailing for the beam following the design model.

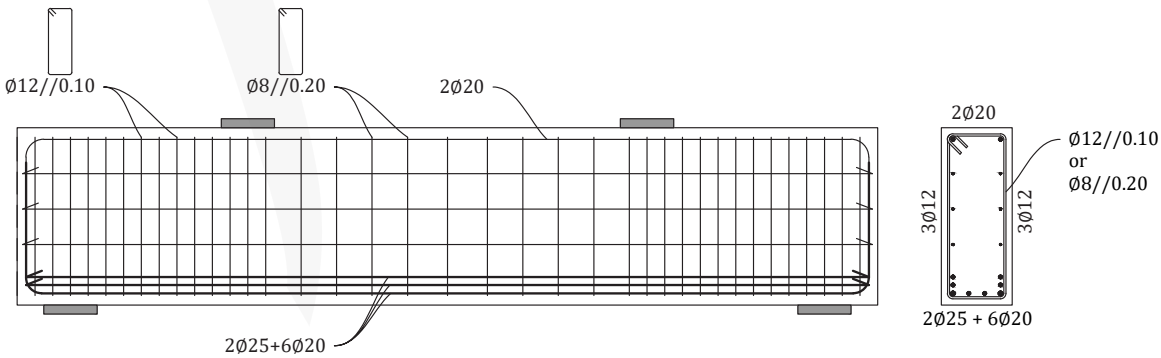


Fig. 3-8 Beam detailing

This document is the intellectual property of the fib – International Federation for Structural Concrete. All rights reserved.
This PDF of fib Bulletin 100 is intended for use and/or distribution solely within fib National Member Groups.

It should be noted that, despite the fact that the reinforcement layout remains the same as LoA I, the understanding of the member and its detailing is more consistent and refined (forces to be anchored over support, load spreading).

3.7.4 Level of Approximation III

Step 1: Apply a lower LoA to provide a first estimate of reinforcement. In this case the reinforcement layout presented in Fig. 3-8 will be analysed.

Step 2: A nonlinear finite element is developed. A simple triangle finite element for the concrete in considered without resistance in tension and a simplified elastic-plastic stress-strain law for compression. The reinforcement is simulated by a 1D element only with axial force and an elastic-plastic strain-stress law for tension and compression, neglecting any tension stiffening.

The output from the analysis is presented in Fig. 3-9a, with the average stress in the stirrups in the clear shear span depicted in Fig. 3-9b.

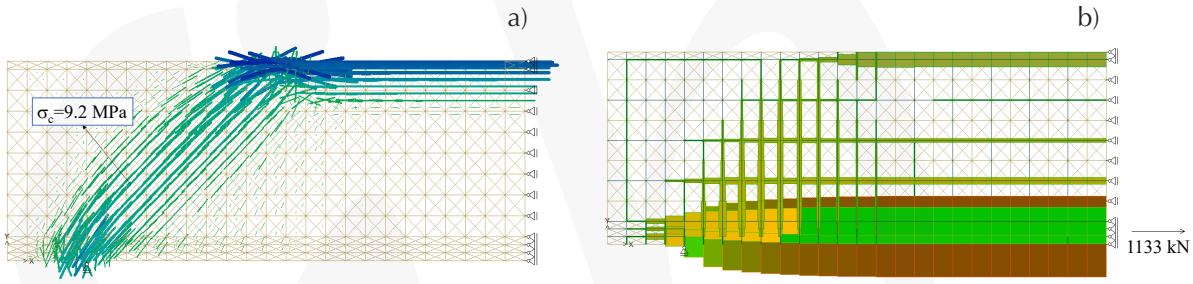


Fig. 3-9 Nonlinear finite element analysis results at ultimate load; a) compression stress fields; b) forces in the reinforcement

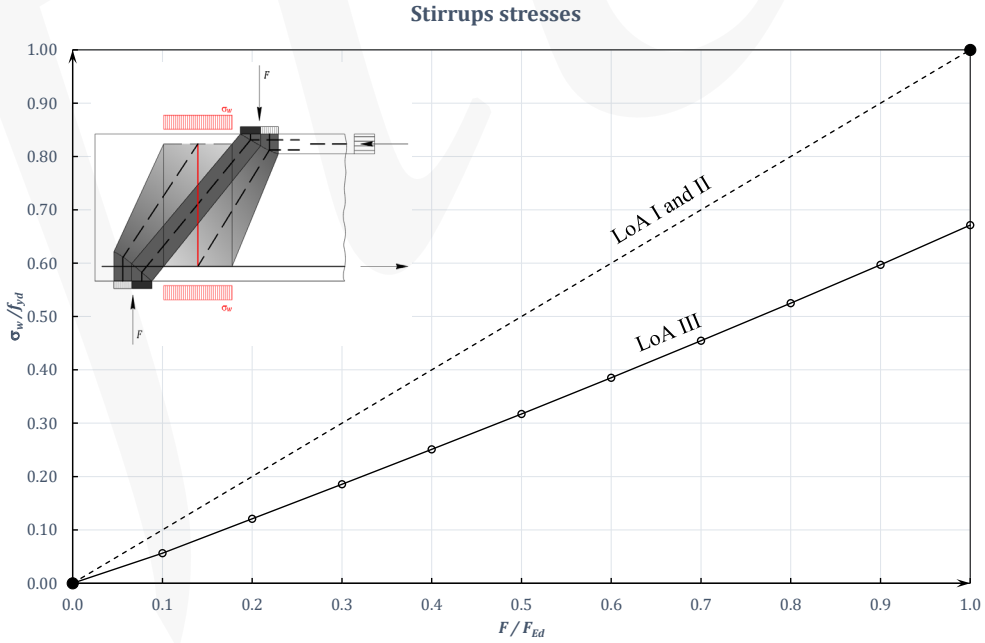


Fig. 3-10 Stresses in stirrups σ_w/f_{yd} vs applied force F under design force F_{Ed}.

This document is the intellectual property of the fib – International Federation for Structural Concrete. All rights reserved.
This PDF of fib Bulletin 100 is intended for use and/or distribution solely within fib National Member Groups.

With the non-linear analysis, it is possible to check the ultimate load and also some ductility aspects. The concrete compression softening due to the presence of transverse tensile strains is also considered to check any premature rupture and steel strains at peak load are lower than the ultimate steel strains. This shows that the semi-empirical Eq. 3-2 is conservative for this case, since in the LoA III analysis the stirrups steel stresses are approximately 300MPa for the design load.

Since no tension stiffening effect is considered it is not possible to draw any conclusion concerning the behaviour at service conditions.

3.7.5 Level of Approximation IV

For LoA IV an appropriate tension stiffening law for the steel was considered. The steel stresses at several load steps are presented in Fig. 3-11, with results for crack widths (w) at different locations and load steps presented in Fig. 3-12.

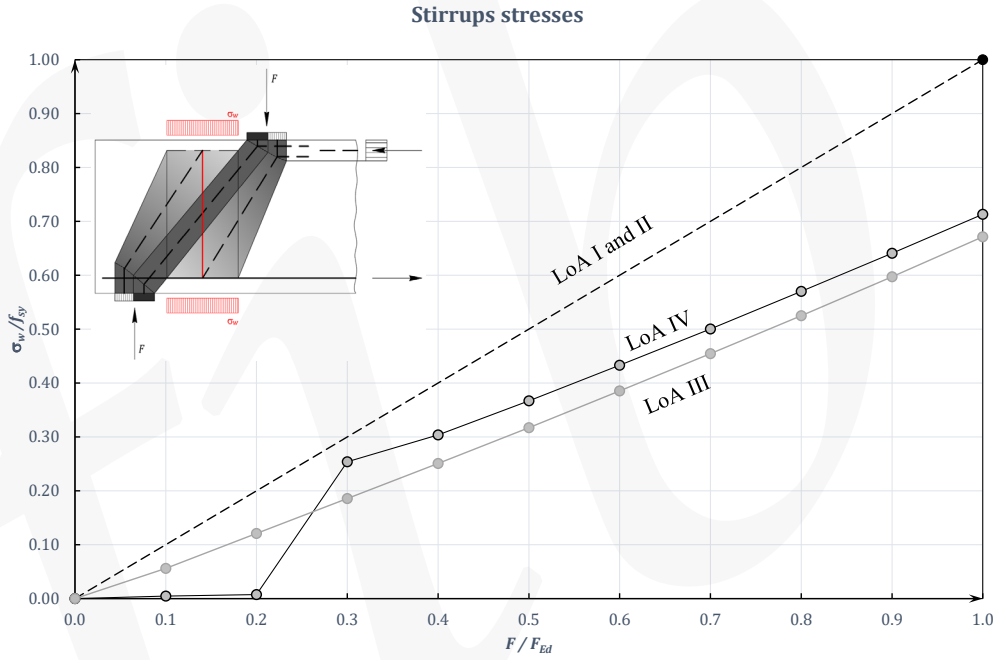


Fig. 3-11 Stresses in stirrups σ_w/f_{yd} vs applied force F under design force F_{Ed}.

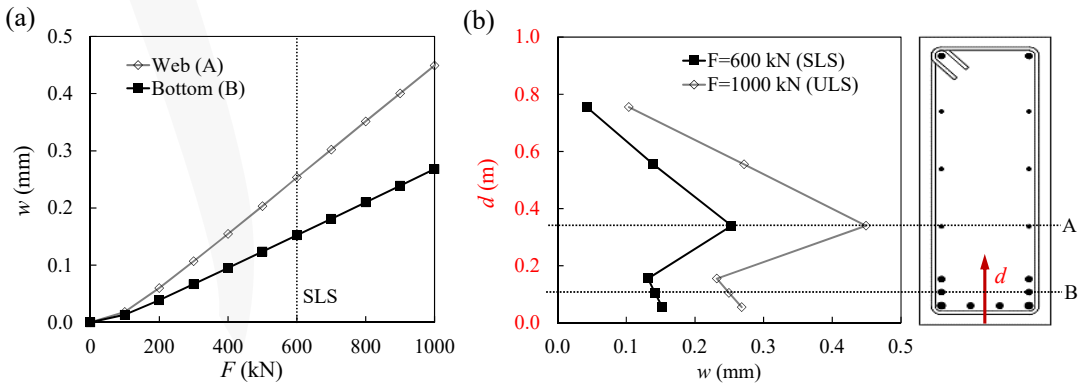


Fig. 3-12 Results of crack widths for LoA IV: (a) evolution for several load steps and two locations; (b) variation through the web for two load steps.

This document is the intellectual property of the fib – International Federation for Structural Concrete. All rights reserved.
This PDF of fib Bulletin 100 is intended for use and/or distribution solely within fib National Member Groups.

With this analysis, it is possible to check the resistance and the serviceability behaviour as well as ductility. Concerning serviceability behaviour, the crack widths at the bottom of the beam at service loads (from F=500 kN to 700 kN) are around 0.15 mm. However, wider crack widths are obtained in the web (see Fig. 3-12b). This is due to the high dependency of the crack spacing on the local amount of reinforcement. While the strains are larger in bottom reinforcement than in web reinforcement, the predicted crack spacing is much larger in the web than at the bottom, resulting in a larger crack width in the web. The maximum crack widths in the web at service loads (from F=500 kN to 700 kN) are acceptable, ranging from 0.20 to 0.30 mm. This direct verification of crack widths is more reliable than the indirect estimations based on the stresses shown for lower levels of approximations. Concerning the ultimate resistance, the concrete compression stresses are always lower than its effective strength, which depends on transverse tension strains induced by the stirrups. Failure is eventually due to bending, i.e. by yielding of the bottom reinforcement and crushing of the compression zone. Stirrup stresses at ultimate load were about 300 MPa, which leads to the conclusion that stirrups are not critical in this case. Note that in LoA I and II the stirrups were obtained by a semi-empirical equation (which is slightly conservative) and the steel area was designed to yield at ultimate load.

3.7.6 Final considerations

Concerning the simple example presented some comments should be mentioned:

- LoA I is the safest and least time-consuming approach. The design model showed that the diagonal compression stresses and the anchorage length at the support are the critical issues. For the LoA II these topics were showed to be less critical.
- In LoA I the width in which the stirrups are distributed must follow the rules for this basic model. In the LoA II, the width may be obtained directly from the stress field model.
- The model refinement, developed for LoA II, provides valuable information, namely that the bottom tie force in the support is lower than in the LoA I. On the other hand, it also allowed the explicit calculation and check of the main compression stresses.
- The check of the CCT and CCC nodes is based in the simplified model (LoA I). In fact, the model considered in LoA II clearly showed that compression stresses in nodal region and the anchorage length are not as critical as determined in LoA I.
- Since LoA II is a redundant strut-and-tie model and compatibility is not explicitly computed in equilibrium models (such as LoA I and II), the stirrups force must be calculated following specific rules presented in technical bibliography. In the LoA III or higher, compatibility is explicitly considered and thus the force in the stirrups is obtained directly from the analysis.
- In LoA III, the obtained compression stresses and stirrup stresses at ultimate load are lower than the lowest LoA. No valuable information for service loads is provided in this level, so service behaviour must be checked indirectly as at the lowest levels.
- In the LoA IV, the most complex and, eventually, time-consuming analysis, is able to provide an explicit check of serviceability behaviour, as well as of deformation capacity.

This document is the intellectual property of the fib – International Federation for Structural Concrete. All rights reserved.
This PDF of fib Bulletin 100 is intended for use and/or distribution solely within fib National Member Groups.

4. Equilibrium-based models

4.1 Introduction

The main scope of this chapter is to provide further guidance for the development of suitable strut-and-tie and stress field models following the previously referred Level-of-Approximation approach, particularly for the application of the LoA I and II. The objective is not to repeat all the already known rules and principles to develop a STM/SFM (such as load path method, model follows elastic trajectories, minimum and maximum angles between struts and ties, etc.) thoroughly described in several technical documents and papers, but to provide understanding for the selection and validation of a chosen design model and, simultaneously, to provide adequate and safe rules for "hand modelling".

In fact, frequently, when using STM/SFM for the design, different engineers may propose different models for the same situation which, sometimes, may lead to quite different reinforcement requirements. This aspect can lead to doubts concerning the suitability of the chosen model, namely ductility and service behaviour.

Several authors[4-1], [4-2] proposed that, in general, adequate service and ductility behaviour are indirectly accounted for if the strut-and-tie model follows the stress trajectories of a linear elastic analysis. Other technical documentation, such as FIP Recommendations[4-3] and EN1992-1-1[4-4], refer to similar procedures, stating: "Possible means for developing suitable strut-and-tie models include the adoption of stress trajectories and distributions from linear-elastic theory or the load path method" and "Verifications in SLS may also be carried out using strut-and-tie models, e.g. verification of steel stresses and crack width control, if approximate compatibility for strut-and-tie models is ensured (in particular the position and direction of important struts should be oriented according to linear elasticity theory)". As pointed out in the *fib* Bulletin 61 *Design examples for strut-and-tie models*[4-5], following this principle, limited ductility is needed, as the redistribution of the inner force flow from the uncracked state to the ultimate load level will be small.

This simple and practical rule has several advantages and may be applied in many situations, especially for regions where little or no experimental evidence is found and no specific rules are provided. It should be considered as a first approach for the development of a suitable design model. The drawback is that it requires a linear elastic analysis in advance with an adequate processing of the output, often with informed decisions to clearly define the compression and tension resultants of the model, since the common reinforcement layout does not match elastic stress trajectories.

Taking as example the beam shown in Fig. 4-1, it is not easy, even for a simple region, to derive an adequate reinforcement layout following the elastic trajectories. It is also not straightforward to reach the stress field model by the interpretation of the main elastic stress trajectories.

https://doi.org/10.35789/fib.BULL.0100.Ch04

This document is the intellectual property of the fib – International Federation for Structural Concrete. All rights reserved.
This PDF of fib Bulletin 100 is intended for use and/or distribution solely within fib National Member Groups.

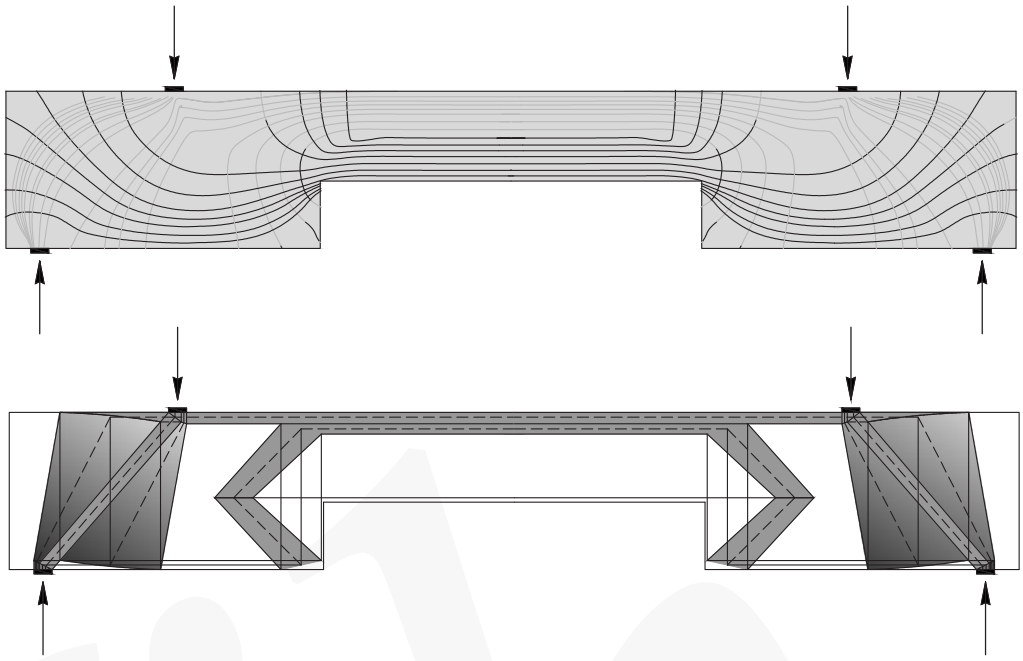


Fig. 4-1 Elastic stress trajectories and stress field model of a dapped beam

These aspects may lead to misunderstanding and potential distrust in using the STM/SFM which, however, should be seen as a pedagogic doubt and a tool for the designer to develop a better insight of the structural behaviour of the region and thus provide an improved design.

It should also be noted that in most cases the STM/SFM may be freely developed, following just some simple and practical rules that are presented in the literature. In fact, concerning ductility aspects for ultimate loads, the assumption that the structure can adapt itself to the chosen design model has been proven by several studies in different discontinuity regions. The deformation capacity of the materials after yielding allows significant stress redistributions leading to a successive formation of new static systems. For this, strut-and-tie models should, in general, be used together with a well distributed minimum reinforcement where no main reinforcement is required, preventing unexpected brittle failures and ensuring that the design load can be reached (special attention should be given to regions where a compression stress field crosses important transversal tensile strains leading to a significant reduction of the effective compression strength of concrete). Concerning service behaviour, the minimum reinforcement must also be adequate to equilibrate a significant proportion of concrete tensile strength after cracking.

Despite the aforementioned aspects regarding the application of STM/SFM for the design of a structural concrete region, there are two main topics that must be clearly addressed: ductility (deformation capacity) and service behaviour. The strut-and-tie method complies with the theory of plasticity and does not explicitly check ductility, namely compression strength softening or excessive reinforcement strains, that may lead to a premature rupture, or serviceability, namely steel stresses and crack widths for service loads.

Following the LoA concept, the highest level may provide valuable output for assessing ductility and serviceability, since the non-linear analysis will provide an adequate prediction of the behaviour at service and ultimate load level. The main objective is, for common basic models that are considered to be representative of most practical situations, to use higher level analysis to establish guidance for the lower level modelling.

This document is the intellectual property of the fib – International Federation for Structural Concrete. All rights reserved.
This PDF of fib Bulletin 100 is intended for use and/or distribution solely within fib National Member Groups.

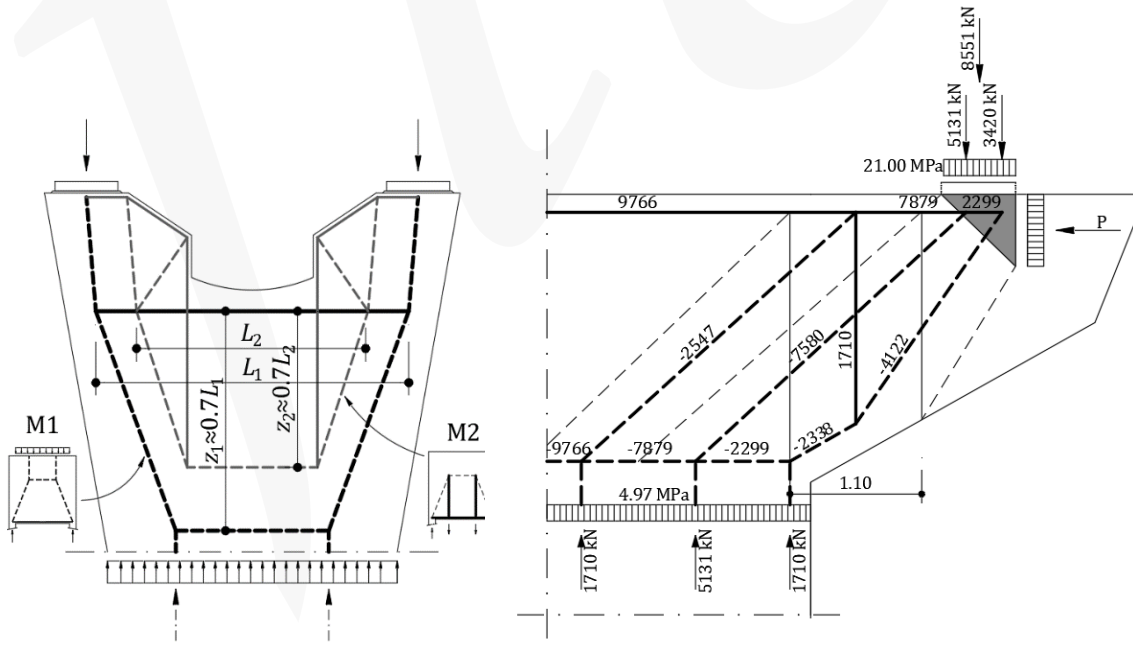
4.2 Complex strut-and-tie models as a combination of simple models

In practice, it is very common to develop tailored STM / SFM for certain regions as a combination of two or more simple (basic) models. This approach is convenient as it takes advantage of the experience of the designer in the use of basic models but allows applying them, by combination, to solve complex cases. Some practical strut-and-tie models for design of complex discontinuity regions are presented in this section. The examples will show how these models can be split into simpler models whose detailed analysis will be presented in the next section.

As a first case, Fig. 4-2a shows the global design model for vertical loads of a column from a viaduct (further details for this case will be given in the chapter of practical examples of this Bulletin). The vertical load at the top of the column represents the vertical load from the deck. The load path defined by the model M1 is identical to that of a common deep beam model and it is easy to observe the similarity also of model M2 for a deep beam with suspended loads.

Another example is shown in Fig. 4-2b for the design model for a corbel of a pier from another viaduct. It represents a case where the load is carried by a combination of actions: a fraction of the load is carried by a direct strut to the support while the rest is carried by indirect support (requiring the presence of stirrups). Also, due to the inclined bottom face of the corbel, a fraction of the vertical load is carried by the bottom compression chord, leading to a reduction of the resultant force in stirrups.

A more complex case is represented by the abutment shear wall shown in Fig. 4-3. The dead load from the viaduct is transferred by pot bearings and the inertial deck forces, due to seismic action, are transferred through damping devices located on the top of the shear wall. Fig. 4-3a) shows the model when the damping device is pushing against the abutment, requiring to modify the strut-and-tie model for a dapped-end beam.



a) *b)*

Fig. 4-2 Strut-and-tie models for the design of discontinuity regions. a) Pile of a viaduct; b) Corbel

This document is the intellectual property of the fib – International Federation for Structural Concrete. All rights reserved.
This PDF of fib Bulletin 100 is intended for use and/or distribution solely within fib National Member Groups.

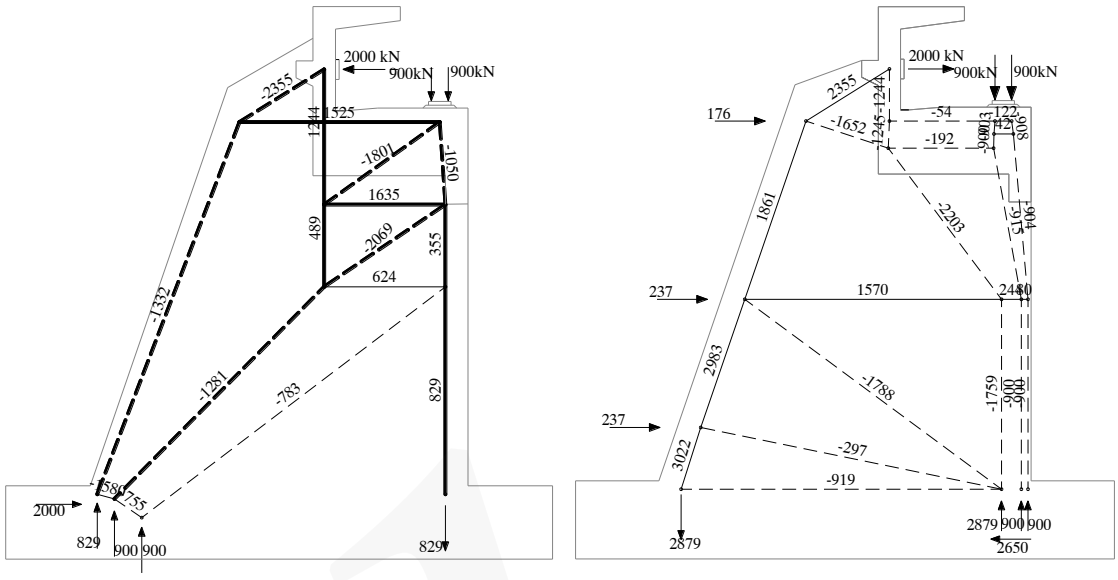


Fig. 4-3 Strut-and-tie model for a fixed abutment of a viaduct. a) seismic action "pushing" the abutment; b) seismic action "pulling" the abutment

Even in rather complex models such as the deep beam of a building shown in Fig. 4-4, it is possible to account for similarities with continuous deep beam models. It can be noted that that it is useful in these cases to develop a realistic load path and, usually, the vertical reactions in the columns are influenced by the selected strut-and-tie model. The locations of the horizontal ties were set in this case at floor levels in order to obtain a simpler and clearer model.

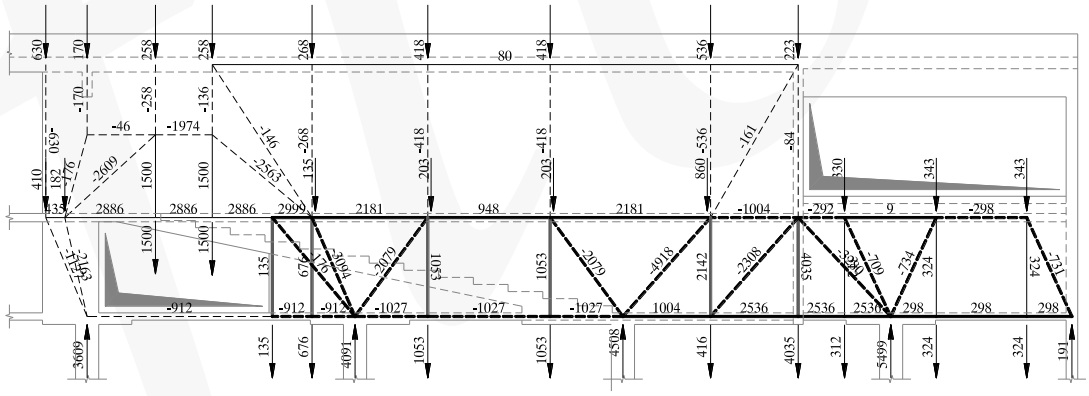


Fig. 4-4 Strut-and-tie model of a deep beam within a building

Following the aforementioned possibilities of combining basic strut-and-tie models to achieve a global design model, the use of adaptive stress field models presented in the following section is also a suitable tool to determine convenient strut-and-tie models for the design of discontinuity regions.

This document is the intellectual property of the fib – International Federation for Structural Concrete. All rights reserved.
This PDF of fib Bulletin 100 is intended for use and/or distribution solely within fib National Member Groups.

4.3 Basic strut-and-tie and stress field models

4.3.1 Introduction

An engineer with some experience in strut-and-tie and stress field modelling, can easily realise that some basic models reoccur in different practical cases and, more importantly, global and complex design models in real situations are usually built up from different basic models.

Studying and assessing these typical basic models will provide guidance for the development of STM. The objective of this chapter is to assess typical basic models, by different possible STM demanding different degrees of stress redistribution and thus different reinforcement layout and checking ultimate load and service behaviour by using a higher-level analysis.

The following basic models are addressed:

- Deep beam with uniform loading
- Deep beam models with uniform suspended loads
- Deep beam / corbels with suspended point loads
- Continuous deep beam models
- Dapped end beam / re-entrant corners
- Spreading of point loads / bottle effect
- Point load near support

4.3.2 Deep beam with uniform loading

The deep beam basic model is a well-known model and some typical stress field models are presented by Muttoni et al.[4-6] in Fig. 4-5. Such models occur in many practical situations e.g. at walls openings (Fig. 4-6a), in prestressed regions (Fig. 4-6b) and in several real design situations (Fig. 4-6c) as shown by Schlaich et al.[4-1].

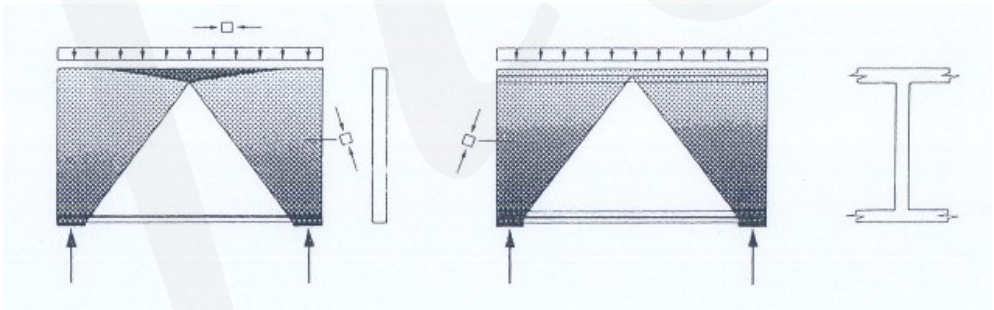


Fig. 4-5 Stress field model for deep beams[4-6]

This document is the intellectual property of the fib – International Federation for Structural Concrete. All rights reserved.
This PDF of fib Bulletin 100 is intended for use and/or distribution solely within fib National Member Groups.

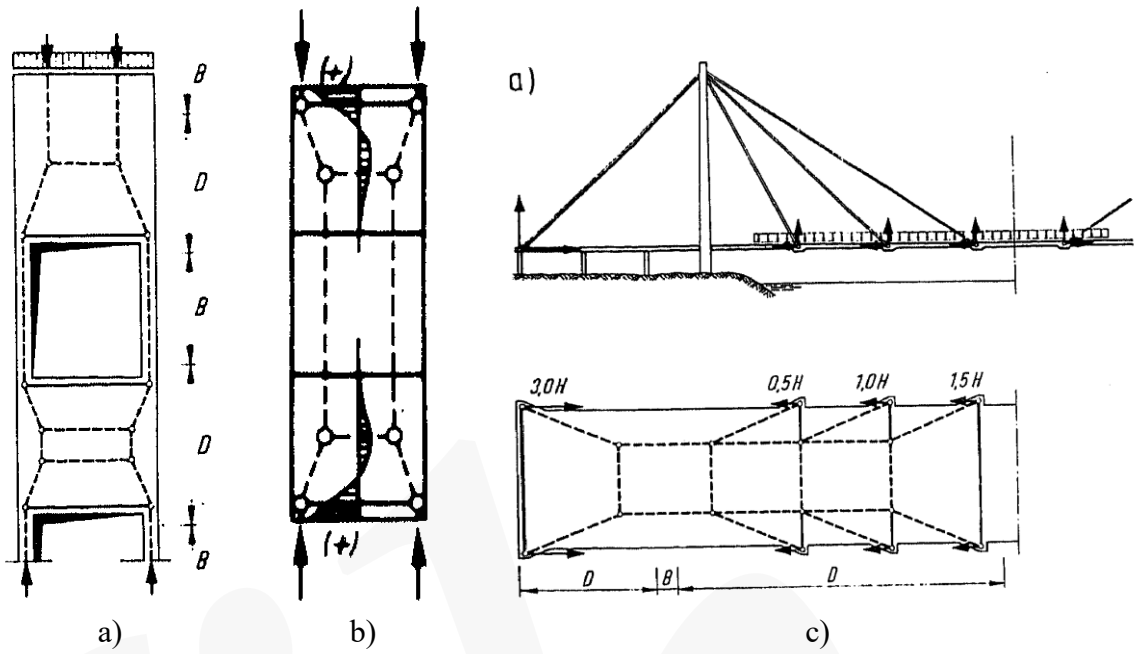


Fig. 4-6 a) Wall with an opening; b) Eccentric prestress; c) Plan STM in a deck of a stay-cable bridge[4-1]

The deep beam models are basically defined by point loads spreading into a distributed load and establishing a very simple strut-and-tie model with smooth deviation of the compression stresses, that leads to a horizontal tension. The reference solution was established long time ago, by Leonhardt and Walther[4-7] and was based on linear elastic analysis and an extensive survey of deep beam tests. The elastic stresses (Fig. 4-7) show a horizontal compression distributed over a large height and tension stresses at the bottom of the deep beam, leading to an inner lever arm z of about 70% of the span L.

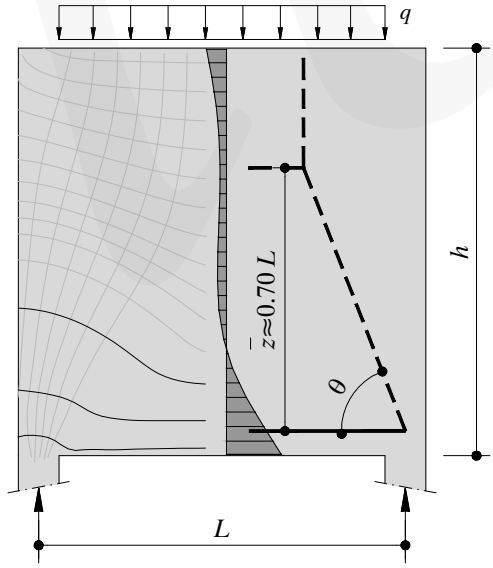


Fig. 4-7 Simply supported deep beam elastic stress trajectories and reference strut-and-tie model

This basic model appears very often in practice and a small variation of angle θ may double or halve the main reinforcement. For this reason, the designer needs to know how close to the reference solution the STM needs to be in order to ensure adequate structural behaviour, at ultimate and service loads.

This document is the intellectual property of the fib – International Federation for Structural Concrete. All rights reserved.
This PDF of fib Bulletin 100 is intended for use and/or distribution solely within fib National Member Groups.

The simple and practical rule stated by Schlaich et al.[4-1], based on energetic principles: "a criterion for optimising a model may be the minimisation of complementary energy of the system, which can be performed in many cases by reducing the number and length of ties", is useful in this case. In fact, increasing the inner lever arm or the angle of the diagonal compression, will always decrease the steel area of the main reinforcement.

Following the aforementioned procedure, several possible design models were developed simulating different alternative stress redistributions (see Fig. 4-8). The Model *R* is the reference model based on the uncracked distribution of stresses. The remaining models foresee larger degrees of stress redistribution which result in smaller reinforcement demands. Based on a design inner lever arm $(z/L)_d$ = 0.92, 1.37 and 1.83, steel areas of 75%, 50% and 37.5% of the reference model with $(z/L)_d$ = 0.69 are obtained. As usual, besides the main reinforcement, the additional minimum web reinforcement of approximately ρ = 0.2% was adopted and the concrete strength was defined in order to avoid concrete crushing at the supports and the ultimate load be governed by steel yielding.

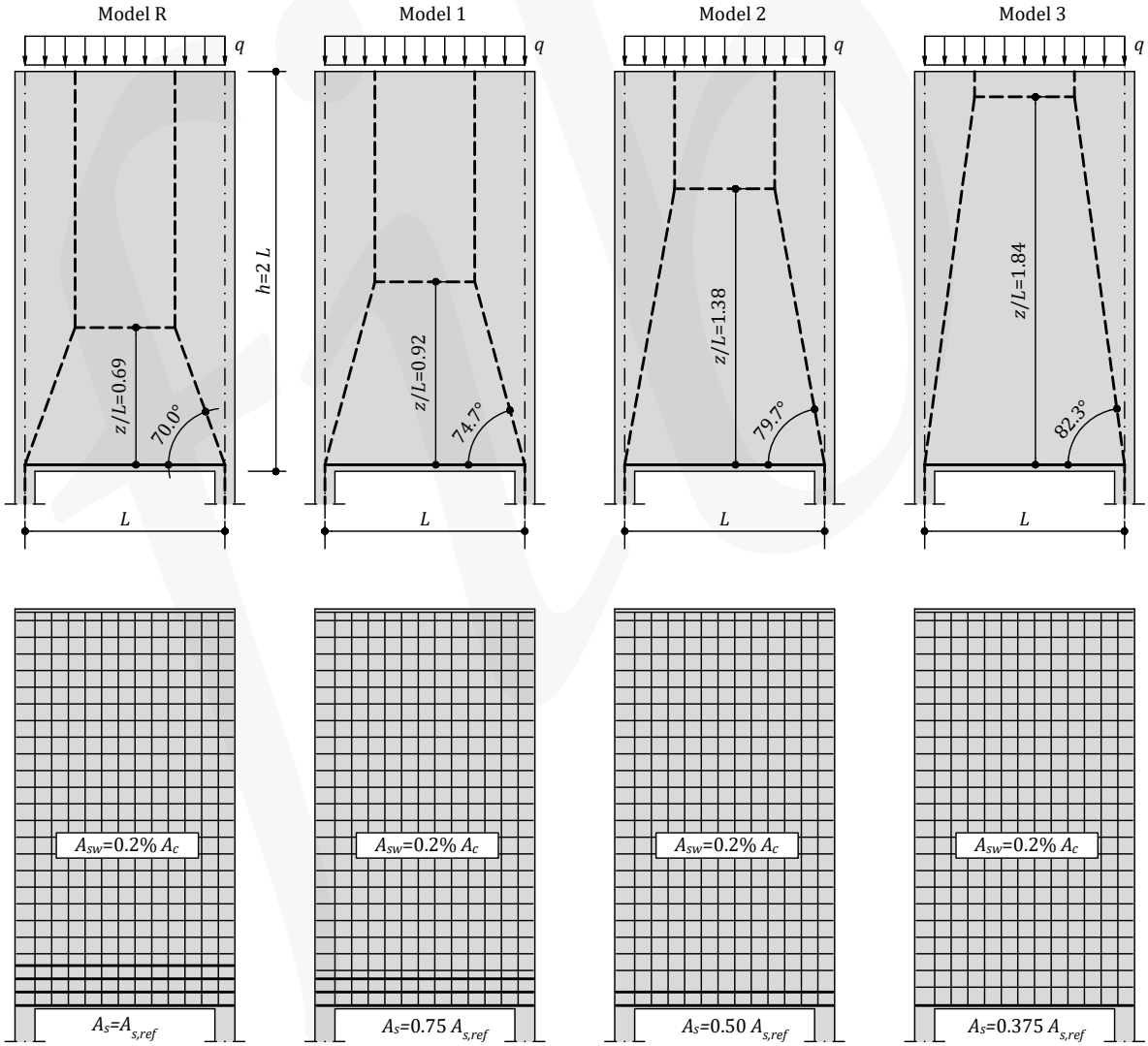


Fig. 4-8 Deep beam with loads on top strut-and-tie model simulating different alternative stress redistribution and corresponding reinforcement layout.

This document is the intellectual property of the fib – International Federation for Structural Concrete. All rights reserved.
This PDF of fib Bulletin 100 is intended for use and/or distribution solely within fib National Member Groups.

Following the different reinforcement layouts obtained by a lower LoA model, several higher LoA analysis were developed for each reinforcement layout to investigate the serviceability response and deformation capacity at ultimate load. Also different reinforcement ratios, for the reference solution, were analysed: reference model with low reinforcement ratio ($A_{s,ref}$ = 2.5 $A_{s,\min}$) and reference model with high reinforcement ratio ($A_{s,ref}$ = 8.0 $A_{s,\min}$).

Knowing that higher steel stresses are related to higher crack widths and that stresses between 200-300 MPa will lead to crack widths between 0.2-0.3 mm, it is possible to conclude that some cases provide poor service behaviour. In fact, implementing 50% of steel area required by the elastic based solution, which represents a variation of 50% of the inner lever arm, and a variation of just 14% of the angle of the diagonal strut, will lead to large crack widths and inappropriate service behaviour, especially for deep beams with low reinforcement ratio (see Fig. 4-9 and Fig. 4-10).

Although the results for the deep beam with higher reinforcement ratios suggest a higher modelling freedom, it is recommended to carry out a more refined analysis when the variation of the inner level arm z produces less than 70% of the reinforcement area. Note that, this practical recommendation is associated with a quite small variation, less than 10%, of the angle of the diagonal strut.

The design load considered for design was reached for all models meaning that the structure had sufficient ductility to reach the ultimate load without any brittle and unexpected rupture.

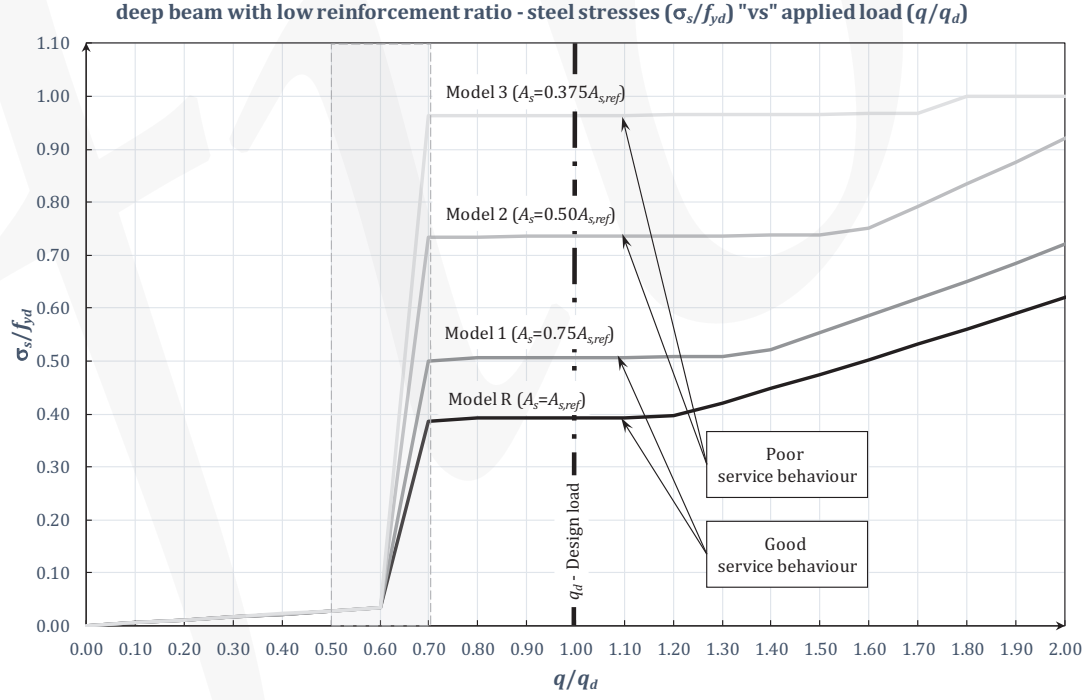


Fig. 4-9 Deep beam with low reinforcement ratio: steel stresses (σ_s/f_{yd}) "vs" applied load (q/q_d)

This document is the intellectual property of the fib – International Federation for Structural Concrete. All rights reserved.
This PDF of fib Bulletin 100 is intended for use and/or distribution solely within fib National Member Groups.

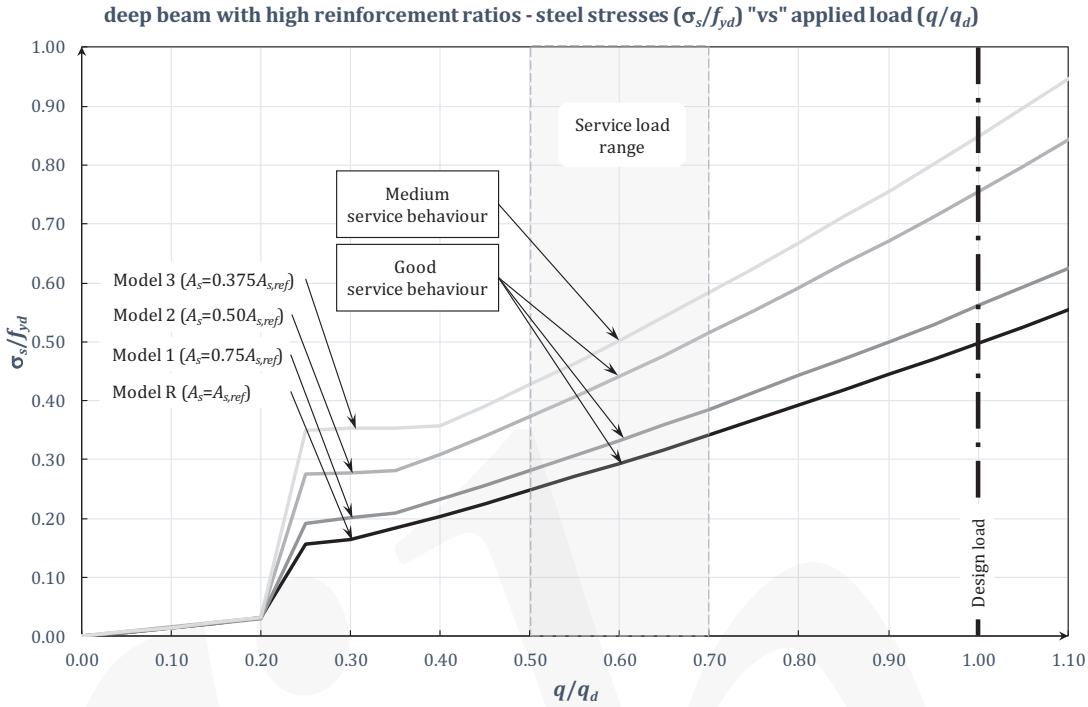


Fig. 4-10 Deep beam with high reinforcement ratio. Steel stresses (σ_s/f_{yd}) "vs" applied load (q/q_d)

4.3.3 Deep Beam with uniform suspended loading

Deep beams with suspended loads is a basic model that occurs in several practical situations, such as deep beam models mentioned before. Fig. 4-11 shows a simple application for a deep beam with an opening.

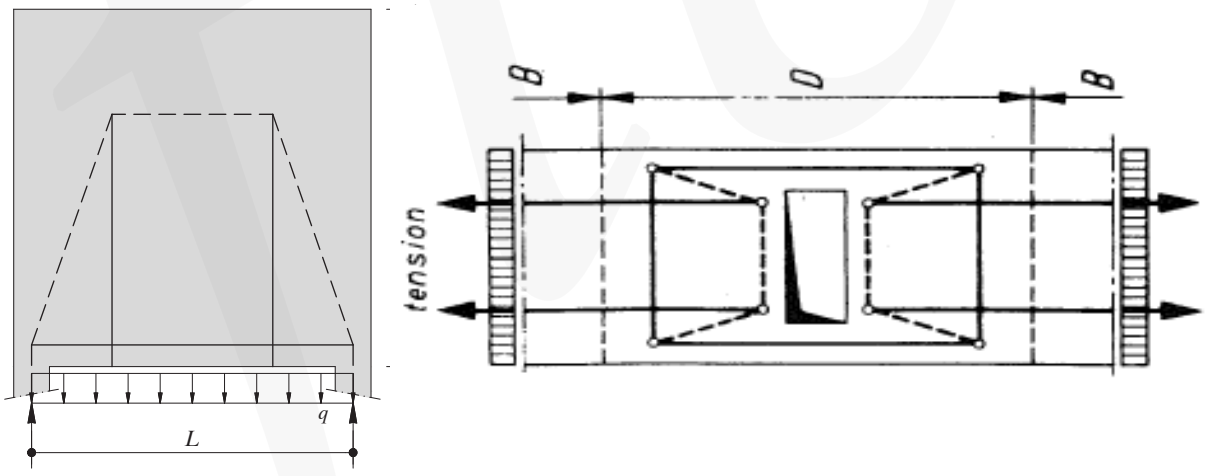


Fig. 4-11 Deep beam with indirect loading a) basic model; b) STM of a wall with opening[4-1]

Similarly to deep beams with loads on top, the main doubt may, as in previous example, be: "what is the suitable inner level arm that provides good service behaviour and resistance for the ultimate load?". For this case the elastic analysis provides an inner level arm of $z = 0.65L$ as shown in Fig. 4-12.

This document is the intellectual property of the fib – International Federation for Structural Concrete. All rights reserved.
This PDF of fib Bulletin 100 is intended for use and/or distribution solely within fib National Member Groups.

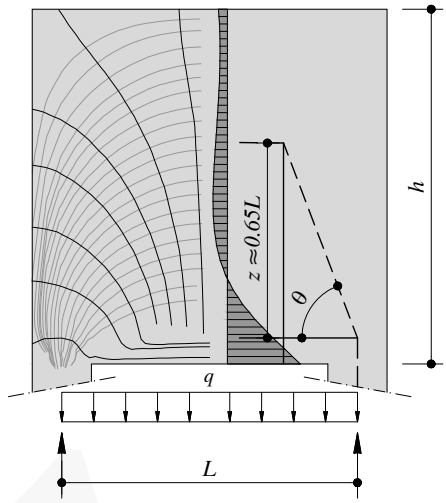


Fig. 4-12 Deep beam with indirect loading, elastic stress trajectories and reference strut and tie model.

As in the previous deep beam example, several design models can be developed simulating different stress redistribution. Model R is the reference model, based on the elastic distribution of stresses. The remaining models assume large stress redistribution and thus quite smaller reinforcement layouts are obtained, 75%, 50% and 37.5% of the reference model (see Fig. 4-13). The additional minimum horizontal web reinforcement of approximately $\rho = 0.2\%$ was adopted.

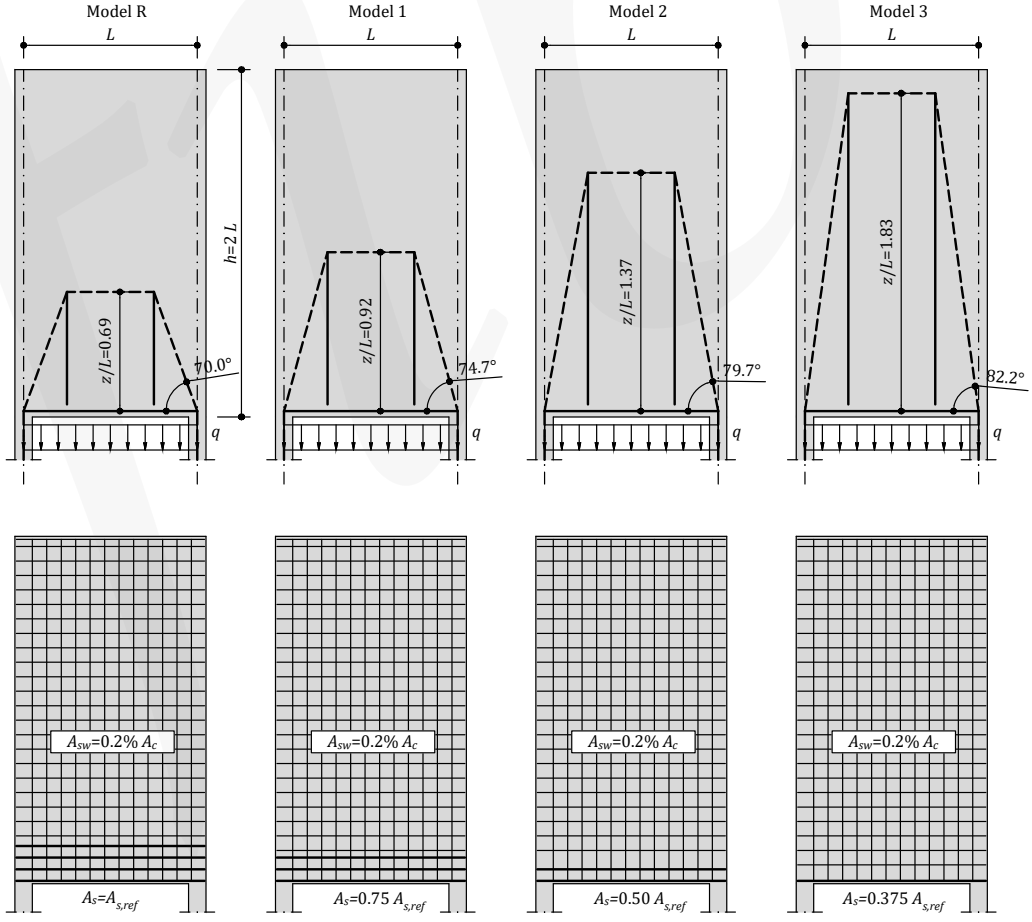


Fig. 4-13 Deep beam with indirect loading strut-and-tie model simulating different alternative stress redistribution and corresponding reinforcement layout.

This document is the intellectual property of the fib – International Federation for Structural Concrete. All rights reserved.
This PDF of fib Bulletin 100 is intended for use and/or distribution solely within fib National Member Groups.

Following the reinforcement layouts, as obtained on the basis of the different design models, a higher LoA analysis was developed, for each case and for different reinforcement ratios in the bottom tie and service behaviour was specifically checked by evaluating steel stresses on the main tie (see Fig. 4-14 and Fig. 4-15).

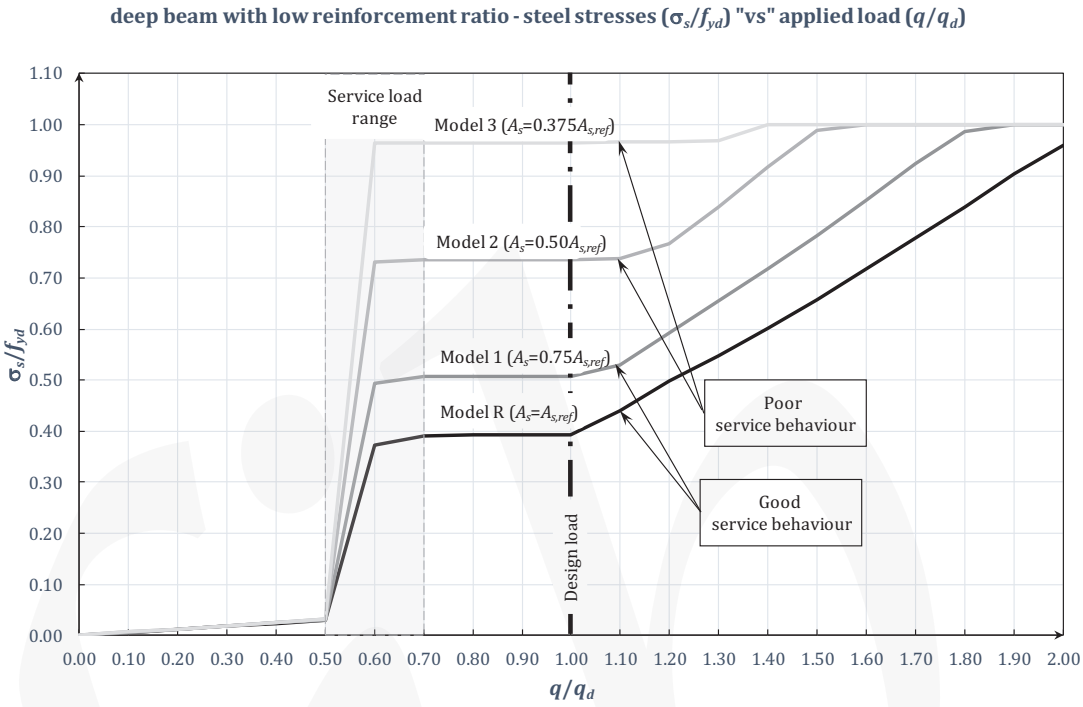


Fig. 4-14 Deep beam with low reinforcement ratio. Steel stresses (σ_s/f_{yd}) "vs" applied load (q/q_d)

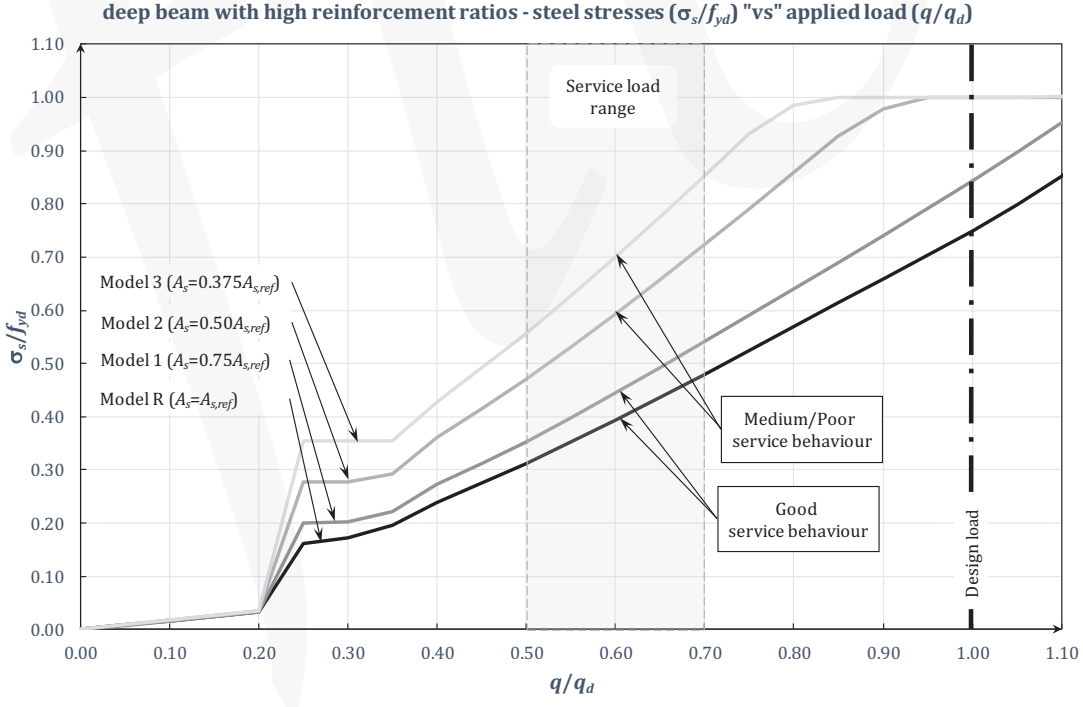


Fig. 4-15 Deep beam with high reinforcement ratio. Steel stresses (σ_s/f_{yd}) "vs" applied load (q/q_d)

This document is the intellectual property of the fib – International Federation for Structural Concrete. All rights reserved.
This PDF of fib Bulletin 100 is intended for use and/or distribution solely within fib National Member Groups.

According to the results presented, inadequate service behaviour may occur for steel quantity less than 50% of the reference, thus leading to the conclusion that it is prudent to avoid large stress redistribution and that a higher LoA analysis case is developed, if similar or larger redistributions are imposed in the design model.

4.3.4 Deep beam / corbels with suspended point loads

A deep beam or corbel with suspended point loads is also very common and may occur in parts of global and more complex models. Fig. 4-16 shows a simple example of the application of this basic model.

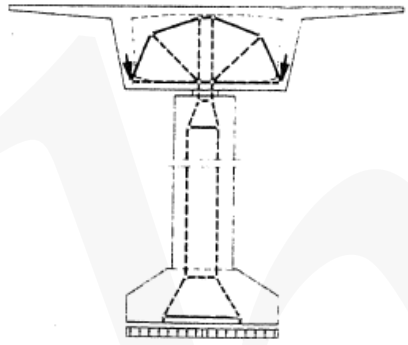


Fig. 4-16 Deep beam with suspended point loading basic model in a bridge deck[4-1]

The elastic stress trajectories are not as clear as desired, since they provide a curved tension path which is not in line with a practical reinforcement layout (Fig. 4-17a) and Fig. 4-17b). To define buildable solutions, the designer must be ingenious and provide a proper reinforcement layout that assures, at least, safety for the ultimate limit state. However, some questions may arise: Is the force suspended by vertical stirrups, inclined reinforcement or by a combination of both (Fig. 4-17c)? What is the amount of load to be transferred by each load path, that provides good service behaviour?

The elastic solution may suggest that half of the load should be carried by each load path and thus the reference model is based on that principle. Model 1 and Model 2 assume significant redistributions and steel stresses at service loads were evaluated (Fig. 4-18).

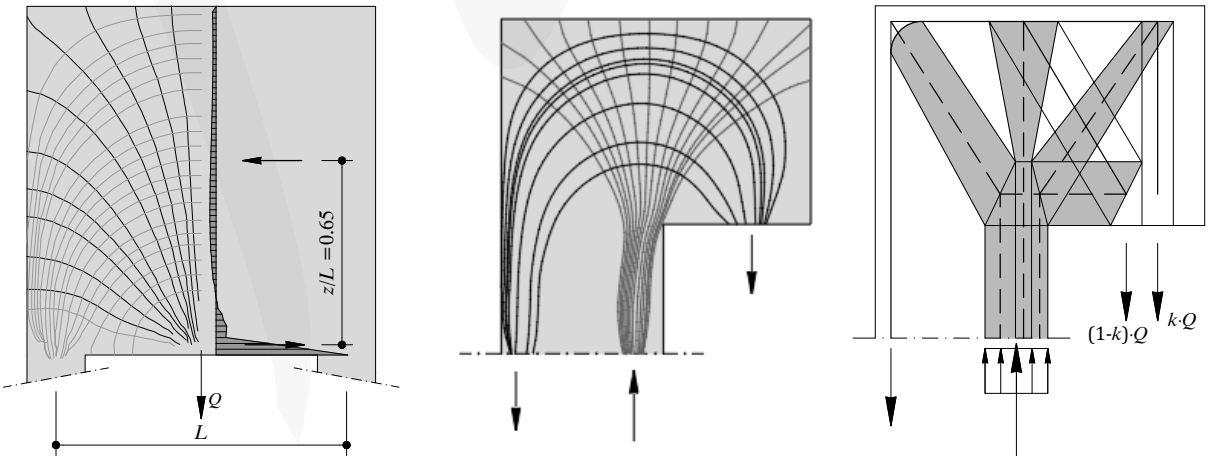


Fig. 4-17 a) Deep beam with suspended point loading elastic stress trajectories; b) Similarity with the elastic stress trajectories of a corbel with suspended point loading; c) Stress field model considering vertical and inclined reinforcement leading to different load paths.

This document is the intellectual property of the fib – International Federation for Structural Concrete. All rights reserved.
This PDF of fib Bulletin 100 is intended for use and/or distribution solely within fib National Member Groups.

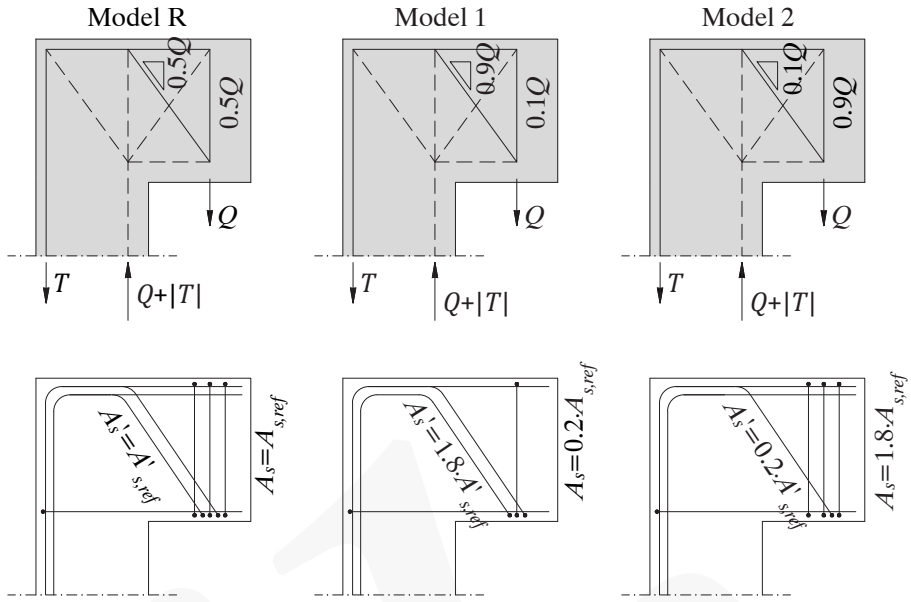


Fig. 4-18 Deep beam with suspended point loading strut-and-tie model simulating different alternative stress redistribution and corresponding reinforcement layout.

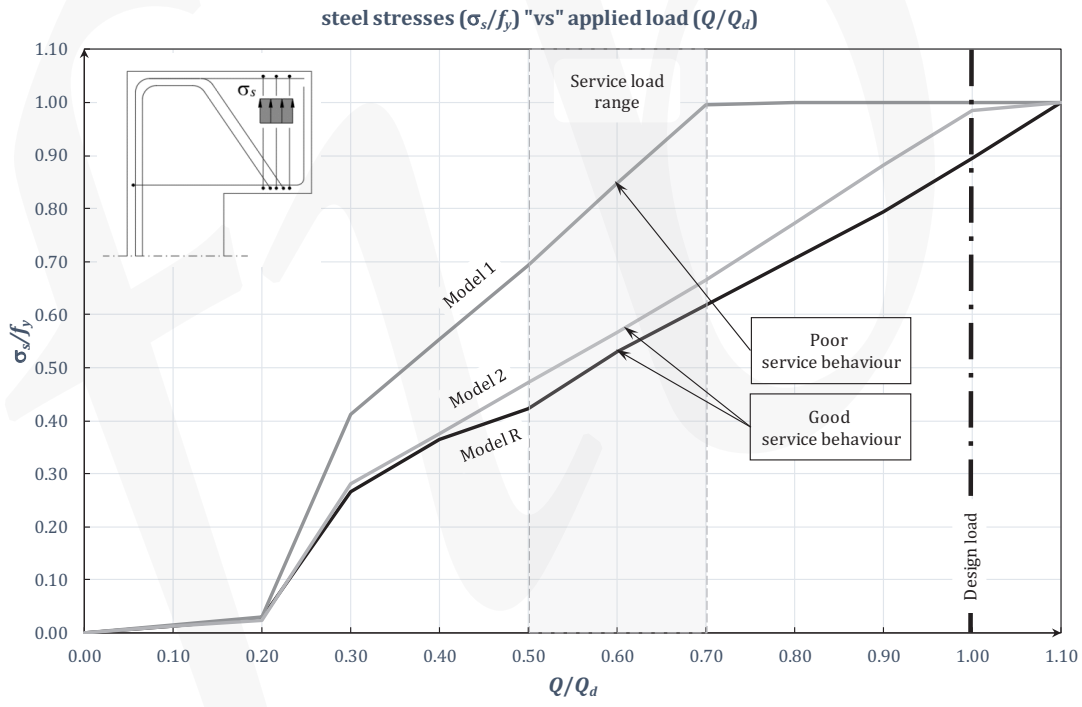


Fig. 4-19 Deep beam with suspended point loading: steel stresses at vertical reinforcement (σ_s/f_{yd}) "vs" applied load (q/q_d)

This document is the intellectual property of the fib – International Federation for Structural Concrete. All rights reserved.
This PDF of fib Bulletin 100 is intended for use and/or distribution solely within fib National Member Groups.

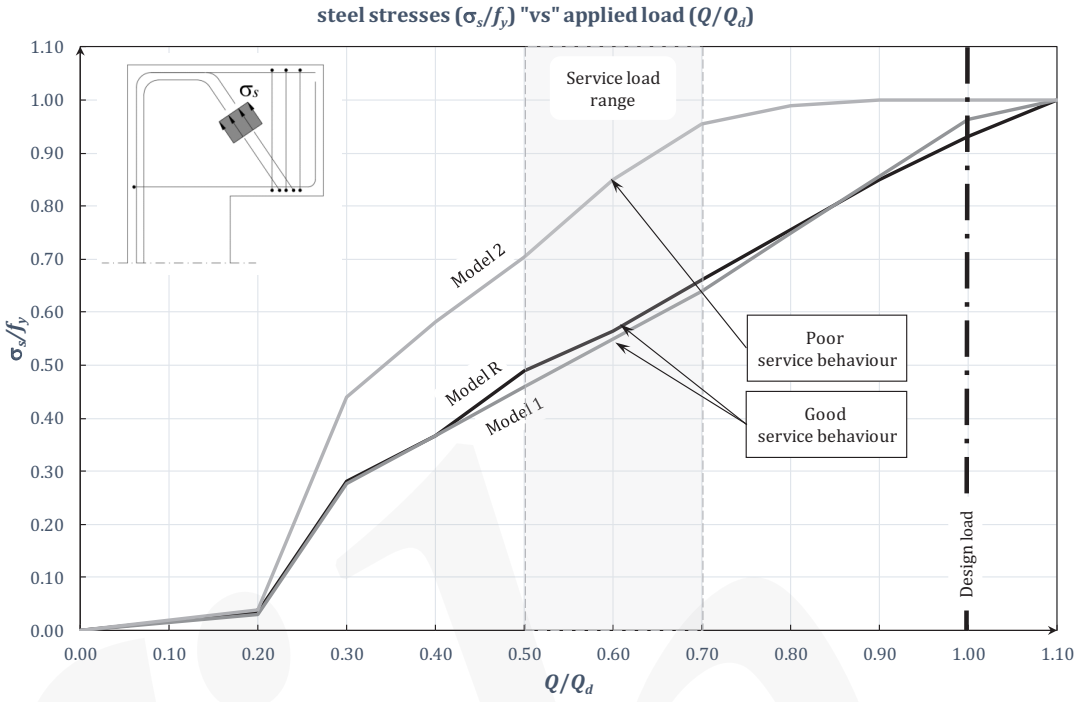


Fig. 4-20 Deep beam with suspended point loading. Steel stresses at inclined reinforcement (σ_s/f_{yd}) "vs" applied load (q/q_d)

It is easy to observe in Fig. 4-19 and Fig. 4-20 that any other redistribution within the range $0.1Q/0.9Q$ to $0.9Q/0.1Q$ will provide intermediate steel stresses that may be obtained by linear interpolation. Following this, the results show that redistribution values of $0.3Q/0.7Q$ to $0.7Q/0.3Q$ do not influence service behaviour and may be the base for the application of the equilibrium models of the lowest LoA.

4.3.5 Continuous Deep Beam models

Continuous deep beams basic models, as illustrated by the stress field in Fig. 4-21c), also occurs in several practical situations as shown in Fig. 4-21a) and Fig. 4-21b).

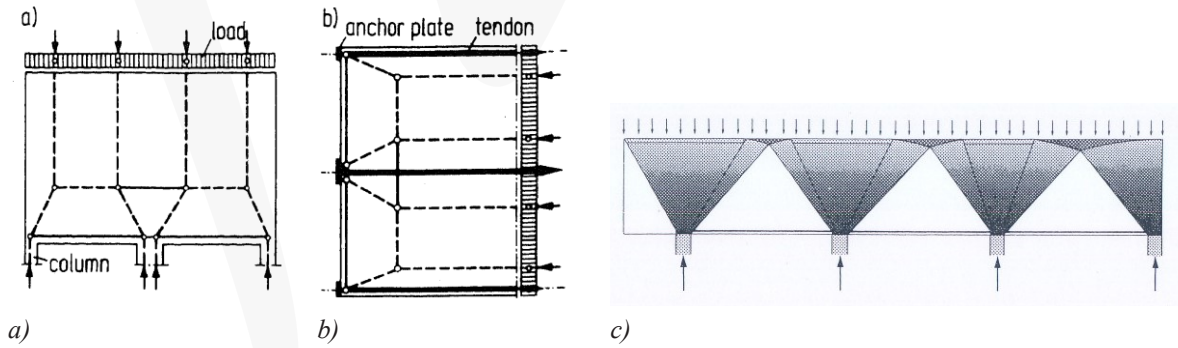


Fig. 4-21 a) Continuous deep beam basic model (Schlaich et al. 1987); b) Continuous deep beam basic model for prestressed anchorage[4-1]; c) Continuous deep beam stress field model[4-6]

The elastic stress trajectories are shown in Fig. 4-22 and suggest an inner level arm of $z = 0.35L$ at the inner support and $z = 0.7L$ at midspan. The elastic reactions are $1.2q{\cdot}L$ for the intermediate support and $0.4q{\cdot}L$ for the outer supports. With this information it is

This document is the intellectual property of the fib – International Federation for Structural Concrete. All rights reserved.
This PDF of fib Bulletin 100 is intended for use and/or distribution solely within fib National Member Groups.

possible to solve the strut-and-tie model, leading to a tension force of $0.2q{\cdot}l$ for the tie over the intermediate support and $0.12q{\cdot}L$ for the bottom midspan tension.

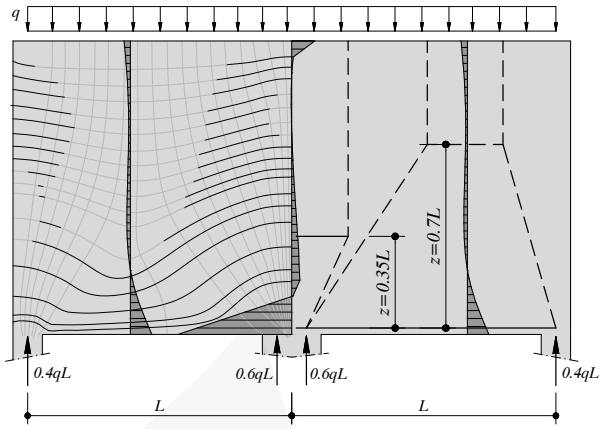
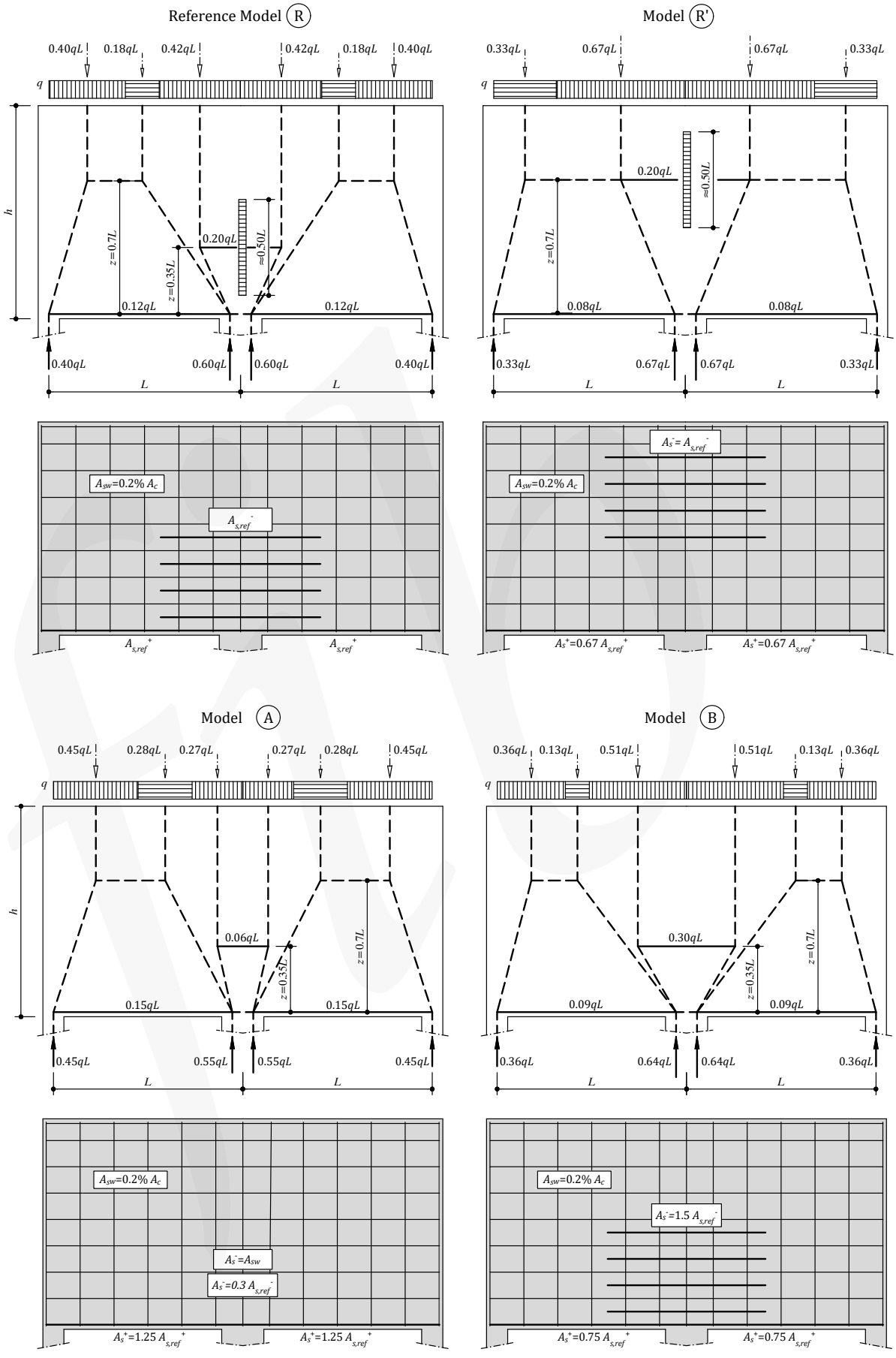


Fig. 4-22 Continuous deep beam elastic stress trajectories and reference strut-and-tie model.

Following the elastic-based strut-and-tie model several different design models are tested in order to simulate different stress redistributions (Fig. 4-23):

- Model R is the reference model, based in the theory of elasticity
- Model R' is a solution where support tension is placed at the same level as the adjacent compression at $z = 0.7L$. The calculation simplicity of this strut-and-tie model makes it particularly useful for design purposes.
- Models A and B were based on the same inner level arm as the elastic solution. The support steel reinforcement areas were set to approximately 30% and 150% of the reference solution, respectively.
- For Model 1 and 2, continuous deep beam full effective height is just as a continuous slender beam. Model 1 was established to provide some reinforcement over the support and near to concrete top boundary and Model 2 assumed the continuous deep beam behaviour as two independent simply supported deep beams and no reinforcement is required for the support region.

This document is the intellectual property of the fib – International Federation for Structural Concrete. All rights reserved.
This PDF of fib Bulletin 100 is intended for use and/or distribution solely within fib National Member Groups.



This document is the intellectual property of the fib – International Federation for Structural Concrete. All rights reserved.
This PDF of fib Bulletin 100 is intended for use and/or distribution solely within fib National Member Groups.

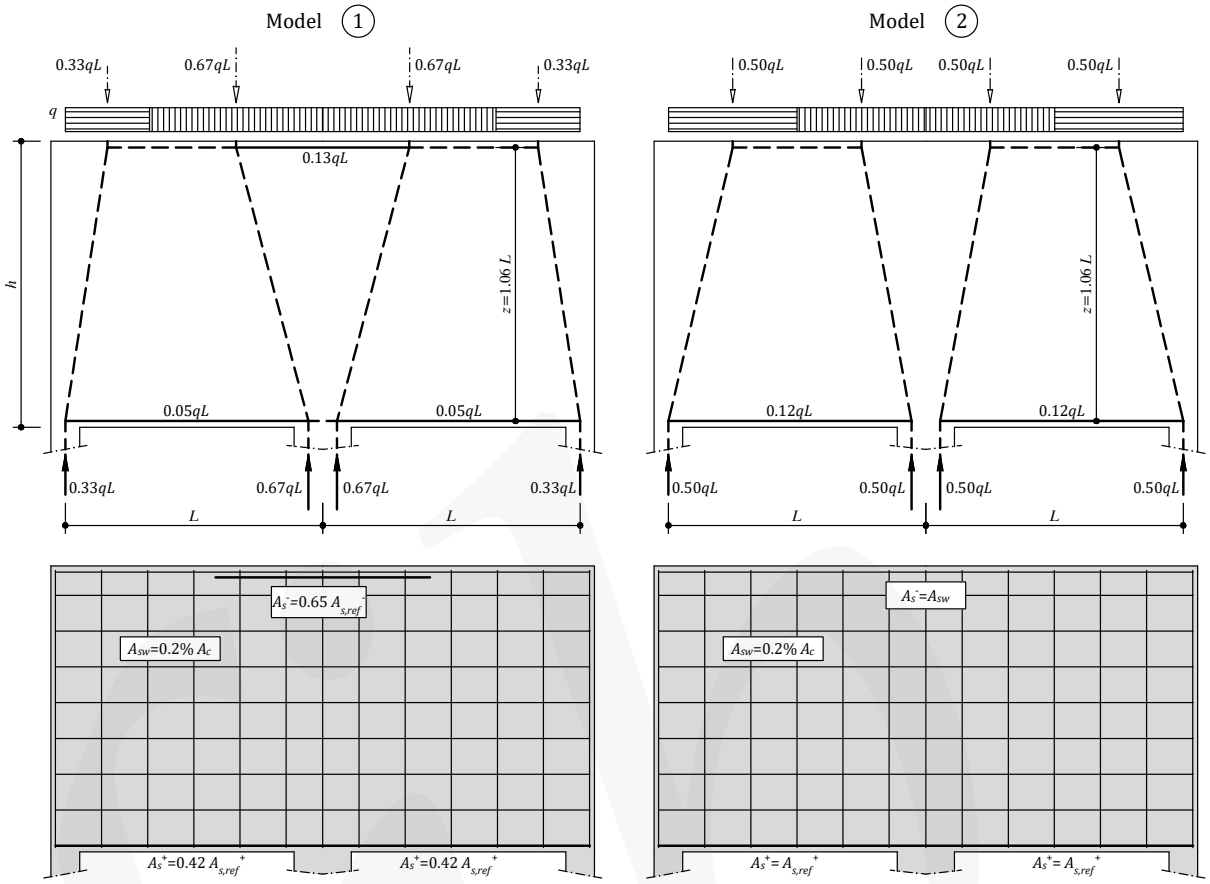


Fig. 4-23 Continuous deep beam strut-and-tie model simulating different alternative stress redistribution and corresponding reinforcement layout.

Following the different design strut-and-tie models, different reinforcement layouts were defined, and different nonlinear analysis were developed, for each case, to evaluate service behaviour and ductility. The service behaviour was, in particular, analysed by assessment of the reinforcement stresses (Fig. 4-24 to Fig. 4-27).

This document is the intellectual property of the fib – International Federation for Structural Concrete. All rights reserved.
This PDF of fib Bulletin 100 is intended for use and/or distribution solely within fib National Member Groups.

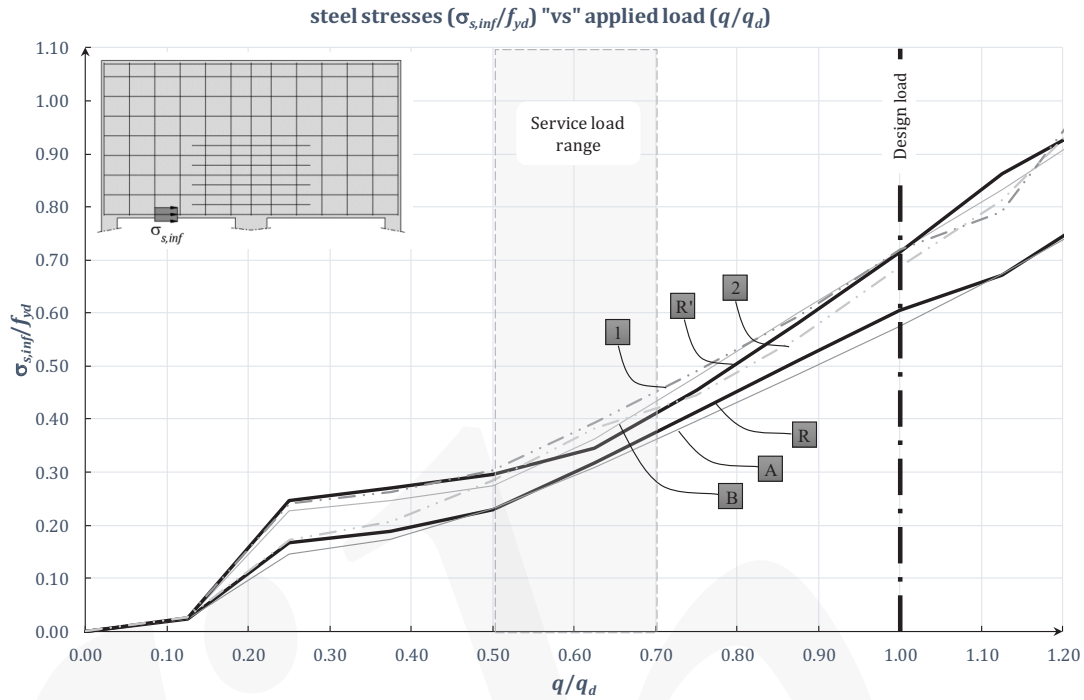


Fig. 4-24 Continuous deep beam steel stresses at bottom reinforcement (σ_s/f_{yd}) "vs" applied load (q/q_d).

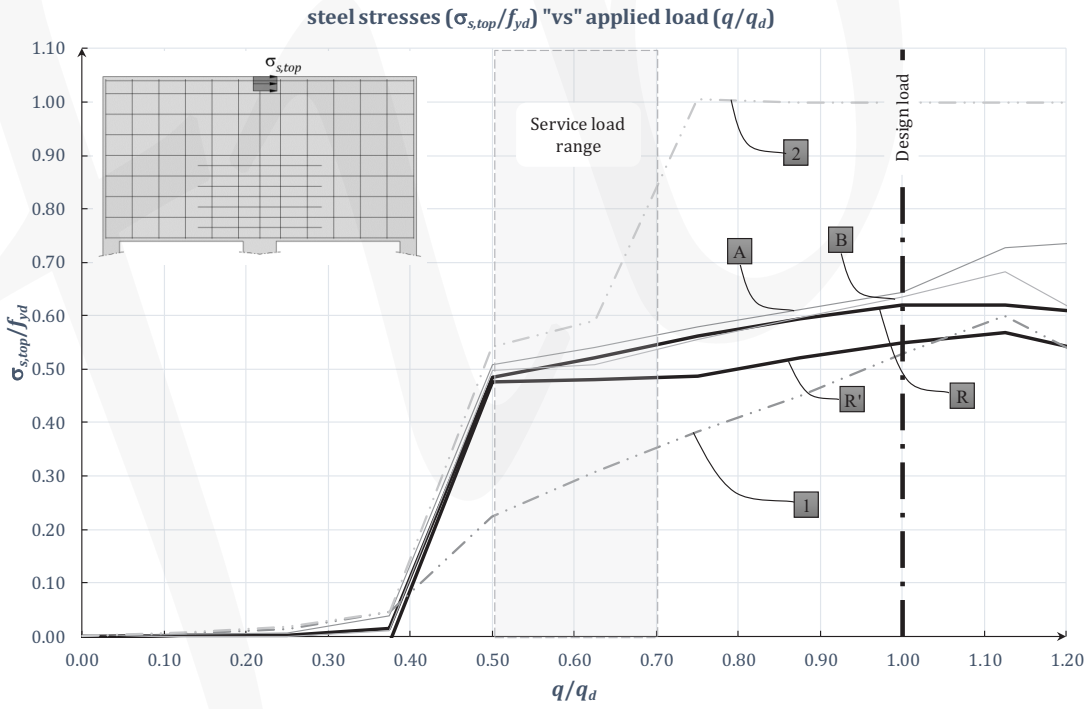


Fig. 4-25 Continuous deep beam steel stresses at top reinforcement (σ_s/f_{yd}) "vs" applied load (q/q_d).

This document is the intellectual property of the fib – International Federation for Structural Concrete. All rights reserved.
This PDF of fib Bulletin 100 is intended for use and/or distribution solely within fib National Member Groups.

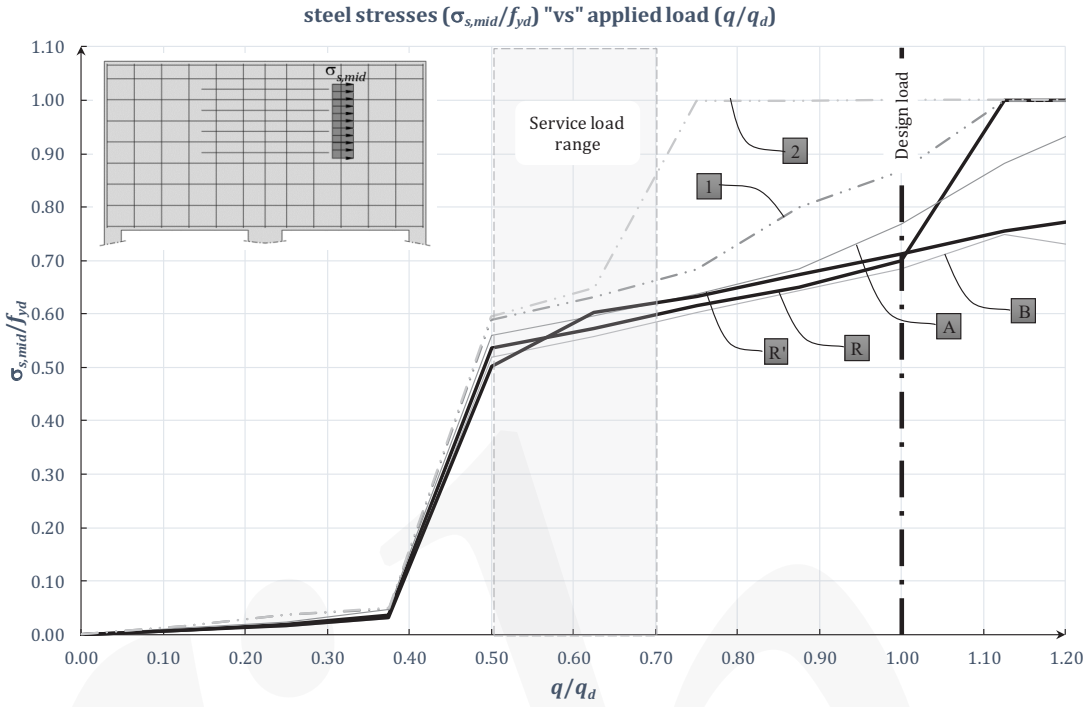


Fig. 4-26 Continuous deep beam steel stresses at the reinforcement over the support at a higher height (σ_s/f_{yd}) "vs" applied load (q/q_d).

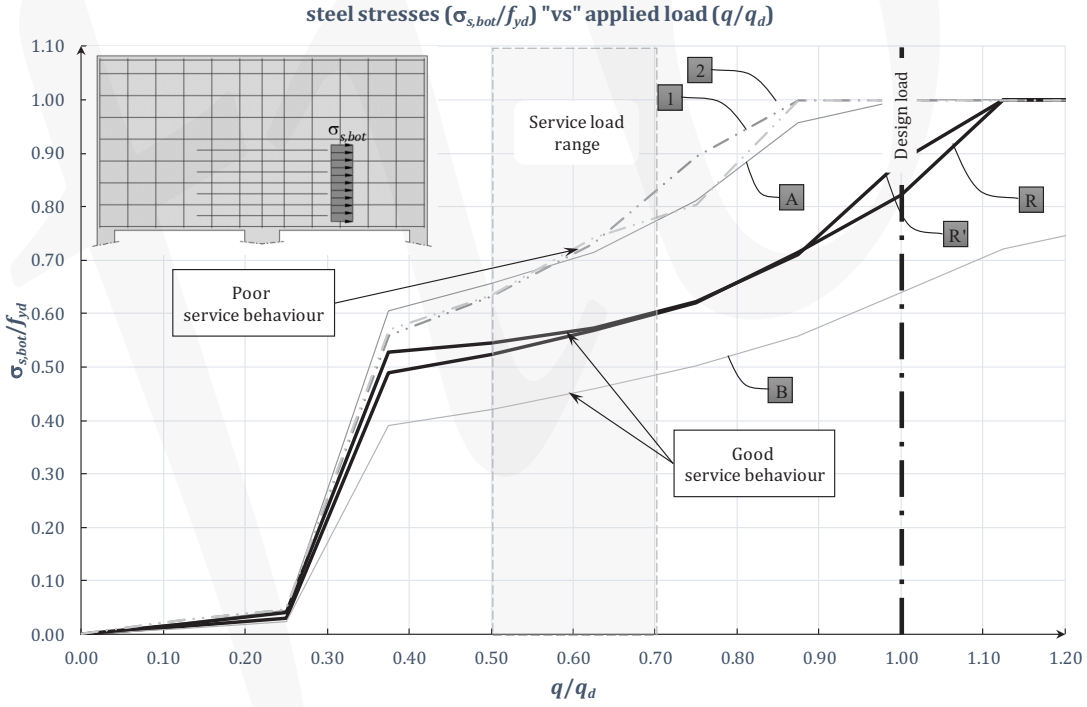


Fig. 4-27 Continuous deep beam steel stresses at the reinforcement over the support at a lower height (σ_s/f_{yd}) "vs" applied load (q/q_d).

All deep beams reach the predicted design load, which means that the structure has sufficient ductility to adapt itself to the chosen model. After concrete cracking occurs at the bottom / mid-span tie, stresses are redistributed and the tensile stresses in the tie over the support increase, keeping the mid span steel stresses approximately constant.

This document is the intellectual property of the fib – International Federation for Structural Concrete. All rights reserved.
This PDF of fib Bulletin 100 is intended for use and/or distribution solely within fib National Member Groups.

Increasing loads leads to cracking at the support region and mid span steel stresses grow with similar slope in all deep beams. For deep beams with low reinforcement ratios over the support - Models A, 1 and 2 - steel stresses can lead to moderate crack widths; indeed for a service load of $q = 0.6\ q_d$, steel stresses of approximately $0.7 f_{yd}$ are obtained (see Fig. 4-26 and Fig. 4-27) which may lead to high crack widths and consequently poor service behaviour. On the other hand, increasing the inner level arm higher than 50% led to steel stresses at service loads that can be considered improper for certain circumstances, as shown for models 1 and 2.

Note that usually, the adopted model for continuous deep beams is influenced by the external support reactions, thus it is worth understanding that the adopted internal redistribution led to variations with respect to the reference model, up to 20% of the external reactions distribution.

The remaining models depict appreciable steel stresses at service loads for all reinforcement levels, showing that there is some arbitrariness for the chosen design model for continuous deep beams and the assumed redistribution is considerably higher than that allowed for slender beams. Nevertheless, in order to prevent inferior service behaviour, extreme stress redistribution should be avoided.

4.3.6 Dapped-end beam / re-entrant corners

The dapped beam models are very common in structural concrete regions. Probably the most common application is in shear walls with openings, as shown in Fig. 4-28.

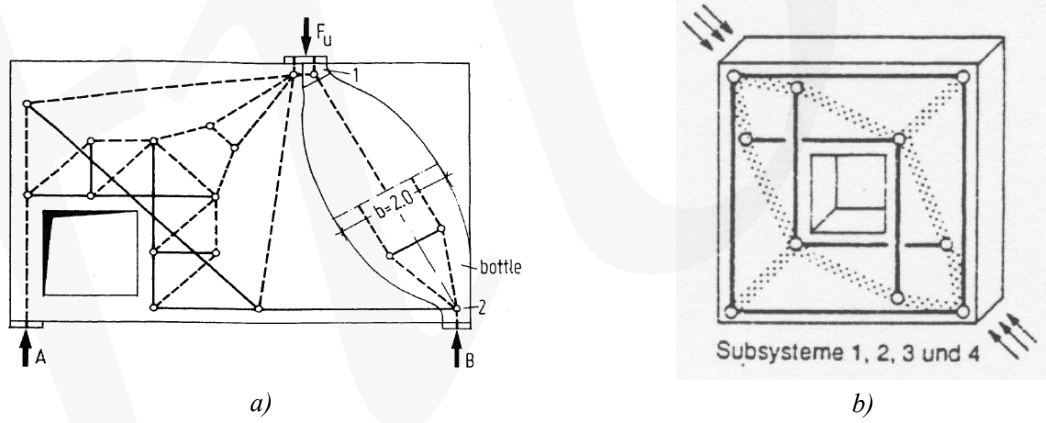


Fig. 4-28 a) Re-entrant corners basic model in a deep beam with an opening[4-1]; b) Re-entrant corners basic model at an opening[4-6]

The elastic solution (see Fig. 4-29) suggests the superposition of the two models, assuming 25% of applied load for the model defined by orthogonal reinforcement and the remaining 75% for the model corresponding to the inclined reinforcement.

Despite some difficulties from the construction point of view, the designer provides some diagonal reinforcement, especially for moderate and high loads, even if not explicitly calculated.

This document is the intellectual property of the fib – International Federation for Structural Concrete. All rights reserved.
This PDF of fib Bulletin 100 is intended for use and/or distribution solely within fib National Member Groups.

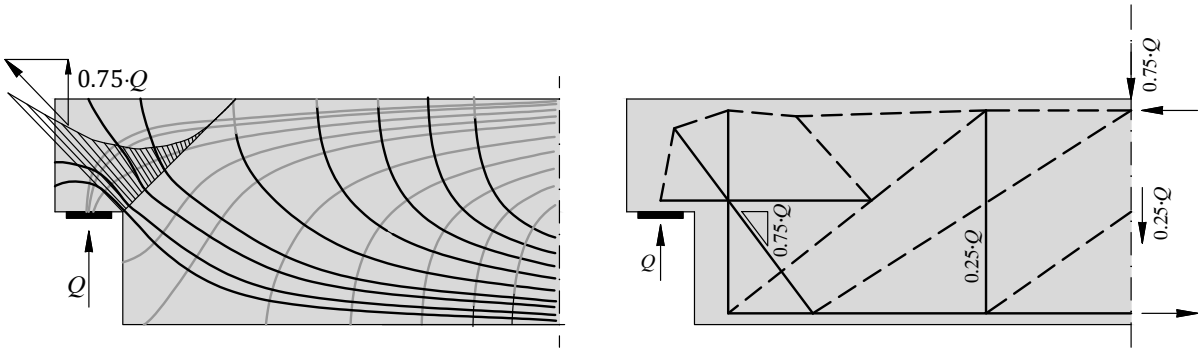


Fig. 4-29 Dapped end beam elastic stress trajectories and reference strut-and-tie model.

For the evaluation of the local behaviour under different reinforcement layouts, three design models were developed (Fig. 4-30): Model R – based on the elastic solution; Model 1 – assuming that 50% of the load is equilibrated by orthogonal reinforcement and the remaining 50% by inclined reinforcement; and, finally, Model 2 – in which only 10% of the load is carried by inclined reinforcement. Combinations of models are performed in many cases as inclined reinforcement is very efficient in terms of structural performance, but difficult to place and anchor.

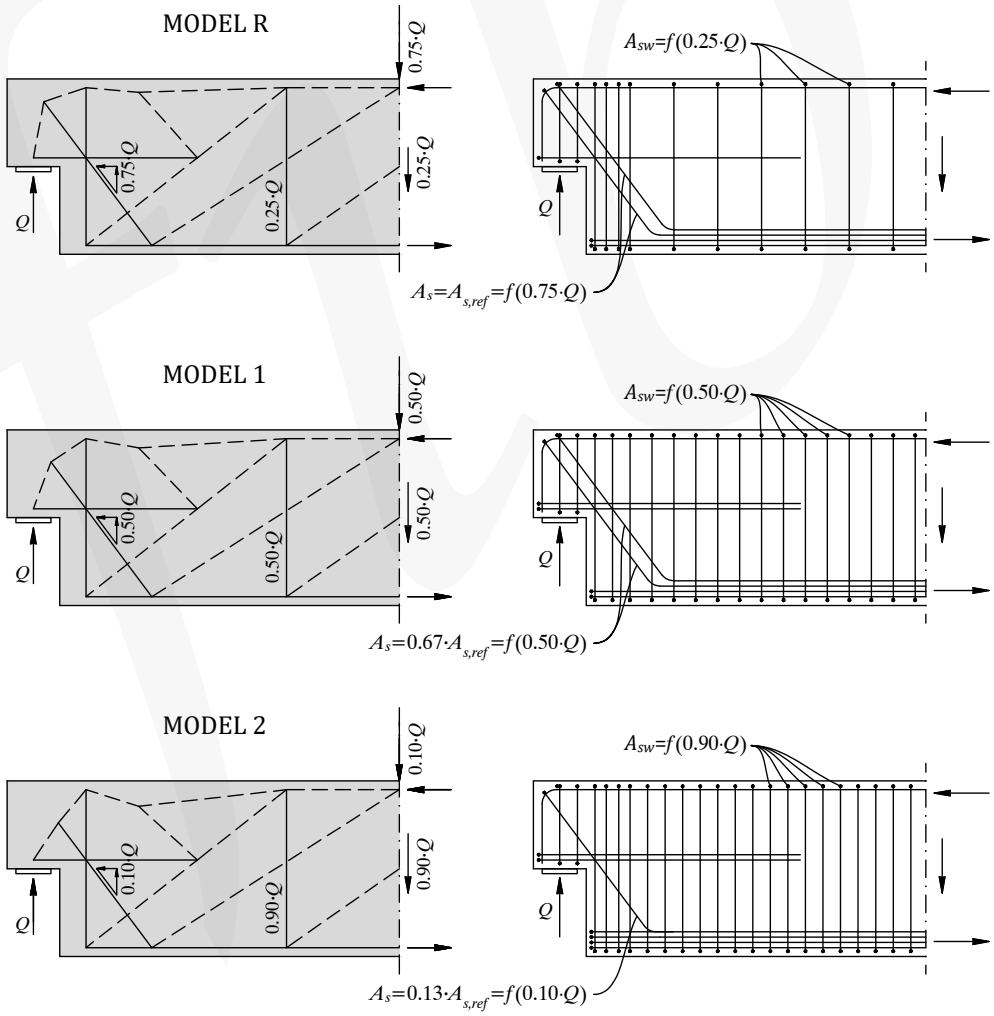


Fig. 4-30 Dapped end beam strut-and-tie model simulating alternative stress redistribution and corresponding reinforcement layout.

This document is the intellectual property of the fib – International Federation for Structural Concrete. All rights reserved.
This PDF of fib Bulletin 100 is intended for use and/or distribution solely within fib National Member Groups.

For these cases, the steel stresses were analysed for different load steps as shown in Fig. 4-31 to Fig. 4-33.

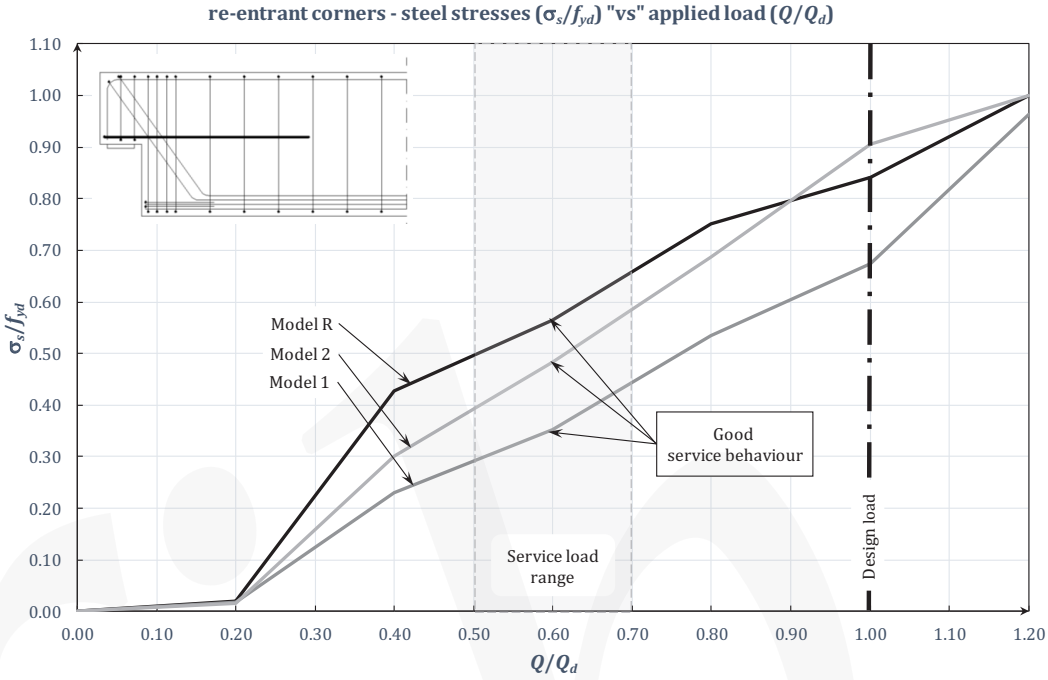


Fig. 4-31 Dapped end beam steel stresses at the horizontal reinforcement (σ_s/f_{yd}) "vs" applied load (q/q_d).

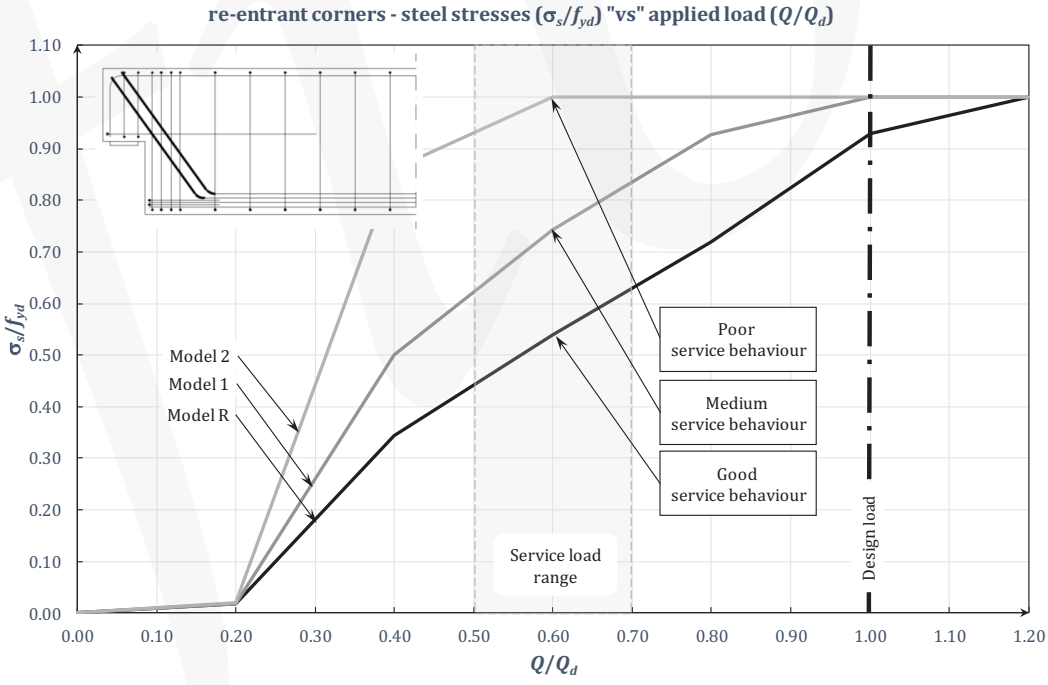


Fig. 4-32 Dapped end beam steel stresses at the inclined reinforcement (σ_s/f_{yd}) "vs" applied load (q/q_d).

This document is the intellectual property of the fib – International Federation for Structural Concrete. All rights reserved.
This PDF of fib Bulletin 100 is intended for use and/or distribution solely within fib National Member Groups.

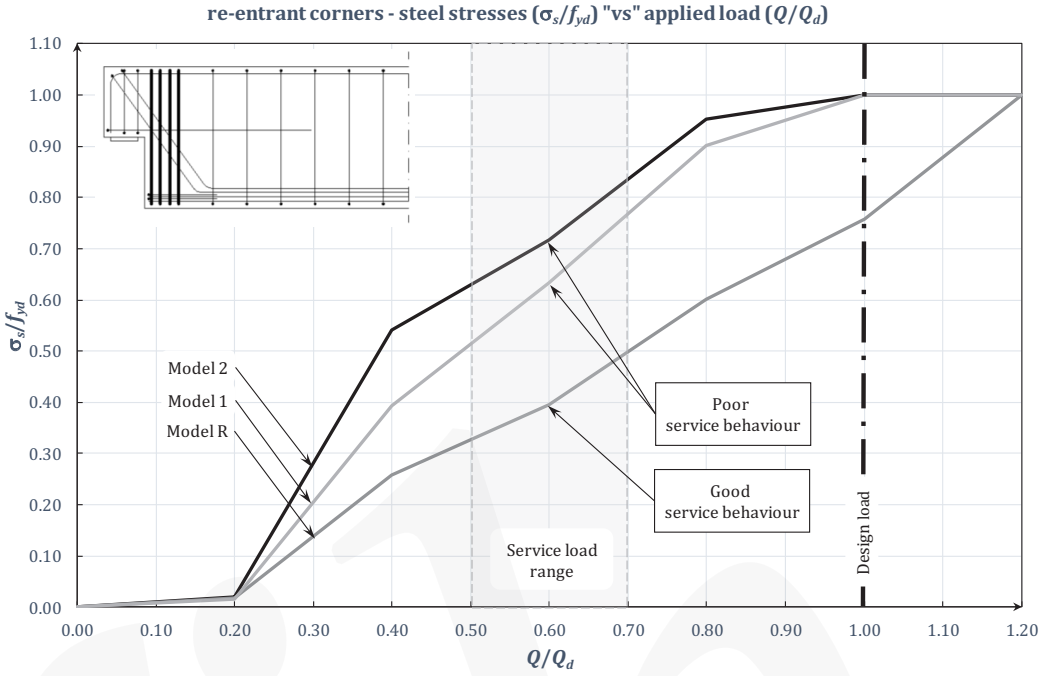


Fig. 4-33 Dapped end beam steel stresses at the vertical reinforcement (σ_s/f_{yd}) "vs" applied load (q/q_d).

The results show that assuming the reference solution (75% of the load equilibrated by inclined reinforcement) a good service behaviour is achieved. However, assuming only 10% for the inclined reinforcement load path leads to high steel stresses that suggests unfavourable service behaviour. Finally, assuming up to 50% for each load path was shown to be an adequate solution with regards to service behaviour.

4.3.7 Spreading of point loads / bottle effect

Spreading of point loads within a concrete region, known as bottle effect, is usually defined by the model shown in Fig. 4-34 mainly based on elastic stresses.

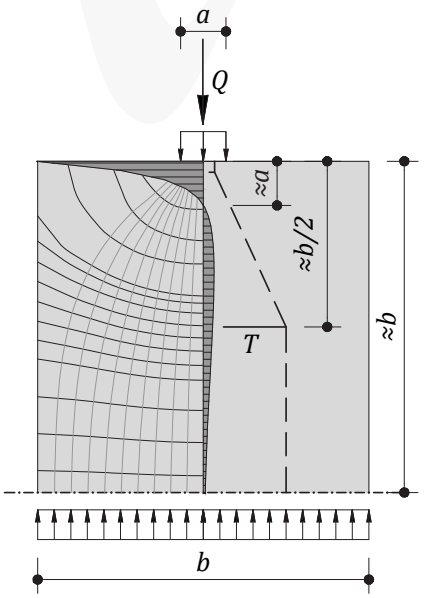


Fig. 4-34 Spreading of point loads stress trajectories and reference strut-and-tie model.

This document is the intellectual property of the fib – International Federation for Structural Concrete. All rights reserved.
This PDF of fib Bulletin 100 is intended for use and/or distribution solely within fib National Member Groups.

The tensile force T may be given by a simple equation, obtained through elastic analysis:

$$T = \frac{Q}{4}\left(1 - \frac{a}{b}\right)$$

Following the elastic solution, several possible design models were detailed and steel stresses at different load increments were evaluated. For the reference model (Model R), the steel area was obtained by applying directly the equation derived by the elastic solution, while the remaining models simulate different possible stress redistribution and, in particular, 70%, 50% and 35% of the reference steel area was considered (Fig. 4-35). Also, different ratios b/a were analysed, with b denoting the concrete width and a the width of the point load.

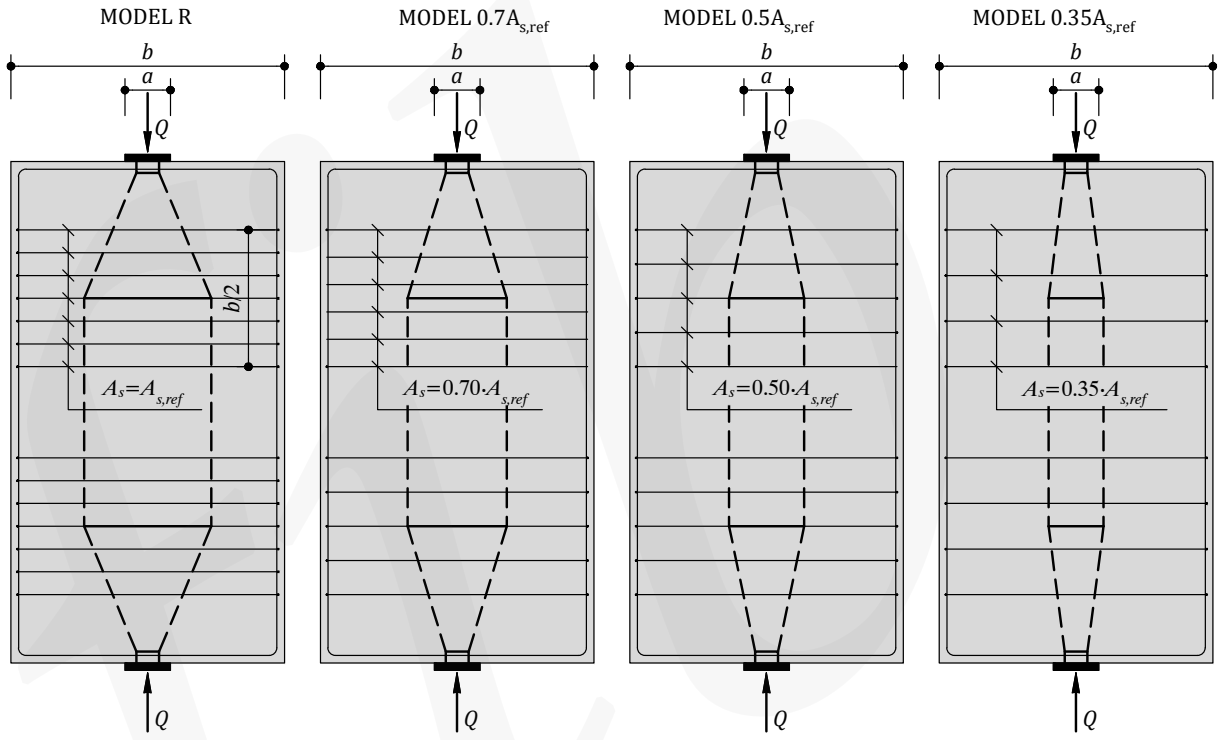


Fig. 4-35 Spreading of point loads strut-and-tie model simulating different alternative stress redistribution and corresponding reinforcement layout.

The steel stresses at each load increment are presented in Fig. 4-36 to Fig. 4-38 and it is possible to show that redistribution up to 70% does not compromise service behaviour.

This document is the intellectual property of the fib – International Federation for Structural Concrete. All rights reserved.
This PDF of fib Bulletin 100 is intended for use and/or distribution solely within fib National Member Groups.

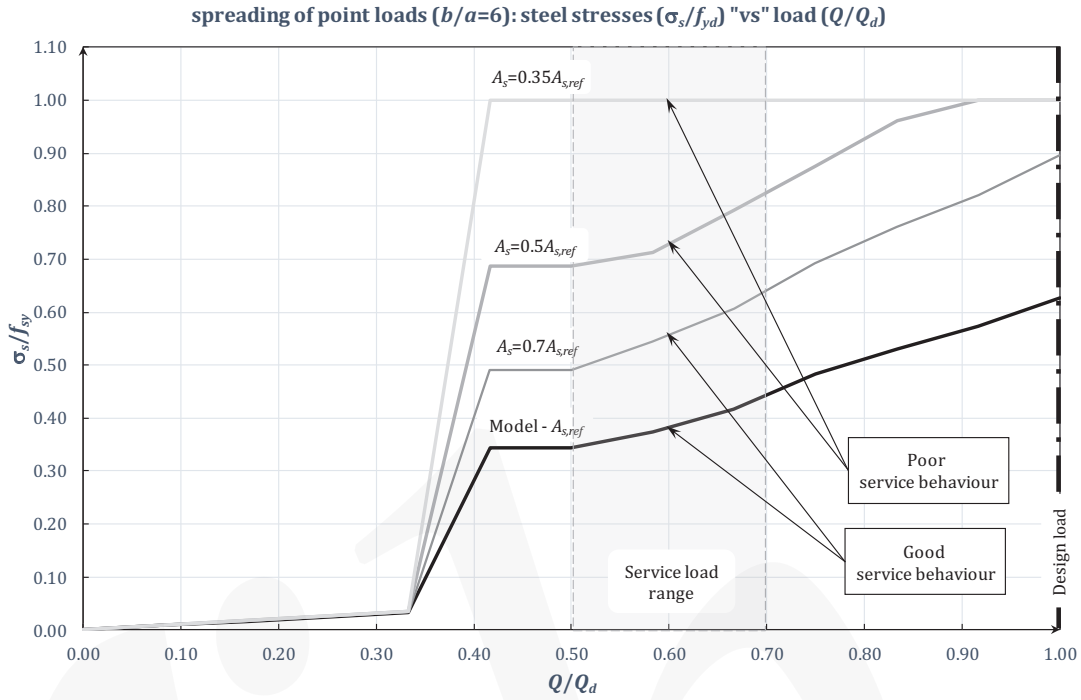


Fig. 4-36 Spreading of point loads, with b/a = 6, steel stresses at the reinforcement (σ_s/f_{yd}) "vs" applied load (q/q_d).

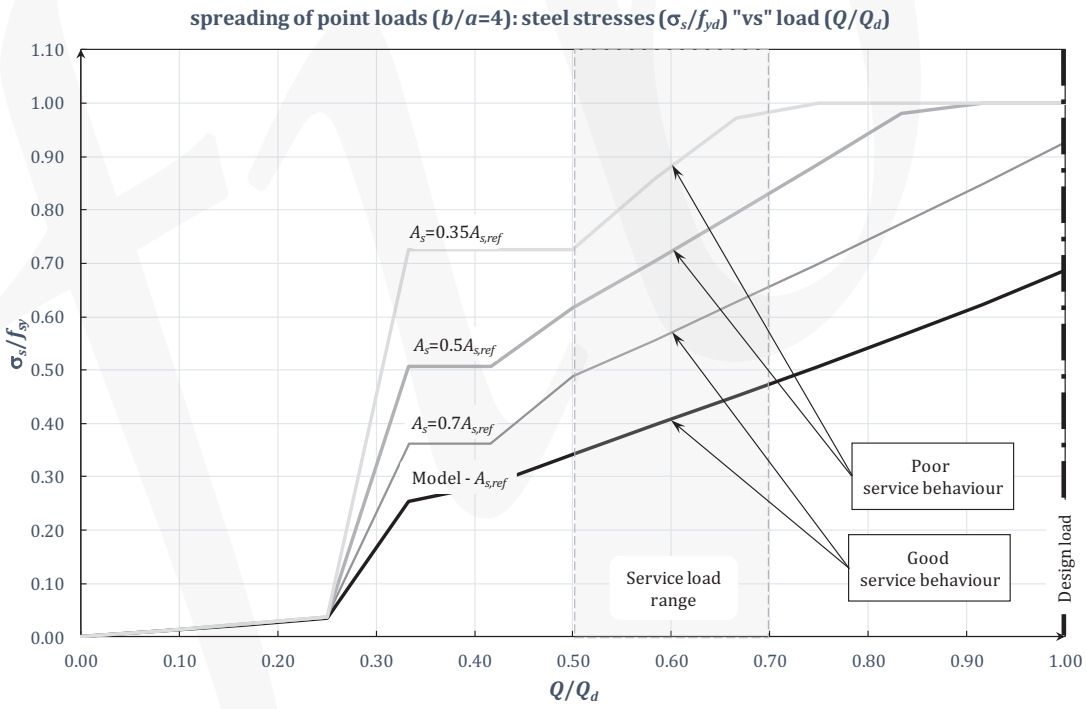


Fig. 4-37 Spreading of point loads, with b/a = 4, steel stresses at the reinforcement (σ_s/f_{yd}) "vs" applied load (q/q_d).

This document is the intellectual property of the fib – International Federation for Structural Concrete. All rights reserved.
This PDF of fib Bulletin 100 is intended for use and/or distribution solely within fib National Member Groups.

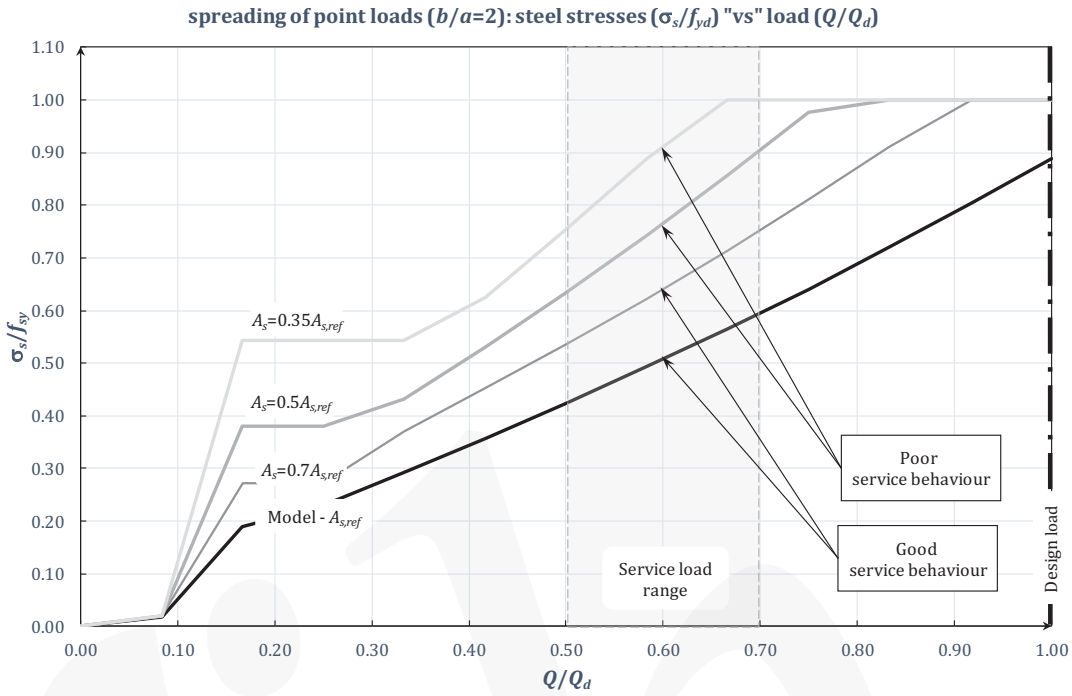


Fig. 4-38 Spreading of point loads, with $b/a = 2$, steel stresses at the reinforcement (σ_s/f_{yd}) "vs" applied load (q/q_d).

In practice, the widths of the point load a and the concrete spreading width b, are not commonly known in every situation; however, a simple and conservative rule may be applied according to the following procedure:

If $T = A_s \cdot f_y$ and $Q = a \cdot t \cdot f_c$ (A_s – steel area, f_y –yielding steel stress, f_c – concrete compression strength, t – wall thickness) then:

$$A_s \cdot f_y = \frac{a \cdot t \cdot f_c}{4}\left(1-\frac{a}{b}\right) \Leftrightarrow \frac{b \cdot t}{2}\frac{A_s}{A_c} \cdot \frac{f_y}{f_c} = \frac{a \cdot t}{4}\left(1-\frac{a}{b}\right)$$

Knowing that $\omega_s = \frac{A_s}{A_c} \cdot \frac{f_y}{f_c} = \rho_s \frac{f_y}{f_c}$ (ρ_s – reinforcement ratio)

$$\omega_s = \frac{1}{2}\frac{a}{b}\left(1-\frac{a}{b}\right)$$

This document is the intellectual property of the fib – International Federation for Structural Concrete. All rights reserved.
This PDF of fib Bulletin 100 is intended for use and/or distribution solely within fib National Member Groups.

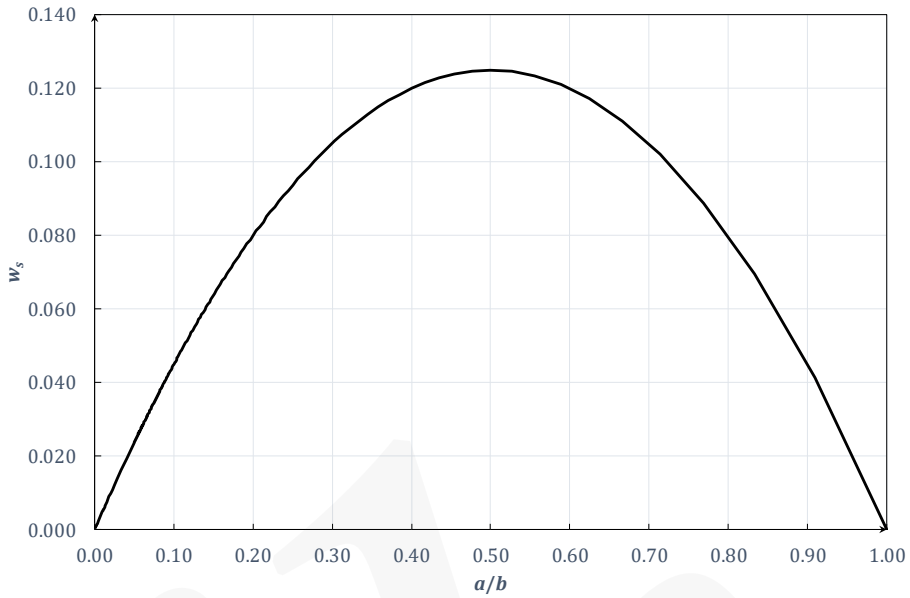


Fig. 4-39 Spreading of point loads: mechanical reinforcement ratio variation with *a/b*.

This simple equation provides the reference reinforcement to equilibrate the tension developing by the spreading of point loads with the maximum occurring for $a/b = 0.5$ leading to $\omega_s = 0.125$ (Fig. 4-39). As showed before, redistribution of about 70% with respect to the reference solution provides acceptable service behaviour; thus, for practical purposes and for avoiding further calculations, the adoption of a "minimum" distributed reinforcement established by $\omega_s = 0.08$ ($\rho_s \approx 0.4\%$) will equilibrate the tensile stresses resulting from every compression stress field spreading within the region and ensure a good service behaviour. This means that the designer, for the lower LoA, may avoid explicitly considering the spreading of point loading in the design model, if this "minimum" reinforcement is provided for the region.

4.3.8 Point load near support

The point load near support is mainly based on a model in which part of the applied load is carried by stirrups (F_w) while the remaining load is transferred directly to the support (see Fig. 4-40b) with two possible stress field models). This solution is also based on the elastic stress trajectories presented in Fig. 4-40a) and several test results, defining the value of the load to be transferred by stirrups as:

$$F_w \leq \frac{Q}{3}\left(2\frac{a}{z} - 1\right)$$

This document is the intellectual property of the fib – International Federation for Structural Concrete. All rights reserved.
This PDF of fib Bulletin 100 is intended for use and/or distribution solely within fib National Member Groups.

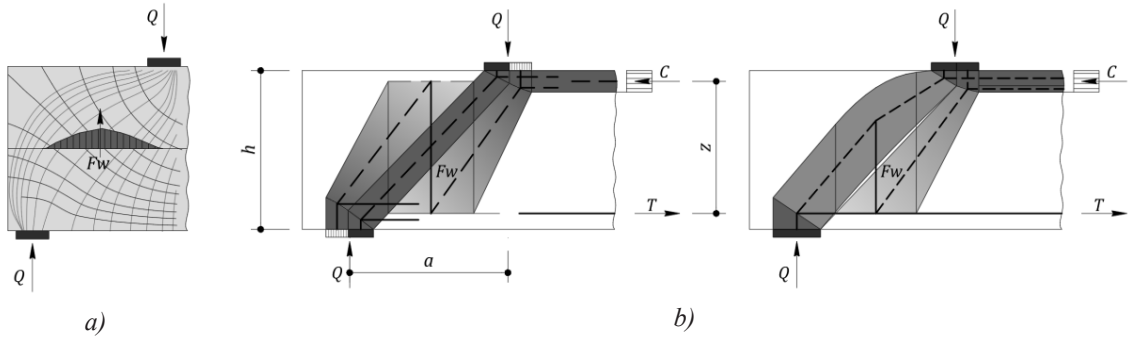


Fig. 4-40 Point load near support stress trajectories and reference stress field models.

To evaluate service behaviour for different levels of stress redistribution, models for different ratios *a/h* were analysed, with a being the distance of the point load to the support and *h* the height of the beam. The solution considered as reference was the one based on the previous discussion, resulting in an area for stirrups of $A_{s,ref}$; several cases with other areas of stirrups A_s were analysed. Fig. 4-41 shows the variation of the stirrups stresses with the applied load *Q*, where Q_d was the design load. It can be observed that a reduction of up to 25% (A_s = 0.75 $A_{s,ref}$) with respect to the reference solution does not influence the service behaviour appreciably. However, larger deviations may, in some cases, lead to unfavourable service behaviour and possible large cracks at service loads.

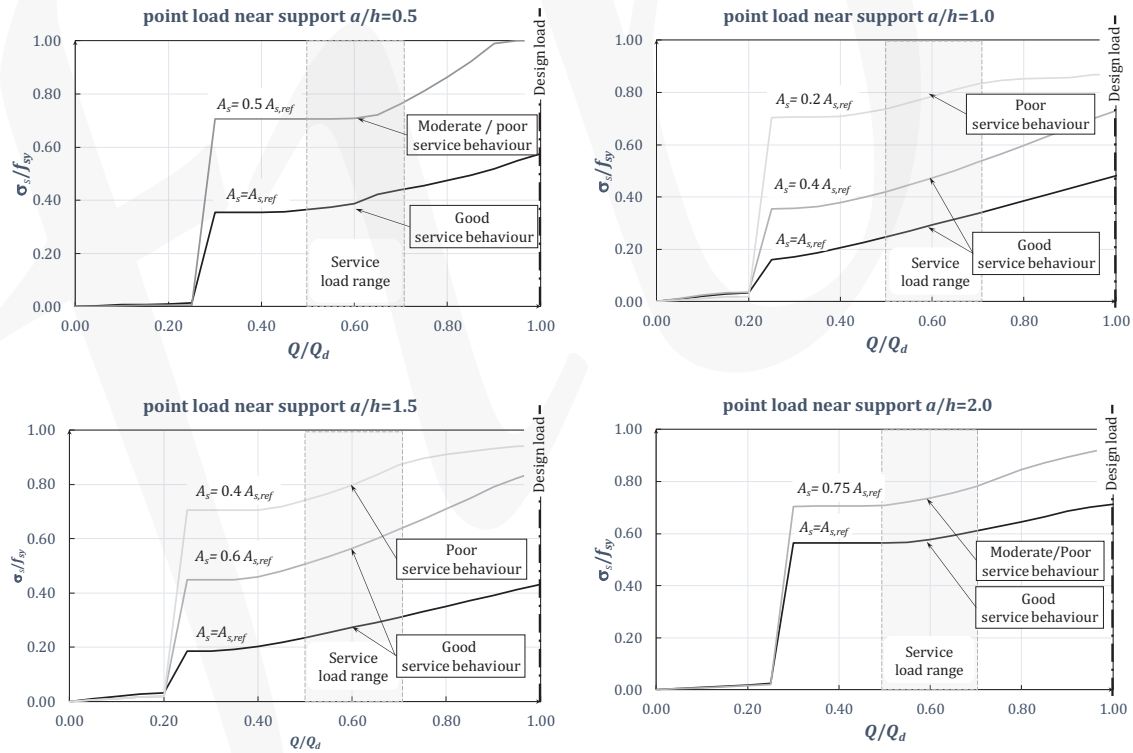


Fig. 4-41 Point load near support steel stresses (σ_s/f_{yd}) vs. applied load (q/q_d) for different distances to the support and reinforcement layout.

4.3.9 Final Remarks – Practical Rules

The assessment of a model for the design of a structural concrete region is mainly influenced by two aspects: ductility and service behaviour.

This document is the intellectual property of the fib – International Federation for Structural Concrete. All rights reserved.
This PDF of fib Bulletin 100 is intended for use and/or distribution solely within fib National Member Groups.

The factors that may affect the ductility of discontinuity regions are essentially the deformation capacity of reinforcing steel after yielding and a brittle concrete rupture. Rupture of reinforcement can be the reason of a premature failure, if the available ductility of the steel prevents the formation of alternative load paths. However, in discontinuity regions, large redistributions usually occur after cracking, provided that, after yielding, moderate steel strains are obtained. The second aspect, an unpredicted concrete failure, is mainly caused by the reduction of the compressive concrete strength due to the presence of large transversal strains. Usually this phenomenon is perceivable for large crack widths, owing to yielding of the reinforcement. However, in most practical cases this effect is not relevant, given that moderate concrete stresses are imposed by the nodal checking and smaller stresses inside the region are obtained. On the other hand, the adoption of minimum distribution reinforcement prevents the formation of large cracks that could cause a brittle failure. These aspects were adequately considered in the above nonlinear analyses and it was found that for the reinforcement layouts analysed, the design ultimate steel strain was not achieved. Simultaneously, transverse tensile strains were adequately considered in the concrete compression constitutive relationship. As a result, it was in all cases verified that this effect was not governing the behaviour.

Concerning service behaviour, the common practical rule: "...if the struts and ties follow the main compression and tension elastic stress trajectories, the ultimate limit state model can be used to check service behaviour...", has been shown to be particularly appropriate. Note that the model orientation on the basis of the elastic solution should not be interpreted as a perfect mapping of the elastic trajectories. An important issue when developing suitable strut-and-tie models is to follow the practical reinforcement layout, provided that the main direction of compression and tension stresses are close to principal stress trajectories. This does not imply that the engineer needs to develop an elastic analysis in every practical situation. The common models presented in technical documentation[4-1], [4-2], [4-3], [4-8] cover most common cases.

In general, the engineer has plenty of freedom for choosing the model for the design of discontinuity regions and judgement and previous knowledge should not be disregarded. The common rules for the development of a suitable strut-and-tie model should be respected, preventing extreme redistributions that can influence service behaviour or even cause a premature failure.

The main objective of this chapter is to provide practical rules for the designers when developing strut-and-tie models for the lowest LoA. If the design model follows these simple instructions, service behaviour is automatically checked, and no further calculation is necessary. Higher redistributions may be allowed, but a higher LoA analysis should then be carried out to check service behaviour and ductility.

In the following all basic strut-and-tie models are presented and corresponding limits of redistribution that prevent the need for further checks, are presented in Fig. 4-42 to Fig. 44-46.

This document is the intellectual property of the fib – International Federation for Structural Concrete. All rights reserved.
This PDF of fib Bulletin 100 is intended for use and/or distribution solely within fib National Member Groups.

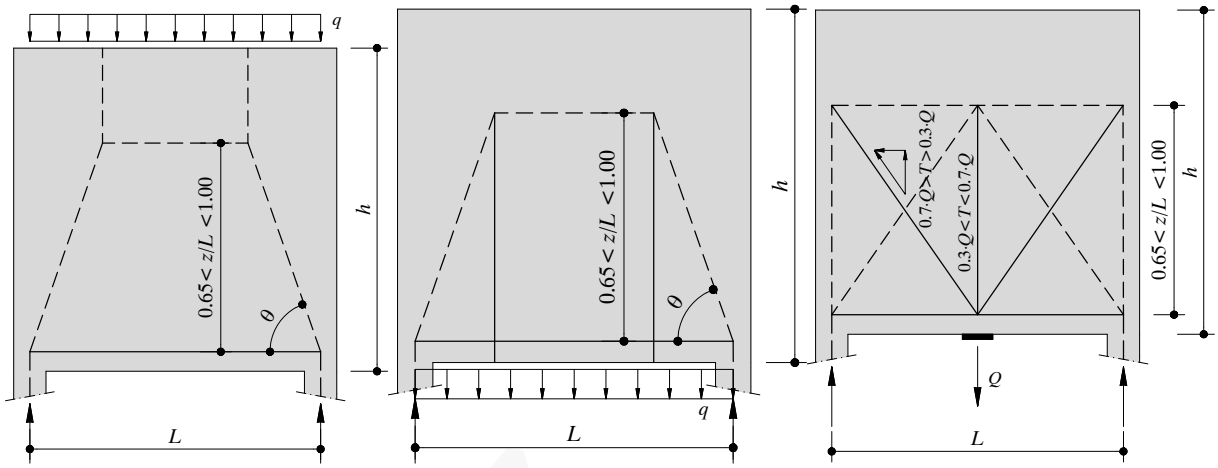


Fig. 4-42 Redistribution limits for simply supported deep beams basic models

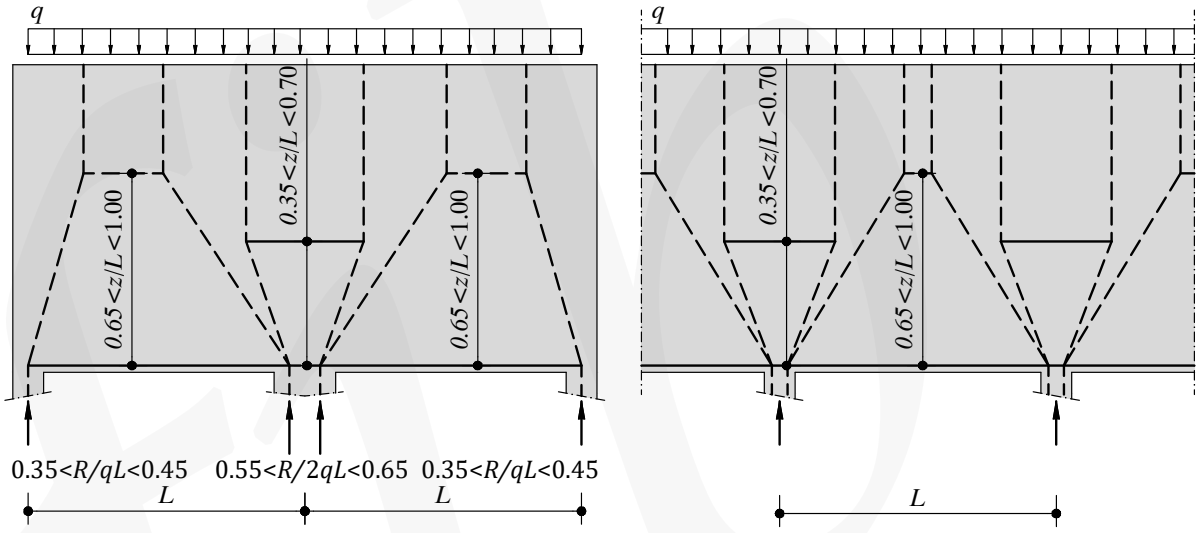


Fig. 4-43 Redistribution limits for continuous deep beams basic models

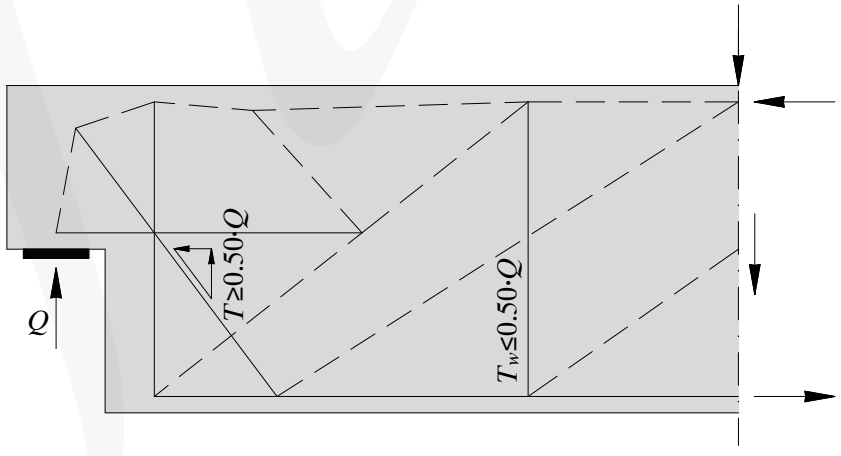


Fig. 4-44 Redistribution limits for re-entrant corners basic models

This document is the intellectual property of the fib – International Federation for Structural Concrete. All rights reserved.
This PDF of fib Bulletin 100 is intended for use and/or distribution solely within fib National Member Groups.

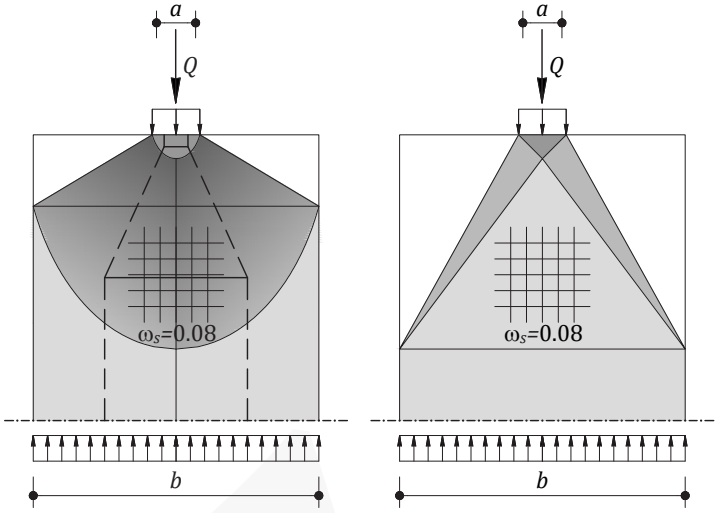
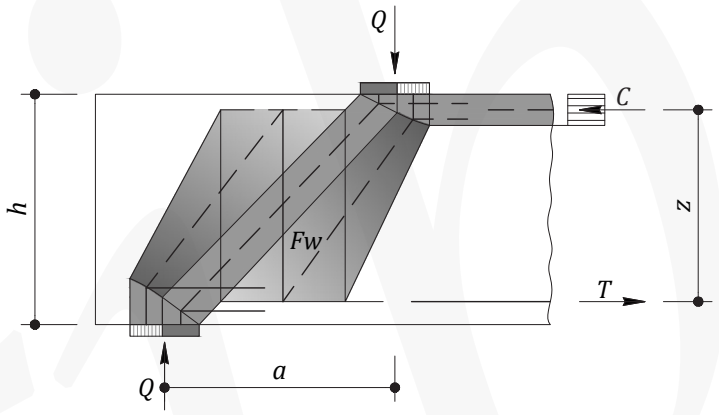


Fig. 4-45 Redistribution limits for spreading of point loads basic models



$$\frac{Q}{4}\left(2\frac{a}{z}-1\right) \le F_w \le \frac{Q}{3}\left(2\frac{a}{z}-1\right)$$

Fig. 4-46 Redistribution limits point loads near support basic models

This document is the intellectual property of the fib – International Federation for Structural Concrete. All rights reserved.
This PDF of fib Bulletin 100 is intended for use and/or distribution solely within fib National Member Groups.

5. Principles of computer modelling

5.1 Introduction

In spite of being recognised as powerful tools, strut-and-tie models and stress fields are essentially used as hand calculation tools and designers are more and more inclined to using other models (e.g. linear elastic finite element calculations) for dimensioning and detailing of structural concrete. Therefore, the use of strut-and-tie models and stress fields might be limited to education and early stage conceptual design, unless they are implemented in user-friendly computational environments to make their application more efficient. The use of computer modelling might overcome the drawbacks of strut-and-tie models and stress fields (i.e. tedious hand application, serviceability and deformation capacity cannot be verified), yet without impairing their advantages of transparency and control over the design.

This chapter introduces several computer modelling strategies to implement the basic ideas of strut-and-tie and stress field models, namely:

- Use of the Finite-Element Method based on the calculation of the displacement field and respecting equilibrium and compatibility conditions,
- Use of the Finite-Element Method based on the optimisation of equilibrium and yield conditions but without explicit calculation of the associated displacement field,
- Adaptive analysis based on strut-and-tie models with the potential to perform optimisation procedures and accounting for a realistic response in reinforcing ties, and
- Implementation of tailored methods (such as the Stringer-Panel-Method) by means of numerical procedures

The choice of the most suitable approach for a given case depends largely on the conditions and outputs required. Some approaches are more suitable for fast and efficient calculations but have some level of simplification (no explicit check of displacement field, simplified assumption on the modelling) while others are more general but generally more time-consuming. In the following, the assumptions and detailed implementation of each approach are discussed, as well as their strengths and potential limitations.

5.2 Compatibility-based Stress field – Finite element method

5.2.1 Introduction

The use of the finite element method (FEM) to determine the stress state in a continuum is a powerful tool for analysing reinforced or prestressed concrete structures. Linear elastic finite element concrete programs are widely used by designers as they allow the analysis of even complex structures in relatively short time, including in many cases user-friendly post-processing modules for automated dimensioning or checking of reinforcement

https://doi.org/10.35789/fib.BULL.0100.Ch05

This document is the intellectual property of the fib – International Federation for Structural Concrete. All rights reserved.
This PDF of fib Bulletin 100 is intended for use and/or distribution solely within fib National Member Groups.

and concrete dimensions. Linear elastic calculations do not reflect the real behaviour of concrete structures, as they neglect the non-symmetric strength of concrete and the non-isotropic behaviour of reinforced concrete in the calculation of internal forces, and only account for these effects in the post-processing, i.e. when dimensioning the reinforcement and checking concrete dimensions, typically carried out using yield conditions based on plasticity theory. While these calculations usually yield safe designs for regions without static/kinematic discontinuities, often unpractical and inefficient reinforcement layouts are obtained[5-1], particularly when the internal force distribution depends on the stiffness of the members or when imposed displacements may occur.

While existing general nonlinear FE programs overcome the aforementioned oversimplifications of linear elastic analysis and allow capturing the real structural behaviour, these methods are not suitable for design purposes. The complexity of the implemented mechanical methods requires high level expertise as well as modelling and interpretation time, while the results might be very sensitive to the choice of material parameters unknown in the design phase. In consequence, non-linear FE-analyses are useful only for research and assessment purposes.

In the method presented next, continuous stress fields fulfilling kinematic compatibility are formulated, which corresponds to a simplified, nonlinear finite element analysis. Contrary to general nonlinear FE-calculations, however, only standard material parameters known at the design stage are required as input and concrete tensile strength is neglected for equilibrium (as discussed in Chapter 2), similarly as in standard structural concrete design. The effective concrete compressive strength is automatically computed from the transverse strains as specified by modern design codes, similar as in compression field analyses accounting for compression softening[5-2], [5-3]. The obtained stress state is in equilibrium with the applied loads and respects the yield conditions of the materials, hence the derived stress fields are lower bound solutions according to Limit Analysis. Fernández Ruiz and Muttoni[5-4] originally proposed and implemented this approach in the method known as Elastic-Plastic Stress Field considering elastic-plastic constitutive relationships, which yields excellent failure load predictions[5-5]. To extend this approach for serviceability as well as deformation capacity verifications Mata-Falcón et al.[5-6] have addressed the consideration of tension stiffening in the approach known as Compatible Stress Field Method[5-7]. While this section focuses on the plane stresses case, the extension to the three-dimensional case is discussed in Section 7.2.

Compatibility-based Stress Fields for plane stress problems use 2D elements to model the concrete and 1D elements to simulate reinforcing or prestressing steel. The use of a discrete representation of the reinforcement allows obtaining the stresses directly in the two materials and yields thus a simpler interpretation of the results. In the following, details about the finite elements, mesh topology dependency, and interpretation of results are given. To conclude, the example introduced in Chapter 1 (see Fig. 1-4) is solved by means of Compatibility-based Stress Fields with different constitutive relationships. The reader is referred to Chapter 2 for details about the mechanical models and constitutive relationships used.

It should be noted that the various stress field approaches based on the classical displacement based finite element method assume coaxiality between the total strain tensor and the stress tensor. This assumption is in fact in agreement with the considerations of Nadai[5-8] and Hencky[5-9]. However, the assumption has been shown not to satisfy the continuity conditions between elastic and plastic regimes[5-10] and also present

This document is the intellectual property of the fib – International Federation for Structural Concrete. All rights reserved.
This PDF of fib Bulletin 100 is intended for use and/or distribution solely within fib National Member Groups.

inconsistencies for unloading. These issues can be solved by considering the coaxiality principle of Saint-Venant[5-11] (later extended by Levy[5-12]) between the increment of plastic strains and the stress tensor. In any case, as stated by Prager[5-13], both cases (coaxial and non-coaxial rigid perfectly plastic materials) yield identical results for proportional loading. A comprehensive review of this aspect can be consulted elsewhere[5-14].

The fact that both coaxial and non-coaxial materials lead to identical results is easy to demonstrate provided that the loading is proportional, and the materials exhibit sufficient plastic deformation capacity without softening behaviour. Despite the relaxation of the condition of coaxiality, the stress fields obtained with the displacement based finite element formulation are in any case lower-bounds of the strength according to limit analysis. This holds true as the stress field is in equilibrium with the actions and fulfils the yield conditions of the materials. With respect to the upper-bound theorem, when the plastic deformations are sufficiently large and non-reversal proportional loading is considered, the elastic deformations can be neglected and the solution obtained for a non-coaxial material converges towards an upper-bound solution (licit mechanism where the stress and increment of plastic strain tensors are coaxial). This also holds true for some cases with no rotation of the strain field during the transition from the elastic to the plastic state or during the plastic phase (as compression chords). The advantage of the procedure for calculating a stress field based on the displacement field is however very significant, as the complete information on the total strain field allows for an estimate of the crack openings and thus of the efficiency factors of concrete, which is not possible (or might be complex) based only on a velocity field. It can also be noted that the same conditions on coaxiality between the stress field and the total strains have been successfully adopted in similar structural models, as for instance in the tension field approach of Wagner for thin steel webs[5-15].

5.2.2 Finite elements

Elements with quadratic interpolation of the displacement field (i.e. 8 node quadrilateral elements or 6 node triangular elements for the 2D case here discussed) are generally recommended avoiding shear locking problems[5-16]. However, implementations of Compatibility-based Stress Fields using finite elements with lower interpolations of the displacement field (i.e. 4 node quadrilateral elements or 3 node triangular elements, known as constant-strain triangles) have shown very good results even for problems with non-uniform distributions of shear, provided an appropriate meshing is used[5-4], [5-7]. The recommendations for meshing will be later discussed in Section 5.2.3.

The basic steps of the finite element method for 2D elements will be illustrated in the following for the simplest finite element, the Constant-Strain Triangle (CST), which has 6 degrees-of-freedom defining the displacement field and a single integration point. Each of its 3 nodes is characterised by 2 displacements (in the horizontal and vertical direction, see Fig. 2-15). The strain state is thus constant and is the result of differential operator L to the matrix of the approximation functions $N(x,y)$. Usually the resulting matrix $B = L \cdot N$ is more useful and relates the strains with nodal displacements directly.

This document is the intellectual property of the fib – International Federation for Structural Concrete. All rights reserved.
This PDF of fib Bulletin 100 is intended for use and/or distribution solely within fib National Member Groups.

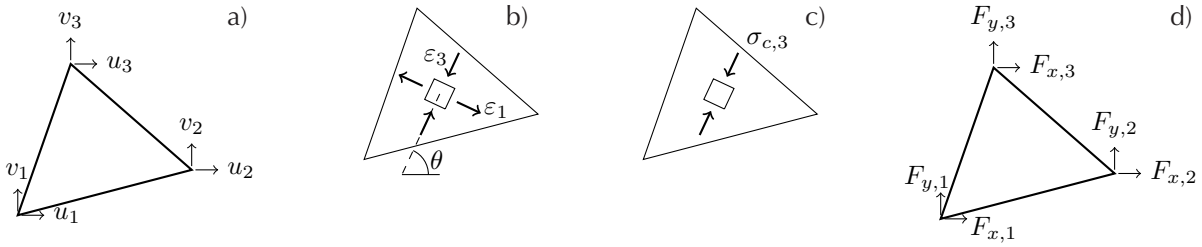


Fig. 5-1 CST Finite element: a) Degrees of freedom; b) Strain state; c) Stress state, d) Equivalent nodal forces to stress state

$$B = \frac{1}{2A}\begin{pmatrix} y_2 - y_3 & 0 & y_3 - y_1 & 0 & y_1 - y_2 & 0 \\ 0 & x_3 - x_2 & 0 & x_1 - x_3 & 0 & x_2 - x_1 \\ x_3 - x_2 & y_2 - y_3 & x_1 - x_3 & y_3 - y_1 & x_2 - x_1 & y_1 - y_2 \end{pmatrix} \tag{5-1}$$

The area of the FE, A, is evaluated with coordinates of the nodes in 2D space.

$$A = \frac{1}{2}\left(x_1 \cdot y_2 + x_2 \cdot y_3 + x_3 \cdot y_1 - x_1 \cdot y_3 - x_2 \cdot y_1 - x_3 \cdot y_2\right) \tag{5-2}$$

The global processing characteristics of FE based on displacement field, is presented below.

$$\begin{Bmatrix} u_1 \\ v_1 \\ u_2 \\ v_2 \\ u_3 \\ v_3 \end{Bmatrix} \underbrace{\vec{N}\begin{Bmatrix} u(x,y) \\ v(x,y) \end{Bmatrix}}_{\vec{B}} \vec{L}\begin{Bmatrix} \varepsilon_{xx} \\ \varepsilon_{yy} \\ \varepsilon_{xy} \end{Bmatrix} \vec{T_p}\begin{Bmatrix} \varepsilon_1 \\ \varepsilon_2 \\ \theta \end{Bmatrix} \vec{D}\begin{Bmatrix} \sigma_1 \\ \sigma_2 \\ \theta \end{Bmatrix} \vec{T_p}^{*}\begin{Bmatrix} \sigma_{xx} \\ \sigma_{yy} \\ \sigma_{xy} \end{Bmatrix} \vec{B^{\intercal}}\begin{Bmatrix} F_{x,1} \\ F_{y,1} \\ F_{x,2} \\ F_{y,2} \\ F_{x,3} \\ F_{y,3} \end{Bmatrix} \tag{5-3}$$

Based on the strain tensor, the principal strains and their orientation can be determined. On this basis, and by applying the constitutive relationships presented in Chapter 2.4, the stress state can be determined (the stresses are constant in the whole element for this particular case, but would be evaluated at each integration point for finite elements with more degrees-of-freedom) and the equivalent internal forces at nodes can be calculated:

$$f_{\text{int}} = t\int_A B^{\intercal} \cdot \sigma \cdot dA = t \cdot A \cdot B^{\intercal}\begin{Bmatrix} \sigma_{xx} \\ \sigma_{yy} \\ \sigma_{xy} \end{Bmatrix} \tag{5-4}$$

According to Hendriks et al.[5-16], the reinforcement should be modelled with the same order of interpolation as for the concrete elements. When using linear interpolations of the displacement field, as in current implementations of Compatibility-based Stress Fields, the reinforcement should be modelled with axial linear element with constant strain and stress. In the general case of inclined bars, the finite element used has two nodes with four degrees of freedom, as represented in Fig. 5-2. This element corresponds thus to a link (resisting only axial forces, without shear or bending strength).

This document is the intellectual property of the fib – International Federation for Structural Concrete. All rights reserved.
This PDF of fib Bulletin 100 is intended for use and/or distribution solely within fib National Member Groups.

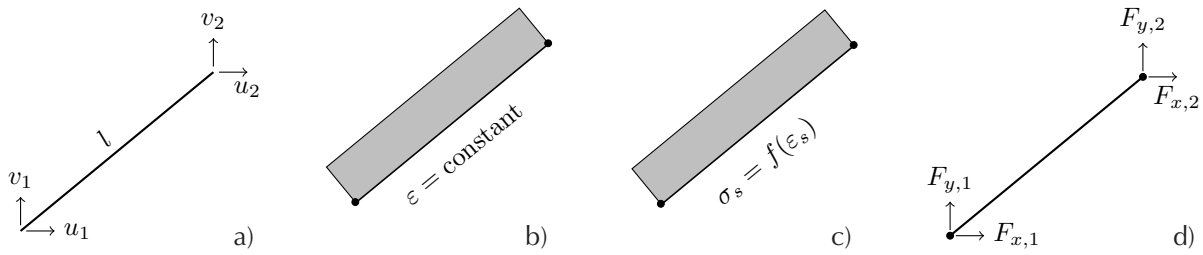


Fig. 5-2 1D Axial finite element: a) Degrees of freedom of displacement field; b) Strain; c) Stress state; d) Equivalent nodal forces to stress state

$$\begin{Bmatrix} u_1 \\ v_1 \\ u_2 \\ v_2 \end{Bmatrix} \vec{B}\{\varepsilon\}\vec{D}\{\sigma\}\overrightarrow{B^T} \begin{Bmatrix} F_{x,1} \\ F_{y,1} \\ F_{x,2} \\ F_{y,2} \end{Bmatrix} \qquad 5\text{-}5$$

The use of independent meshes for concrete and reinforcement has the benefit of leading to regular meshes with a finite element size independent of the spacing between bars. In this case, concrete and reinforcement finite elements do not share nodes and either an embedded discretization, or multi-point constraint (MPC) elements should be introduced to connect both meshes, as shown in Fig. 5-3. It should be noted that only the displacement in the direction of the reinforcement should be constrained by the MPC elements (no dowel effect considered).

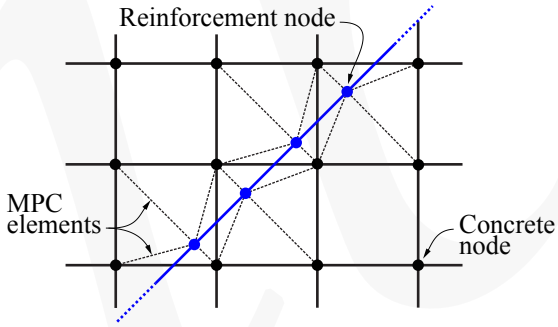


Fig. 5-3 Reinforcing bar FE mapped to concrete FE mesh using multi-point constraint (MPC) elements.

The bond between concrete and steel allows a composite response of the two materials, and the forces can be transfer between them. These bond stresses have a limit, usually denoted as fbd, that is used to evaluate the anchorage length, for instance. If this length is not available, slippage between reinforcement and concrete occurs that may govern the response. In regions such as column-beam joints, the global deformation is influenced by slippage occurring inside these regions[5-17].

An explicit bond stress-slip modelling can be introduced into the model, using spring-like elements to connect the concrete elements to the reinforcement. More specifically, to examine the favourable effect of transverse compression a 3-node, zero-length finite element can be used. This element has two nodes connected to the concrete FE and the third to reinforcement FE. A team[5-18] tested this approach to evaluate an experimental program. The multi-point constraint elements can be used in conjunction with bond elements.

This document is the intellectual property of the fib – International Federation for Structural Concrete. All rights reserved.
This PDF of fib Bulletin 100 is intended for use and/or distribution solely within fib National Member Groups.

The problems to be solved in compatibility-based stress fields are intrinsically nonlinear, so an iterative scheme is necessary to solve the system. The usual approach consists of a Newton-Raphson method or similar approaches, like the Modified and Quasi Newton-Raphson method that can lead to algorithms that are less time-consuming. The formulation is based on an expansion to Taylor's series:

$$f\left(x\right) \approx f\left(x_0\right) + \frac{\partial_f}{\partial_x}\left(x - x_0\right) \rightarrow K^{(i)} \cdot \Delta x^{(i+1)} = f - f_{\text{int}}^{(i)} \qquad 5\text{-}6$$

To obtain information about the deformation capacity of the elements, methods that allow the simulation to continue beyond a local or global maximum in the load-deflection response should be used (e.g. the arc-length procedure).

A convergence criterion has to be used for determining equilibrium on the iterative procedure. The criterion is often a norm of the residual force vector, the incremental displacement vector or a norm based on energy. The choice depends on the problem and the software, but norms based on displacements only should be avoided[5-16]. The actual value of the criteria should be defined based on preliminary tests.

5.2.3 Mesh topology considerations

The finite element model (FEM) has an associated mesh topology which can affect the results. When using the CST finite elements is important to correctly choose its orientation to avoid numerical errors. For the case of a shear failure dominated reinforced concrete beam modelled with constant strain triangles Muttoni et al.[5-5] reported a variation up to 17% on the ultimate load depending on the FE orientation. Based on this analysis, a zig-zag FE distribution, as shown in Fig. 5-4 was recommended.

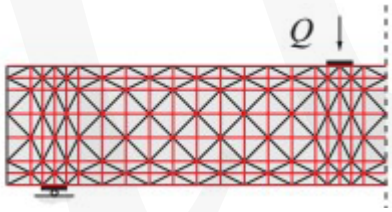


Fig. 5-4 Recommended finite element orientation for concrete triangular elements

Reinforcing bars located at the same level from beam soffit are transformed into a single element with the same area, since plane modelling is employed, see Fig. 5-5. Yet, for bond stress evaluation, it is necessary to account the correct perimeter of the single element, based on the actual diameters and number of bars.

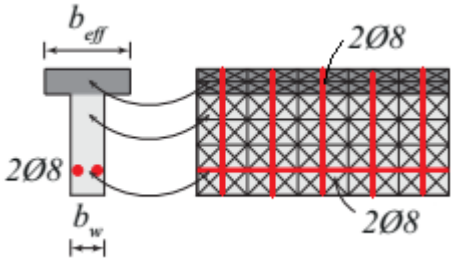


Fig. 5-5 Discretization of reinforcing bars (adapted from Muttoni et al.[5-5]).

This document is the intellectual property of the fib – International Federation for Structural Concrete. All rights reserved.
This PDF of fib Bulletin 100 is intended for use and/or distribution solely within fib National Member Groups.

When the bars are arranged in layers and then share nodes with the concrete elements, bar discretization must be adapted depending on the mesh size unless concrete and reinforcement are meshed independently. For a coarse mesh size, a reasonable simplification would be to group the bars into a single element. For a fine mesh size, the distribution should respect the position of each layer, with concrete elements between them. The use of independent meshes for concrete and reinforcement allows respecting the real position of the reinforcement regardless of the mesh size, see Fig. 5-3.

In the method presented, redirection of concrete stresses is either performed by the reinforcement or by acting loads. To obtain a good simulation in the former case, the spacing between reinforcing bars is instrumental and might be used to define the reference length for the finite elements. As a general recommendation, the mesh size should not be larger than the spacing of the transversal reinforcement. However, capturing some failure modes might require the use of a smaller mesh size. Therefore, the mesh size sensitivity of every model should be always evaluated, as indicated e.g. in *fib* Model Code 2010[5-20], in which it is prescribed that the values obtained from a sound model should not vary significantly from those evaluated from two other mesh sizes.

A parametric study on mesh size sensitivity carried out by Muttoni et al.[5-5]showed that the results are independent of the mesh size in the cases of: (i) uniaxial compression, (ii) uniaxial tension and, (iii) uniform shear. Yet, in the case of I beams with thin webs developing non-uniform shear, some dependency on the mesh size is observed. This dependency is larger for sections with thin webs and large amounts of transverse reinforcement, which fail due to concrete crushing. The smaller the mesh the more pronounced this strain localization effect is. Using the tension stiffening the mesh size sensitivity is reduced[5-7]. In this case, the failure owing to insufficient ductility of the reinforcement is consistently captured without relying on concrete compression softening. Nevertheless, for practical cases and regularly spaced reinforcement matching the mesh size it can be concluded that, generally, the results show an acceptable mesh size sensitivity.

Another aspect related to mesh size is the stress concentration produced in concrete elements smaller than the distance between reinforcing bars. The deviation of the compressive stresses by the reinforcement requires these stresses to converge where the bars are actually located. This implies mesh-dependent stress concentration, which is limited, in any case, by the yield condition. Three models with different degrees of refinement are presented in Fig. 5-6 to show this effect, where a panel subjected to pure shear is modelled with different mesh sizes. Note the concentration of stresses for the nodes where the reinforcements are in the refined models. These cases may be relevant when the spacing between stirrups is large. Spreading the reinforcement to match the concrete mesh can avoid mesh-dependent stress concentration.

This document is the intellectual property of the fib – International Federation for Structural Concrete. All rights reserved.
This PDF of fib Bulletin 100 is intended for use and/or distribution solely within fib National Member Groups.

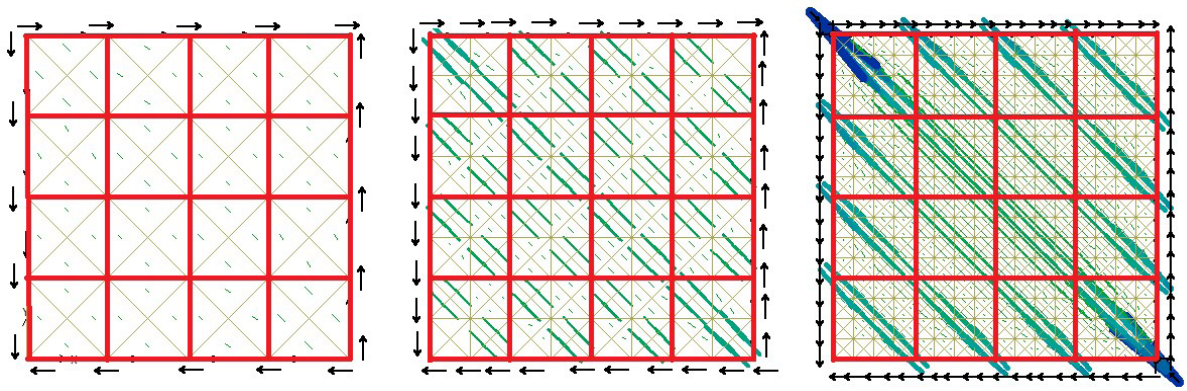


Fig. 5-6 Stress concentration dependent of mesh size

The aspect ratio of finite elements for concrete (i.e. the ratio between the largest to the smallest characteristic dimension of an element) can potentially influence the results as well. In general, the maximum recommended ratio in the literature on the finite element method, is limited to 1:3[5-20], [5-21]. However, Muttoni et al.[5-5] observed very reduced variations in the ultimate load (below 2%) when using different meshes with aspect ratios from 1:1 to 1:5 in a simply supported I-beam with two-point loads.

5.2.4 Additional considerations

Concrete finite elements located at the cover of the members cannot deviate the compression field as concrete tensile strength is always neglected in equilibrium in the Compatibility-based Stress Field method. To avoid local numerical instability in the cover, a modelling strategy is to neglect the cover region.

The previous approach might be excessively conservative, particularly when the cover thickness is not limited with respect to the overall depth of the member. A practical approach suitable to regions outside zones presenting strong discontinuities, is to extend the reinforcement to the free surface allowing to deviate the concrete stresses. A post-processing verification is necessary to check that the equivalent concrete tensile stress is in an acceptable range.

The previous approach should be avoided whenever spalling is expected in this region, as in beam-column joints or dapped-end beams (see Fig. 5-7) as in such cases failure may be governed by the stresses on the cover and by its spalling. Suitable modelling in these cases can be performed by introducing axial elements (perpendicular to the free edge), with a strength defined based on the tensile strength and fracture energy of concrete. In this respect, adopting for the cover a fictitious tensile strength of approximately 20% of the actual one is normally sufficient to avoid issues associated with spalling and to provide a realistic estimate of the strength[5-22], [5-5].

This document is the intellectual property of the fib – International Federation for Structural Concrete. All rights reserved.
This PDF of fib Bulletin 100 is intended for use and/or distribution solely within fib National Member Groups.

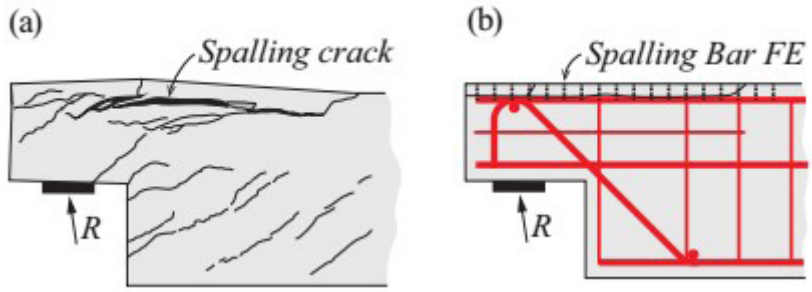


Fig. 5-7 Spalling cracks and link FE to simulate spalling strength; (a) crack pattern from tests; (b) Model geometry with spalling bar finite element (figure adapted from Muttoni et al.[5-5]).

An alternative approach to automatically check the anchorage region without explicitly introducing bond elements is by reducing the reinforcing bar diameter to limit its stress and thus to fulfil the bond strength (f_b), see Fig. 5-8.

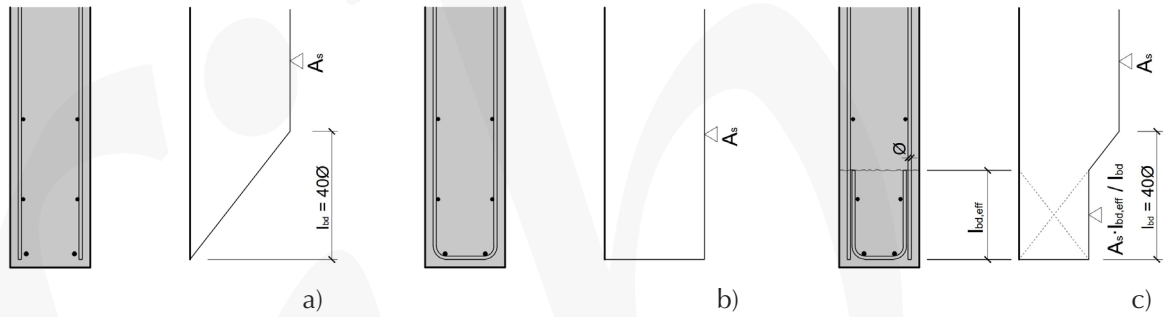


Fig. 5-8 Equivalent cross-section area to limit the bond stress at the end of the reinforcing bar. (a) near the reinforcement end (linear reduction) (b) Continuous reinforcement (no reduction); (c) reinforcement overlapped (adding reduced areas)

In cases where high bond stress occurs and governs the structural capacity, it is necessary to use explicit bond elements between the reinforcement and the concrete to evaluate the bond stresses and eventually the slip displacement between materials (see Section 5.2.2). These elements add a new degree-of-freedom for each reinforcement node. As discussed in Chapter 2, a simple elastic-plastic relationship for the slip-bond shear stresses using a high elastic stiffness (virtually rigid-plastic behaviour) allows for automatically verifying the anchorage of reinforcement according to code requirements.

Loads and reactions can be applied either directly on the corresponding nodes, or through a plate (with finite dimensions, width and thickness, as well as material properties). While the first approach is straightforward, it might lead to excessive pressures for concentrated forces when they are applied to a single node. This might be overcome by distributing the force into several nodes (according to the dimensions of the distribution plate), assuming a uniform stress distribution or even taking into account the stiffness of the plate (see e.g. Meléndez[5-23]). This approach allows meshing the concrete region independently of the dimensions of the plate.

When introducing a plate in the model, it should be realised that a very thick plate leads to high compression stresses near the edges of the plate, while a more flexible one presents a more uniform distribution. Hence, on a refined model, the correct dimensions, width and thickness must be used to get a more accurate solution. In case of modelling the plate with finite elements sharing nodes with the concrete elements, stresses perpendicular to

This document is the intellectual property of the fib – International Federation for Structural Concrete. All rights reserved.
This PDF of fib Bulletin 100 is intended for use and/or distribution solely within fib National Member Groups.

the direction to the load appear. To reduce this effect, it is possible to use a soft interface material, between the concrete and the plate to minimise the contribution of the plate in the concrete compression, see Fig. 5-9. A more refined version of this approach is to model the plate and use link elements between the plate and concrete to avoid friction effects.

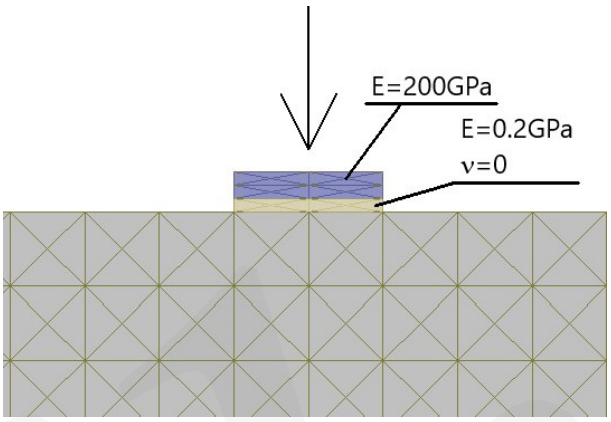


Fig. 5-9 Local modelling for concentrated load - Steel plate with a soft material

As a conclusion, it can be noted that the approach based on finite elements described in this section can be validated and be used with confidence for practical applications.

5.2.5 Interpretation of results

A critical evaluation of the results is fundamental for a correct analysis. Since the analysis shall comply with the requirements of limit analysis, it is necessary to check the structural ductility. This is generally ensured if the structural capacity is governed by reinforcement yielding (with a sufficiently ductile reinforcement). In these cases, the overall force-displacement curve of the structure should present a clear yield plateau. Otherwise, either reinforcement failure due to insufficient ductility occurs, or the response of concrete in compression is influencing the maximum load carried by the structure (particularly at the areas where the presence of positive transverse strains reduces the effective compression strength). These cases are, in general, mesh dependent and therefore it is advisable to evaluate the problem with different mesh sizes.

The analysis of the results should include checking of:

1. the global equilibrium, considering the distribution of loads and support reactions;
2. stresses in main reinforcement;
3. concrete compression stresses, with incidence on the zones next to the point loads and high transverse strains; and
4. the local equilibrium through the resultant forces at a section cut.

5.2.6 Example

The wall with an opening presented in Chapter 1, with the distribution of reinforcement presented in Fig. 1-7 (distributed reinforcement of $\phi 8$ @ 0.15 in each direction and face; principal horizontal reinforcement of 2 $\phi 16$ and 2 $\phi 12$ over and under the opening, respectively) was analysed again and some results are shown next. The modelling options and data used is also discussed.

This document is the intellectual property of the fib – International Federation for Structural Concrete. All rights reserved.
This PDF of fib Bulletin 100 is intended for use and/or distribution solely within fib National Member Groups.

A level-of-Approximation 3 is used, using the elasto-plastic relationships for the material response.

Materials:

Concrete C40

Strength	f_c = 40 MPa
Modulus of elasticity	E_c = 36.3 GPa (From Model Code 2010)[5-19]
Partial security factor	γ_c = 1.5
Equivalent plastic strength	$f_{cp} = \frac{40\ \text{MPa}}{1.5}\left(\frac{30}{40}\right)^{\frac{1}{3}} = 24.2\ \text{MPa}$
Concrete thickness	t = 20 cm

Steel S500B

Strength	f_y = 500 MPa
Modulus of elasticity	E_s = 200 GPa
Partial security factor	γ_s = 1.15
Plastic strength (?)	f_{yp} = 435 MPa

Loads

Point load	Q_k = 667 kN
Partial load factor	γ_F = 1.5
Applied load	Q_d = 1'000 kN
Width	b = 30 cm

Mesh size

The reference case for the mesh size is reinforcement spacing, i.e. 15 cm, in this case. All relevant geometry coordinates must be included in the grid that defines the mesh.

- X grid = [0; 0.7m; 1,95m; 2,65m] – from boundaries
- X grid = [0.05m; 0.65m; 2.0m; 2.60m] – from cover definition (distance from edge to reinforcing bar = 5cm)
- X grid = [0,20m; 0.35m; 0.50m; 0.80m; 0.95m; 1.10m; 1.25m; 1.40m; 1.55m; 1.70m; 1.85m; 2.00m; 2.15m; 2.30m; 2.45m] – from reinforcement position
- Y grid = [0; 2.20m; 2.85m; 3.55m] – from boundaries;
- Y grid = [0.05m; 2.15m; 2.90m; 3.50m] – from cover definition;
- Y grid = [0.20m; 0.35m; …; 2.00m; 2.30m; 2.45m; 2.60m; 2.75m; 3.05m; 3.20m; 3.35m] – from reinforcement position

The load is applied directly to the nodes.

This document is the intellectual property of the fib – International Federation for Structural Concrete. All rights reserved.
This PDF of fib Bulletin 100 is intended for use and/or distribution solely within fib National Member Groups.

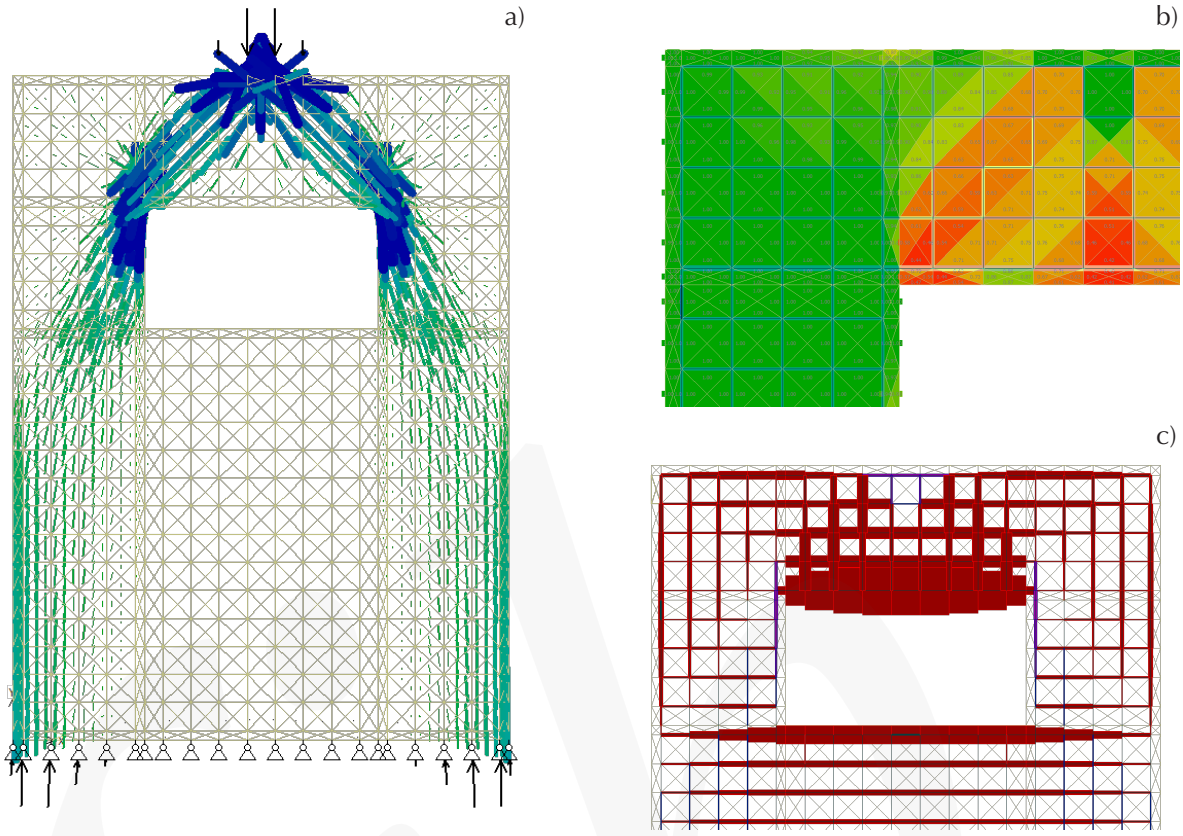


Fig. 5-10 Results for wall model: a) Principal stress in concrete. The size of the lines is proportional to the stress level and its orientation reflects the angle of the principal directions; b) Effect of transverse strains on concrete strength; c) Axial forces on the reinforcements

Comments:

- Due to symmetry, the load is divided in half and develops two diagonal struts near the top corners of the opening. The horizontal reinforcement, that yields, governs the variation of the angle. At the bottom of the opening, the distributed reinforcement allows for the deviation of the struts and they are concentrated near the lateral boundaries.
- A secondary load path, with tensile forces near the external edge of the corners is not significant due to the small amount of the reinforcement present
- The strut-and-tie model that can be derived from the results is shown in Fig. 5-11.

This document is the intellectual property of the fib – International Federation for Structural Concrete. All rights reserved.
This PDF of fib Bulletin 100 is intended for use and/or distribution solely within fib National Member Groups.

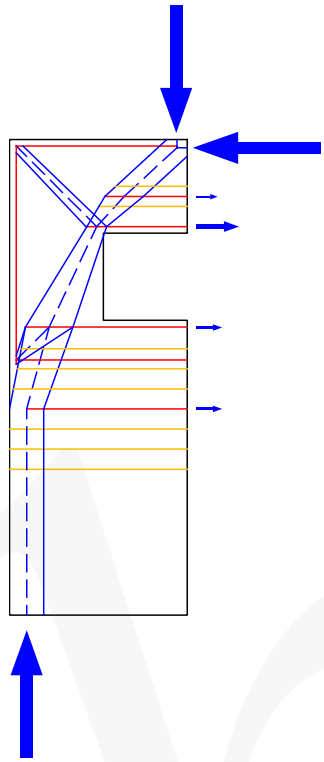


Fig. 5-11 Strut-and-tie model for Ultimate Limit State, derived from a LoA III modelling

To evaluate the influence of some options in modelling, a parametric investigation was performed as presented in Fig. 5-12:

- w/o cover – Model without cover.
- w/ cover + w/o plate – Model with cover and extended reinforcement. Load applied with point loads;
- w/ plate – Model with load applied in a plate with 3cm of thickness;
- w/ plate + soft - Model with load applied in a plate with 3cm of thickness and a soft material with 2cm;
- w/ Tension stiffening + Hardening – Model with load applied with point loads. The steel was modelled with Tension stiffening;
- w/ Tension stiffening – Model with load applied with point loads. The steel was modelled with Tension stiffening but without Hardening;

This document is the intellectual property of the fib – International Federation for Structural Concrete. All rights reserved.
This PDF of fib Bulletin 100 is intended for use and/or distribution solely within fib National Member Groups.

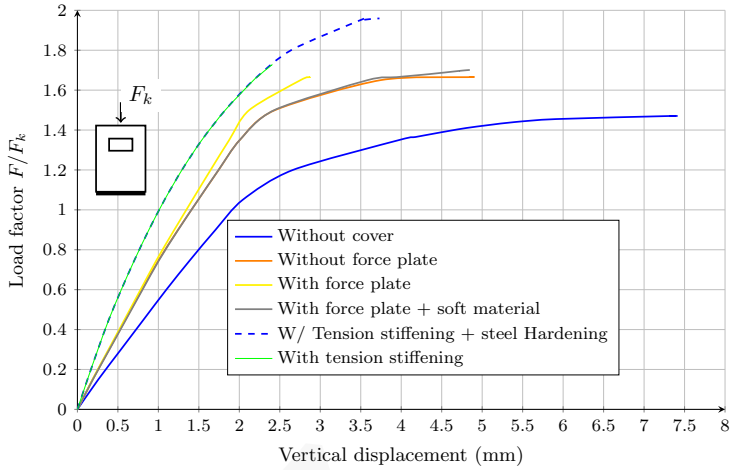


Fig. 5-12 Load-vertical displacement for different modelling options

In terms of strength, which is the basic outcome of Elastic-Plastic Stress Fields (EPSF), all models provide fairly comparable estimates (except when strain hardening is considered, yielding to a higher strength). Depending on the modelling approach, some differences yet appear in the deformation capacity of the elements. The responses with increased ductility correspond to cases where the tension-stiffening is neglected, while the deformation capacity reduces (increasing the strength) when this phenomenon is considered.

A Level of Approximation IV can also be used to check the Service Limit State as, for instance, crack opening and deformation. In Fig. 5-13, the stresses on the first two layers of reinforcement over the opening (ϕ16) and (ϕ8 Horizontal) and on the most stressed stirrup (ϕ8 Vertical) are presented (the values depend on the creep coefficient). From the analyses, it can be observed that cracking at the middle section occurs for a load equal to 30% of peak load; The service behaviour cannot be modelled with bare bars due to the difference on stiffness. The influence of creep and shrinkage is more pronounced in main reinforcement, at the top of the opening.

Materials:

Concrete C40

(Average) strength	f_c = 48 MPa
Modulus of elasticity	E_c = 36.3 GPa (From Model Code 2010)
Creep	φ = 1
Equivalent modulus	$E_{c,\varphi}$ = 18.15 GPa
Partial security factor	γ_c = 1.0
Equivalent plastic strength	$f_{cp} = \frac{48\ \text{MPa}}{1.0}\left(\frac{30}{48}\right)^{\frac{1}{3}} = 41.0\ \text{MPa}$
Concrete thickness	t = 20 cm
Shrinkage	ε_{cs} = -0.23 mm/m

Steel S500B

Strength	f_y = 500 MPa
Modulus of elasticity	E_s = 200 GPa
Partial security factor	γ_s = 1.0
Plastic strength	f_{sy} = 500 MPa

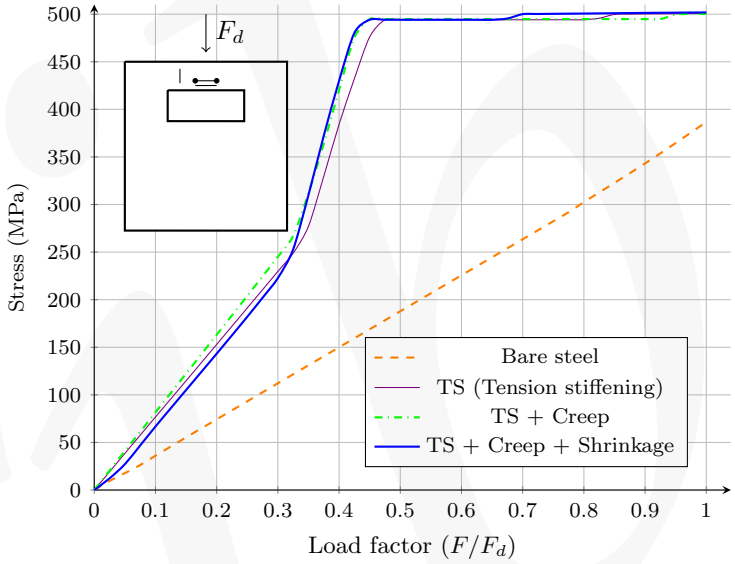
This document is the intellectual property of the fib – International Federation for Structural Concrete. All rights reserved.
This PDF of fib Bulletin 100 is intended for use and/or distribution solely within fib National Member Groups.

Properties for defining Tension stiffening

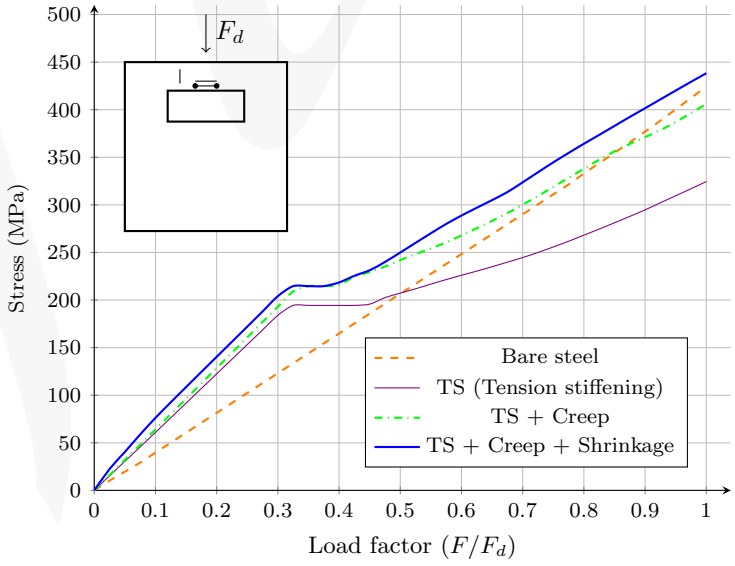
Concrete Tensile strength	f_{ct} = 3.5 MPa
Effective concrete area f8	$A_{c,8}$ = 130mm^2
Effective concrete area ϕ12	$A_{c,12}$ = 20 cm · (2 · 5 cm) = 200 cm^2
Effective concrete area ϕ16	$A_{c,16}$ = 20 cm · (2 · 5 cm) = 200 cm^2

Loads

Point load	Q_k =667 kN
Partial safety factor for load	γ_F = 1.0
Applied load	Q_d = 667 kN
Width	b = 30 cm

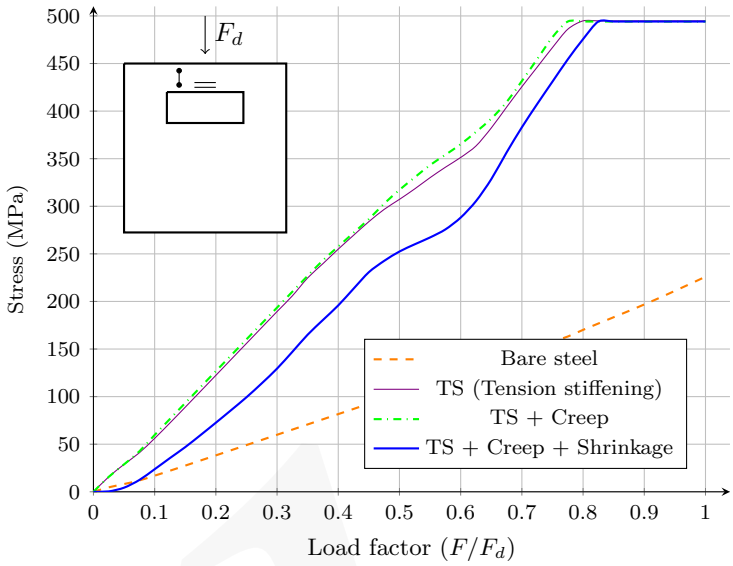


a) Stress on principal reinforcing bar (ϕ16) over the opening



b) Stress on horizontal reinforcing bar (ϕ8) over the principal reinforcement

This document is the intellectual property of the fib – International Federation for Structural Concrete. All rights reserved.
This PDF of fib Bulletin 100 is intended for use and/or distribution solely within fib National Member Groups.



c) Stress on vertical reinforcing bar ($\phi 8$)

5-13 Stresses on reinforcing bars; results for: (i) Bare steel without creep and shrinkage;(ii) Steel with tension stiffening effect without creep and shrinkage; (iii) Steel with tension stiffening effect with creep and without shrinkage, and (iv) Steel with tension stiffening effect with creep and shrinkage

5.3 Finite Element Limit Analysis of Reinforced Concrete Structures

5.3.1 Introduction

This section gives a brief introduction to the concept of Finite Element Limit Analysis (FELA), which provides a general framework for numerical stress field modelling. The concept combines a stress-based variant of the finite element method, convex optimisation algorithms and the theory of plasticity to determine the load-carrying capacity of reinforced concrete structures. The applicability of the method will be demonstrated by means of some examples and the advantages and challenges related to application of the concept are discussed. It is possible to establish upper- as well as lower bound FELA formulations. Only the lower bound concept is discussed in this section.

A general formulation of the theory of rigid plastic structures was established in the 1930s by Gvozdev[5-24], who already at that time demonstrated examples of application to reinforced concrete members in bending. The work of Gvozdev, however, remained unknown to the Western world until an English translation was published in 1960. Meanwhile, in the 1950s, similar theories were formulated independently in the West, mainly by Prager[5-25] and Drucker[5-26]. Braestrup[5-27] has recently published a detailed historical review of the development of limit analysis and plastic theory. The work by Gvozdev and by Prager & Drucker includes the formulation of the important extremum principles. These are the upper bound theorem, the lower bound theorem and the uniqueness theorem. Based on these theorems, researchers and engineers have over the years developed practical methods for determination of the load carrying capacity of structures with plastic material behaviours. Most well-known are perhaps the yield line method[5-28] and the strip method for analysis of slabs[5-29]. The yield line method is consistent with the upper bound theorem while the strip method is based on the lower bound theorem. These methods, along with the lower bound strut-and-tie models and the stringer-panel models, are widely used by structural

This document is the intellectual property of the fib – International Federation for Structural Concrete. All rights reserved.
This PDF of fib Bulletin 100 is intended for use and/or distribution solely within fib National Member Groups.

engineers. The methods are extremely useful because practical problems can be solved approximately in this way by simple hand calculations. This is possible mainly because solutions based on the upper bound methods do not require engineers to solve the equilibrium equations, while solutions based on lower bound methods need not fulfil compatibility requirements.

The upper- and lower-bound methods mentioned above were originally developed as hand-calculation methods by which a given structural problem can be formulated as an optimisation problem, either by minimising an upper-bound solution or, by maximising a lower-bound solution. However, the quality of the solutions obtained by hand calculations depends in many cases on the experience and engineering intuition of the structural engineers. And often there are too many optimisation parameters to be handled by manual calculations. Hence, hand-calculated solutions might be too conservative if a lower-bound method is used, while upper bound solutions might on the other hand be unsafe. As improvements, many computer-based procedures have therefore been developed to assist the engineers in obtaining the most optimal solutions. These improvements, however, have their limitations, primarily because they adopt the assumptions of the particular hand calculation methods as a basis for numerical automated analysis. For instance, the optimal solution according to the strip method would in many cases still be a lower-bound solution as the method does not account for torsional moments. Likewise, when using software-based methods to determine the most critical yield line patterns in slabs, the engineer obtains the most critical load parameter. However, being an upper-bound method, the engineer would not be able to determine the internal forces (moments and transverse shear forces), nor the distribution of reactions.

In the end, it seems obvious that a general numerical tool to model stress fields and the load-carrying capacity of various types of reinforced concrete structures must somehow adopt the finite element method as a fundamental basis. However, to have practical relevance, such a design tool must be able to handle large-scale problems with reasonable computational time. The framework of such a tool will be described in the following.

5.3.2 Lower bound optimisation problem

The task of determining the load-carrying capacity of a rigid-plastic structure can be formulated as an optimisation problem. Based on the lower bound theorem, the optimisation task would be to look for the stress field (among all possible stress fields that satisfy the equilibrium and the static boundary conditions) that provides the highest load factor λ without violating the yield conditions. Obviously, the size of the problem and the number of stress fields that can be investigated in practice would be very limited, unless computer-based methods are adopted. That is, the problem has to be solved numerically. The method described in the following uses a mesh discretisation known from the finite element method in order to translate the continuum mechanical problem into a numerical format. The method is therefore called Finite Element Limit Analysis (FELA). However, except from the similar mesh discretisation procedures, the analysis strategy required in FELA is distinctly different than what is normally used in the classical finite element method. In FELA there is no unique relationship between stresses and strains since the concept is based on the assumption of rigid-plastic material. This eventually means that in a lower bound formulation of FELA, the response of each finite element (and in the end the response of the entire structure) cannot, as done in classical FEM, be based on

This document is the intellectual property of the fib – International Federation for Structural Concrete. All rights reserved.
This PDF of fib Bulletin 100 is intended for use and/or distribution solely within fib National Member Groups.

an approximation of the displacement field (the shape functions). Instead, equilibrium elements are used (the term lower-bound elements is also used). In simple terms, this means that instead of having a stiffness matrix, equilibrium elements are formulated by directly establishing the equilibrium equations that relate the forces acting on the element to the stress field assumed within the element. The stress field of each element is described by a number of stress variables at the "nodes" of the element and can, similar to the shape functions of classical finite elements, be more or less sophisticated (e.g. linear stress variation versus quadratic stress variation).

The fact that the lower bound formulation of FELA only involves equilibrium and yield conditions has the consequence that the number of stress variables to be determined will, in general, exceed the number of equations that are available. So, unlike a linear elastic problem where only one solution exists, there can in principle be an unlimited number of admissible stress fields (solutions) for a problem formulated in FELA. For illustration, the reader may think of a continuous beam over two spans subjected to a uniform load. Here, the moment diagram of course varies parabolic, but if only equilibrium conditions are considered, then the hogging moment at the intermediate support (the redundant) has no unique solution unless compatibility conditions as well as yield conditions are imposed. Of course, according to the lower-bound theorem, the admissible stress field to be selected is the one that maximises the load factor. This turns in fact the problem into an optimisation problem where the optimisation conditions consist of equations of equilibrium and the yield conditions in the form of inequalities. The general lower bound FELA problem can therefore be stated as follows:

$$\begin{aligned} &\text{maximize} && \lambda \\ &\text{subjected to} && H\beta = R\cdot\lambda + R_0 \\ & && f(\beta_i) \le 0, \quad i = 1, 2, \ldots, m \end{aligned} \qquad 5\text{-}7$$

where vector R_o is the constant part of the load acting on the model (e.g. dead load) and $R\cdot\lambda$ is the scalable part of the load with R representing e.g. the live load. The constraints of the optimisation problem consist of a set of linear equalities (which ensure equilibrium) and a set of inequalities (ensuring that the stress field does not violate the yield criteria or yield function, $f(\beta i)$). In Equation 5-7, H is the global equilibrium matrix, β is the stress vector and m the number of check points for the yield function. It is a fundamental presumption of plastic theory that yield criteria are convex[5-30]. Thus (5-7) represents a convex optimisation problem. The first framework for FELA as well as lower bound finite elements to model solids, plates and slabs were presented in the beginning of the 1970s[5-31], [5-32]. These pioneer works adopted linear programming to optimise the load carrying capacity. To do so, the convex and non-linear yield conditions had to be linearised resulting in a multiple of linear constraints. Since then, much more advanced optimisation techniques, such as second-order cone programming and semidefinite programming, have been developed. These techniques have shown to be extremely suitable and efficient to the type of constraints, i.e. the yield conditions, often encountered in structural concrete mechanics[5-33], [5-34], [5-35], [5-36], [5-38]. The plane-stress problems presented herein will be formulated as second-order cone optimisation problems. More details can be found in the following.

While the solution to problem (5-7) does not produce the displacement field directly, one can in fact obtain a collapse mode, i.e. a velocity field, from the problem known as dual optimisation problem. The dual problem is linked to the primal problem (5-7) via the

This document is the intellectual property of the fib – International Federation for Structural Concrete. All rights reserved.
This PDF of fib Bulletin 100 is intended for use and/or distribution solely within fib National Member Groups.

complementarity condition, which states that plastic strains can only occur when the stress state is on the yield surface[5-39]. From this, the plastic strain rates and corresponding velocities can be determined under the assumption of associated flow (i.e. the normality condition, which is a requirement for both the upper and lower bound theorem). Solving a lower bound problem will therefore not only give a safe and statically admissible stress field, but also the velocity field associated with the determined stress field.

5.3.3 Equilibrium finite elements for analysis of plane stress problems

Equilibrium elements to analyse various types of structural problems have been developed since the 1970's[5-39], [5-40], [5-41], [5-42]. More recently, tailor-made elements to model reinforced concrete structures and precast reinforced concrete structures have also been formulated[5-36], [5-38], [5-43], [5-44]. Here, only a brief description of the finite elements required to model reinforced concrete structures in plane stress conditions will be given. This includes:

- A plane, triangular element to model the concrete, which may contain an orthogonal mesh of reinforcement
- A linear element to model discrete reinforcing bars/stringers

To model plane stress fields, the favoured element is a triangular element with a linear stress variation (LST element). Poulsen & Damkilde[5-42] have proposed such an element. The linear stress field means that it is sufficient to check the yield function in the corners of the element to ensure a safe stress field. Using higher order stress variations would lose this property, hence making it difficult to ensure a strict lower bound solution. The stress field within an LST element, see Fig. 5-14, can be fully described by linear combinations of the stress vectors at the vertices of the element. The stress variables of an element are given in global coordinates and appear as follows:

$$\sigma_{el} = \begin{bmatrix} \sigma_1 \\ \sigma_2 \\ \sigma_3 \end{bmatrix}, \text{ and } \sigma_i = \begin{bmatrix} \sigma_{xi} \\ \sigma_{yi} \\ \tau_{xyi} \end{bmatrix} \qquad 5\text{-}8$$

where σ_i is the stress state in the i_{th} corner node. The stress variables are shown in Fig. 5-14 together with the tractions q_i given in local coordinates of the element boundary, which must be in equilibrium with adjacent elements (i.e. condition of traction continuity). Due to the linear variation of the stress field, traction continuity must be enforced at both ends of each of the three element boundaries. As usual, the traction q_i can be expressed by linear combinations of the stresses σ_i by means of coordinate transformations, see e.g. Poulsen & Damkilde[5-42] and Herfelt[5-38] for details. In addition to the conditions of traction continuity, internal equilibrium between the stress field and the external load must also be ensured. The element is subjected to surface load γ_x and γ_y acting uniformly on the entire surface area A of the element. The applied load is equivalent to the two nodal forces q_x and q_y acting in the centre of the element as shown in Fig. 5-14. That is:

$$q_{el} = \begin{bmatrix} q_x \\ q_y \end{bmatrix} = A \begin{bmatrix} \gamma_x \\ \gamma_y \end{bmatrix} \qquad 5\text{-}9$$

This document is the intellectual property of the fib – International Federation for Structural Concrete. All rights reserved.
This PDF of fib Bulletin 100 is intended for use and/or distribution solely within fib National Member Groups.

The conditions of internal equilibrium as well as traction continuity altogether results in a total of 14 equilibrium equations for the element, which may be written as:

$$q_{el} = h_{el} \cdot \sigma_{el} \qquad 5\text{-}10$$

where h_{el} is called the element *equilibrium matrix*. A detailed derivation of h_{el} can be found in above mentioned references. In this context, it is noted that the global equilibrium matrix H mentioned in Equation (5-7) is established by assembling h_{el} of all elements. As discussed, the forces acting on the element edges are the tractions, hence, external line loads are therefore applied as tractions. The line loads may vary linearly. Point loads can approximately be applied in the same manner, where an appropriate length is chosen.

Reinforced concrete structures normally contain an orthogonal mesh of reinforcement as well as concentrated reinforcing bars acting as ties/stringers. The mesh reinforcement is normally modelled as a smeared contribution where perfect bond with the concrete is assumed. This means that the stresses carried by the mesh reinforcement (especially if the tensile strength of concrete is neglected) can be incorporated into the stress field of the LST element by interpreting σ_{el} as so-called *total stresses*. It is in fact only a matter of bookkeeping of the yield criteria for concrete and reinforcement, respectively, to separate the portion carried by the concrete from the portion carried by the mesh reinforcement.

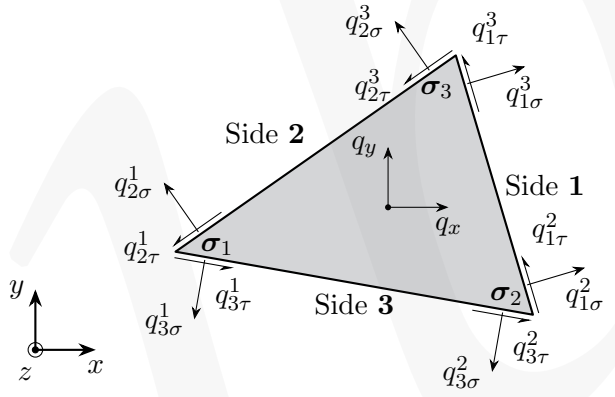


Fig. 5-14 LST element – a lower bound finite element with linear variation of stresses

To model a concentrated reinforcing bar, it is necessary to consider its interaction with the concrete and for this reason, an equilibrium bar element is needed. The stress field (i.e. variation of the axial force) assumed for the bar element must in this context be compatible with the linear variation of the shear stress, that can act along the boundary of the LST element. Hence, a quadratically varying axial force is required. Such an element is illustrated in Fig. 5-15.

The necessary equilibrium equations of the bar element can be established by considering an infinitesimal length of the bar subjected to a linearly varying shear force. This is what gives rise to the quadratic variation of the axial force. At the ends of the bar element, equilibrium is enforced in global coordinates, hence, for bar elements with a free end, i.e. no adjacent bar elements, the axial force is therefore required to be zero.

This document is the intellectual property of the fib – International Federation for Structural Concrete. All rights reserved.
This PDF of fib Bulletin 100 is intended for use and/or distribution solely within fib National Member Groups.

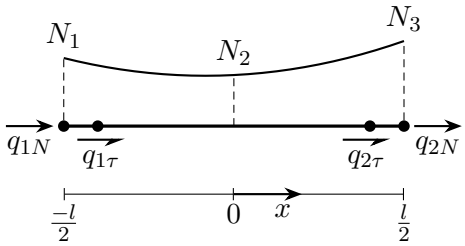


Fig. 5-15 Lower bound bar element with stress variables and nodal forces.

5.3.4 Yield criterion for plane stress states

As mentioned above, the stress field within the LST element represents the total stresses, which comprise stresses carried by the concrete and the orthogonal mesh reinforcement, respectively. This may be expressed as follows when the total stresses are transformed to the coordinate system (x',y') of the mesh reinforcement:

$$\begin{pmatrix} \sigma_{x'm} \\ \sigma_{y'm} \\ \tau_{x'y'm} \end{pmatrix} + \begin{pmatrix} \tilde{\sigma}_{x's} \\ \tilde{\sigma}_{y's} \\ 0 \end{pmatrix} = \begin{pmatrix} \cos^2\phi & \sin^2\phi & 2\sin\phi\cos\phi \\ \sin^2\phi & \cos^2\phi & -2\sin\phi\cos\phi \\ -\sin\phi\cos\phi & \sin\phi\cos\phi & \cos^2\phi - \sin^2\phi \end{pmatrix} \begin{pmatrix} \sigma_x \\ \sigma_y \\ \tau_{xy} \end{pmatrix} \qquad 5\text{-}11$$

where ϕ is the angle between the (x,y)-system, to which σ_{el} is referred, and the (x',y')-system, see Fig. 5-16. Subscript *m* indicates concrete stresses (matrix material) and subscript *s* indicate reinforcement stresses (steel). Note that as usual, reinforcement steel is assumed to act as bars unable to carry shear stresses (i.e. dowel action is neglected). Note further that and $\tilde{\sigma}_{x's}$ and $\tilde{\sigma}_{y's}$ are known as equivalent reinforcement stresses, which means that the axial force in each bar is smeared over a representative area of the concrete cross section. That is:

$$\begin{pmatrix} \tilde{\sigma}_{x's} \\ \tilde{\sigma}_{y's} \end{pmatrix} = \frac{1}{t} \begin{pmatrix} A_{sx'} & 0 \\ 0 & A_{sy'} \end{pmatrix} \begin{pmatrix} \sigma_{sx'} \\ \sigma_{sy'} \end{pmatrix} \qquad 5\text{-}12$$

where $A_{sx'}$ and $A_{sy'}$ are the reinforcement area per unit length in the two orthogonal directions, t is the out of plane thickness of the concrete and $\sigma_{sx'}$ and $\sigma_{sy'}$ are the stresses carried by the mesh reinforcement. In the following, the reinforcement is assumed to have a tensile yield stress of fy while the compression strength is neglected. Hence, $\sigma s_{x'}$ and $\sigma_{sy'}$ shall not exceed fy and furthermore be non-negative. This results in the following linear yield criterion for the reinforcement:

$$\begin{aligned} 0 \le \tilde{\sigma}_{x's} &\le \frac{A_{sx'}}{t} f_y \\ 0 \le \tilde{\sigma}_{y's} &\le \frac{A_{sy'}}{t} f_y \end{aligned} \qquad 5\text{-}13$$

A similar yield criterion applies to the stresses of the bar elements representing concentrated reinforcement ties/stringers. It should be noted that it is possible to include the compression strength of the reinforcement in the yield criterion. This may e.g. be useful in regions close to the supports, where a significant fraction of the reaction may be carried by the reinforcement.

This document is the intellectual property of the fib – International Federation for Structural Concrete. All rights reserved.
This PDF of fib Bulletin 100 is intended for use and/or distribution solely within fib National Member Groups.

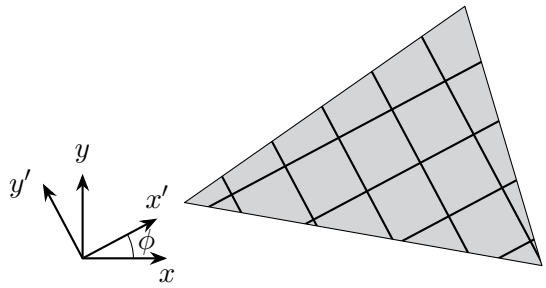


Fig. 5-16 Direction of the orthogonal reinforcement mesh (x′,y′) within the LST element.

For limit analysis of concrete, it is normal to adopt a Mohr-Coulomb failure criterion with a tension cut-off[5-30]. Furthermore, the tension cut-off usually corresponds to the assumption of zero tensile strength. When dealing with plane stress problems, this simplified criterion takes the following form:

$$\begin{aligned} \sigma_{1m} &\le 0 \quad (a) \\ -\sigma_{2m} - \upsilon \cdot f_c &\le 0 \quad (b) \end{aligned} \qquad 5\text{-}14$$

where $\sigma_{1m} \ge \sigma_{2m}$ are the principal concrete stresses, f_c is the standard uniaxial compression strength of the concrete and υ is the effectiveness factor, which accounts for the fact, that concrete is not a rigid-perfectly plastic material[5-30]. This factor, which is also discussed elsewhere in this bulletin, can be implemented in FELA with different levels of sophistication – an issue that will be discussed further later on. The largest and the smallest principal stress in the plane, where the concrete is subjected to a plane stress state, can be obtained by the transformation formulas. Criterion (5-14a) and (5-14b) can therefore be formulated in terms of the concrete stresses in the (*x′*, *y′*)-system as follows:

$$\begin{aligned} &\frac{\sigma_{x'm} + \sigma_{y'm}}{2} + \sqrt{\left(\frac{\sigma_{x'm} - \sigma_{y'm}}{2}\right)^2 + \tau_{x'y'm}^2} \le 0 \quad (a) \\ &-\left(\frac{\sigma_{x'm} + \sigma_{y'm}}{2} - \sqrt{\left(\frac{\sigma_{x'm} - \sigma_{y'm}}{2}\right)^2 + \tau_{x'y'm}^2}\right) - \upsilon \cdot f_c \le 0 \quad (b) \end{aligned} \qquad 5\text{-}15$$

The following auxiliary variables are introduced[5-45]:

$$\begin{aligned} \alpha_1 &= -\frac{1}{2}\left(\sigma_{x'm} + \sigma_{y'm}\right) \quad (a) \\ \alpha_2 &= \frac{1}{2}\left(\sigma_{x'm} - \sigma_{y'm}\right) \quad (b) \\ \alpha_3 &= \upsilon \cdot f_c - \alpha_1 \quad (c) \end{aligned} \qquad 5\text{-}16$$

By substituting the auxiliary variables into (5-15), the following reformulation of the Mohr-Coulomb criterion with zero tension cut-off for plane stress problems is obtained:

$$\begin{aligned} \sqrt{\alpha_2^2 + \tau_{x'y'm}^2} - \alpha_1 &\le 0 \quad (a) \\ \sqrt{\alpha_2^2 + \tau_{x'y'm}^2} - \alpha_3 &\le 0 \quad (b) \end{aligned} \qquad 5\text{-}17$$

This document is the intellectual property of the fib – International Federation for Structural Concrete. All rights reserved.
This PDF of fib Bulletin 100 is intended for use and/or distribution solely within fib National Member Groups.

It is important to mention here that the reformulation of (5-14) into (5-17) is not just an exercise of mathematical manipulation, but in fact a result, which is crucial for the further implementation of the optimisation problem. From the criteria in (5-17), the reader may note that the surfaces of two quadratic cones in the $(\alpha_2, \tau_{x'y'm}, \alpha_1)$- and in the $(\alpha_2, \tau_{x'y'm}, \alpha_3)$-space, respectively, are obtained when the inequality sign is replaced by an equality sign. It can therefore be shown that the reformulated criteria perfectly fits the format of second-order programming, see e.g. Nielsen[5-45] and Poulsen et al.[5-46] which also contains a reformulation the Mohr-Coulomb criterion with non-zero tension cut-off into a seconder-order cone format. A procedure for how to establish the conical criteria in matrix form for implementation in FELA can also be found in Poulsen et al.[5-46]. The practical implication of this is that the problem can be solved extremely fast by use of interior point methods. In fact, modern and commercial solvers in this respect (see e.g. MOSEK ApS[5-47]) are capable of solving optimisation problems with hundreds of thousands of variables and constraints in a matter of minutes on a standard laptop. For details, see e.g. Herfelt[5-38].

5.3.5 Examples

To demonstrate the applicability of FELA, a few calculation examples are presented below. The calculated results are compared with analytical and elastic-plastic FE-solutions and convergence as well as computational times are discussed.

5.3.5.1 Deep beam with isotropic mesh reinforcement - uniform load and uniform shear reactions

The first example is a deep beam subjected to a uniformly distributed pressure, p, acting on the top boundary. The beam is reinforced with an isotropic mesh reinforcement and supported along the left and right boundaries in the y-direction, i.e. shear supports, see Fig. 5-17. The beam is not supplied with any concentrated bars at the bottom boundary. The exact plastic solution to this problem is well known[5-30] and given as:

$$p^* = \frac{4\Phi \cdot h^2 \cdot \upsilon \cdot f_c}{\left(1+\Phi\right)L^2} \leq \upsilon \cdot f_c \qquad 5\text{-}18$$

where Φ is the mechanical reinforcement ratio defined as:

$$\Phi = \frac{A_s}{t}\frac{f_y}{\upsilon \cdot f_c} \qquad 5\text{-}19$$

Here, f_c is the uniaxial compression strength of concrete, f_y is the yield stress of the reinforcement, t is the thickness of the member, υ is the effectiveness factor and A_s is the area per. unit length of the isotropic reinforcement mesh. Using h = 2 m, L = 6 m, $\upsilon \cdot f_c$ = 20 MPa, and Φ= 0.075, the exact limit load for the deep beam is p^* = 0.62 MPa. The symmetry is utilised for the computations and only half of the beam is analysed using a structured mesh. The right side of Fig. 5-17 shows one of the adopted mesh configurations while the left side of the figure shows the triangular zones with homogeneous stress fields, which form the basis of the exact solution (Eq. 5-18).

This document is the intellectual property of the fib – International Federation for Structural Concrete. All rights reserved.
This PDF of fib Bulletin 100 is intended for use and/or distribution solely within fib National Member Groups.

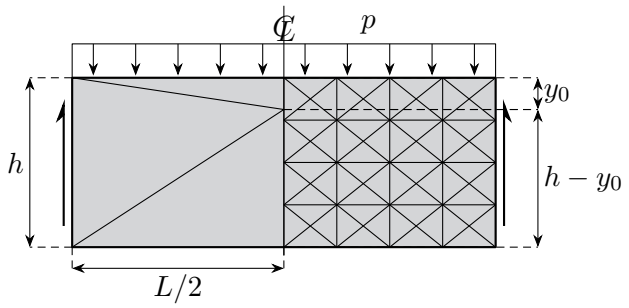


Fig. 5-17 Deep beam with isotropic mesh reinforcement subjected to uniform pressure p at top face. Left side indicates the homogeneous triangular stress fields of the exact solution and right side shows one of the mesh configurations adopted for numerical analysis (n_{el} = 64).

Table 5-1: Limit load, p, of the deep beam vs. number of finite elements n_{el}, error relative to the exact solution and computational time.

n_{el}	p [MPa]	Error [%]	Time [s]
64	0.5555	10.42	0.15
256	0.6053	2.40	0.68
1'024	0.6177	0.39	3.57
4'096	0.6191	0.17	16.18
16'384	0.6193	0.13	67.36

The results obtained by FELA are summarised in Table 5-1. It is notable that the result, p, approaches the exact limit load, p^*, from below as n_{el} and thereby the model fineness increases. This is a general and consistent feature of FELA when lower bound elements are used. A similar consistency in terms of result convergence cannot be obtained in non-linear FE-analyses of concrete structures, where a rough element mesh may result in a load carrying capacity which can be much higher than the correct solution. Hence, the fact that lower bound solutions are always obtained with FELA, even when using a very rough element mesh, is an important feature from a practical point of view. Another important feature of FELA is the computational efficiency, especially when it comes to large-scale problems. As shown in Table 5-1, the increase in computational time is approximately proportional to the problem size, n_{el}.

5.3.5.2 Deep beam with opening and with combination of mesh reinforcement and concentrated bars

Fig. 5-18 shows a deep beam with an opening, reinforced with a mesh reinforcement as well as concentrated reinforcement bars. The example is a benchmarking case first introduced by Schaich et al.[5-48] to demonstrate application of the classical strut-and-tie method. The example has since been used several times, see e.g. Muttoni et al.[5-49] and Niketic[5-50]. Here, the example is modelled by use of the aforementioned LST element with incorporation of the mesh reinforcement and by use of the lower bound bar element

This document is the intellectual property of the fib – International Federation for Structural Concrete. All rights reserved.
This PDF of fib Bulletin 100 is intended for use and/or distribution solely within fib National Member Groups.

to represent the concentrated reinforcement bars. In the calculation the yield stress of the reinforcement is taken as f_y = 435 MPa and the uniaxial compression strength of concrete is f_c = 20 MPa. For convenience υ = 1.0 has been adopted, which will be further discussed below. The beam is analysed using an unstructured mesh, and the results obtained by FELA are summarised in Table 5-2, where the limit load, *F*, and the required computational time are shown for different mesh densities, n_{el}. Note that the load *F* is in the model modelled as a line load distributed over a length of 0.70 m.

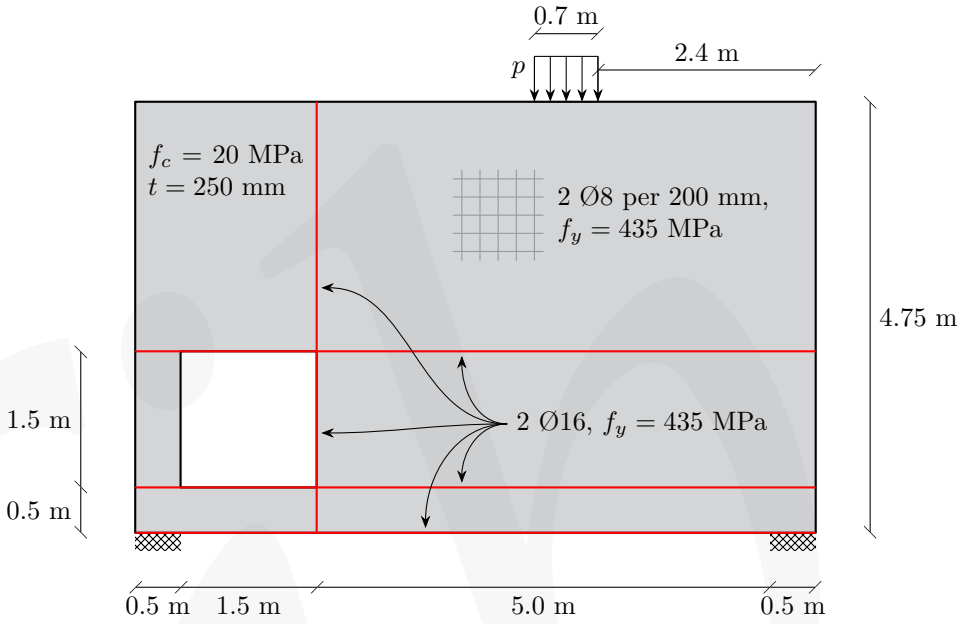


Fig. 5-18 Deep beam with opening. Reinforcement is shown schematically and assumed to be anchored by U-bars along the boundaries.

Table 5-2: Limit load, *F*, of the deep beam with opening vs. number of finite elements, n_{el}, and computational time.

Number of elements, n_{el}	Collapse load *F* [kN]	Computational time [s]
875	2'437	2.26
2'046	2'662	5.81
3'513	2'694	7.78
5'361	2'700	13.01
7'886	2'711	38.41
12'083	2'712	65.29

This document is the intellectual property of the fib – International Federation for Structural Concrete. All rights reserved.
This PDF of fib Bulletin 100 is intended for use and/or distribution solely within fib National Member Groups.

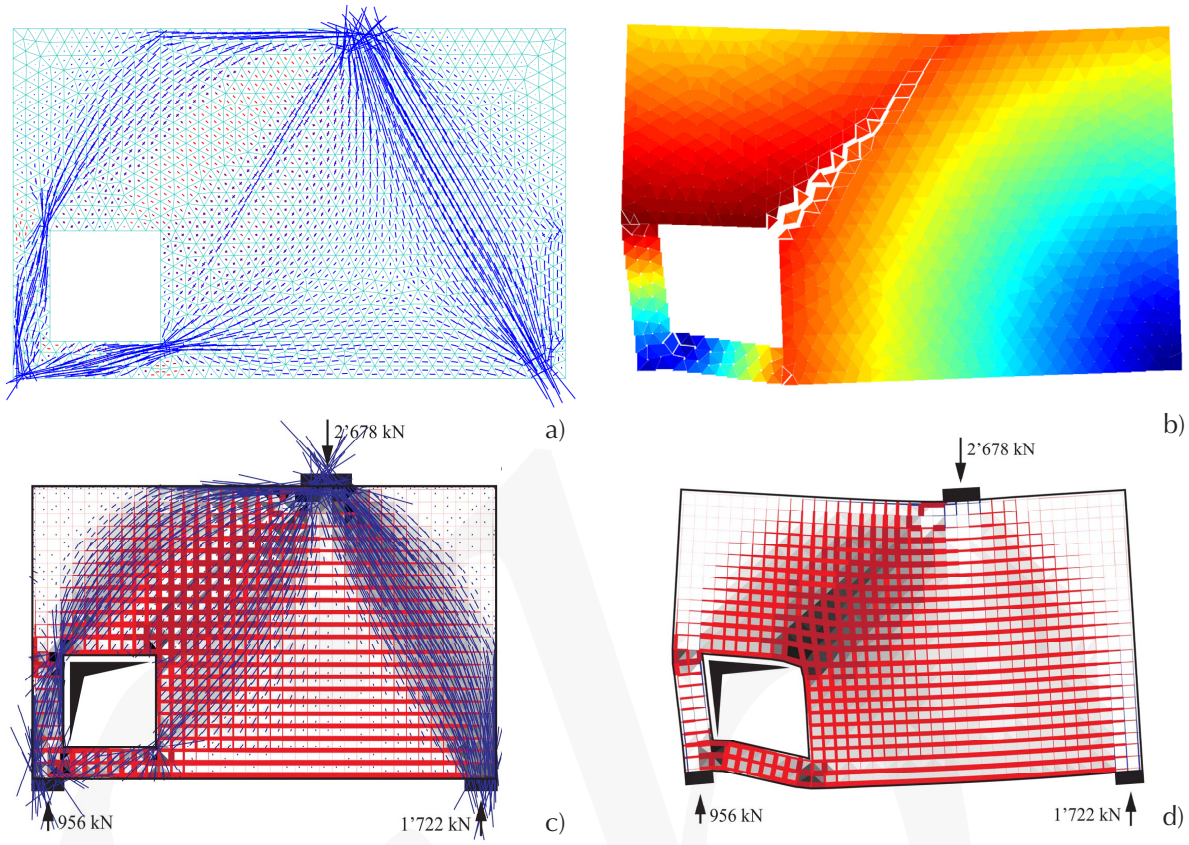


Fig. 5-19 (a) and (b) shows results obtained by use of FELA, principal stresses (blue indicates compression and red indicates tension) & collapse mode for model with n_{el} = 2046. (c) and (d) are elasto-plastic results (adapted from Niketic[5-50]), showing principal compression stresses in concrete and tension stresses in reinforcement & displacements at collapse load.

Like in the previous example, the calculated limit load increases as the mesh is refined, which is to be expected for a lower bound model. Furthermore, the computational time here is also nearly proportional to the problem size. The convergence tendency suggests that F = 2'712 kN may be taken as the load carrying capacity of the established model. To indicate how the structure carries the ultimate load, the corresponding principal stress field has been plotted in Fig. 5-19a. The stresses correspond to the total stresses determined within the LST element and stresses in the concentrated bars are not shown. It can be seen that the stress field to the right of the load resembles a direct compression strut that runs from the load to the support. To the left of the load, the stresses have to deviate around the opening. Consequently, the stress field here presents a more complex system of struts and ties. Note also that the stress field in the part below the opening and in the part to the left of the opening clearly indicate shear- and bending actions similar to the behaviour of restrained beams. As described above, it is possible from the results of FELA to extract information about the collapse mechanism in the form of a velocity field (i.e. the plastic strain increments). The result is shown in Fig. 5-19b,and based on engineering judgments the mechanism is consistent with the corresponding stress field. The collapse mechanism clearly identifies development of four plastic hinges in the beam- and column parts at the opening (as suggested by the stress field). Furthermore, the deviation of the load path around the opening gives rise to a local tension failure mode (development of a diagonal crack), which shows that the mesh reinforcement is at yield in this region. As mentioned, this benchmarking example has been used in several

This document is the intellectual property of the fib – International Federation for Structural Concrete. All rights reserved.
This PDF of fib Bulletin 100 is intended for use and/or distribution solely within fib National Member Groups.

studies. The problem has, for instance, been analysed under similar assumptions for the material response by Muttoni et al.[5-49], see also Niketic[5-50]. They used an elasto-plastic finite element model, where the reinforcement (mesh as well as concentrated bars) are modelled as individual bars with perfect bond to the concrete. Furthermore, the model neglects the tensile strength of the concrete and has the possibility - during the incremental load-displacement analysis - to determine the value of the effectiveness factor υ at each point based on the calculated transverse strains (further discussions are provided below). Fig. 5-19c and Fig. 5-19d show the results obtained by Muttoni et al., where the collapse load was found to be F = 2'678 kN. This is practically the same as the result obtained by FELA and also checked manually with rigid-plastic upper-bound solutions[5-50]. It is furthermore interesting to see the similarities between the stress field obtained by the elasto-plastic FE-analysis and the stress field found by use of FELA. It is also notable that the displacements at the ultimate load found by an elasto-plastic calculation corresponds very well to the collapse mechanism predicted by use of FELA. However, it is here important to emphasise that the FELA model only gives velocities, not absolute displacements. This imposes some limitations on how the FELA results can be interpreted. For instance, it is not possible to use the collapse mechanism to evaluate whether or not the structure has sufficient deformation capacity. It is on the other hand possible to use the mechanism to evaluate, qualitatively, if the type of collapse can be classified as ductile or as brittle. In this example, Fig. 5-19b strongly suggests a ductile type of failure (flexural failure). Furthermore, it is in this case not surprising that the two models lead to practically the same load carrying capacity even though the FELA model assumes a constant value of $\upsilon = 1$ everywhere. As indicated by the collapse mechanism in Fig. 5-19b and confirmed by the displacement field in Fig. 5-19d, crushing of the concrete only takes place in zones which represent plastic hinges, i.e. failure by bending and not by shear action. This means that υ, even when modelled in a refined manner in the elasto-plastic model, is expected to be near to unity in the zones with crushing failure. This way of extracting qualitatively information from the FELA collapse mechanism is instrumental for a proper engineering judgment of the obtained results. If, for instance, the collapse mechanism from FELA has shown indications of shear failure in the concrete, then a recalculation with a lower ν-value (or alternatively an adaptive determination of υ as discussed in the next section) would be recommended in order to determine the best estimate of the load carrying capacity.

5.3.6 Discussion and concluding remarks

The two calculated examples demonstrate that the concept of Finite Element Limit Analysis is a useful tool to determine numerically the load carrying capacity of reinforced concrete structures. The method provides information about the collapse load, the stress field and the corresponding collapse mechanism. Compared to classical non-linear FE-analyses, FELA has the practical advantage of being very computational effective. This is true in regards to computational efforts as well as numerical stability. In fact, from a practical point of view, the issue of numerical stability may be even more important than computation time. With FELA, it is always possible to determine a collapse load, which is consistent with the model input and assumptions. When dealing with classical non-linear FE-analysis, on the other hand, numerical instability may prevent the outcome of meaningful results.

This document is the intellectual property of the fib – International Federation for Structural Concrete. All rights reserved.
This PDF of fib Bulletin 100 is intended for use and/or distribution solely within fib National Member Groups.

It should be noted though, that the above-mentioned advantages come with a cost. As shown in the calculated examples, FELA only provides information about the collapse mechanism but not the absolute displacements. A direct evaluation of the required deformation capacity is therefore not possible. In this context, FELA has the same drawback as any other rigid-plastic lower bound methods (e.g. the classical strut-and-tie method and Hillerborg's strip method). This entails that in practice, engineers have to perform an indirect verification of the deformation capacity to ensure that the plastic redistribution of stresses can take place as assumed in the FELA solutions. For simple cases, the obtained collapse mechanism together with guidelines and detailing rules provided in codes and standards are probably sufficient to verify the deformation capacity. For complex problems, a direct verification in the form of a detailed non-linear FE-analysis is recommended. In this context, the computational efficiency of FELA should be used to run a series of rigid-plastic calculations covering all relevant load combinations. And based on the obtained FELA results and the extracted collapse mechanisms, the engineer can select a few cases, that show relatively brittle types of collapse mechanism. These cases can then be subjected to a detailed and more time-consuming non-linear FE-analysis to verify the deformation capacity.

Coupled to the problem of deformation capacity is the issue of the effectiveness factor υ. This factor depends partly on the brittleness of the concrete and partly on the magnitude of the tensile strain, ε_1, transverse to the compression field (see e.g. Nielsen and Hoang[5-30]). The later dependency is a challenge to handle within the FELA concept, first and foremost because FELA assumes rigid-plastic behaviour. Secondly, the computational advantages of having convex yield conditions disappear if the strain-based dependency has to be correctly incorporated. This is so because υ displays a non-convex dependency on the transverse strain, which in the literature is frequently modelled by $\upsilon = 1/(k_1+k_2\cdot\varepsilon_1)$, where k_1 and k_2 are calibration constants.

In practical applications of FELA, the challenges related to the implementation of the ν-factor can be handled with different levels of sophistication. For simple cases, it is probably sufficient to adopt constant values of ν, that can be found in standards and text books. The recommended ν-factors depend on the type of action/failure (e.g. the ν-value for crushing of concrete due to flexural actions is different from the value adopted for crushing of concrete due to shear actions). This means that based on the stress field and the collapse mechanism of an initial FELA calculation, it is possible to refine the model by adopting - in the various zones of the model - the ν-factor that is most representative for the expected state of stress within the zone. For more complex cases with a multiple of load combinations, sound engineering judgments are required, and it is recommended to carry out calculations based on lower- and upper limits for the ν-factor. The obtained results should then form the basis for selection of cases to be examined in detail concerning deformation capacity (as discussed above).

To incorporate the effectiveness factor into FELA in a more sophisticated manner, a different and two- steps approach is needed. In this approach, the effective yield criterion for a representative reinforced element must be numerically determined in advanced once and for all. For plane stress problems, for instance, this would mean that the effective yield criterion of a reinforced concrete membrane should be determined for all combinations of stresses and with account of how the concrete- and the reinforcement stresses are redistributed in order to reach the yield point. The effective yield criterion may e.g. be established by use of a non-linear FE-model taking into account cracking and rotation of

This document is the intellectual property of the fib – International Federation for Structural Concrete. All rights reserved.
This PDF of fib Bulletin 100 is intended for use and/or distribution solely within fib National Member Groups.

the compression field. The result is an effective yield criterion, which lies within the ideal yield criterion assuming $\nu = 1$ (analytical yield criteria for the latter case can be found in Nielsen and Hoang[5-30]. The effective yield criterion will in some parts be non-convex due to the above-mentioned dependency of ν on the strain state. These parts should be appropriately approximated to render a full convex criterion, that can be adopted in the FELA model. A closed-form approximation of the effective yield criterion has e.g. been formulated by Herfelt et al.[5-51].

5.4 Adaptive Stress Field Method

5.4.1 Introduction

This chapter intends to present an energetic approach named, Adaptive Stress Field Models[5-52], that employs the convenient simplifications inherent to the stress field method to develop a tool for the nonlinear analysis of discontinuity regions. The interpretation of the flow of forces provided by the method offers a unique awareness of the structural behaviour along the loading process, which is considered especially important for an adequate evaluation of the outputs. The internal stress redistribution due to the nonlinear behaviour of the materials is accomplished introducing the concept of adaptive structures to stress field systems and, in particular, model follows energy. The configuration of the model at each load step is thus obtained following the minimum complementary energy principle. It intends to follow consistently the stress field model concept, by setting an initial stress field distribution and choosing the appropriate variables that will be adjusted later (model geometry and/or forces). The mechanical properties of elements under compression and tension are obtained directly from the geometry of the stress fields, accounting for the nonlinear constitutive relationships of the materials. Therefore, a detailed study of the behaviour of each element is presented, based on the constitutive relationships of the materials. Special attention is given to the behaviour of reinforced concrete ties since the global energy is deeply influenced by the tensile stress fields.

5.4.2 Formulation

A plane and uniaxial stress state is assumed for each of the three types of elements: ties, fan shaped struts and prismatic shaped struts. Prismatic struts are assumed to have constant compressive stresses - obtained simply by dividing the resultant force by the stress field area, whereas fan struts have compressive radial stresses with hyperbolic variation along their length. On a reinforced concrete tie element, the bond constitutive relationship leads to different steel and concrete stresses along the length of the tie. The stress field resultants are obtained by nodal equilibrium and the stress state in each element is described afterwards.

The mechanical properties of the stress fields are based on their geometry and stress state, and current structural analysis techniques are applied. Stress redistribution is simulated following the adaptive structures concept, in particular, form follows energy, in which the model configuration is adjusted according to the minimum global energy, the latter obtained as the sum of the computed energy of each element of the model and at each load step.

This document is the intellectual property of the fib – International Federation for Structural Concrete. All rights reserved.
This PDF of fib Bulletin 100 is intended for use and/or distribution solely within fib National Member Groups.

Adaptive structures can be defined as systems whose mechanical or geometrical characteristics are adapted according to a specific optimisation process. Several optimisation criteria are possible: e.g. minimise structure weight by changing element section and/or structural geometry; optimise axial forces on bars by adjusting element cross-section; adapt structural geometry according to minimum energy criteria, form follows energy.

Model follows energy concept consists of minimising complementary energy according to Eq. 5-20.

$$U = \int_V \int_\sigma \varepsilon \cdot d\sigma \cdot dV \qquad 5\text{-}20$$

satisfying equilibrium and compatibility conditions, where U should in particular depend on the structure configuration, V is the integration domain, and σ and ε are the element's stress and strain, respectively. The node position or angles between bars are set as variables and will be called adaptive variables.

For truss structures, the application of this methodology is computationally effortless since each element is subject only to axial force. The equilibrium equations can be obtained from nodal equilibrium in the global referential ($\Sigma F_x = 0$, $\Sigma F_y = 0$) and are condensed in Eq. 5-21. Also, compatibility equations are obtained by establishing a relationship between nodal displacement and bar elongation defined by Eq. 5-21 (see Fig. 5-20).

$$T \cdot N + F = 0 \qquad 5\text{-}21$$

$$D + T^T \cdot \delta = 0 \qquad 5\text{-}22$$

where:

- Matrix T represents the cosines and sines of each bar angle with horizontal direction.
- Vector N includes the axial forces of the elements.
- Vector F represents the applied forces at nodes in the global referential.
- Vector D contains the total axial elongation of the elements.
- Vector δ contains the nodal displacements in global coordinates.

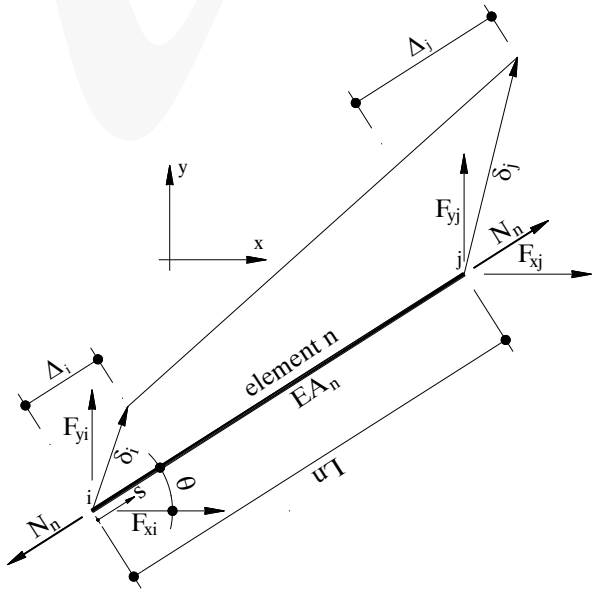


Fig. 5-20 Forces and displacements of the element

This document is the intellectual property of the fib – International Federation for Structural Concrete. All rights reserved.
This PDF of fib Bulletin 100 is intended for use and/or distribution solely within fib National Member Groups.

Finally, adaptation of geometry and/or stress distribution of the models is obtained by solving the minimisation problem for Eq. 5-23 where U is the global complementary energy defined in Eq. 5-20.

$$\min\ U,\ \text{with the constraints } T \cdot N + F = 0 \text{ and } D + T^T = 0 \qquad 5\text{-}23$$

5.4.3 Compression Stress Fields

Prismatic stress fields are no more than a particular case of a fan shape stress field. The quantification of their stresses is obtained by merely dividing the resultant compression force by its loading area. Fan shape stress fields are in general non-centred and the definition of the node boundary geometry is established according to equilibrium conditions of an infinitesimal strut within the fan. The node boundary curve is defined by a 2nd order polynomial (see Fig. 5-21b) and the radial stresses at each boundary are defined according to Eq. 5.4-5 and Eq. 5.4-6 where σ_I, σ_{II} and σ'_I, σ'_{II} are the principal stresses in the start and end node of the fan, according to Fig. 5-21a.

$$\sigma_r = \sigma_{II} \frac{1+\tan^2\alpha}{\frac{\sigma_{II}}{\sigma_I}+\tan^2\alpha} \qquad 5\text{-}24$$

$$\sigma'_r = \sigma'_{II} \frac{1+\tan^2\alpha}{\frac{\sigma'_{II}}{\sigma'_I}+\tan^2\alpha} \qquad 5\text{-}25$$

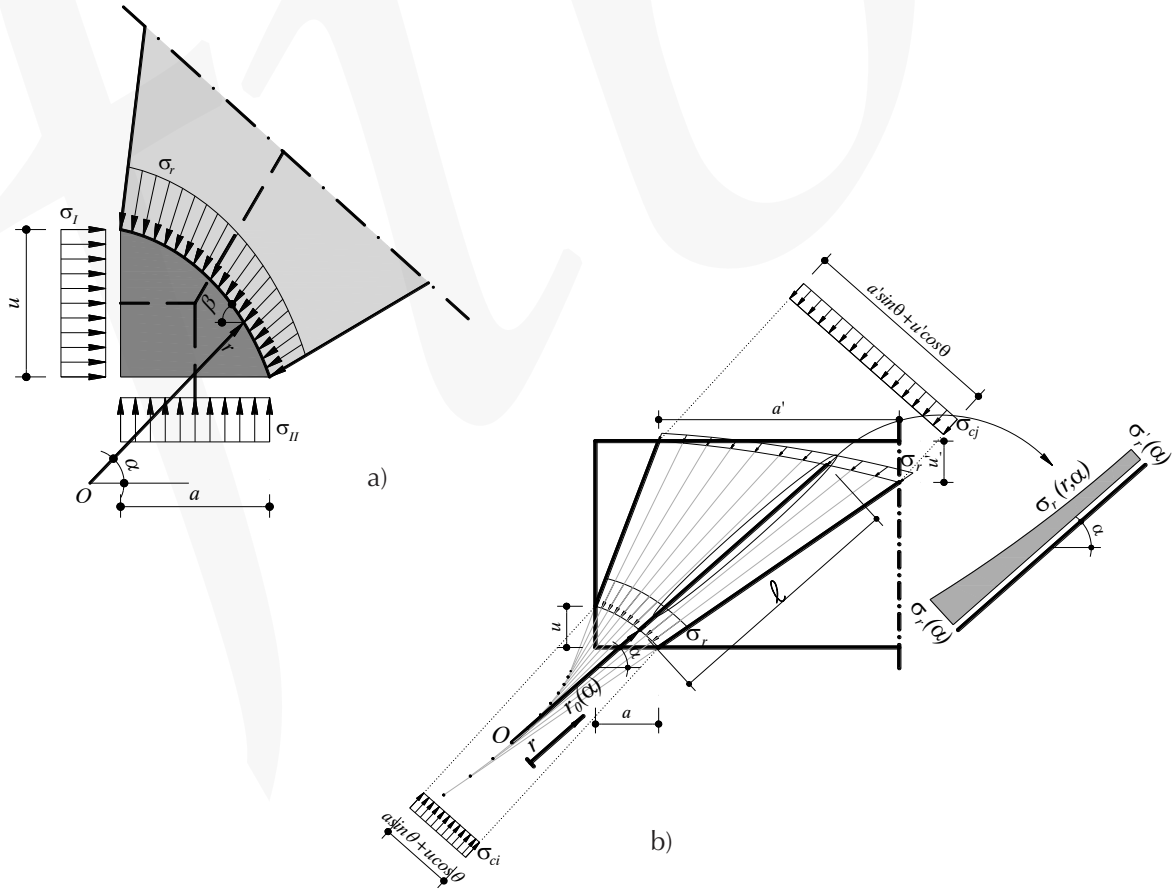


Fig. 5-21 a) Principal stresses at the node b) Radial stresses of a non-centred fan

This document is the intellectual property of the fib – International Federation for Structural Concrete. All rights reserved.
This PDF of fib Bulletin 100 is intended for use and/or distribution solely within fib National Member Groups.

The stresses along each chord within the fan vary hyperbolically, from the value σ_r into σ'_r at each radial angle α, and are obtained according to geometric and equilibrium conditions of an infinitesimal width of a specific chord (see Eq. 5-26). For practical and computational implementation, it is feasible and reliable to consider a linear stress distribution in simulating the behaviour of the fan. In this case the stresses are calculated according to the nodal dimensions, as shown in Fig. 5-21.

$$\sigma_r\left(r,a\right)=\sigma_r\frac{r_0\left(\alpha\right)}{r} \qquad 5\text{-}26$$

with

$$r_0\left(\alpha\right)=\frac{\sigma'_r\cdot l}{\sigma_r-\sigma'_r} \qquad 5\text{-}27$$

The distribution of concrete strains is obtained by the common hyperbolic σ_c-ε_c curve according to Eq. 5-28. Factor η_ε in Eq. 5-28 is meant to predict the reduction of the concrete strength, caused by the presence of transversal strains. This reduction usually occurs in compression stress fields crossing tensioned reinforcement and is mainly due to the bond induced by the reinforcement between the cracks and the friction stresses, leading to transverse tensile stresses and strains in concrete. Other reasons for this reduction are also the smaller effective width of the crack surface and the disturbances induced by the reinforcement. This effect was evaluated by several authors[5-53], [5-54], [5-55], [5-56], [5-57] and is usually simulated through a decrease of concrete compressive peak value on the basis of the applied transversal tensile strains, ε_1 [5-2].

$$\frac{\sigma_c}{f_c}=\eta_\varepsilon\frac{\alpha\cdot\varepsilon_{cc}-\varepsilon_{cc}^2}{\left(1+\beta\cdot\varepsilon_{cc}\right)} \qquad 5\text{-}28$$

with

$$\alpha=\frac{E_c}{E_{c1}};\beta=\frac{E_c}{E_{c1}}-2;E_{c1}=\frac{f_c}{\varepsilon_{c1}}=\varepsilon_{cc}=\frac{\varepsilon_c}{\varepsilon_{c1}};\eta_\varepsilon=\frac{1}{0.8+0.34\varepsilon_1/\varepsilon_{c1}} \qquad 5\text{-}29$$

The complementary energy, u_{compl}, Eq. 5-30 represents the area behind the stress-strain curve and may be computed by Gauss integration within the fan area (see Fig. 5-22):

$$u_{compl}=\int_{\sigma_1}^{\sigma_2}\varepsilon\cdot d\sigma;U_{compl}=\int_0^L\int_{A_c}u_{compl}\,dA\cdot ds \qquad 5\text{-}30$$

where A is the fan area, L the length of the fan and ds an infinitesimal length along fan axis.

This document is the intellectual property of the fib – International Federation for Structural Concrete. All rights reserved.
This PDF of fib Bulletin 100 is intended for use and/or distribution solely within fib National Member Groups.

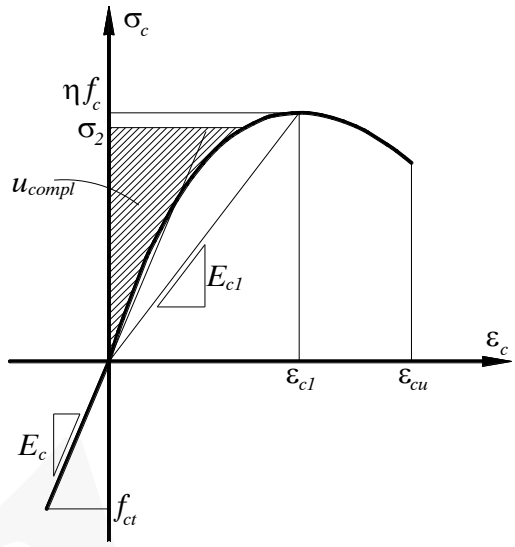


Fig. 5-22 Stress-strain relationship of the concrete

5.4.4 Tension Stress Fields

The global internal energy is mainly influenced by ties, especially after cracking of concrete. To properly simulate the behaviour of a structural concrete region, under service loads and for post-yielding phases, special attention to tension stress fields is required. In general, technical documents define constitutive relationships for reinforced concrete ties assuming a stabilised crack pattern, which is not suitable for some discontinuity regions. In fact, situations of non-stabilised cracking are commonly observed, e.g. load near support, dapped end beam, and others. In such cases the crack pattern is usually characterised by a main crack that has a relevant effect on the global structural behaviour. This phenomenon can be related to the stress distribution along the tie length, in which the length of the tie with constant stresses may not be enough to allow the formation of a stabilised crack pattern.

To properly simulate a reinforced concrete tie element, the approach presented in the Tension Chord Model by Marti et al.[5-58], is employed. This model establishes equilibrium conditions for an infinitesimal reinforced concrete tie (Fig. 5-23), allowing the determination of concrete and steel stress variation along the element length (Eq. 5-31 to Eq. 5-33).

$$N = N_s + N_c = A_s \cdot \sigma_s + A_c \cdot \sigma_c \qquad 5\text{-}31$$

$$d\sigma_c = \frac{4\tau_b \cdot \rho}{\phi} + \frac{q}{A_c} \qquad 5\text{-}32$$

$$d\sigma_s = \frac{4\tau_b}{\phi} \qquad 5\text{-}33$$

Concrete in tension has a linear σ_c-ε_c relation ($\sigma_c > 0$ – tension) until it reaches its tensile strength f_{ct}, with the Young's modulus of E_c. The reinforcing bars have a bi-linear σ_s-ε_s relation with the stiffness E_s in the elastic branch until the yielding stress f_y with hardening E_t after yielding, defined by the steel ductility until the ultimate strain ε_{su} and steel strength f_{su}. A rigid plastic relationship for bond stresses was shown to be adequate[5-58] to simulate a reinforced concrete tie with $\tau_{b0} = 2f_{ct}$ and $\tau_{b1} = f_{ct}$ before and after yielding of reinforcement steel, respectively.

This document is the intellectual property of the fib – International Federation for Structural Concrete. All rights reserved.
This PDF of fib Bulletin 100 is intended for use and/or distribution solely within fib National Member Groups.

Compatibility conditions and constitutive relationships for concrete in tension, steel and bond, together with suitable integration of strains, allow the calculation of the crack widths, the total elongation and the element mean strain (Eq. 5-34 to Eq. 5-37 and Fig. 5-24).

$$\rho = \frac{A_s}{A_c} \qquad 5\text{-}34$$

$$w_k = \int_0^{s_r} \left(\varepsilon_s - \varepsilon_c\right) dx \qquad 5\text{-}35$$

$$s = \int_0^{L} \left(\varepsilon_s - \varepsilon_c\right) dx \qquad 5\text{-}36$$

$$\varepsilon_{sm} = \frac{S}{L} \qquad 5\text{-}37$$

Fig. 5-24 shows stress, strain and slip variation along the length of the element in two identical ties with different "anchorage" length. Quite different crack patterns, steel and concrete stresses are obtained. As expected, the tie with larger lengths of variable axial load reveals a stiffer behaviour, evident in the stress-mean strains curves shown in Fig. 5-25. It is worth mentioning that a reliable model for stabilised and non-stabilised cracking is essential for the application of the Adaptive Stress Field Models in structural concrete regions, since substantially different complementary energies are computed and thus different global behaviour.

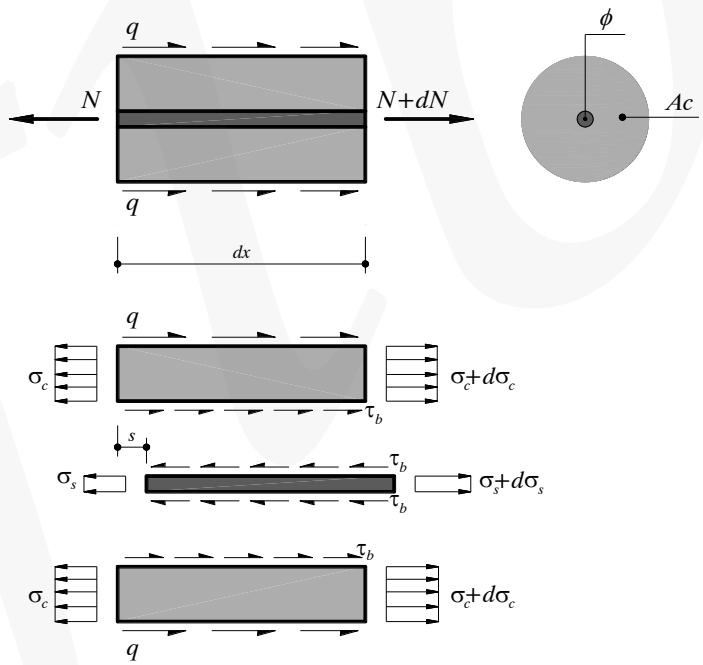


Fig. 5-23 Infinitesimal reinforced concrete tie

This document is the intellectual property of the fib – International Federation for Structural Concrete. All rights reserved.
This PDF of fib Bulletin 100 is intended for use and/or distribution solely within fib National Member Groups.

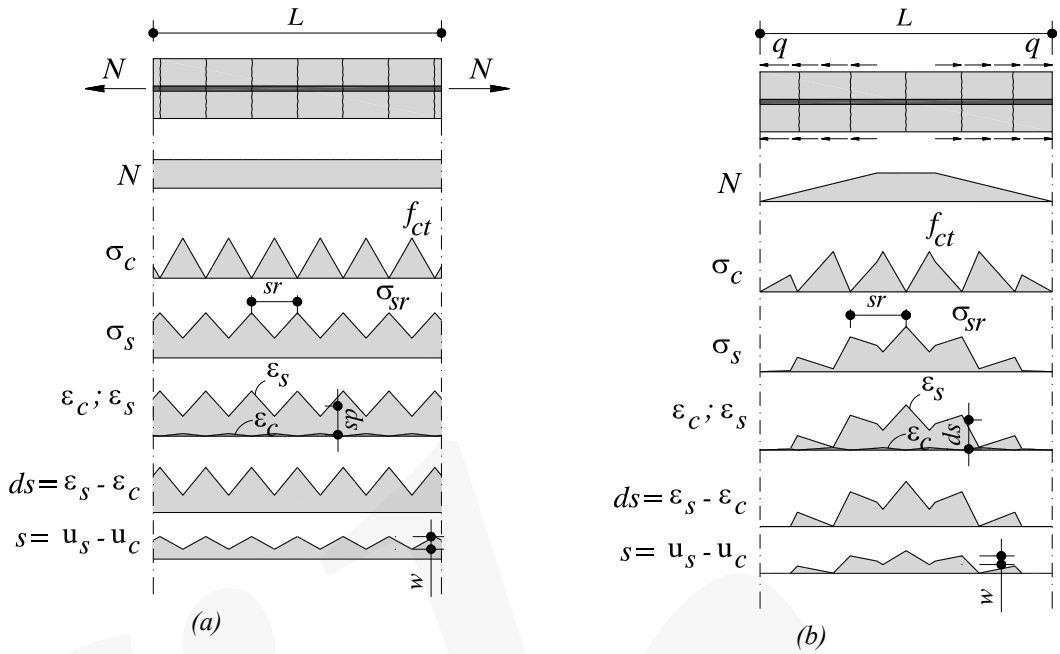


Fig. 5-24 Steel and concrete stresses and strains, slip and crack width of a reinforced concrete tie. a) Stabilised cracking; b) Non-stabilised cracking

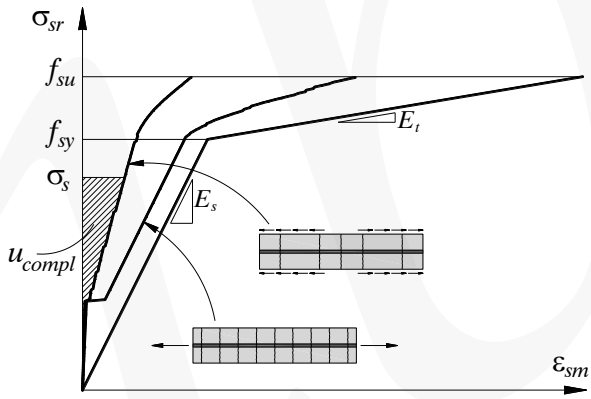


Fig. 5-25 Reinforced concrete tie constitutive relationships for stabilised and non-stabilised cracking

The complementary energy is defined by Eq. 5-38 and represents the area behind the stress-mean strain curve.

$$u_{compl} = \int_{\sigma_1}^{\sigma_2} \varepsilon_{sm} \cdot d\sigma ; U_{compl} = \int_0^L \int_A u_{compl} \cdot dA \cdot ds \qquad 5\text{-}38$$

5.4.5 Test Example

In order to illustrate the behaviour of an adaptive stress field model, a simple example of two bars is presented (Fig. 5-26). To clearly understand an adaptive structure, first elements 1 and 2 are assumed to be linear elastic with the same axial stiffness $E \cdot A$ and the intention is to "optimise" the shape of the structure according to the least complementary energy. Setting θ as the adaptive variable and minimising the global complementary energy, the shape is initially set to an angle of 60º as shown in Eq. 5-39 to Eq. 5-41.

This document is the intellectual property of the fib – International Federation for Structural Concrete. All rights reserved.
This PDF of fib Bulletin 100 is intended for use and/or distribution solely within fib National Member Groups.

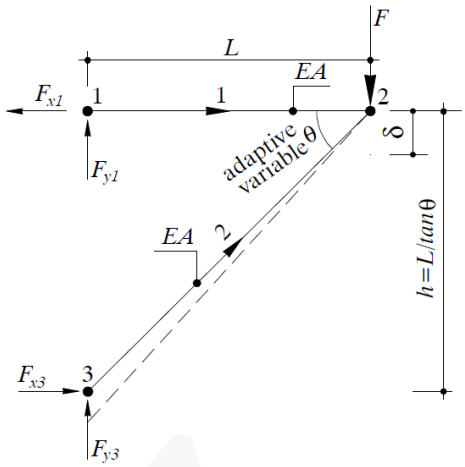


Fig. 5-26 Test example – geometry

$$U_1 = \frac{1}{2}\frac{F^2 \cot^2\theta \cdot L_1}{E \cdot A_1} \qquad 5\text{-}39$$

$$U_2 = \frac{1}{2}\frac{\frac{F^2}{\sin^2\theta} L_2}{E \cdot A_2} \qquad 5\text{-}40$$

$$\frac{\partial U}{\partial \theta} = 0 \Rightarrow 2\cos^3\theta + 3\cos^2\theta - 1 = 0 \Rightarrow \theta = \frac{\pi}{3} = 60° \qquad 5\text{-}41$$

For the example of Fig. 5-25 is now assumed that element 1 will have a nonlinear behaviour, with a bi-linear σ-ε constitutive relationship with an "elastic" branch and a "plastic" branch and element 2 is considered only with elastic (Fig. 5-26).

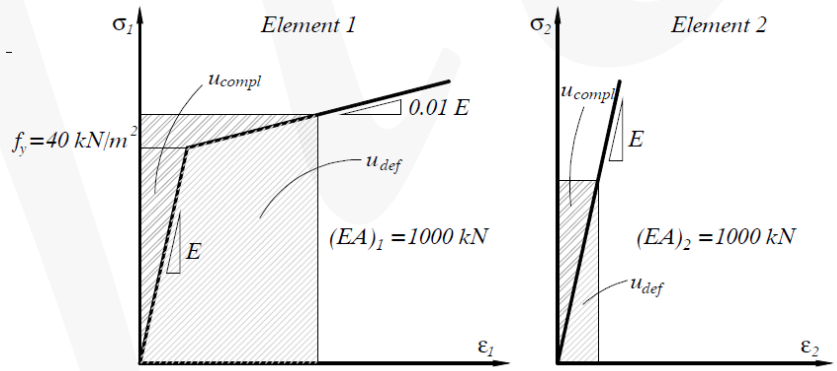


Fig. 5-27 Test example - constitutive relationships of the elements

It is possible to calculate the shape of the structure when both elements are at the elastic branch as obtained before, resulting an angle of θ= 60°, and develop a similar analysis with element 1 having the "plastic" branch stiffness and element 2 having the elastic stiffness $(E{\cdot}A)_1 = 0.01\ (E{\cdot}A)_2$. For this case the shape of the structure that minimises the complementary energy is given for an angle of θ = 76.59°.

Performing an analysis for both structural configurations without modifying the angle of the structure during the analysis, two different force-displacements curves F-δ (applied

This document is the intellectual property of the fib – International Federation for Structural Concrete. All rights reserved.
This PDF of fib Bulletin 100 is intended for use and/or distribution solely within fib National Member Groups.

force vs displacement – see Fig. 5-28a) are obtained. These results are compared with an incremental nonlinear adaptive analysis for all load steps and it is possible to observe the geometry adaptation in Fig. 5-28b along the load incremental process. Adaptive nonlinear analysis adjusts structural geometry to follow the different linearized stages. In the "uncracked" stage the adaptive variable remains unchanged at $\theta = 60°$. After cracking, steel stresses and geometry adjustment tend to the "plastic branch" geometry.

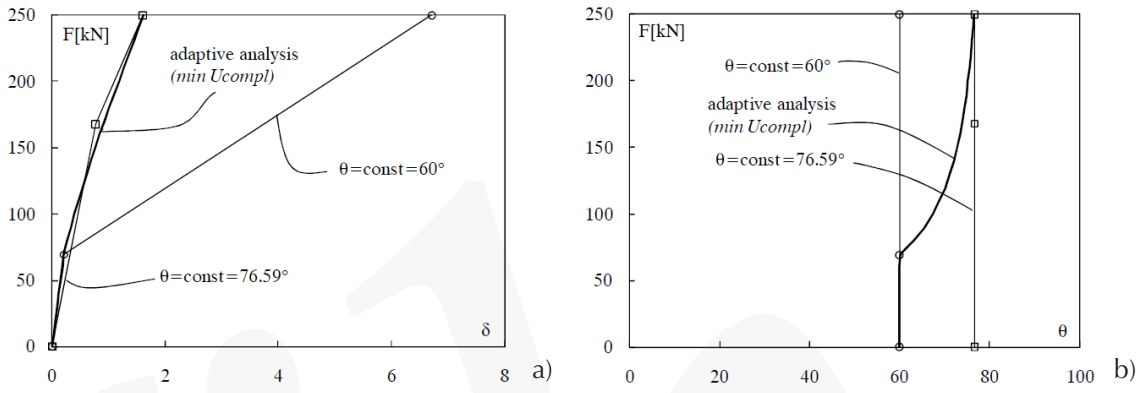


Fig. 5-28 Adaptive analysis of the test example. a) Applied force vs vertical displacement of point 2; b) Applied force vs model shape given by angle θ.

5.4.6 Application of the Adaptive Stress Field method to a deep beam test

The methodology presented is compared with the well-known Leonhardt and Walther[5-59] deep beam tests. Two simply supported beams, *WT2* and *WT3*, were in particular analysed.

The dimensions, loading and steel reinforcement layout of deep beams *WT2* and *WT3* are represented in Fig. 5-29. Tests have shown considerable redistribution of internal stresses due to cracking. Experimental ultimate loads reached P_u = 1'195 kN and P_u = 1'290 kN, for deep beams *WT2* and *WT3*, respectively (Fig. 5-34 and Fig. 5-35). At rupture, deep beam *WT2* exhibited yielding of the bottom reinforcement and maximum compression stresses at supports of about $1.06f_{cu}$. With regards to deep beam *WT3*, bottom steel stresses of about 370 MPa and support compression stresses of about $1.2f_{cu}$ were measured. Steel reinforcement detailing at the node region, where U-loops were adopted, improved concrete confinement and increased concrete resistance.

Numerical results agree quite well with tests at all load stages (Fig. 5-31 and Fig. 5-33). Note that mean steel strain was measured in the tests via strain gauges glued on bars and that the results depend on the crack location and strain gauge position. The increase of concrete compression resistance at the supports was not considered in the numerical model, leading to ultimate load values (P_u = 1'100 kN) slightly lower than the experimental results.

This document is the intellectual property of the fib – International Federation for Structural Concrete. All rights reserved.
This PDF of fib Bulletin 100 is intended for use and/or distribution solely within fib National Member Groups.

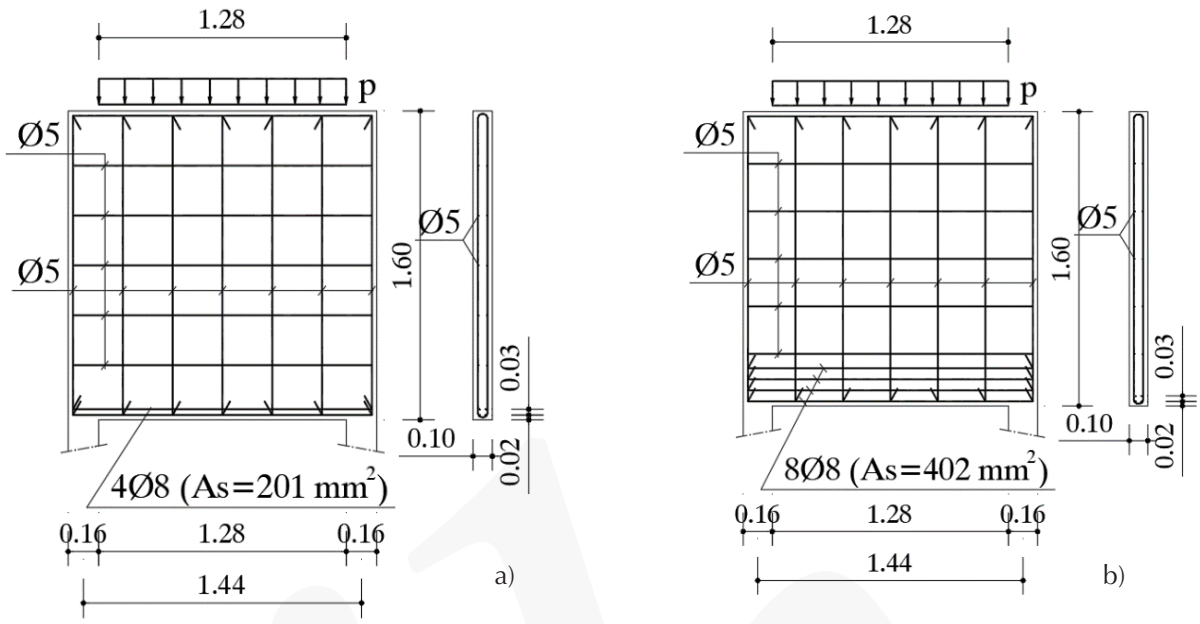


Fig. 5-29 Deep beams geometry and reinforcement layout[5-59]. a) *WT2*; b) *WT3* (dimensions in m).

The adaptive variables in the stress field analysis are node horizontal coordinates of web reinforcement.

It should be pointed out that the stiffness reduction related to cracking of the main tie induces significant internal stresses redistributions, evident in the stress field model configurations (Fig. 5-30 and Fig. 5-32), or in the internal lever arm (z/L) variation. These aspects are particularly relevant for the *WT2* test, where the available ductility allowed full utilisation of the beam effective depth. Fig. 5-34 and Fig. 5-35 shows the agreement of numerical and test crack pattern for ultimate load.

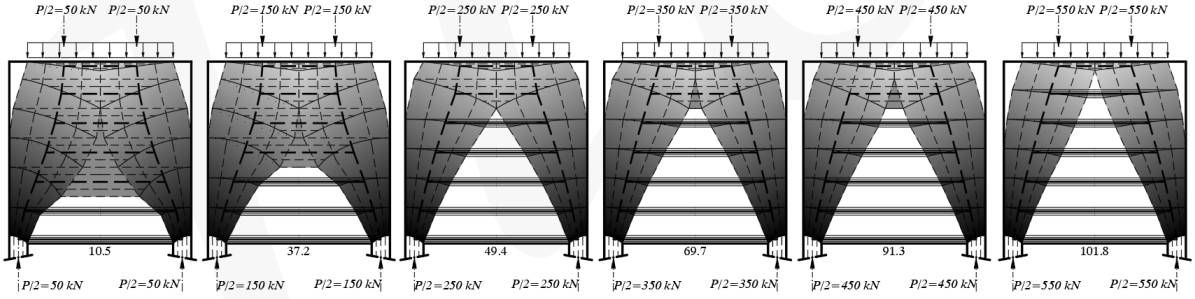


Fig. 5-30 *WT2* adaptive stress field model for several load steps

This document is the intellectual property of the fib – International Federation for Structural Concrete. All rights reserved.
This PDF of fib Bulletin 100 is intended for use and/or distribution solely within fib National Member Groups.

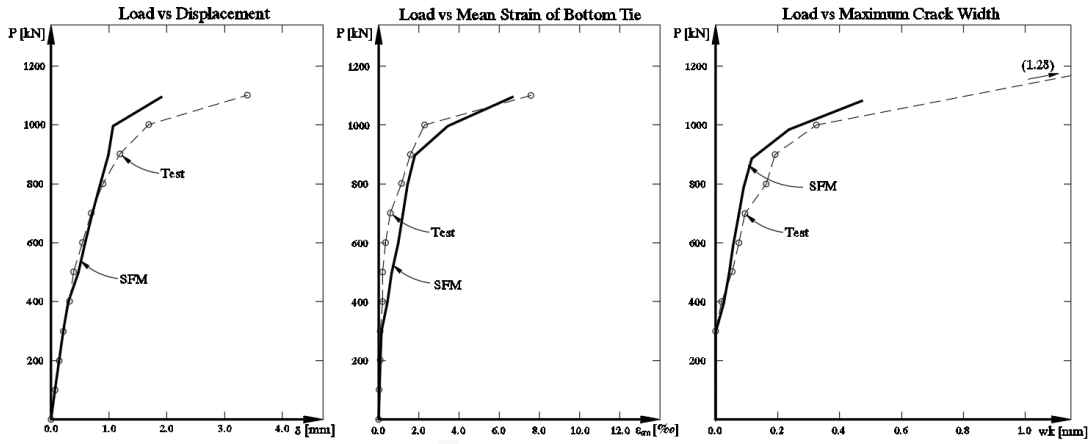


Fig. 5-31 Test and adaptive stress field model (ASFM) results comparison for *WT2*

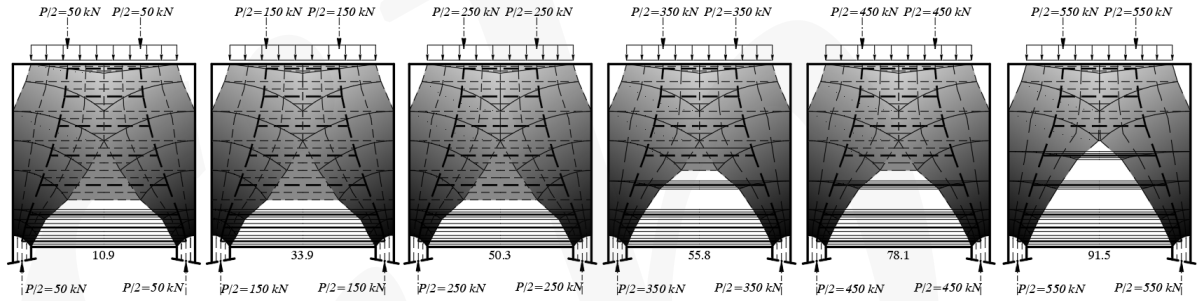


Fig. 5-32 *WT3* adaptive stress field model for several load steps

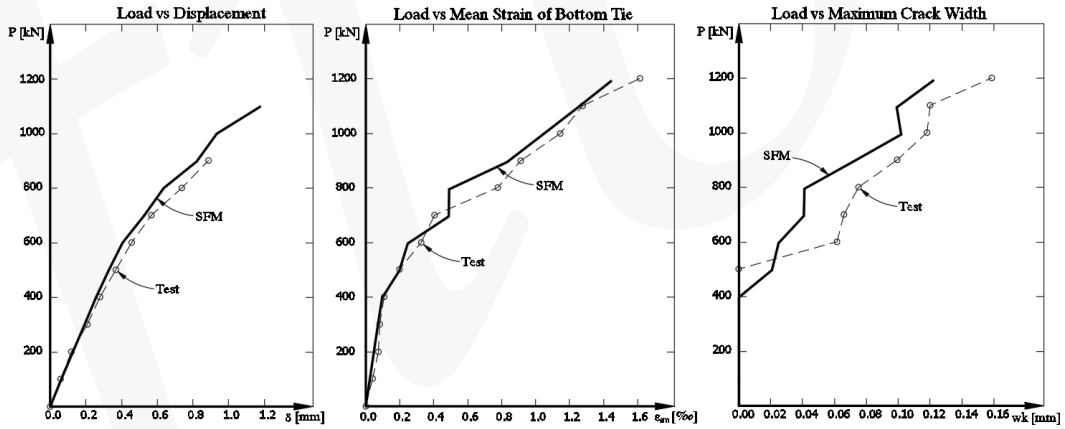
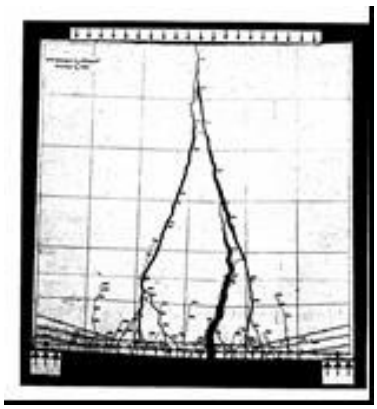


Fig. 5-33 Test and adaptive stress field model (ASFM) results comparison for *WT3*

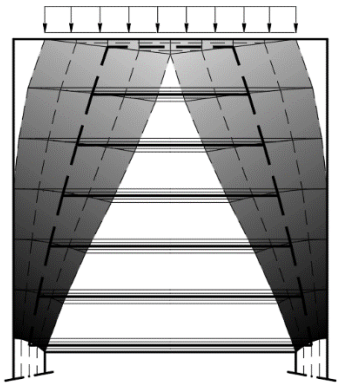
This document is the intellectual property of the fib – International Federation for Structural Concrete. All rights reserved.
This PDF of fib Bulletin 100 is intended for use and/or distribution solely within fib National Member Groups.

Test (P_u = 1'195 kN)

Adaptive Stress Field



a)

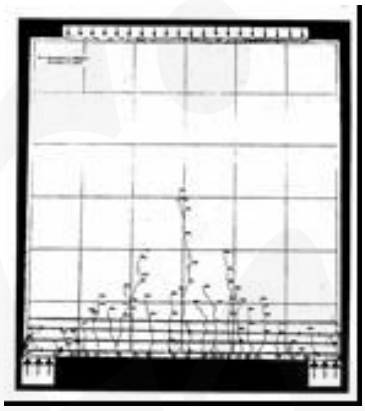


b)

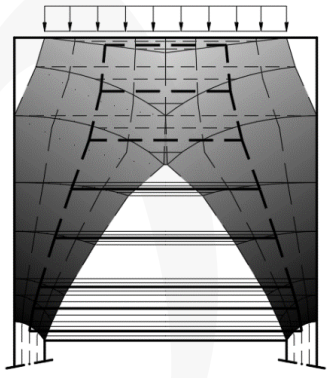
Fig. 5-34 WT2 numerical and test crack pattern for ultimate load. a) Test[5-59]; b) Adaptive stress field model

Test (P_u = 1'290 kN)

Adaptive Stress Field



a)



b)

Fig. 5-35 WT3 numerical and test crack pattern for ultimate load. a) Test[5-59]; b) Adaptive stress field model

In general, numerical results agreed quite well with the ones obtained experimentally. The force-strain and force-crack width curves obtained by the adaptive stress field analysis, follow closely the response during the test stages: uncracked; cracked and post-yielding. One aspect that needs to be clarified regarding specimen *WT2* is the considerable difference between test results and numerical predictions regarding crack width. In fact, the usual way of calculating crack widths may not be appropriate for cases with yielding of reinforcement.

The Adaptive Stress Field Model approach has been shown to be quite powerful, while its graphical output facilitates the visualisation of structural behaviour for all load stages. However, it is not yet easily applicable in practice owing to the complexity in developing automatic stress fields and programming their adaptation according to the minimum system energy. It is desirable that a fully automatic and more user-friendly software will be developed in the near future to facilitate application of the adaptive stress field technique in design practice.

This document is the intellectual property of the fib – International Federation for Structural Concrete. All rights reserved.
This PDF of fib Bulletin 100 is intended for use and/or distribution solely within fib National Member Groups.

5.5 Stringer-Panel Models

5.5.1 Introduction

For the design of D-regions, to the present day, structural designers rely mostly on the Strut-and-Tie Model (STM) or on the application of stress fields. The Stringer-Panel Model (SPM) presented here is a companion method which can be used in its own right, but which may also be applied to determine a proper strut-and-tie model, or used in combination with the STM.

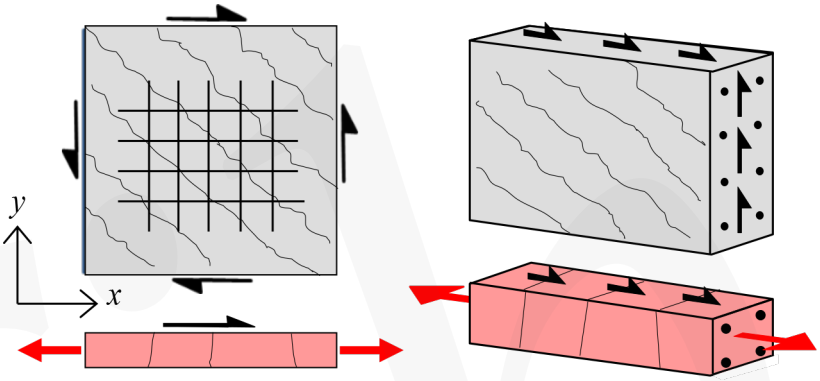


Fig. 5-36 Two different member types are used: panels (shown in grey) and stringers (shown in red if tensile). The shear membrane force depicted has positive sign.

In the SPM, two different member types are used, stringers and panels; see Fig. 5-36. The panels transfer shear membrane forces, which are uniform over the whole area of a panel. The stringers transfer normal forces. Because the stringers are loaded by the uniform shear forces of the panels, the normal force varies linearly over the path of a stringer.

As for the relation to the STM, much of the knowledge concerning that method also applies to the SPM. However, some difficulties in the STM are thought to be circumvented by the application of the SPM. The SPM is advantageous at least for two particular classes of design: (i) applications in which strict serviceability and durability requirements need to be met, and (ii) applications comprising cyclic loading as, for example, in the case of seismic action.

5.5.1.1 Increased importance of serviceability state

The STM essentially had its roots in the era of plasticity, an approach which has a pronounced focus on the consideration of ultimate strength. Since the development of this approach, the serviceability state of structures has received continuously increasing attention. The large freedom enjoyed by the structural designer in the STM came at the cost of not paying attention to serviceability. Keeping to near-linear solutions is considered important, from a durability perspective, in many regions of the world. In many structures, the reinforcement needed for the serviceability limit state has become a more decisive consideration than reinforcement for the ultimate limit state. Where reinforcement for serviceability state has been well determined, the required additional reinforcement for ultimate limit state often will be merely a local adaptation – the SPM is advantageous in such cases.

This document is the intellectual property of the fib – International Federation for Structural Concrete. All rights reserved.
This PDF of fib Bulletin 100 is intended for use and/or distribution solely within fib National Member Groups.

5.5.1.2 Seismic analysis

In seismic regions, the attention of structural designers is on the phenomenon of reversed loading. In the STM, each load cycle requires different models for the loading in one direction and the loading in the reverse direction. The SPM obviates this need: the same model is suitable for both directions of loading.

5.5.2 Concept of the Stringer-Panel Model

In structural concrete design, the stringer-panel method was already introduced by M.P. Nielsen in *Limit Analysis and Concrete Plasticity* (1998)[5-60]. In that book, the method was suggested in the context of lower-bound solutions in plasticity. As such, the SPM belongs to the family of stress field methods.

In general, five design steps are distinguished in the SPM, similar to the STM, albeit slightly adapted:

- Define the D-region to be considered and evaluate the body and boundary forces. All loads must constitute a set of equilibrating forces, horizontally, vertically, as well as rotationally.
- Choose a stringer-panel model and solve for the member forces in stringers and panels.
- Select the appropriate bundle of reinforcing steel in the tension stringers and distribute the reinforcement in the panels. Strictly speaking, the requirement of proper anchoring of the stringer reinforcement is replaced by the bond check. Nevertheless, for safety reasons, anchoring should always be undertaken, so as to address potential bond failure in highly tensioned regions. Mesh reinforcement always needs anchoring along edges (in the form of u-bars).
- Evaluate the dimensions of the compression stringers and check the concrete stress in the panels. For compressed stringers, an effective width must be selected, accounting for the spacing between stringers and free edges.
- Distributed reinforcement is required to ensure sufficient ductility capacity in the D-region. In the SPM, this is more naturally ensured, owing to the required two-way structural panel reinforcement.

Fig. 5-37 shows an exploded view of a simple stringer-panel example and the distribution of normal forces in the stringers. It is a simply-supported beam, loaded by a concentrated force halfway across its span. Of course, the structural engineer does not need the SPM to address this problem, but it is chosen for cognitive reasons. The model consists of seven stringers and two panels. The loading is a set of equilibrating forces. Locations where panel corners join are called nodes. The example in Fig. 5-37 has six *nodes*. A shear membrane force n_{xy} acts at the edges of each panel. As a result, the stringers are loaded axially by uniformly-distributed shear forces, evoking normal forces N that vary linearly over the path of a stringer. In the figure, this linear distribution is manifested by the gradient of the stringer's axial force diagrams, coloured in green and red, where green is used for compression and red for tension.

This document is the intellectual property of the fib – International Federation for Structural Concrete. All rights reserved.
This PDF of fib Bulletin 100 is intended for use and/or distribution solely within fib National Member Groups.

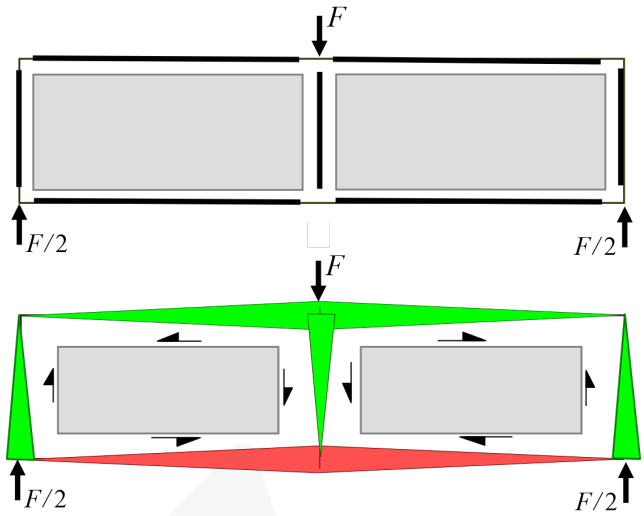


Fig. 5-37 Example of simple stringer-panel model. Panels, shaded in grey, are loaded by shear force resultants. These forces act in opposite directions on the stringers. Red diagrams indicate tensile forces, green diagrams compressive forces.

Because no membrane normal forces n_{xx} and n_{yy} are considered, we only deal with membrane shear forces n_{xy}. Therefore, we will skip the index *xy*, and denote the membrane shear force by the symbol *n*. Furthermore, we will often not be working with this uniform membrane shear force *n* but with the shear resultant *S*, which is the integral of the uniform membrane shear force over the path of the panel edge. In square panels, the shear resultants on the horizontal and vertical faces are equal, but in rectangular panels they are not. In the latter case they differ by the aspect ratio of the shear panel. In a stringer, the adjacent shear resultants *S* determine the difference between the normal force at the one end and at the other end of the stringer.

5.5.2.1 Anchorage of stringers

Fig. 5-37 does not correspond to general knowledge that the tensile force in the main reinforcement will become constant over the path of the reinforcing bar in ultimate limit state, as a result of cracking and loss of bond between the reinforcing bar and concrete. For this reason, appropriate anchorage is always needed, also when the normal force at the stringer end is zero and even when the slip strength would be sufficient. Anchorage must be based on the maximum tensile force that occurs in the reinforcing bar under consideration. The following rationale lies behind this approach: consider a reinforced concrete stringer with maximum tensile force at the right-hand end and zero force at the anchored free left-hand end. Over the path of the stringer length a distributed shear force acts, which balances the tensile force at the right-hand end. As long as no slip occurs, the reinforced concrete stringer will keep tensioned over the path of the stringer. After slip has fully developed, the reinforcement is bondless and the maximum tensile force occurs over the full path of the stringer up to the anchorage. Now the concrete stringer is loaded at the left-hand end by the anchorage force, and the stress state in the concrete stringer has changed from tensile into compression, yet still equilibrating the distributed shear force over the path of the stringer length. In this stage, the maximum compression occurs at the anchorage end of the stringer and the zero value at the right-hand end. This member will still perform well in the stringer-panel model. In reality, the situation at ultimate limit state may be in between the two cases; the tensile force at the right-hand end will be transferred to the concrete with a combination of bond stresses and anchorage force.

This document is the intellectual property of the fib – International Federation for Structural Concrete. All rights reserved.
This PDF of fib Bulletin 100 is intended for use and/or distribution solely within fib National Member Groups.

5.5.2.2 Levels of Approximation and SPM

Elsewhere in this Bulletin four Levels of Approximation (LoA) have been discussed for the strut-and-tie method. In general, the four levels apply to stringer-panel models as well.

5.5.2.2.1 LoA I, II

Level I regards the conception or design of new structures and level II is appropriate for the design of a new structure as well as for a general or brief assessment of an existing member. In LoA I and II the constitutive relationship is rigid-plastic and the forces in stringers and panels are calculated on the basis of equilibrium equations alone. If the model is statically determinate, the exact solution is obtained, and in case of redundancy, the structural engineer has the freedom to make choices before applying equilibrium equations. In the latter case, considerable redistribution of stresses may occur, if the choice differs substantially from the linear-elastic solution. LoA I will in general refer to coarse models, which often will be statically determinate or have a low degree of indeterminacy, and LoA II to more refined models with a moderate degree of redundancy.

5.5.2.2.2 LoA III, IV

In levels III and IV, compatibility considerations are included, and less rigid material laws are applied. These levels are at stake when serviceability requirements must be met. In general, LoA III may be restricted to linear-elastic or elastic-plastic material behaviour, whereas in LoA IV advanced non-linear material properties of any kind may be applied. LoA III and IV may be used for the design of a member in a complex loading state or a more elaborate assessment of a structure. Research on nonlinear modelling in LoA IV has been performed at TU Delft[5-61] and ETH[5-62].

5.5.2.3 Degrees of freedom in stringers and panels

To perform a stiffness analysis, the degrees of freedom (dofs) per element type must be defined. A stringer element has always three dofs, one at either of the two ends and one in the middle of the element; see the definition in the left-hand part of Fig. 5-38. Note that the middle one is not the displacement of the location halfway along the element length but is rather the weighted average of the displacements over the path of the element. This dof is denoted by the arrow on the dashed line. Likewise, the degrees of freedom at the panel edges are average displacements. At this dof the uniformly-distributed membrane shear between stringers and panels is transferred (the aforementioned shear resultant S) from the one to the other.

Stringers and panels can be imitated by elements from the library of standard FEA program packages. The elements to be used are shown in the right-hand part of Fig. 5-38. The stringer has three nodes and the panel eight, and two degrees of freedom are defined in each node. The FEA software must allow to specify orthotropic material behaviour in panels, for only shear rigidity is non-zero. All degrees of freedom in mid-side nodes normal to panel edges have to be put to zero, because no stiffness occurs in these directions. Alternately, to avoid this, one might allow small normal rigidities in the panels (say 0.1% of the shear rigidity).

This document is the intellectual property of the fib – International Federation for Structural Concrete. All rights reserved.
This PDF of fib Bulletin 100 is intended for use and/or distribution solely within fib National Member Groups.

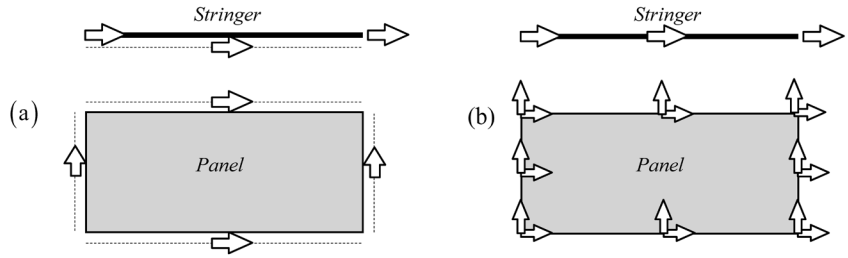


Fig. 5-38 Degrees of freedom. (a) Definition of stringers and panels. (b) Imitation of stringers and panels with standard FEA software.

5.5.2.4 Statical determinacy

Simple stringer-panel models will often be statically determinate. Where this is the case, member forces can be determined by equilibrium considerations alone. More complicated models will generally be statically indeterminate.

In case of statically determinate models, the structural designer has no freedom in choosing the stress distribution. For indeterminate cases, he/she does have such freedom and may make choices to render the structure under consideration statically determinate. If, in case of redundant models, the structural designer wants to keep close to the linear-elastic solution, he/she needs stiffness method software to determine the stress distribution.

5.5.2.5 SPM considered as a design method with stress fields

The stringer-panel model is part of the family of stress field methods. For the simply supported beam of Fig. 5-37, the stress field is demonstrated in Fig. 5-39, where the left-hand half of the structure is shown. We shall first discuss the top part of the figure. The uniform shear membrane force in the panel requires distributed horizontal and vertical reinforcement and evokes distributed, inclined compressive concrete struts. These struts represent a uniaxial stress state: in the case of equal horizontal and vertical reinforcement, under an angle of 45 degrees. This field of struts is denoted by the pattern of dots in the figure. The distributed reinforcement is represented by the mesh of parallel horizontal and vertical lines. The red line at the bottom of the figure is the stringer reinforcement. This stringer is loaded by a distributed horizontal shear force, which is the resultant of the forces in the distributed vertical reinforcement and the distributed inclined concrete struts. Alike, a vertical distributed shear force occurs, causing the stress field to widen at the vertical edges of the structural element.

An enlargement of the small rectangular element at the upper boundary of the structure is depicted at the bottom part of Fig. 5-39. Here, the red vertical lines represent distributed reinforcement of the panels. The black triangles are incremental nodes, loaded by a force from an inclined strut, a horizontal compressive force and the vertical distributed reinforcement. It will be seen that the force in the stringer is built up from left to right across the stress field.

This document is the intellectual property of the fib – International Federation for Structural Concrete. All rights reserved.
This PDF of fib Bulletin 100 is intended for use and/or distribution solely within fib National Member Groups.

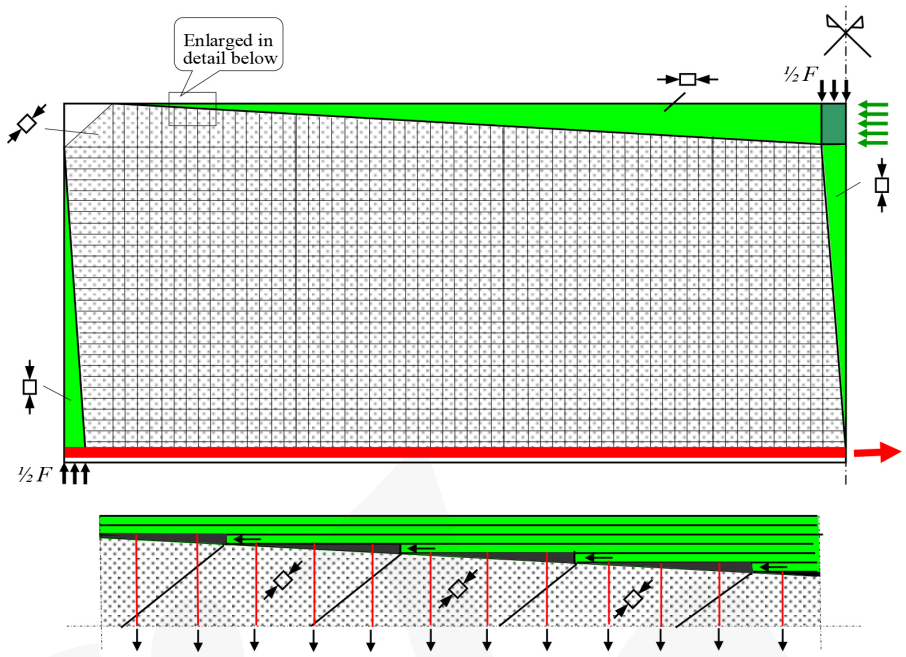


Fig. 5-39 Stress field in the left half of the simply-supported beam of Fig. 5-37.

5.5.3 Dimensioning the stringers, panels and nodes

5.5.3.1 Detailing of reinforcement

The detailing of reinforcement is based on the stringer tensile forces and the panel stress field in the ultimate limit state, in which concrete and steel reinforcement deform plastically.

For the tensile stringers, we apply bundle reinforcement. Knowing the normal force N and the adopted steel design stress f_{sd}, we calculate the required steel area A as $A = N / f_{sd}$. A stringer needs not be anchored if there is enough length to build up – through bond – the stringer force from zero to the yield force. If this is not the case, two solutions are possible. The first one is to use higher quantity of steel. The other solution is to realise anchorage via looped bars. If the anchoring strength is equal to the yield force of the stringer, no bond stresses are needed at all, and a compression force can occur over the full length of the stringer.

The distributed reinforcement in the panels can be based either on the assumptions of equal reinforcement ratios in the horizontal and vertical directions or on different ratios. In the case of equal ratios, the distributed concrete struts in the panel at yielding of the reinforcement have an inclination angle of 45 degrees, and the compressive stress σ_c in the concrete will be twice the uniform shear stress $|\sigma_{xy}|$. The required steel ratio ρ of the distributed reinforcement is calculated from the equations $n_{sx} = n_{sy} = |n|$, where n_{sx} and n_{sy} are the forces per unit width in the reinforcement in the x- and y-direction respectively and n the membrane shear force. The structural engineer has freedom in applying different amount of distributed reinforcement in x- and y-direction. If he/she does so, the following holds true:

$$\begin{aligned} n_{sx} &= k|n| \\ n_{sy} &= k^{-1}|n| \\ n_c &\left(k + k^{-1}\right)|n| \end{aligned} \qquad 5\text{-}42$$

This document is the intellectual property of the fib – International Federation for Structural Concrete. All rights reserved.
This PDF of fib Bulletin 100 is intended for use and/or distribution solely within fib National Member Groups.

Factor k is defined as $k = \tan \alpha$, where α is the angle between the x-axis and the normal to the compressive concrete struts in the panel. The total reinforcement is minimal for $k = 1$.

In structures a minimum distributed reinforcement will always be available. Call the strength of this mesh n_{min}; this is the membrane shear force which the mesh can carry. Sometimes, if choosing $k = 1$, n_{sx} (or n_{sy}) may be smaller than n_{min}. In that case, we could choose $n_{sx} = n_{min}$, obtaining a larger value of k and more reduction in y-direction. Codes normally limit the choice of k (between say 0.4 and 2.5) to avoid large shear cracks in SLS.

The obtained total amount of reinforcement will in general not be less than that when the strut-and-tie method is applied, and will certainly not be less if the engineer applying the STM allows himself/herself a considerable degree of freedom in choosing the load path. SPM pays off owing to its ease of application and better control over crack width.

5.5.3.2 Check of concrete compressive stress in stringers and panels

For checking purposes, one may rely on Model Code 2010[5-19] or the recommendations of Schlaich et al.[5-48]. The concrete compression design stress f_{cd} is related to the characteristic compressive strength f_{ck}, which in turn depends on the designated code of practice, and the partial safety factor γ_c for the concrete in compression. The concrete compression design stress f_{cd} must be multiplied by the effectiveness factor ν in order to account for cracking, either parallel or skew to the struts. For explanation the reader is referred to *Limit Analysis and Concrete Plasticity* by Nielsen and Hoang[5-30]. The following values are proposed in Schlaich et al.[5-48]:

- $\nu = 1.0$ for an undisturbed and uniaxial state of compressive stress;
- $\nu = 0.8$ if tensile strains in the cross direction or transverse tensile reinforcement may cause cracking parallel to the strut, with normal crack width; this applies also to node regions where tension steel bars are anchored or crossing;
- $\nu = 0.6$ as above but for skew cracking or skew reinforcement.

5.5.3.3 Design of nodes

For the design of nodes and checking of the compressive stress, the reader is referred to Schlaich et al.[5-48] and to the Model Code 2010[5-19].

5.5.4 Dapped beam end

The major part of a beam with a dapped end will meet the requirements of Bernoulli beam theory and classical theory for the design of structural concrete beams holds true. However, it does not hold for the dapped end. Focusing on the design of this D-region, an example of a 0.68 m-deep, 0.30 m-wide beam shown on the left-hand diagram of Fig. 5-40, is to be detailed for a support reaction R of 230 kN. The first step is to make a decision about the extent of the D-region. Following that choice, a decision has to be made as of which horizontal and vertical stringer lines occur and which external load is applied to the D-region; see the right-hand diagram in Fig. 5-40. Horizontal stringers must at a minimum be applied: (i) in the top compression zone of the beam, (ii) at the horizontal reinforcement in the dapped end, and (iii) at the horizontal reinforcement in the bottom part of the beam, as denoted by numbers 1, 2 and 3, respectively, in the figure. Vertical stringer lines are at least needed: (i) at the support reaction, (ii) on the right of the re-entrant corner and, (iii) at the end of the D-region, as denoted by

This document is the intellectual property of the fib – International Federation for Structural Concrete. All rights reserved.
This PDF of fib Bulletin 100 is intended for use and/or distribution solely within fib National Member Groups.

numbers 4, 5 and 6, respectively. Furthermore, the structural designer has to make an estimate of the distance from the horizontal top stringer to the beam's top face and from the tensile bottom stringer to the beam's bottom face. The designer must also choose a position for vertical stringer 5, to the right of the re-entrant corner. Here, a spacing of 240 mm is introduced between this stringer and the support reaction, accounting for cover and the expected width of a bundle of stirrups. In all these considerations regarding the model, engineering judgement and experience play an important role, as in strut-and-tie modelling. In between the stringer lines, three shear panels are applied.

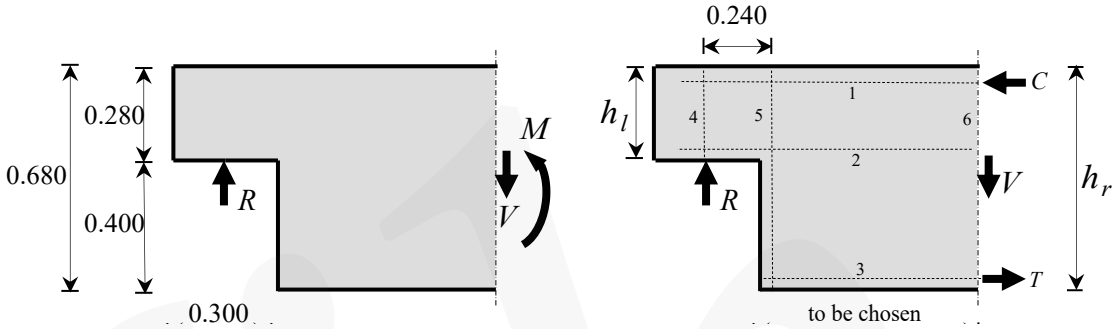


Fig. 5-40 Dapped beam end (left). Stringer lines and loading (right). Dimensions in m.

After the scheme of horizontal and vertical lines has been worked out, the extent of the external loading acting on the D-region needs to be defined. In Fig. 5-40, the bending moment *M* at the end of the D-region is replaced by a force *C* in the compression zone and a force *T* in the tension zone. The vertical shear force *V* is equal to the support reaction *R*. The four forces *C*, *T*, *V* and *R* must be a horizontally and vertically, as well as rotationally, equilibrating set. If desired, one may account for the dead weight of the D-region and/or distributed load on top of the region, but they are neglected here for simplicity.

5.5.4.1 Extent of D-region

On choosing the proper extent of the D-region in the SPM, the rules applied in the STM are equally valid. These rules are based on Saint-Venant's principle, which helps determine the distance between the disturbance and the cross-section where Bernoulli beam theory starts to hold true. In the example of a beam with a recess, the disturbance occurs at the position at which the beam depth changes from h_l (left of the recess) to h_r (right of the recess); refer to Fig. 5-40.

In the left-hand part of the beam, beam theory is violated over a distance h_l from the disturbance; in the right-hand part, beam theory is violated over a distance h_r from the disturbance. Thus, the D-region has length $h_l + h_r$, implying that in this case, the whole dapped end on the left-hand side of the D-region must be included, while on the right-hand side the D-region extends over a distance of 0.680 m from the re-entrant corner. For other cases, the extent of the D-region has to be determined accordingly.

This document is the intellectual property of the fib – International Federation for Structural Concrete. All rights reserved.
This PDF of fib Bulletin 100 is intended for use and/or distribution solely within fib National Member Groups.

Fig. 5-41 is a reminder of the strut-and-tie model recommended in Schlaich et al.[5-48] for the dapped end problem. At first glance, it seems to show a lesser extent to the right of the re-entrant corner than the effective beam depth h, but after spreading the vertical tie T_2 over the length l_2, it becomes clear that the extent $l_1 + l_2$ is approximately equal to the depth h. We can make a similar choice in the SPM. In Fig. 5-41, the inclined struts to the left and right of the re-entrant corner have the same inclination angle, ϑ_1. The equivalent condition in the SPM is that the corresponding panels have the same aspect ratio. Henceforth, we will continue with this SPM.

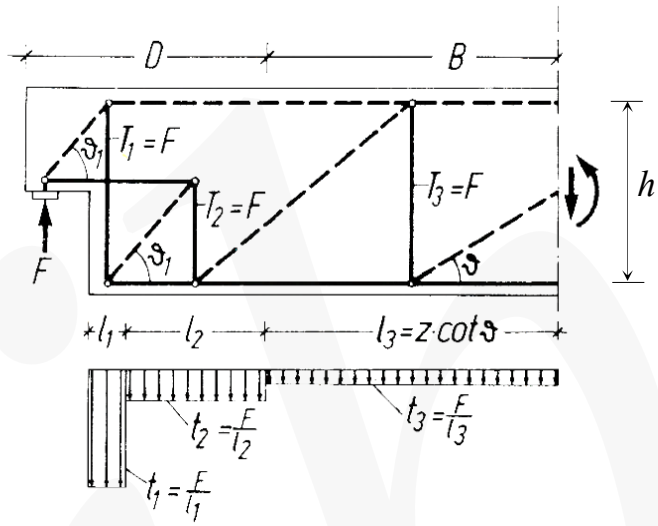


Fig. 5-41 Recommended strut-and-tie model in PCI Journal 1987.

5.5.4.2 Stringer-panel model

The model obtained is depicted in Fig. 5-42a, in which the panel size has been slightly reduced for clarity. The model consists of five horizontal stringers, five vertical ones and three shear panels. The shear panels are numbered from 1 to 3 (circled in the diagram). As in concrete beam design, we assume the shear force at the end of the D-region to be uniformly distributed over the height of the model. We split it into an upper part of 76.7 kN and a lower part of 153.3 kN, in proportion to the panel heights of 0.200 m and 0.400 m. The aspect ratio of the panel with height 0.400 m must be 1.2. Thus, it has a length of 0.480 m. The two horizontal forces acting on the D-region are 276 kN each, acting in opposite directions. The set of forces 230 kN, 76.7 kN, 153.3 kN and (twice) 276 kN is in perfect equilibrium.

This document is the intellectual property of the fib – International Federation for Structural Concrete. All rights reserved.
This PDF of fib Bulletin 100 is intended for use and/or distribution solely within fib National Member Groups.

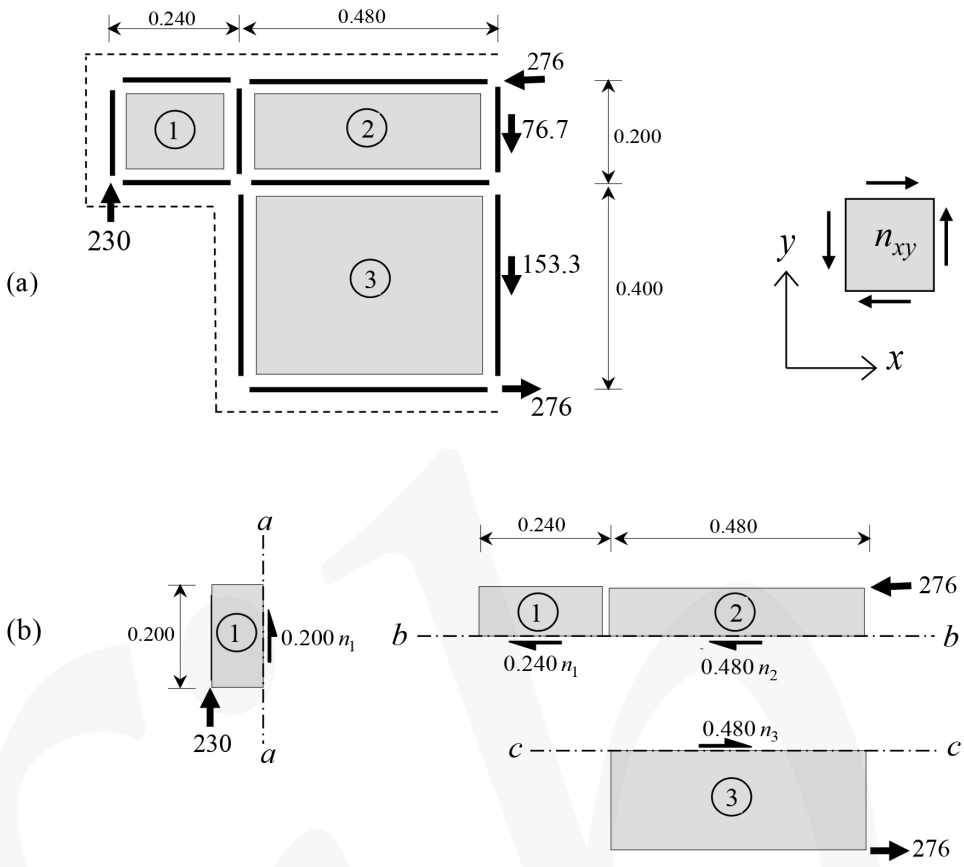


Fig. 5-42 Part (a): Stringer-panel model and external loading. Forces in kN; dimensions in m. Positive sign of membrane shear forces is shown. Part (b): Equilibrium of three free bodies is considered.

5.5.4.3 Solution

The model is statically determinate. Hence, the solution of the member forces is obtained from equilibrium considerations alone and the structural engineer cannot make free choices. A convenient way is to first calculate the membrane shear force n of the three panels, and to derive the stringer forces from the obtained membrane shear forces.

We can draft three equilibrium equations for the three unknown membrane shear forces n_1, n_2, and n_3. First, we consider the vertical equilibrium of the free body left of a vertical cut a-a over panel 1. For this free body is referred to Fig. 5-42b. Next, the horizontal equilibrium of the free body above a horizontal cut b-b over the panels 1 and 2 is considered, and finally, the horizontal equilibrium of the free body below a horizontal cut c-c over panel 3. Accounting for the sign convention shown in Fig. 5-42a, and definition of the membrane shear forces per unit length, we obtain the three equations

$$\begin{aligned} 230 + 0.200 n_1 &= 0 \\ 276 + 0.240 n_1 + 0.480 n_2 &= 0 \\ 276 + 0.480 n_3 &= 0 \end{aligned} \qquad 5\text{-}43$$

The solution is n_1 = -1'150 kN/m, n_2 = 0 and n_3 = -575 kN/m. Fig. 5-43a shows the shear resultants acting on the full panel edges, while Fig. 5-43b shows the same resultants acting with opposite sign on the stringers (action equals reaction). From this loading the stringer forces are easily calculated, shown in Fig. 5-43c, coloured red for tension and

This document is the intellectual property of the fib – International Federation for Structural Concrete. All rights reserved.
This PDF of fib Bulletin 100 is intended for use and/or distribution solely within fib National Member Groups.

green for compression. The solution is surprising: one of the three panels remains stress-less. The zero-membrane shear force n_2 will always occur if the extent of the D-region is chosen on the basis of equal aspect ratio. If not, a non-zero value will be obtained for the membrane shear force n_2; always small, however, in comparison to n_1 and n_3.

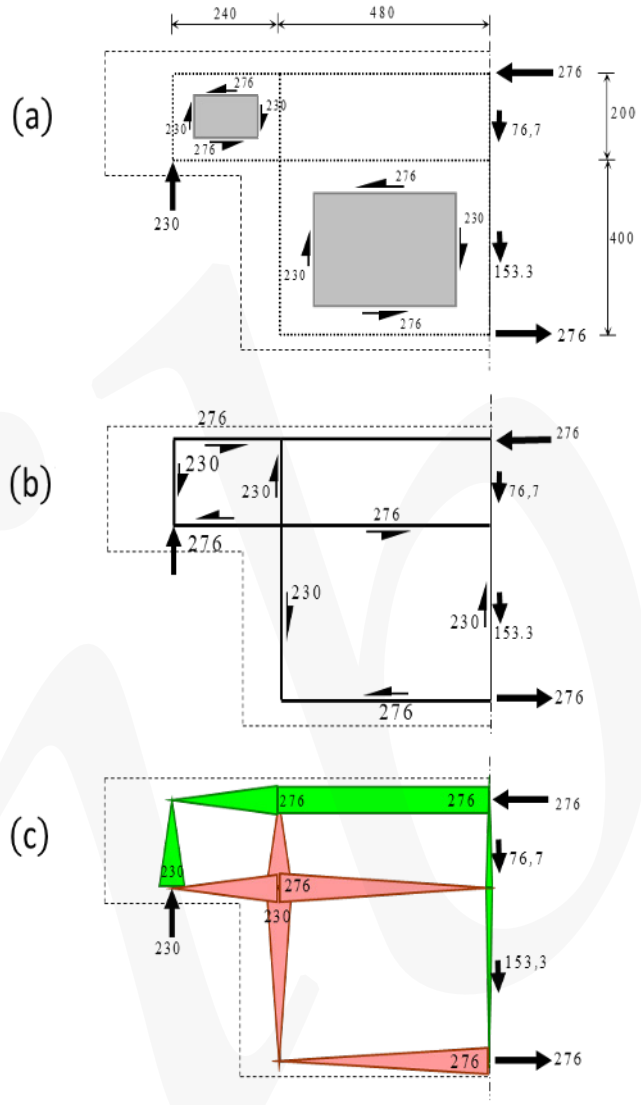


Fig. 5-43 Member forces for support reaction of 230 kN. (a) Panel shear resultants, (b) shear resultants acting as load on the stringers, (c) calculated stringer forces. Forces kN; dimensions m.

5.5.4.4 Remark

Here above, three equilibrium equations have been derived in which the membrane shear forces n_1, n_2 and n_3 are the unknowns. Alternately, one could have used the shear resultants S_1, S_2 and S_3. The derivation of the stringer forces may result somewhat easier.

5.5.4.5 Stringer reinforcement

The horizontal stringers in the dapped end have to carry a tensile force of N = 276 kN. For steel quality with design strength f_{sd} = 435 N/mm^2, this tensile force requires 276'000/435 = 634 mm^2 of reinforcement. Three bars with diameter 18 mm will be sufficient: $3(\pi/4)\cdot 18^2 = 763$ mm^2.

This document is the intellectual property of the fib – International Federation for Structural Concrete. All rights reserved.
This PDF of fib Bulletin 100 is intended for use and/or distribution solely within fib National Member Groups.

The vertical tensile stringers (hangers) carry a tensile force of N = 230 kN, equal to the support reaction. The designer has to decide whether he/she applies a Z-shape bent reinforcing bar or prefers stirrups for the hanger stringers. In the left-hand picture of Fig. 5-44, the hanger reinforcement is depicted as a bent reinforcing bar, and in the right-hand picture with stirrups. Here, the option with stirrups is adopted. For steel design stress f_{sd} = 435 N/mm^2, two stirrups with bar diameter of 14 mm are sufficient. This being so, four bars are available, with a total cross-section area of $4\cdot(\pi/4)\cdot 14^2$ = 616 mm^2. The resisting strength is 616·435/1000 = 268 kN, which is larger than 230 kN.

After detailing, the structural designer has a better indication as to the horizontal distance between support reaction and hanger reinforcement, and may decide to iterate or not, depending on how much the distance differs from the estimated 240 mm in the chosen model. In the right-hand picture of Fig. 5-44, at the bottom of the dapped end and at the bottom of the beam, a loop anchorage has been chosen for the two horizontal main reinforcing bars.

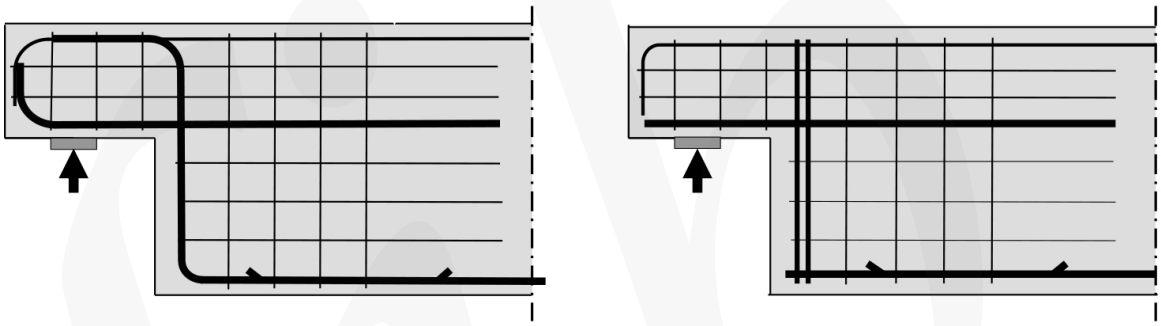


Fig. 5-44 Concentrated and distributed reinforcement. Left: the hanger reinforcement consists of one Z-shape bent reinforcing bar. Right: the hanger consists of two stirrups.

5.5.4.6 Panel reinforcement

The distributed two-way mesh reinforcement in the panel areas must be based on the membrane shear forces:

$$\begin{aligned} |n_1| &= 1'150 \text{ kN/m} \\ |n_2| &= 0 \\ |n_3| &= 575 \text{ kN/m} \end{aligned} \qquad 5\text{-}44$$

It is essential that the distributed reinforcement be a two-way mesh; refer to Fig. 5-44. The amount of reinforcement in each direction must be based on the absolute value of the membrane shear force.

5.5.4.6.1 Panel 1

The membrane shear force is n_1 = 1'150 N/mm. The design steel strength is f_{sd} = 435 N/mm^2. This requires a distributed steel area A_s = 1'150/435 = 2.64 mm^2/mm. For this area, stirrups (or hairpins) with diameter of 10 mm and spacing of 50 mm will suffice (3.14 mm^2/mm). Horizontal reinforcement is required over the length of the dapped end. This reinforcement is extended as far as the end of panel 2, increased with an appropriate

This document is the intellectual property of the fib – International Federation for Structural Concrete. All rights reserved.
This PDF of fib Bulletin 100 is intended for use and/or distribution solely within fib National Member Groups.

bond length. Hairpins should be used. Vertical reinforcement is required over the length of the dapped end and can consist of stirrups.

5.5.4.6.2 Panel 3

The membrane shear force is n_3 = 575 N/mm, and the required steel area is 1.32 mm²/mm. For this area, stirrups (or hairpins) with diameter of 8 mm and spacing of 75 mm will be appropriate (1.34 mm²/mm). Vertically, we apply stirrups, which –in any case– must be extended over the length 480 mm of panel 3. In reality, they will also extend over the area of panel 2. Horizontally, the reinforcement consists of hairpins which extend to the end of panel 3, increased by an appropriate bond length.

5.5.4.7 Check of stringers under compression

As an example, we will consider the upper horizontal compressed stringer. The maximum compressive force is N = 276 kN and the concrete design strength is chosen as f_{cd} = 26 N/mm². The stringer is crossed orthogonally by a tension stringer; hence, we adopt the effectiveness factor ν = 0.8 and will work with the effective concrete compressive strength 0.8·26 = 20.8 N/mm². The required stringer concrete cross-section area must be A_c = 276'000/20.8 = 13'269 mm². Because the thickness of the beam is 300 mm, the stringer must have a width of 13'269/300 = 44.2 mm, namely 22.1 mm on each side of the stringer centre line. The distance from the centre line of the stringer to the upper boundary of the beam has been taken as 40 mm, which is sufficient. Should the required stringer width prove larger than was assumed, an iterative procedure has to be initiated. An alternate solution is adding compression reinforcement, or accounting for the reinforcement which anyway occurs for framing purposes.

5.5.4.8 Check of concrete stress in panels

For equal steel area in *x*- and *y*-direction the concrete compressive stress in the panels will be twice the nominal shear stress in the panel. This compressive stress must be less than or equal to $\nu \cdot f_{cd}$. Because the distributed reinforcement intersects the inclined concrete 'struts', we use the effectiveness factor ν = 0.6. Therefore, the effective design strength is 0.6·26 = 15.6 N/mm².

In panel 1, the nominal shear stress is $\tau_c = n_1/t$, where t is the thickness of the beam. Hence τ_c = 1'150 (N/mm)/300 (mm) = 3.8 N/mm². The concrete compressive stress is $\sigma_c = 2\tau_c$ = 7.6 N/mm², which is less than the strength 15.6 N/mm², as required. The nominal shear stress in panel 3 is half the value of panel 1, hence also sufficiently small.

5.5.5 Deviating columns in building

The case will be considered of deviating columns in a building. Fig. 5-45a is a sketch of the structure. The two high-strength circular concrete columns have a diameter of 0.25 m and horizontal spacing of 5.0 m. For the transmission of the vertical force 3'700 kN from the one column to the other, a connecting wall is inserted between the two floor slabs and the two columns. The wall thickness and slab thickness is 0.25 m, and the mid-plane to mid-plane distance of the slabs is 3.0 m. At the left-hand and right-hand wall edge, a chord occurs of cross-section 0.45·0.45 m², continuations of the columns.

This document is the intellectual property of the fib – International Federation for Structural Concrete. All rights reserved.
This PDF of fib Bulletin 100 is intended for use and/or distribution solely within fib National Member Groups.

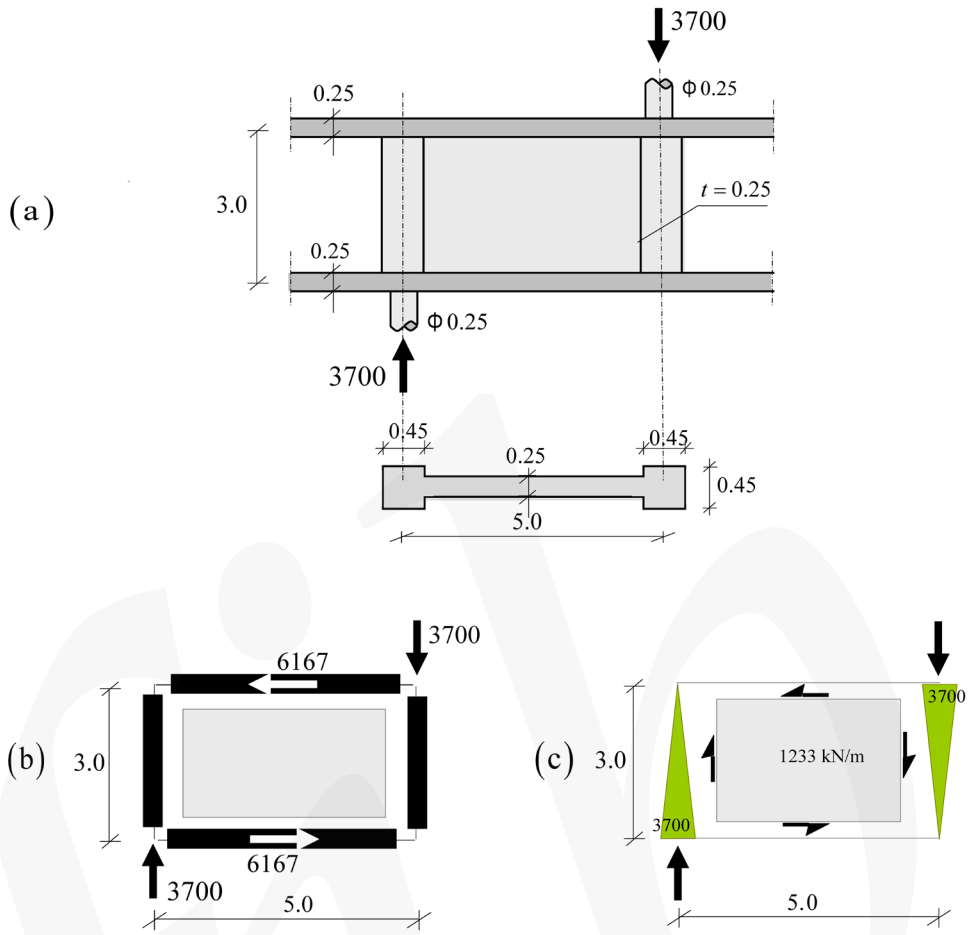


Fig. 5-45 (a) Deviating columns and connecting wall, not to proper scale. (b) Stringer-panel model and equilibrating loading set in kN. (c) Stringer forces in kN and panel shear membrane force in kN/m. All dimensions in m.

Fig. 5-45b depicts the simple stringer-panel model and the load on the model. The two opposite vertical loads of 3'700 kN equilibrate the two opposite horizontal shearforces of 6'167 kN. The slabs act these horizontal forces on the wall. They occur at the interfaces between wall and slabs.

The horizontal stringers are the slab parts at the top and base of the wall (depth and width of stringers 0.25 m). The vertical stringers are the chords with area 0.45·0.45 m^2.

The model is statically determinate and is solved with exceptional ease. The solution is presented in Fig. 5-45c. The green colour in the vertical stringers denotes compression. The compressive forces decrease linearly from 3'700 N to zero. The horizontal stringers remain stressless, for the shear load similarly, 6'167 kN is transferred directly to the panel. The shear membrane force is 1'233 kN/m.

This document is the intellectual property of the fib – International Federation for Structural Concrete. All rights reserved.
This PDF of fib Bulletin 100 is intended for use and/or distribution solely within fib National Member Groups.

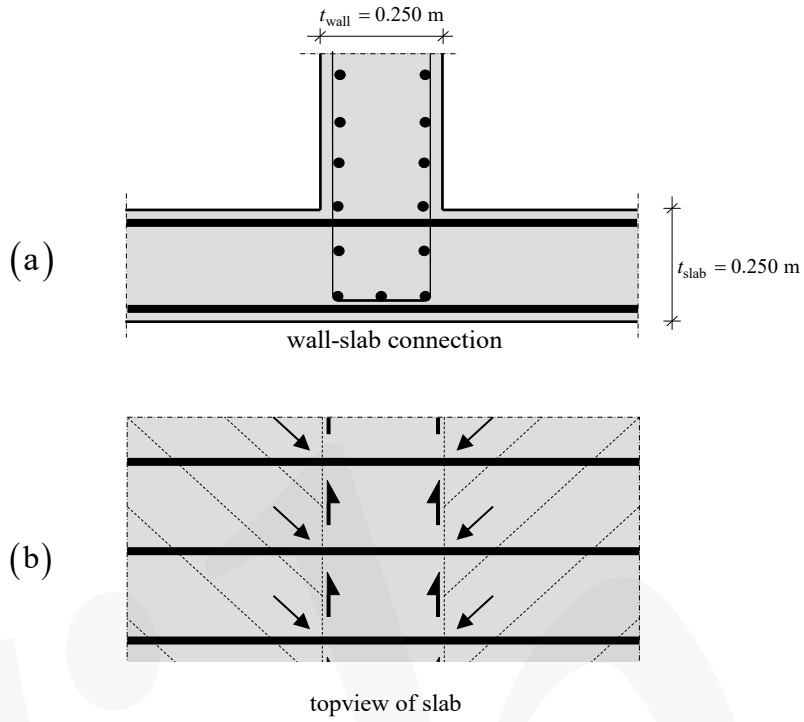


Fig. 5-46 Wall-slab connection

Choosing an equal amount of mesh reinforcement in both panel directions, the amount must be designed on the basis of:

$$n_{sx} = n_{sy} = 1'233 \text{ kN/m}$$

The yield stress is $f_y = 500$ MPa and the partial safety factor $\gamma_s = 1.15$. Hence, the design strength of the reinforcement mesh is $f_{sd} = 500/1.15 = 435$ MPa. The required steel area is

$$A_{sx} = A_{sy} = 1'233'000/435 = 2'834 \text{ mm}^2/\text{m}$$

A mesh at both wall sides $\phi 14$, spacing of 100 mm, will suffice, providing 3'077 mm^2/m. It is important that the reinforcing bars are well anchored. In fact, both the horizontal and the vertical bars must be implemented as stirrups, as is depicted (for the vertical stirrups) in Fig. 5-46a.

The compressive stress in the concrete struts is twice the nominal shear stress

$$\sigma_c = 2 \times \{1'233'000/(250 \times 1'000)\} = 9.9 \text{ MPa}$$

This is fine, for the effective design strength is

$$\nu f_{cd} = 0.6 \times 20 = 12.0 \text{ MPa}$$

where ν is the effectiveness factor and f_{cd} the design strength.

This document is the intellectual property of the fib – International Federation for Structural Concrete. All rights reserved.
This PDF of fib Bulletin 100 is intended for use and/or distribution solely within fib National Member Groups.

5.5.5.1 Reinforcement in wall-slab connection and concrete stress

Fig. 5-46b presents a top view of the slab at the location of the wall. The shearing force of 6'167 kN (refer to Fig. 5-45b) is transferred between slab and wall in two faces. Each face has a depth of 250 mm. The shear force n per unit length in each face is

$$n = 1'233/2 = 616 \text{ kN/m}$$

A distributed set of inclined concrete struts develops, as is the case in the wall. In the direction normal to the wall, distributed reinforcement is required, half the amount required in the wall, because of spreading in two faces. A mesh ϕ14, spacing of 200 mm, will do.

The concrete stress is also half, due to spreading in two faces

$$\sigma_c = 9.9/2 = 5.0 \text{ MPa},$$

which again is less than the design strength of 12.0 MPa.

5.5.5.2 Design of concrete vertical stringers

The vertical stringers are the continuation of the high-strength circular columns with diameter 250 mm. Their load is N = 3'700 kN; hence, the required strength is

$$N_{cd} = 3'700 \text{ kN}$$

The stringers have been given a square cross-section of area 450·450 mm^2. The design concrete stress is f_{cd} = 20 MPa, and the effectivity factor ν = 1.0. Hence the resistance is

$$N_{cd} = (450 \times 450 \times 20)/1'000 = 4'050 \text{ kN}$$

For framing purposes, 8 longitudinal bars ϕ12 are foreseen in the stringers, and also stirrups ϕ8, at a spacing of 150 mm.

5.5.6 Building wall with opening

The wall with opening in-between two floors discussed in Chapter 1.2 is now considered (see Fig. 5-47). The height of the wall is 3.55 m, including the thickness of the top floor. The width of the wall is 2.65 m and the thickness 0.20 m. The load consists of a central point load of 1'000 kN at the top of the wall.

In this Section, the concrete characteristic strength is f_{ck} = 30 MPa and the characteristic steel yield stress is f_{sk} = 500 MPa. The partial safety factor for concrete is γ_c = 1.5 and for steel γ_s = 1.15. Hence, the design strengths are f_{cd} =30/1.5 = 20 MPa and f_{sd} =500/1.15 = 435 MPa, for concrete and steel, respectively.

This document is the intellectual property of the fib – International Federation for Structural Concrete. All rights reserved.
This PDF of fib Bulletin 100 is intended for use and/or distribution solely within fib National Member Groups.

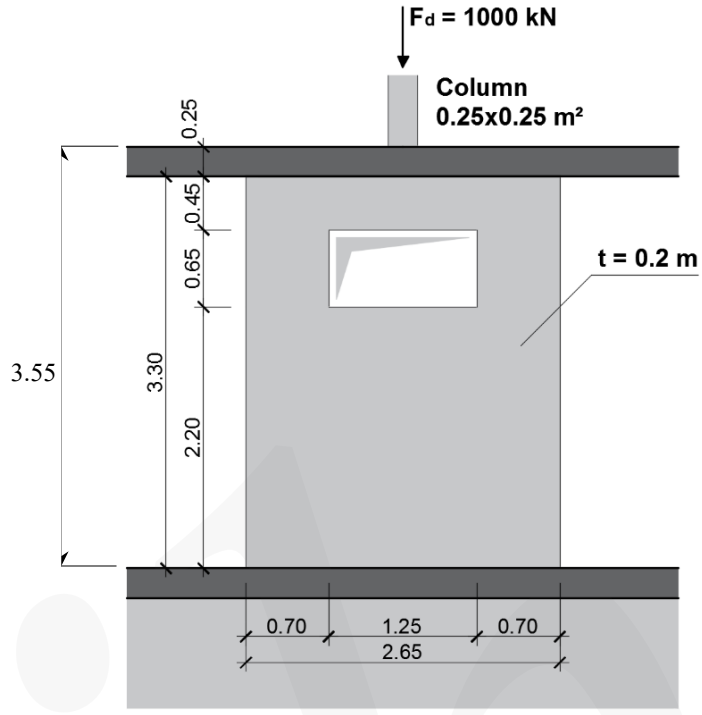


Fig. 5-47 Scheme of the wall structure. Dimensions in m.

5.5.6.1 Modelling of the structure

In fact, the whole wall structure is one single D-region. The first step in the modelling is to determine a set of equilibrating loads. We will do so in two different ways. Firstly, elasticity-inspired. Secondly, plasticity-inspired. In the first way, the opening in the wall is the disturbance, and the D-region extends to the bottom of the wall, since the wall height below the horizontal bottom line of the opening (2.20 m) is less than the wall width (2.65 m). In the case that the height is equal to or greater than the width, a uniform distribution of the vertical support reaction is expected at the base of the wall, due to Saint-Venant's principle. In the case under consideration, the difference between the height 2.20 m below the opening and the width 2.65 m is sufficiently small to start from such a uniform distribution at the base.

Fig. 5-48 shows the applied stringer-panel model. The loading consists of the single downward point load of 1'000 kN at the top of the wall and five upward point loads at the base of the wall, with a total of 1'000 kN.

In the plasticity-inspired way, we abandon applying Saint-Venants principle and feel free to propose a distribution of the vertical support forces at the base and choose locations of the horizontal stringer forces in the vertical axis of symmetry of the wall.

This document is the intellectual property of the fib – International Federation for Structural Concrete. All rights reserved.
This PDF of fib Bulletin 100 is intended for use and/or distribution solely within fib National Member Groups.

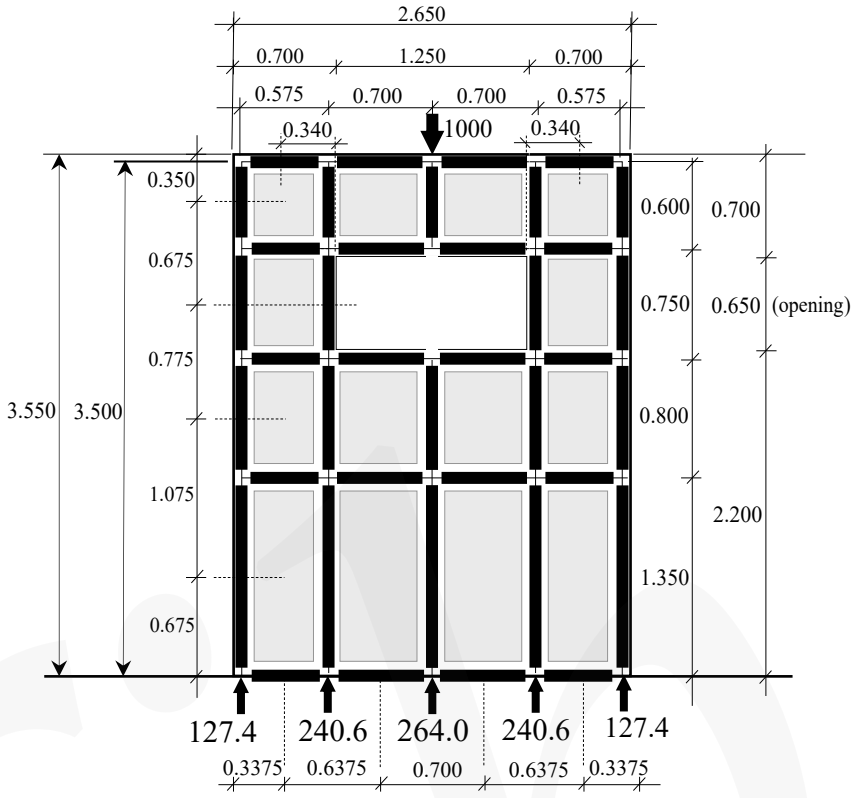


Fig. 5-48 Applied stringer-panel model. Dimensions in m. Force in kN.

The dimensions of the model grid follow from the dimensions in Fig. 5-48.

A spacing of 0.05 m between the free structure edges and the outer stringers is adopted. It is expected that the cross-section area of the vertical stringers to the left and right of the opening is not sufficient to limit the compressive concrete stresses. Therefore, a spacing 0.075 m is chosen at the vertical edges of the opening. The value of the five vertical base forces (elasticity-inspired) is included in the figure.

This statically indeterminate example will be considered for two different levels of approximation. First, a LoA I design is performed. The analysis starts from plasticity considerations, and the design problem is solved on the basis of equilibrium alone. Next, a LoA III design is performed. In this case, a linear-elastic stiffness analysis is executed, hence, kinematic relationships, constitutive laws and equilibrium relationships are all taken into account. In both design approaches, the left-hand wall half is considered.

5.5.6.2 Plastic analysis (LoA I)

The plasticity approach consists of four steps:

- Select a proper set of external equilibrating loads.
- Determine the degree of statically indeterminacy (m).
- Choose a value for the membrane shear force in m panels.
- Determine the membrane shear force of all other panels by considering the equilibrium of properly-chosen free body parts of the structure.
- Derive the value of the stringer forces from the membrane shear forces.

This document is the intellectual property of the fib – International Federation for Structural Concrete. All rights reserved.
This PDF of fib Bulletin 100 is intended for use and/or distribution solely within fib National Member Groups.

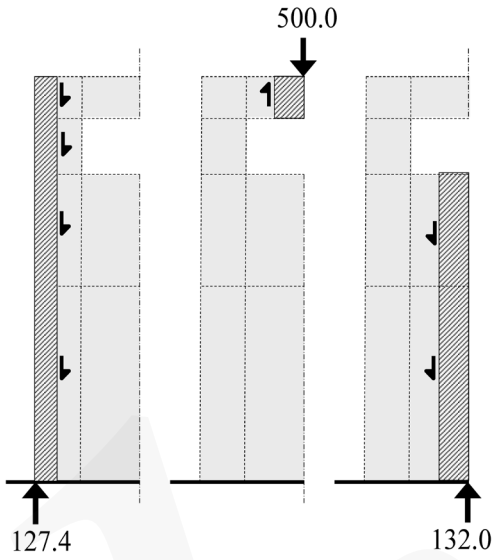


Fig. 5-49 Three free body equilibrium options (hatched areas). Forces in kN.

For the half wall, the membrane shear force *n* of seven panels must be determined. Only three free bodies can be selected for which an equilibrium equation can be derived, all in vertical direction; they are hatched in Fig. 5-49. Hence, the degree of redundancy is *m* = 7–3=4, and at forehand the value of four panel membrane shear forces has to be chosen.

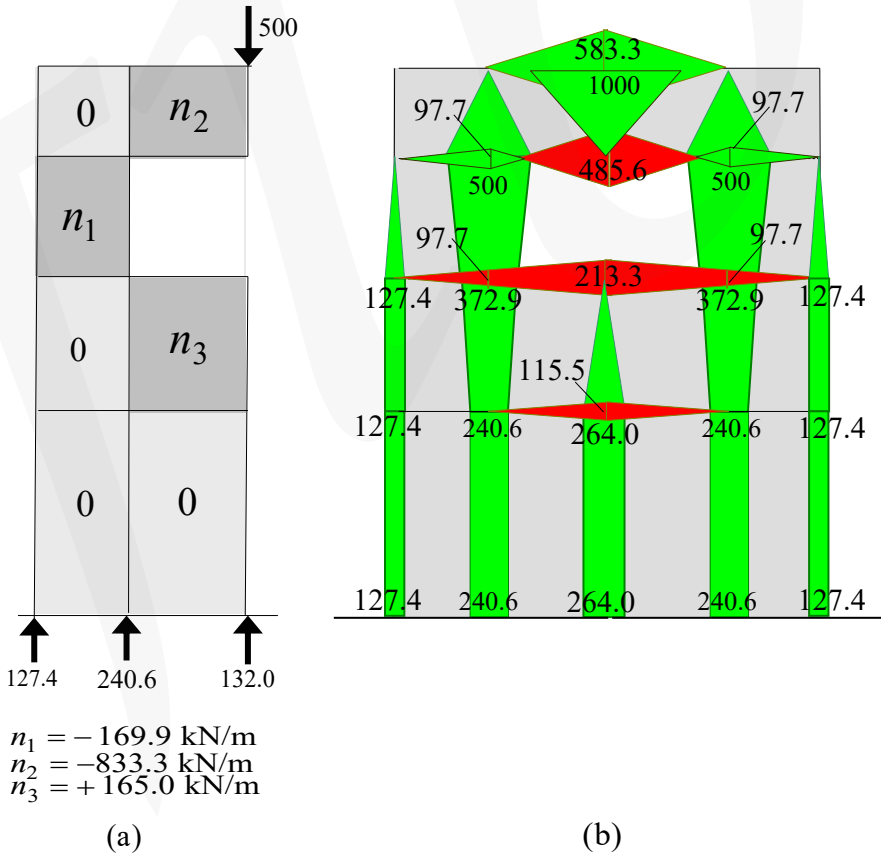


Fig. 5-50 Choice 1: Zero membrane shear forces chosen in four panels.

This document is the intellectual property of the fib – International Federation for Structural Concrete. All rights reserved.
This PDF of fib Bulletin 100 is intended for use and/or distribution solely within fib National Member Groups.

The plastic analysis will be performed twice. In both analyses four zero panel values are assumed, be it not in the same panels. The main difference between the two plastic analyses regards the choice of the external equilibrating forces. Choice 1: elasticity-inspired. Choice 2: chosen freely.

5.5.6.3 Choice 1. Elasticity-inspired load

Fig. 5-50a shows the four panels at which the membrane shear force is zero. The panels with the three unknown membrane shear forces are n_1, n_2 and n_3, and these panels have been shaded darker. The obtained n-values are given in the figure. The membrane shear forces of Fig. 5-50a yield the stringer forces shown in Fig. 5-50b.

For the minimum panel reinforcement a distributed mesh ϕ8 in two directions is chosen at both sides of the wall with a spacing of 200 mm. The area of this mesh is $2\cdot(5\pi/4)\cdot8^2$ = 503 mm^2/m, 0.25% of the concrete area. The strength is n_{min} = (503·435)/1'000 = 218.8 kN/m. This is sufficient for all panels except above the opening.

The panels above the opening carry a shear membrane force of 833.3 kN/m, requiring 833'300/435 = 1'916 mm^2/m. This is obtained by a distributed mesh reinforcement ϕ12 in two directions, at both sides of the wall, with a spacing of 100 mm. The area of this mesh is $2\cdot(10\pi/4)\cdot12^2$= 2'262 mm^2/m. The strength is (2'262·435)/1'000 = 984.0 kN/m. The horizontal bars may be extended into the corner panels for anchoring. The vertical bars are installed as stirrups; refer to Fig. 5-51.

The tensile force in the tie above the opening is N = 485.6 kN. With a design steel stress f_{yd} =435 N/mm^2, the required steel cross-section area is 485'600/435 =1'116 mm^2. This is satisfied by 4ϕ20. This area is $4(\pi/4)\cdot20^2$ =1'257 mm^2.

The force in the tie below the opening is 213.3 kN. The required area is 213'300/435 = 490 mm^2. This is satisfied by 3ϕ16, with area of $(3\pi/4)\cdot16^2$ = 603 mm^2.

In the wall region with mesh ϕ8-200, the highest shear membrane force is 169.9 N/mm. Because of the thickness 200 mm, the nominal shear stress is τ =169.9/(200)=0.85 MPa. The concrete compressive stress σ_c in the panels is twice the value of the nominal shear stress τ, hence σ_c = 1.70 MPa. The effective design strength is $\nu\cdot f_{cd}$ = 0.6·20 = 12.0 MPa, which is sufficient.

In the region with mesh ϕ12-100, the membrane shear force is 833.3 N/mm. Hence, the nominal shear stress is τ = 833.3/200 = 4.17 MPa; the concrete stress is twice this value: σ_c = 8.34 MPa, which is less than the effective design stress of 12.0 MPa.

This document is the intellectual property of the fib – International Federation for Structural Concrete. All rights reserved.
This PDF of fib Bulletin 100 is intended for use and/or distribution solely within fib National Member Groups.

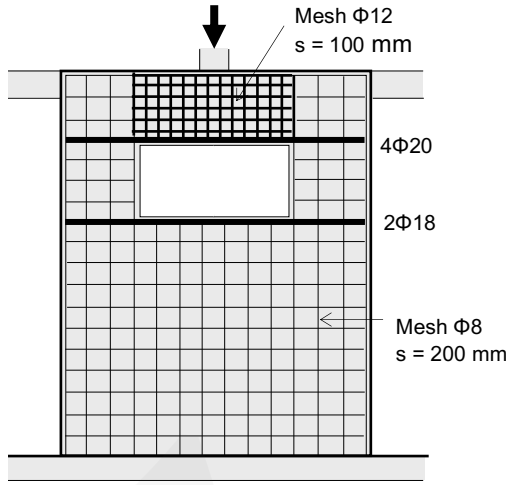


Fig. 5-51 Reinforcement lay-out for Choice 1 (LoA I).

The largest compressive stringer force occurs in the vertical stringer at the location where the point load is applied. The vertical force 1000 kN acts (neglecting spreading) on an area of 200·250 = 50'000 mm^2, and at the location, compressive stresses occur in two orthogonal directions. The compressive stress is 1'000'000/50'000 =20 MPa. Because of the effectivity factor $\nu = 1.0$, the design strength is $\nu \cdot f_{cd}$=1.0×20 =20 MPa. This value is not surpassed.

At the same location the horizontal compressive stringer force is 583.3 kN. The required stringer area is 583'300/20=29'165 mm^2. A larger area is at disposal, because the stringer is located in the top floor slab. The spacing between the stringer axis and the top of the wall is 50 mm; therefore, the width of the stringer is 100 mm. In transverse direction a width is needed 29'165/100 = 292 mm. Accounting for the wall thickness of 200 mm, only 46 mm extra floor width at each wall side has to be allocated. The stringer force can be easily carried.

The next largest compressive force occurs in the vertical stringer to the left and right of the opening. The force is 500 kN. Because no tensile bars are crossing where this force occurs, the effectivity factor $\nu = 1.0$, and the design strength $\nu \cdot f_{cd}$ = 20 MPa. The stringer has a width 2·75=150 mm. Accounting for the wall thickness t = 200 mm, the stringer cross-section area is 150·200=30'000 mm^2. Hence, the compressive concrete stress is σ_c = 500'000/30'000 = 16.67 MPa, which is smaller than 20 MPa.

5.5.6.4 Choice 2. Plasticity-inspired load

Fig. 5-52a shows the freely chosen external load and the four panels to which a zero-membrane shear force is assigned. The panels with the three unknown membrane shear forces are n_1, n_2 and n_3 again have been shaded darker. The main difference with Choice 1 is the external load on the wall half.

The obtained membrane shear forces n_1, n_2 and n_3 are given in Fig. 5-52a. The absolute value of the membrane shear forces n_1 and n_2 are very close to each other and have (practically) the same value as n_2 in Choice 1. Hence, these panels require the same reinforcement, ϕ12, spacing 100 mm, both wall sides. For all other panels the minimum reinforcement is sufficient (based on n_{min} =218.8 kN/m). For the distributed reinforcement, refer to Fig. 5-53.

This document is the intellectual property of the fib – International Federation for Structural Concrete. All rights reserved.
This PDF of fib Bulletin 100 is intended for use and/or distribution solely within fib National Member Groups.

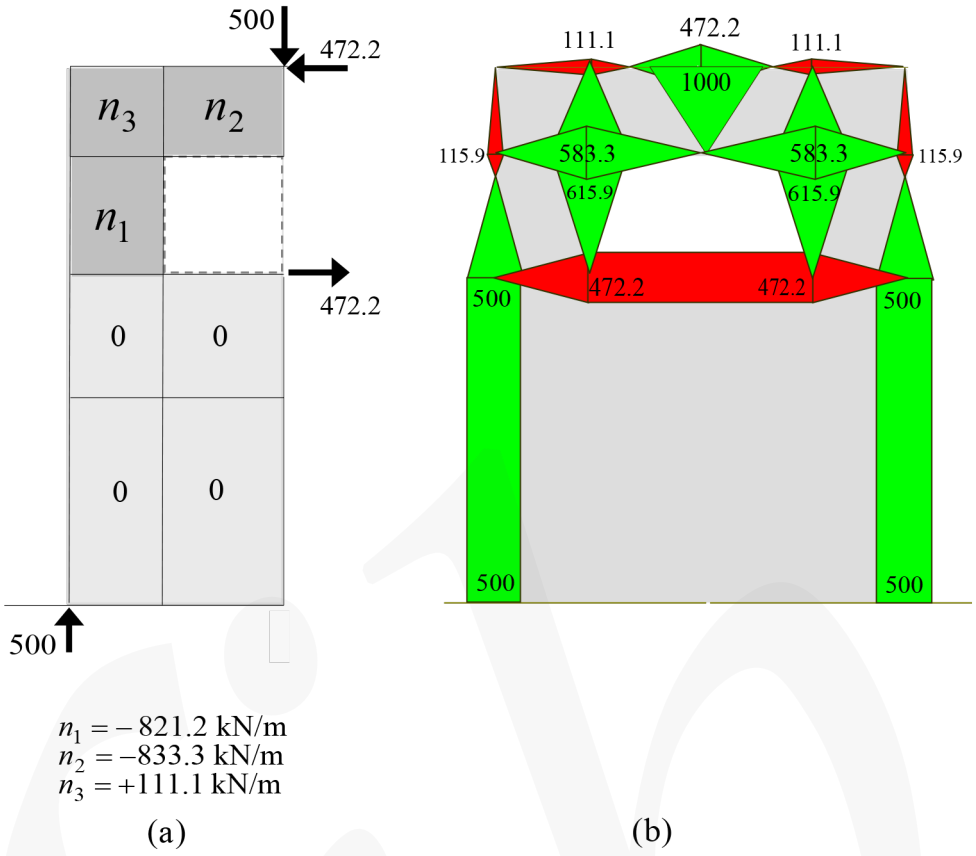


Fig. 5-52 Choice 2. Zero membrane shear forces chosen in four panels.

From the membrane shear forces in Fig. 5-52a, the stringer forces shown in Fig. 5-52b are derived. The force in the tie above the opening is zero. At the upper edge of the wall tensile forces 111.1 kN occur which require 255 mm² steel cross-section; 2ϕ14 will do.

The force in the tie below the opening is 472.2 kN. The required steel area is 1'086 mm². This is satisfied by 4ϕ20 (1'257 mm²).

The forces in the two horizontal tension stringers above and below the opening sum to 583 kN, less than 699 kN for the same ties in case of Choice 1. It is interesting to also compare with the strut-and-tie solution of Fig. 1-6a. There, also no horizontal tie is needed, and tensile forces occur at the upper edge of the wall. The sum of the two horizontal tie forces in that analysis is 564 kN, close to the solution 583 kN of Choice 2.

This document is the intellectual property of the fib – International Federation for Structural Concrete. All rights reserved.
This PDF of fib Bulletin 100 is intended for use and/or distribution solely within fib National Member Groups.

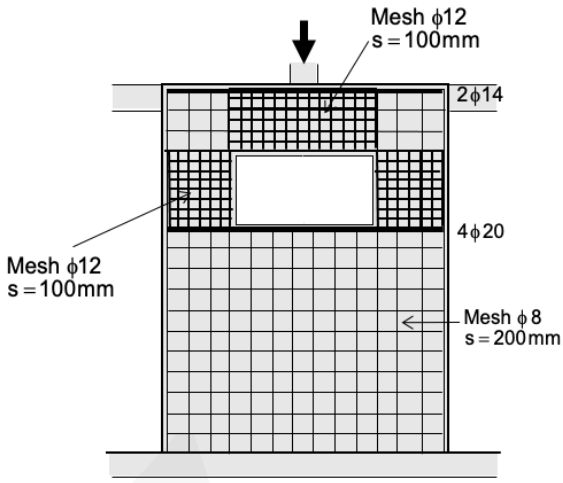


Fig. 5-53 Reinforcement lay-out for Choice 2 (LoA I).

The check for the compressive concrete stresses in the panels need not be repeated. The same distributed reinforcement arrangements occur, with permissible concrete compressive stresses.

The check for the largest compressive stringer force in the vertical stringer at the location where the point load is applied occurs in the exactly the same way as in Choice 1. At the same location the horizontal compressive stringer force becomes 472.2kN, less than in Choice 1, hence again permissible. The next largest compressive force occurs in the vertical stringer to the left and right of the opening. Now the force is 615.9 kN. The stringer has a width 2·75 = 150 mm. Accounting for the wall thickness t = 200 mm, the stringer cross-section area is 150·200 = 30'000 mm^2. The compressive concrete stress is σ_c = 615'900/30'000 = 20.5 MPa. Because no tensile bars are crossing where the force 500 kN occurs, the effectivity factor is ν = 1.0, and the design strength is $\nu \cdot f_{cd}$ =20 MPa. Strictly speaking, the strength limit is surpassed, and an iteration has to be performed with a slightly adapted geometry of the mesh. This is not performed here.

5.5.6.5 Stiffness analysis (LoA III)

First, the stiffness properties of the stringers and panels for the uncracked Serviceability Limit State (SLS) have been determined. The stiffness of a stringer depends on E, A and l, the modulus of elasticity $E = 3\times10^6$ kN/m^2, the cross-section area A and length l, respectively. The area is $A = b \cdot t$, where t is the wall thickness and b the width of the stringer. The width is chosen as the sum of the half widths of the two adjacent panels. In the case of an edge stringer, only one half panel width is concerned, but now the spacing between stringer and free edge must be included, referring to the dimensions to the left of and below the model in Fig. 5-48. The same holds for stringers along the opening. The length l is also derived from the grid in the figure.

The mechanical property of a panel depends on G, t, a and b, where the shear modulus $G = 1.5\cdot10^6$ kN/m^2, the wall thickness t = 0.20 m and the lengths a and b of the panel edges differ per panel. The value of G is chosen for a zero Poisson's ratio. A non-zero value has little meaning, because of the impossibility of modelling lateral interaction between stringers. The values a and b are derived from the grid (spacing between stringers) in Fig. 5-48.

This document is the intellectual property of the fib – International Federation for Structural Concrete. All rights reserved.
This PDF of fib Bulletin 100 is intended for use and/or distribution solely within fib National Member Groups.

The adopted stiffness properties for uncracked members will of course lead to a lower bound that can be used for ULS design. However, in reality, cracking may already occur in SLS, reducing the stiffness of panels and tension stringers, primarily depending on the applied reinforcement. The structural designer may account for this reduction by choosing smaller values of G or E for the members which appear to be in tension and investigate its effect on the lower bound solution. This would require one or more iterations. Here we will refrain from this.

Different widths should be used in checking whether the obtained forces in panels and stringers satisfy code requirements. For that purpose, in order to prevent that the same concrete area is used for stringers and panels, the width of stringers should be restricted. To mention an example, in Denmark the stringer width is restricted to a maximum 20% of the smallest width of the adjacent panels in order to fulfil the assumptions of the stringer model.

Again, the analysis is restricted to the left-hand half of the wall. The boundary conditions in the considered model (half structure) consist of zero horizontal degrees of freedom in the axis of symmetry. Furthermore, in order to prevent a free body displacement, one of the vertical degrees of freedom has to be set to zero. The central base degree of freedom has been chosen.

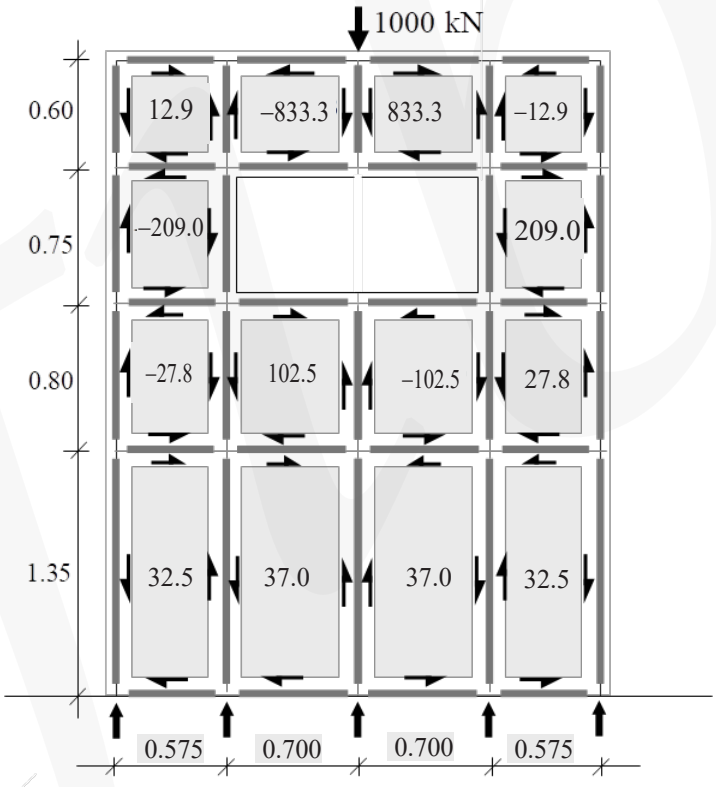


Fig. 5-54 Panel membrane shear forces in kN/m. Dimensions in m.

5.5.6.6 Results of analysis

The analysis results are depicted in two figures. For the membrane shear forces, we refer to the panel centres in Fig. 5-54. The stringer forces are plotted in Fig. 5-55. Strikingly, the top corner panels of the model appear hardly to contribute to the force transfer. The membrane shear force in the corner panels is very small compared to the

This document is the intellectual property of the fib – International Federation for Structural Concrete. All rights reserved.
This PDF of fib Bulletin 100 is intended for use and/or distribution solely within fib National Member Groups.

panels above the opening. Therefore, at the level of the upper horizontal edge of the opening, practically all load is transferred downward through the vertical stringers either side of the opening (the half point load is 500.0 kN and the obtained normal force in the vertical stringer is 507.8 kN).

At the level of the lower horizontal edge of the opening, about 70% of the load 500.0 kN is in the stringer nearest to the opening and the other 30% in the stringer nearest to the outer wall edge. In the four panels below the opening, the 70% force starts spreading in two directions, to the left and the right, causing the compressive force in the middle vertical stringer to develop in the lowest four panels, leading to the distribution of the vertical stringer forces along the base line which were the load input, according to a uniform distribution of support reactions.

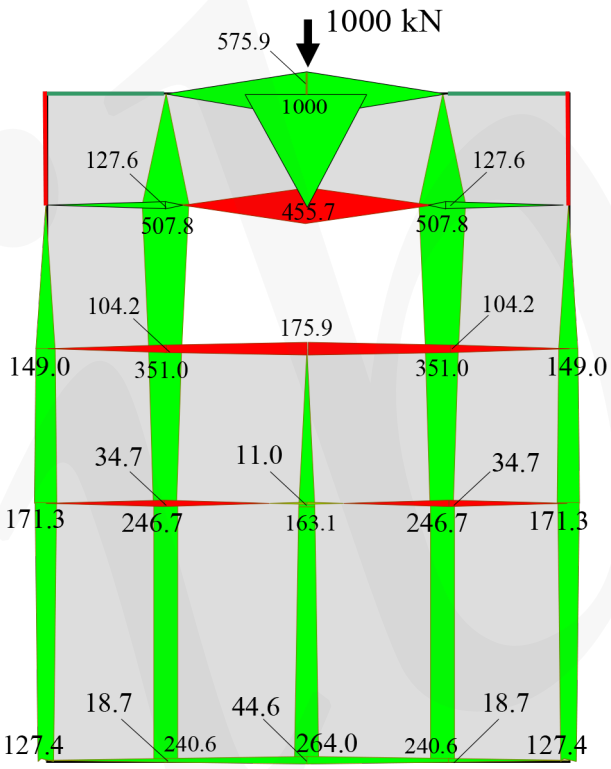


Fig. 5-55 Stringer forces in kN. Dimensions in m.

The distributed reinforcement stays the same as in the plastic analysis for all panels; refer to Fig. 5-56.

The tensile force in the tie above the opening is N = 455.7 kN. With a design steel stress of f_{sd} = 435 N/mm^2, the required steel cross-section area is 455'700/435 = 1'048 mm^2. This is satisfied by 4ϕ20. This area is 4·(π/4)·202 = 1'256 mm^2; refer to Fig. 5-56.

The tensile force in the tie below the opening is 175.9 kN. The required area is 175'900/435 = 404 mm^2. This is (within 0.5% accuracy) satisfied by 2ϕ16, with area of (2π/4)·16^2 = 402 mm^2.

Because the distributed reinforcement is the same as in the plastic analysis, the compressive concrete stresses are sufficiently limited.

The highest compressive stringer force 1'000 kN occurs in the vertical stringer at the location where the point load is applied. This force size has already been checked here above.

This document is the intellectual property of the fib – International Federation for Structural Concrete. All rights reserved.
This PDF of fib Bulletin 100 is intended for use and/or distribution solely within fib National Member Groups.

The next highest compressive stringer force 575.9 kN also occurs at the position where the point load is applied. In Section 5.5.6 has already been shown that the larger compressive force 583.3 kN is permissible.

The compressive force in the vertical stringers to the left and right of the opening is 507.8 kN. Here before, it was already shown that a larger force 596.0 is permissible.

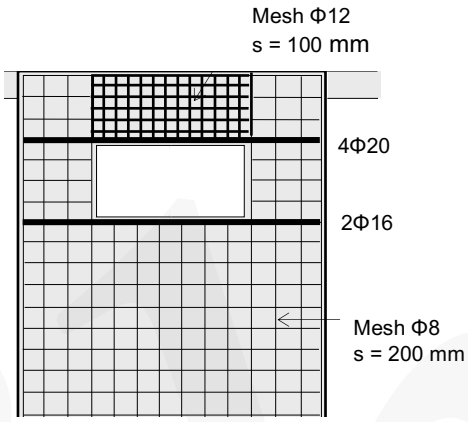


Fig. 5-56 Reinforcement lay-out for stiffness analysis (LoA III)

Repeating the analysis with a rigid base with zero vertical displacements yields almost the same solution. The resultant of the support reactions per half wall is again 500 kN, but the position of the resultant moves 0.028 m outward. In comparison with the solution for a uniform distribution of base reactions, the differences in the member forces in the upper half of the wall are far less than 1%.

5.5.6.7 Strut-and-tie model

Fig. 5-57 depicts the coarsest strut-and-tie model that can be derived from the stringer-panel results. The resultant of the three vertical stringer forces per half wall is 500 kN at each horizontal line; however, the position of the resulting vertical force differs per line. On the level of the upper horizontal opening edge, the resultant is chosen at the vertical stringer line, yielding the distance 0.575 m to the leftmost (and rightmost) stringer, as indicated in the picture. For lower levels, the position is determined on the basis of the vertical stringer forces from the SPM analysis, yielding the distances 0.404 m and 0.493 m to the leftmost (and rightmost) stringers, as indicated in the picture. The distance at the base is 0.613 m. The obtained horizontal tie forces above and below the opening are close to the stringer forces of the SPM solution in Fig. 5-55. The sum of the two tie forces is 632 kN in SPM and 639 kN in STM, a difference of 1%.

This document is the intellectual property of the fib – International Federation for Structural Concrete. All rights reserved.
This PDF of fib Bulletin 100 is intended for use and/or distribution solely within fib National Member Groups.

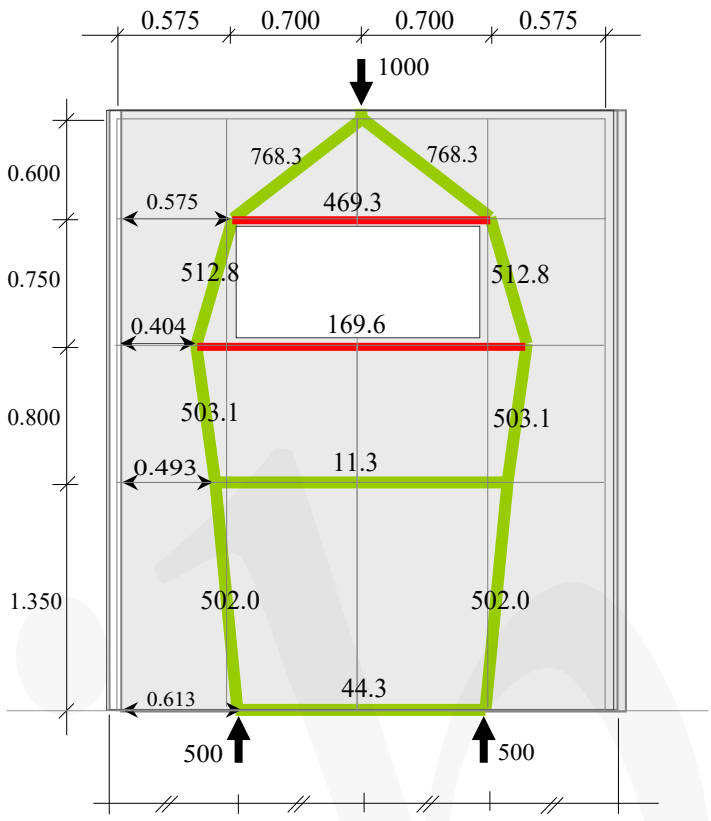


Fig. 5-57 Strut-and-tie model. Forces in kN. Dimensions in m.

5.5.7 Outlook

In the preceding sections of this Chapter the discussion of SPM has been restricted to orthogonal models with rectangular panels and linear-elastic constitutive relationships. The application of SPM is definitely not limited to these options. In this Section, three extensions are briefly examined: (i) non-orthogonal model shapes, (ii) non-linear constitutive material laws, (iii) 3D-structures and (iv) panels with advanced stress field.

5.5.7.1 Non-orthogonal model shapes

The stringer-panel concept is not necessarily restricted to modelling with rectangular panels. Panels of quadrilateral shape can be used as well[5-61], [5-62]. An example of such models is shown in Fig. 5-58. The diaphragm above a support of a box girder bridge is loaded by the shear flow according to beam theory. This loading is introduced in the model in the middle node of the stringers concerned.

Not all stringers are in line with global orthogonal axes *x* and *y*, but this does not cause any problem. However, it does for non-rectangular quadrilateral panels. Still four degrees of freedom are defined, but the stiffness relationship between these dofs and the corresponding element forces is more complex than for rectangular elements. The membrane shear force will not be uniformly distributed over the panel area. As a rule, the analysis cannot be done anymore by hand, even for simple models. This is because equilibrium equations soon become too complicated, even if the solution could be obtained by equilibrium equations alone. Furthermore, because of the non-uniform membrane shear force, interpretation of the results obtained requires a skilful user. For interested structural engineers, a program for linear-elastic material behaviour (SPM.py) is freely available on the Internet (http://heronjournal.nl/42-3/SPM/). A user manual with some examples is also included.

This document is the intellectual property of the fib – International Federation for Structural Concrete. All rights reserved.
This PDF of fib Bulletin 100 is intended for use and/or distribution solely within fib National Member Groups.

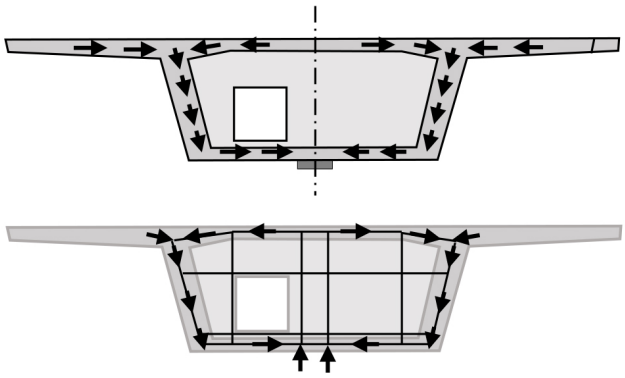


Fig. 5-58 Diaphragm above an intermediate support in box girder bridge with both rectangular and quadrilateral panels. Above: flow of shear stresses from beam theory of box girder. Below: stringer-panel model with loading in middle-node of stringers.

5.5.7.2 Non-linear constitutive material laws

Non-linear constitutive relationships can be of any kind. In SPM, one has to distinguish between different types of non-linearity for stringers and panels.

For stringers, it is appropriate to distinguish tensile and compressive forces. In the compression domain, usually an elastic-plastic law is applied. In the tension domain three phases must be considered, corresponding to three distinct branches in the N-ε diagram

1. un-cracked phase, in which the elasticity modulus of plain concrete determines the linear-elastic branch;
2. the crack-developing phase with a tension-stiffening branch;
3. the phase with yielding main reinforcement, determining a horizontal plastic branch.

Handling of non-linearity in panels is more complex because the stress state is not uniaxial as in stringers. For the two-dimensional stress state in panels it is recommended to use the modified compression field theory as implemented by Hoogenboom[5-61], in the specialised software SPanCAD, employing AutoCAD as graphical user-interface. This application is typical LoA IV. This academic software has stressed the potential of nonlinear SPM, but only recently it has seen its way into the building and infrastructure engineering software sector. Additionally, part of the work of Heinzmann[5-62] also regards SPM, but no publicly accessible software has yet been made available.

5.5.7.3 3D-structures

In 3D-models the composition of stringers and panels is in three-dimensions. Two examples are shown in Fig. 5-59, a box type of bridge of varying depth and a caisson for founding a bridge pier. Now a 3D-arrangement of degrees of freedom does occur, but, for the rest, the degree of complexity hardly increases.

This document is the intellectual property of the fib – International Federation for Structural Concrete. All rights reserved.
This PDF of fib Bulletin 100 is intended for use and/or distribution solely within fib National Member Groups.

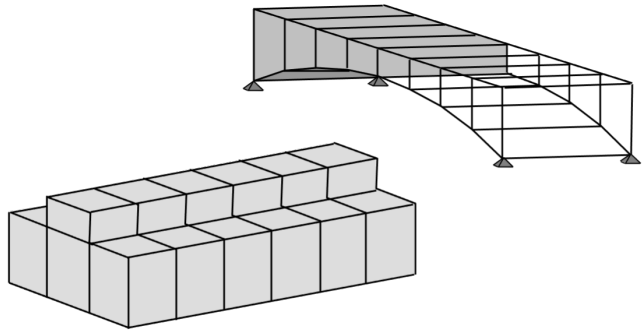


Fig. 5-59 Examples of 3D-structures, a caisson and a curved box girder bridge.

5.5.7.4 Panels with advanced stress field

In this Bulletin, the stress field in panels has been restricted to a uniform membrane shear force n. The concept can be extended to equilibrating stress fields in which all membrane forces n_{xx}, n_{yy} and n_{xy} play a role. Hoogenboom[5-61] has done so by defining five independent stress modes, three uniform modes n_{xx}, n_{yy} and n_{xy}, a mode in which n_{xx} varies linearly in x-direction and a mode in which n_{yy} varies in y-direction. The result is a panel which is loaded on each edge by a uniform shear traction and a uniform normal traction. Hence, by necessity, the set of panel degrees of freedom has to be increased; at each edge, not only a degree of freedom in the direction of the edge occurs, but also normal to the edge. Interested readers are referred to Hoogenboom[5-61]. Such an enhanced model is not particularly needed for design purposes, but can facilitate the assessment of existing structures. As such, it would fall into LoA IV.

This document is the intellectual property of the fib – International Federation for Structural Concrete. All rights reserved.
This PDF of fib Bulletin 100 is intended for use and/or distribution solely within fib National Member Groups.

6. Practical examples

6.1 Use of strut-and-tie models and stress fields for assessment of existing critical structures

Strut-and-tie models and particularly their combination with stress fields, has shown to be a very suitable tool for analysing the strength of existing structures. One of the most interesting advantages of this approach is that the estimate of the strength can be gradually refined as needed, by considering more refined stress fields, through a Levels-of-Approximation approach. Thus, simple estimates of the strength can be rapidly calculated while, for critical structures, more detailed and time-consuming analyses can be consistently performed.

The following example shows the application of such approach to the evaluation of a critical member (riegel element, deep transfer beam) for the Troll A gas production platform in the North Sea (Norway), Fig. 6-1. The 370 m high concrete gravity-based structure was installed in 1996 as the largest structure ever transported and installed in sea. The platform was built by Norwegian Contractors and is operated by Equinor (formerly Statoil).

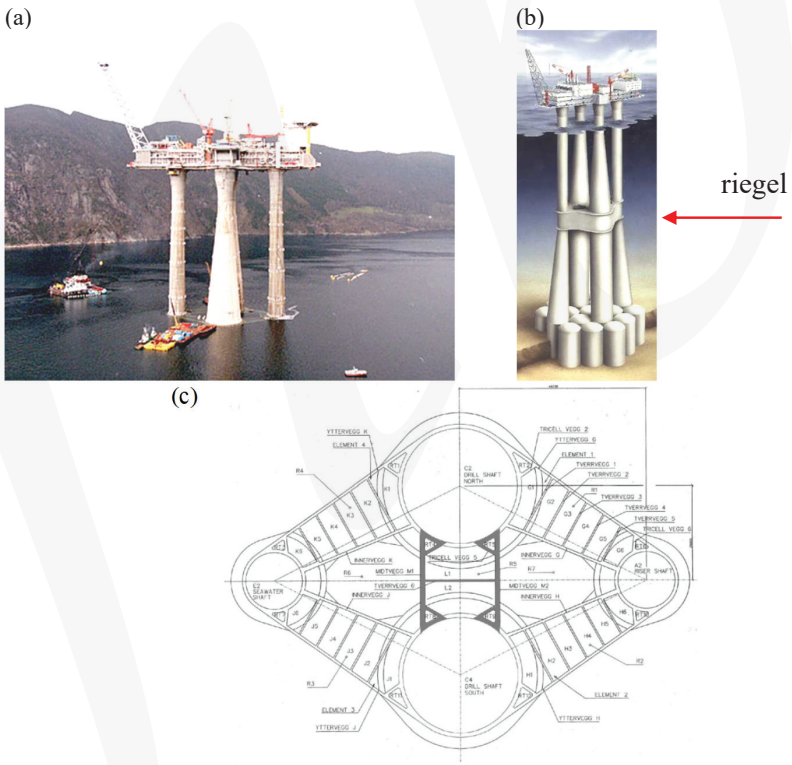


Fig. 6-1 Troll A offshore platform: (a) during tow to field ; (b) view and location of the investigated member; and (c) horizontal view of the inner riegel walls

Following a potential increase of the topside weight, a preliminary analysis indicated that the shear strength of the riegel element connecting the four shafts was potentially critical and its strength was investigated in detail. The geometry of the inner walls of the riegel is

https://doi.org/10.35789/fib.BULL.0100.Ch06

This document is the intellectual property of the fib – International Federation for Structural Concrete. All rights reserved.
This PDF of fib Bulletin 100 is intended for use and/or distribution solely within fib National Member Groups.

shown in Fig. 6-2. They have a total height of almost 30 meters and a minimum thickness of 1.2 meters. The element is heavily prestressed in the longitudinal and transverse directions, leading to crushing of the compression field as the governing failure mode.

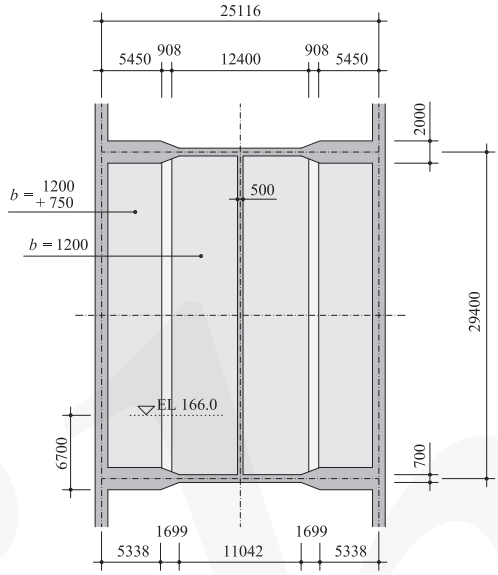


Fig. 6-2 Inner riegel wall: view and geometry (dimensions in [mm])

For this case, a simple check of the strength can be directly performed based on the strength of the compression field:

$$V_{Rd} = \eta_{\varepsilon} \cdot f_{cd} \cdot b_w \cdot z \cdot \sin\alpha \cdot \cos\alpha \qquad 6\text{-}1$$

The maximum strength of the stress field (lower-bound of the failure load) can be obtained for an angle of the compression field α = 45° (this can be easily obtained by equalling the derivative of the shear strength to zero), refer to Fig. 6-3a.

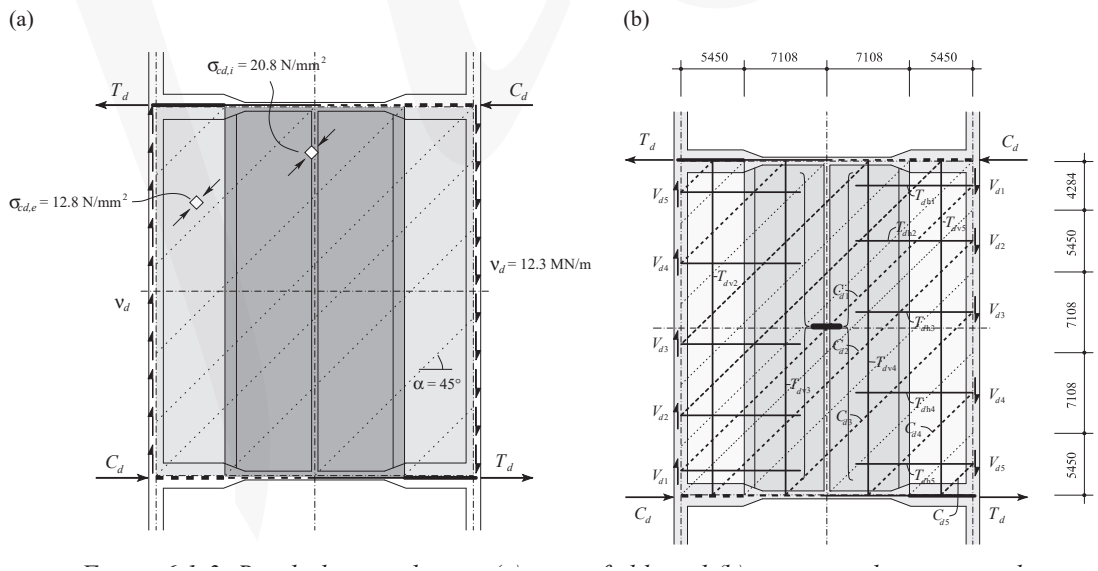


Fig. 6-3 Rigid-plastic solution: (a) stress field; and (b) corresponding strut-and-tie model

This document is the intellectual property of the fib – International Federation for Structural Concrete. All rights reserved.
This PDF of fib Bulletin 100 is intended for use and/or distribution solely within fib National Member Groups.

Thus:

$$V_{Rd} = \frac{1}{2}\eta_{\varepsilon} \cdot f_{cd} \cdot b_w \cdot z \qquad 6\text{-}2$$

Where $f_{cd} = \eta_{fc} \cdot f_{ck} / \gamma_c$ (= 34.6 MPa in the investigated case, to account for the brittleness factor and the safety format). With respect to the transverse strain reduction factor (η_{ε}), values between 0.55[6-1] and 0.6[6-2] are usually adopted. Adopting for instance the value 0.6 (σ_{cd} = 20.8 MPa), gives:

V_{Rd} = 363 MN

In addition to this simple analysis, the significance of the structure as well as some peculiarities (concrete in the bottom part of the wall was slightly less resistant than in its top part) ponied to the need for a more refined analysis. The results were performed using the elastic-plastic stress field method (refer to Section 5.2), leading to a failure load V_{Rd} = 396 MN (9% higher than that corresponding to the rigid-plastic analysis). The main results are shown in Fig. 6-4 and Fig. 6-5.

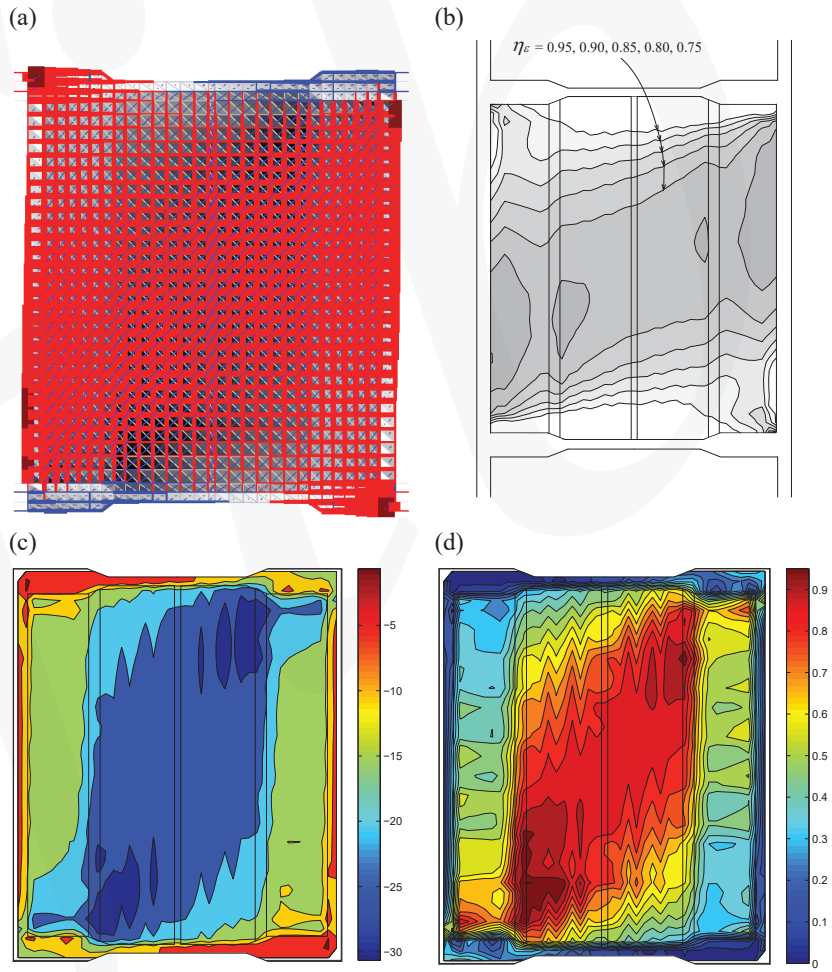


Fig. 6-4 Elastic-plastic stress field analysis: (a) stresses in the reinforcement (brown referring to yielding); (b) coefficient η_{ε}; (c) compressive stress in the concrete; and (d) utilization ratio ($\sigma_{cd}/(\eta_{\varepsilon} f_{cd})$

This document is the intellectual property of the fib – International Federation for Structural Concrete. All rights reserved.
This PDF of fib Bulletin 100 is intended for use and/or distribution solely within fib National Member Groups.

The elastic-plastic stress field analysis results confirm those of the rigid-plastic analysis, while allowing for some refinements:

No yielding of the reinforcement occurs in the shear panel (refer to Fig. 6-4 a where yielded reinforcement is drawn in brown)

Failure occurs by concrete crushing (Fig. 6-4d) in the shear panel. Some regions in the bottom part show a weaker behaviour as the in-situ concrete strength during casting was actually lower

- The angle of the compressive stresses is close to 45° (Fig. 6-5a)
- The value of the transverse strain reduction factor is about 0.7 (Fig. 6-5b), relatively similar to the rigid-plastic assumption, yet higher

The stresses in the concrete (Fig. 6-4c) are similar (slightly higher) to those calculated according to the rigid-plastic model (Fig. 6-3a) explaining the increase in strength.

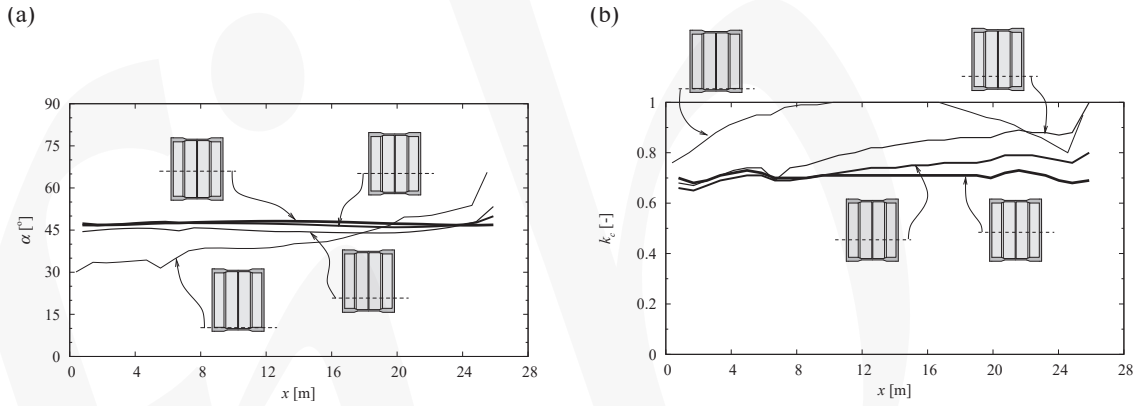


Fig. 6-5 Elastic-plastic stress field analysis (horizontal sections at location of dashed lines): (a) angle of the compression field; and (b) coefficient η_ε

This example shows thus that refinement in the analyses, while keeping the same theoretical ground, leads to consistent results and allow the engineer to gain understanding of the structural behaviour.

6.2 Use of strut-and-tie models and stress fields for conceptual design of new structures

The use of strut-and-tie models in combination with stress fields is an efficient way to approach the design of new structures, where the shape is to be defined or optimised. This is typically the case of bearing walls, where the location of openings, columns and supports has to be defined together with the architects. The example presented hereafter shows how these tools can be used at different stages of a project, from the conceptual design stage to the tender or building project.

The example refers to the Léman School (Renens, Switzerland), see to Fig. 6-6. The building was characterised by large inner spaces and patios and a reduced number of columns inside the school. This was made possible by arranging a number of bearing

This document is the intellectual property of the fib – International Federation for Structural Concrete. All rights reserved.
This PDF of fib Bulletin 100 is intended for use and/or distribution solely within fib National Member Groups.

walls supported on a limited number of columns (Fig. 6-6b). The project was built in 2007 and 2008 by the architects Espósito et Javet (Switzerland) and the structural design and analysis of the main bearing walls was performed by Muttoni et Fernández consulting engineers (Switzerland).

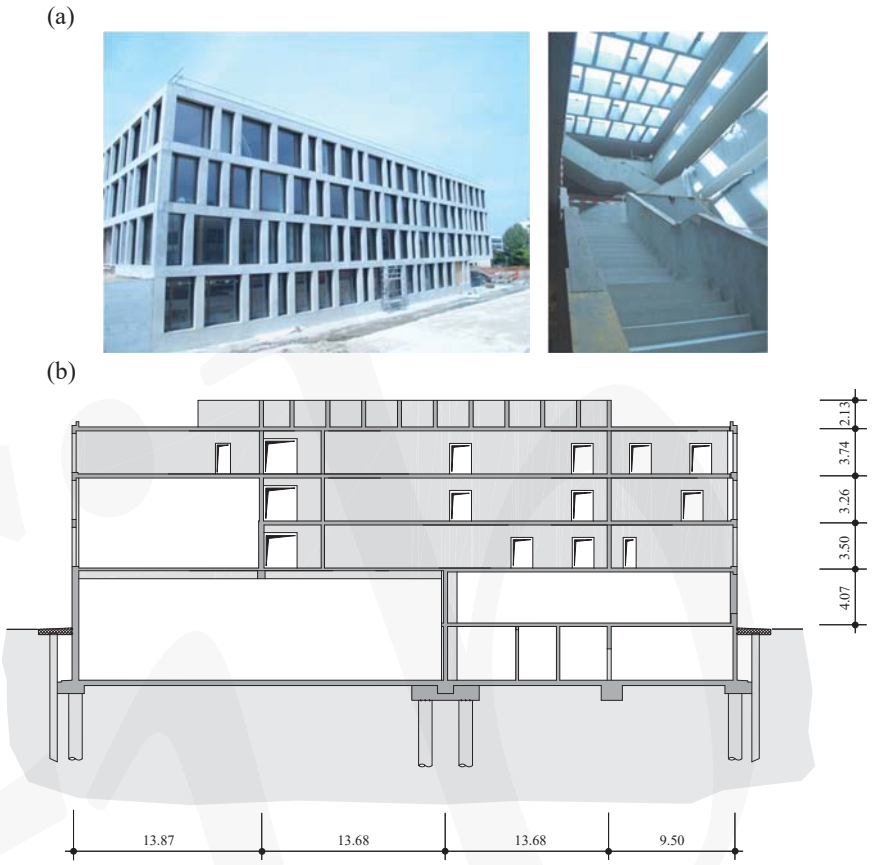


Fig. 6-6 Léman school: (a) photographs during construction; and (b) investigated wall

The conceptual design of the walls was performed by using equilibrium-based approaches, such as strut-and-tie models. This allows determining the main load-carrying actions, as well as establishing the location of the most significant openings and tension ties. Fig. 6-7 shows a preliminary analysis of the location of the main struts and ties. It can be noted that some local conflicts may arise (refer to Fig. 6-7a), but they can be solved by locally deviating the struts in the surrounding concrete by arrangement of local ties. Near the supports, however, such openings are no longer possible.

It is interesting to note that different load-carrying actions are possible. For instance, in Fig. 6-7a, the load is carried by two arches requiring only reinforcement in the bottom region of the wall. However, also the load near the central support can be carried by a top reinforcement and two curved struts (Fig. 6-7b), corresponding to the continuity reinforcement of a continuous beam. The amount of load carried by each action can be selected by the designer at this stage, on the basis of experience or to ensure a satisfactory behaviour at SLS (cracking).

This document is the intellectual property of the fib – International Federation for Structural Concrete. All rights reserved.
This PDF of fib Bulletin 100 is intended for use and/or distribution solely within fib National Member Groups.

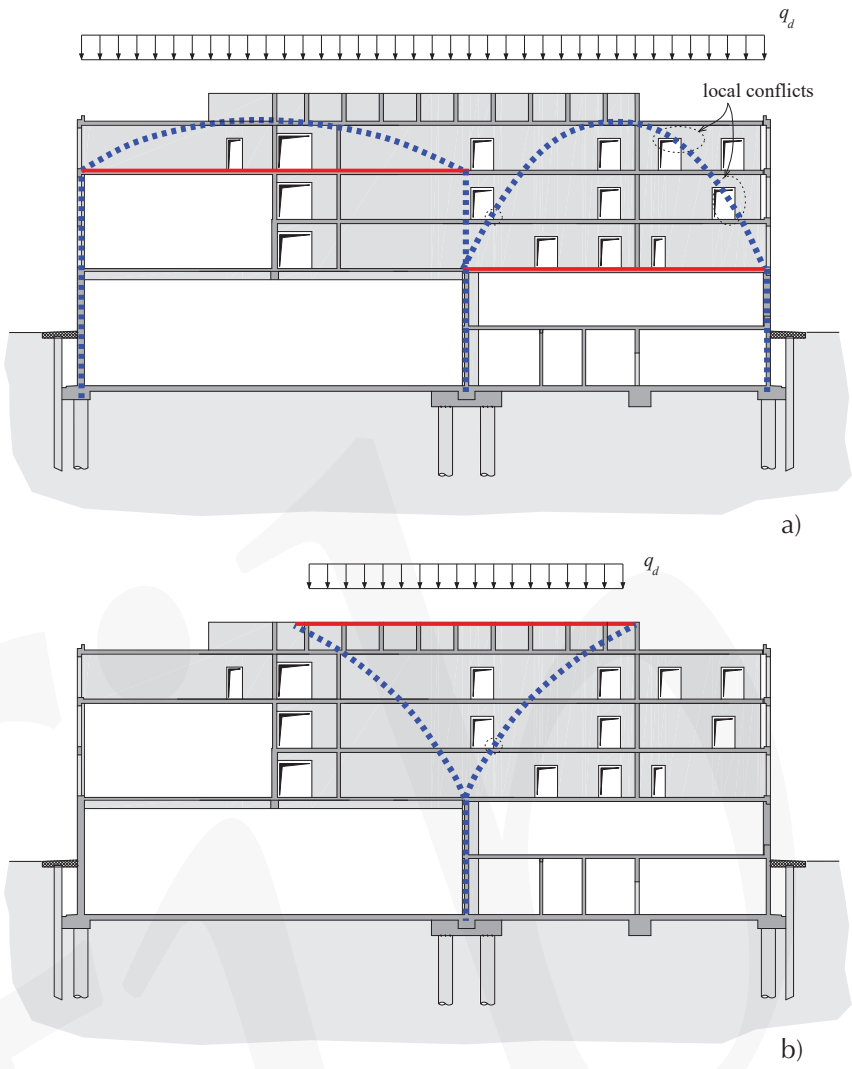


Fig. 6-7 Load-carrying actions in the wall: (a) arching action; and (b) cantilever action

The main reinforcement was designed according to a strut-and-tie model, where the continuity reinforcement over the intermediate support (Fig. 6-7b) was estimated on the basis of a continuous beam behaviour. For the tender and building project, a more detailed estimate (or a confirmation of the adopted values) of the load carried by each load-carrying action in Fig. 6-7 is required. This can be performed by means of accounting for compatibility conditions to satisfy SLS requirements, using, for instance, the elastic-plastic stress field method.

The results of this approach are presented in Fig. 6-8. They show that the final response of the structure is a combination of the previously discussed load-carrying actions (Fig. 6-8a). The amount of post-tensioning (Fig. 6-8b) can also be tailored in order to satisfy the cracking and deflection (Fig. 6-8c) criteria.

This document is the intellectual property of the fib – International Federation for Structural Concrete. All rights reserved.
This PDF of fib Bulletin 100 is intended for use and/or distribution solely within fib National Member Groups.

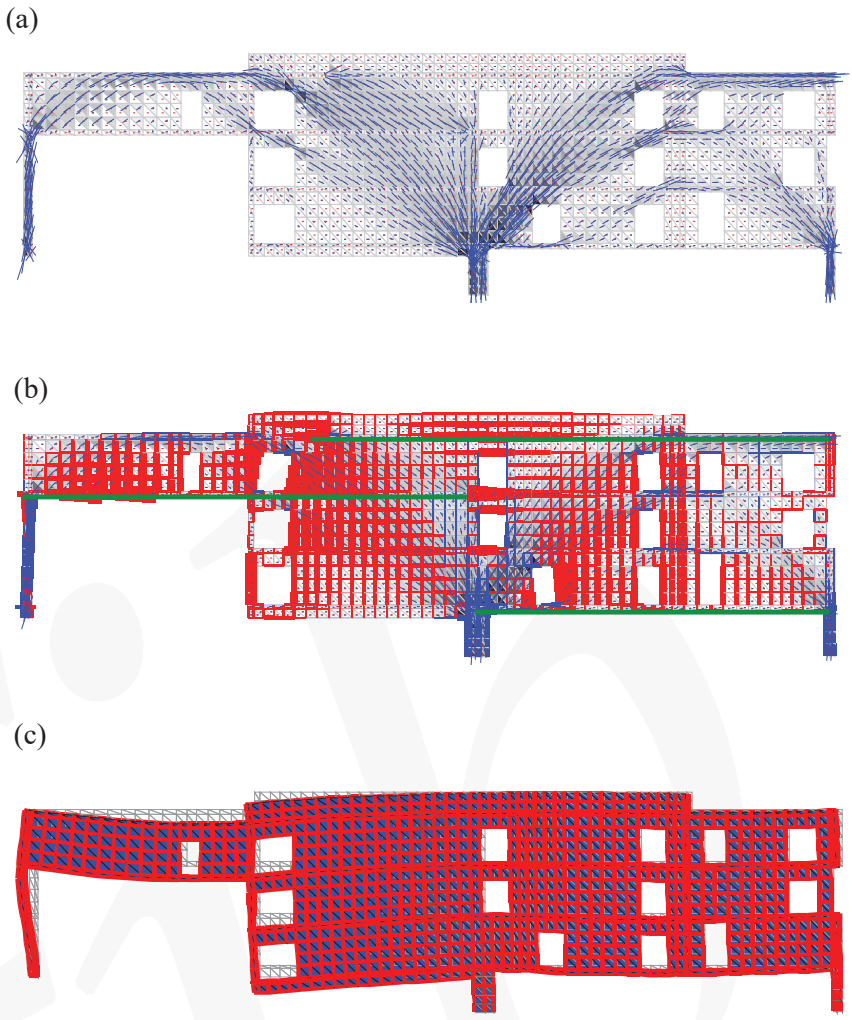


Fig. 6-8 Analysis of the wall by means of elastic-plastic stress fields: a) compression field principal directions; (b) stresses in the reinforcement (green for post-tensioning tendons); and (c) deflected shape

As for the previous example, it is clear that the method is consistent and allows the designer to gain understanding of the structure and of its critical regions. The different levels of approximation yield consistent results and allow a transition between simple (hand-made) calculations to more complex (computer-aided) analyses.

It is however advised that once the Elastic-Plastic Stress Field (EPSF) model is finalised and checked (sum of forces, integration of sectional forces), manual checks are performed in the critical regions. This is, for instance, the case for the load introduction at the supports (columns), where suitable detailing is required to transfer the forces by means of continuous high-strength (f_{yk} = 700 MPa) compression reinforcement.

6.3 Applications to the assessment of a bridge

The assessment of existing bridges by means of design formulas provided in codes of practice leads to safe estimates of the actual strength and might not be sufficient to ensure the load bearing capacity of the structure. In such cases, a more detailed analysis is justified in order to avoid or to minimise strengthening of the structure. This section

This document is the intellectual property of the fib – International Federation for Structural Concrete. All rights reserved.
This PDF of fib Bulletin 100 is intended for use and/or distribution solely within fib National Member Groups.

presents an example of how such refined analyses can be performed for bridge assessment. To that aim, the Elastic-Plastic Stress Fields (EPSF) will be used (according to Fernández Ruiz and Muttoni[6-3]).

The use of the EPSF for the assessment of bridges is particularly suitable as it allows consideration of a number of issues:

- Fulfilment of static and kinematic conditions, providing an exact solution according to limit analysis (and thus, maximising the strength);
- Accurate modelling of the geometry and reinforcement layout;
- Possibility to consider bond and reinforcement development conditions, as well as of stress increase in prestressing tendons;
- Local estimate of the strength reduction factor accounting for transverse cracking and the corresponding angle of the compression fields.

Fig. 6-9 shows for instance a typical box-girder bridge built in Europe (Switzerland) in the 1960's with high levels of prestressing. Evaluation of such bridges using current design provisions reveals, in many cases, insufficient shear strength due to the low reinforcement ratios used at the time, together with the limits on the compression field angles and associated value of the strength reduction factor of concrete to account for transverse cracking.

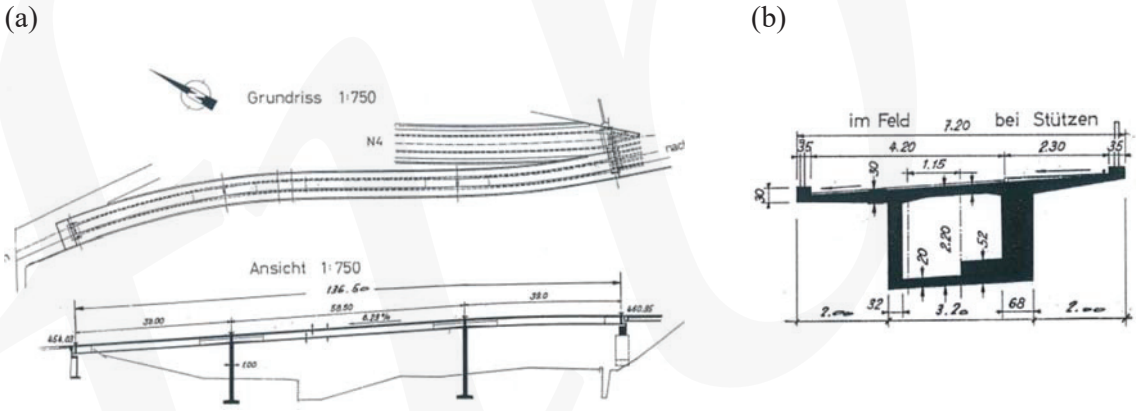


Fig. 6-9 Mosi bridge (Switzerland): (a) plan view; (b) cross-section at mid span (left) and over the supports (right)

In these cases, and in order to avoid any unnecessary strengthening, it is usually justified to perform a detailed analysis by means of EPSF. This approach allows accounting for the favourable effect of prestressing on the strength reduction factor due to transverse cracking (lower reductions for higher levels of prestressing) allowing reduction of the inclination of the compression field beyond the values usually proposed in codes of practice. Additionally, the favourable effect of the variation of the stress in the prestressing tendons in the failure region can also be accounted for. In particular, in this kind of bridges, it is important to suitably model the presence of ducts by locally reducing the width of the web[6-4], [6-5], [6-6].

To do so, a finite element model can be developed accounting for the actual geometry, reinforcement and tendon layout. The results for the region near the abutment (identified as the shear-critical region) are shown in Fig. 6-10. The critical location of the load is identified as the one closest to the support but outside of the fan region (no direct strut). The analysis predict quite low angles for the compression field (below 20°, Figs. 6-10a,d) particularly close to the support. This behaviour largely enhances the capacity to transfer shear forces

This document is the intellectual property of the fib – International Federation for Structural Concrete. All rights reserved.
This PDF of fib Bulletin 100 is intended for use and/or distribution solely within fib National Member Groups.

(activation of larger amounts of stirrups). In addition, due to the large prestressing forces, the strength reduction factor due to cracking (Figs. 6-10c) yields also larger values of the strength reduction factor than those predicted by codes of design (typically ranging from 0.55-0.65).

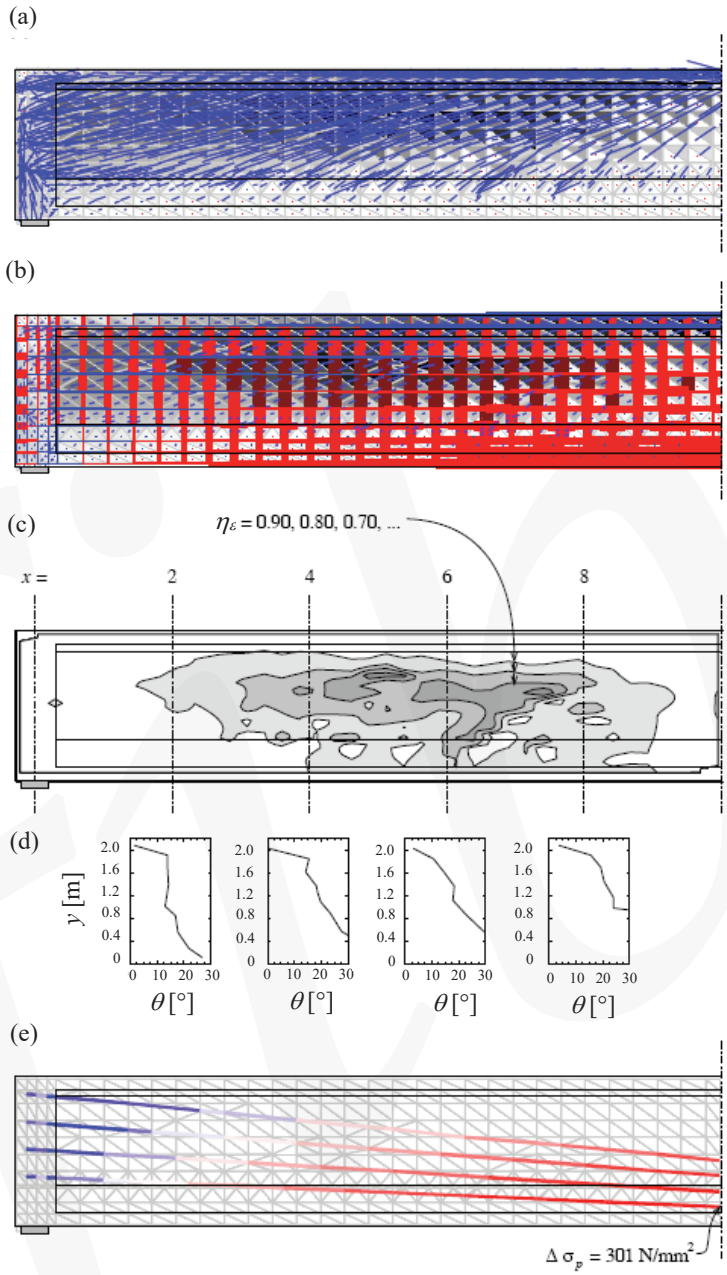


Fig. 6-10 EPSF analysis of the region near the abutment: (a) direction of compressive stresses; (b) reinforcement stresses (brown indicates steel yielding); (c) strength reduction factor due to concrete cracking; (d) angles of the compression field at selected sections; and (e) change in the stresses in the prestressing tendons

Two additional positive effects are also considered in this case by the EPSF results:

- The first refers to the capacity of the compression flange to carry shear forces (refer to Fig. 6-10a,d). This load-carrying action is normally neglected when performing stress field design for a new structure, but may be a fairly relevant contribution particularly for largely prestressed structures[6-5], [6-6].

This document is the intellectual property of the fib – International Federation for Structural Concrete. All rights reserved.
This PDF of fib Bulletin 100 is intended for use and/or distribution solely within fib National Member Groups.

- The second refers to the increase in the force of the inclined tendons (Fig. 6-10e). This beneficial influence occurs at some distance from the support, but contributes to the enhancement of shear capacity. It can be noted that this effect may even be more significant in the regions of the web near intermediate supports (where the tendon is activated by bending).

This example shows that the EPSF is a consistent tool to account for the various strength reserves that, despite not being usually considered during the design of new structures, they may significantly increase the shear capacity of a member under assessment, preventing unnecessary strengthening.

6.4 Padre Cruz Viaduct

6.4.1 Description of structure

The Padre Cruz viaduct is a multi-span bridge in Lisbon with a deck of 32.5m width, maximum spans of 100 m and a total length of approximately 900 m (see Fig. 6-11). This example shows the application of strut-and-tie and stress field models for the design of the main piers of the viaduct for vertical loads. Different levels of approximation analysis are developed to illustrate the application and the differences of each level/approach.



Fig. 6-11 General view after construction (2007)

Fig. 6-12 and Fig. 6-13 show the longitudinal section of the bridge and a transverse section near the support, respectively. The pier section is variable along the height and the section geometry is defined in Fig. 6-14a. The reinforcement layout, presented in Fig. 6-14b was mainly governed by two load combinations: vertical loads and seismic action.

This document is the intellectual property of the fib – International Federation for Structural Concrete. All rights reserved.
This PDF of fib Bulletin 100 is intended for use and/or distribution solely within fib National Member Groups.

The properties of the materials for the piers were:

Concrete C40. Steel S500. Prestress Y1860/1670.

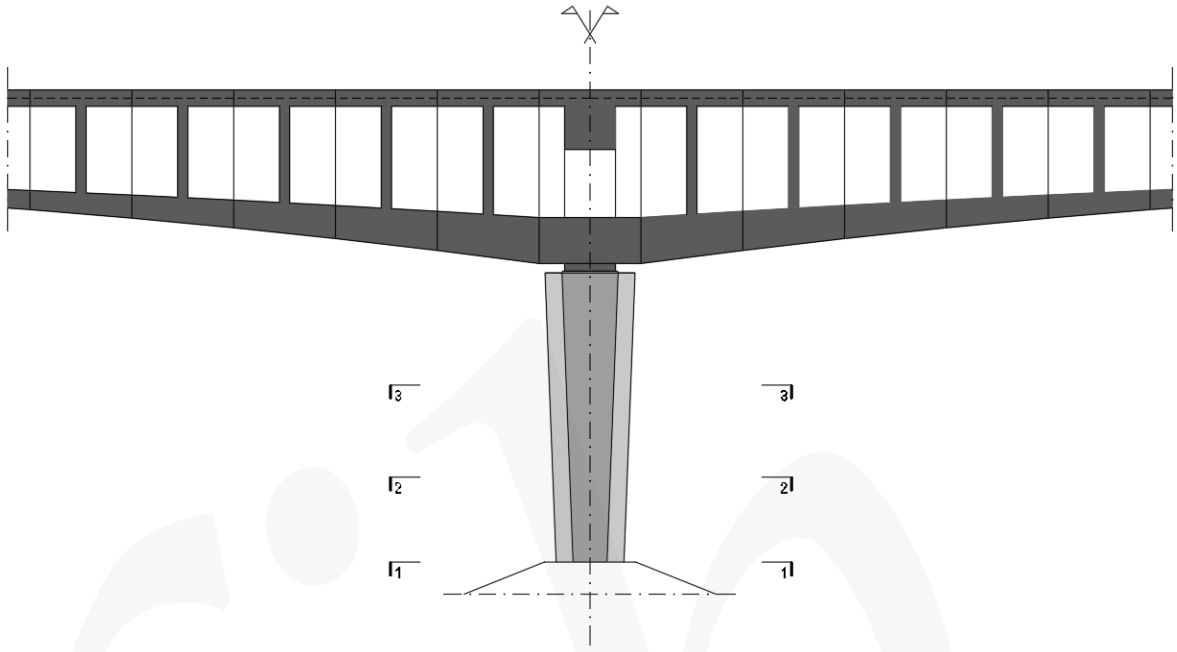


Fig. 6-12 Longitudinal section

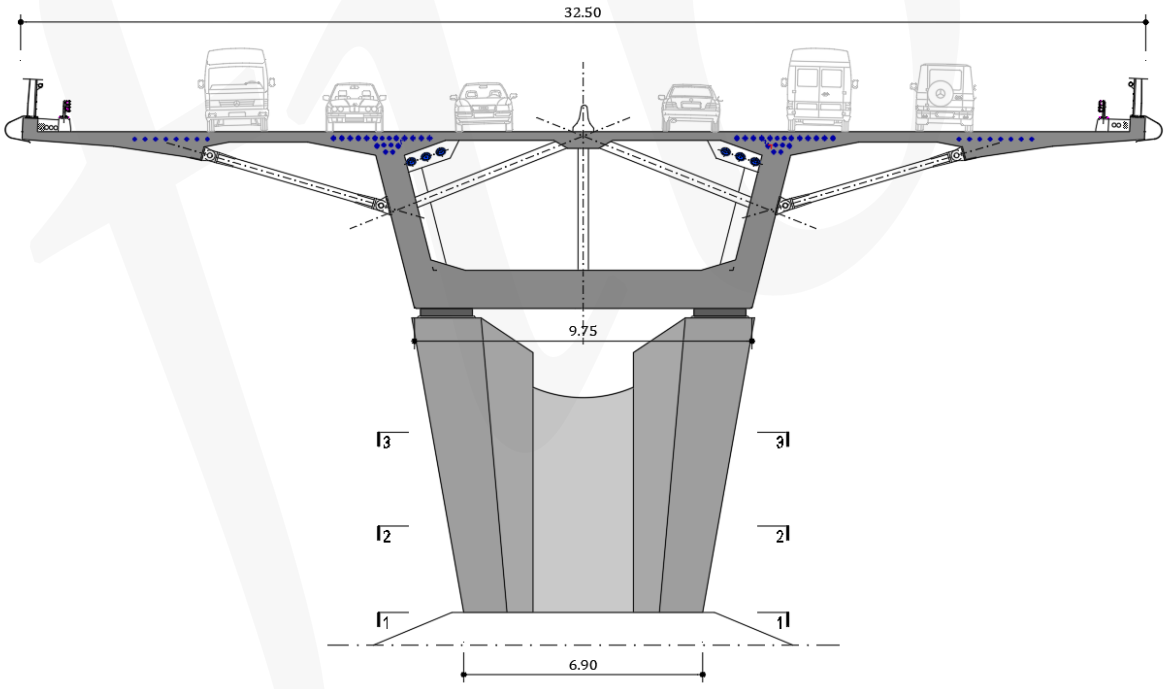


Fig. 6-13 Deck section at the supports region and column front view

This document is the intellectual property of the fib – International Federation for Structural Concrete. All rights reserved.
This PDF of fib Bulletin 100 is intended for use and/or distribution solely within fib National Member Groups.

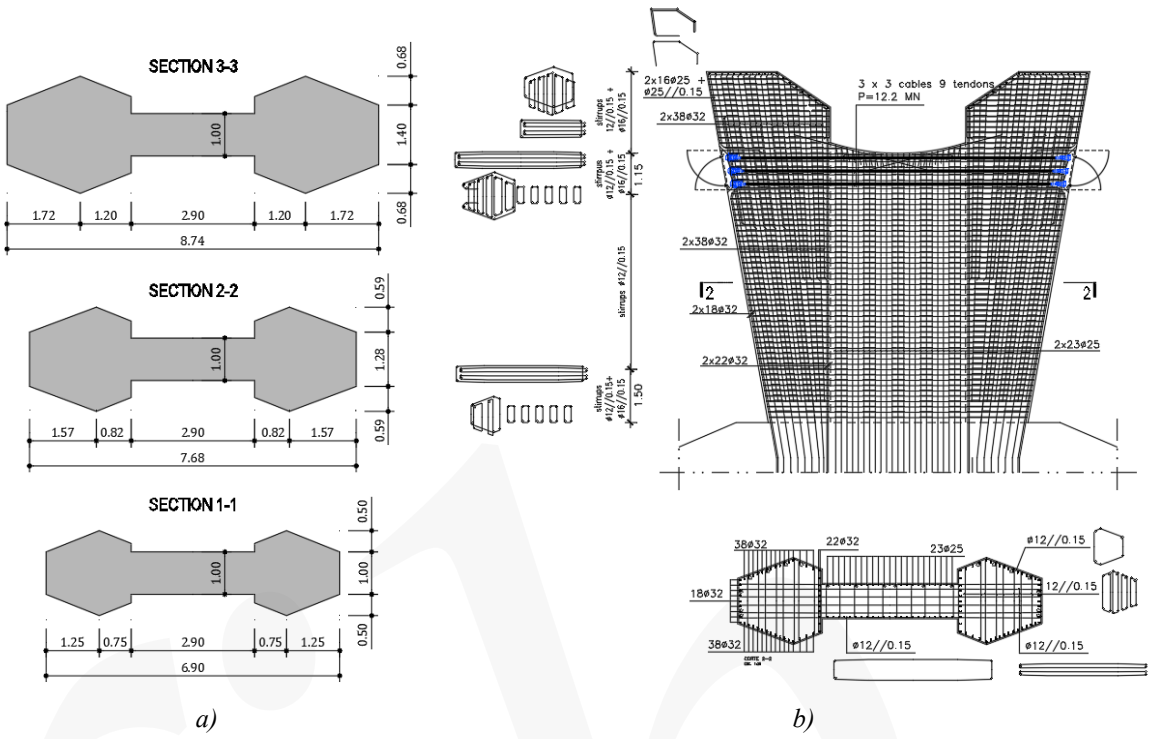


Fig. 6-14 a) Pier section; b) Reinforcement layout

6.4.2 LoA I Model

The design model presented in this and the next chapter was, in fact, the design model of the pier for the vertical loads at the design stage, however the example is being presented as a check of the already defined reinforcement layout to be extended to the remaining levels of approximation.

The model for the lowest LoA is mainly based on the combination of two simple and basic strut-and-tie models presented in Section 4, even if it looks like a more complex and elaborate model. The model is presented in Fig. 6-15, where the load path defined by model M1 is identical to a common deep beam model with top loads, so the inner level arm z_1 was set to approximately $0.7L_1$. It is easy to observe the similarity of model M2 with a deep beam with suspended loads, though the same ratio between the inner level arm z_2 and the distance L_2 was used. Since the practical rules presented earlier for each basic model were followed, namely the inner level arms of each basic model, ductility and service behaviour topics are automatically checked and no further calculations to check service behaviour are necessary.

This document is the intellectual property of the fib – International Federation for Structural Concrete. All rights reserved.
This PDF of fib Bulletin 100 is intended for use and/or distribution solely within fib National Member Groups.

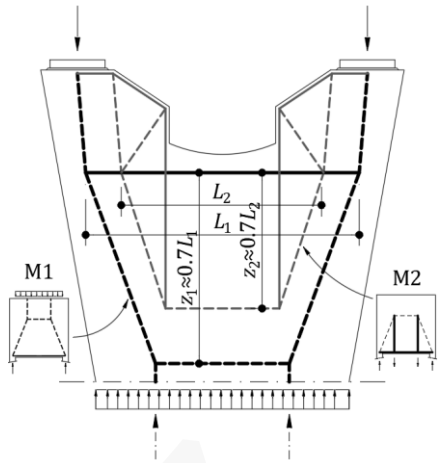


Fig. 6-15 Draft strut-and-tie model based in the combination of two basic models

The resultant model can then be calculated and the forces in the struts and ties are obtained (Fig. 6-16a). The geometry of the model is also presented in Fig. 6-16b.

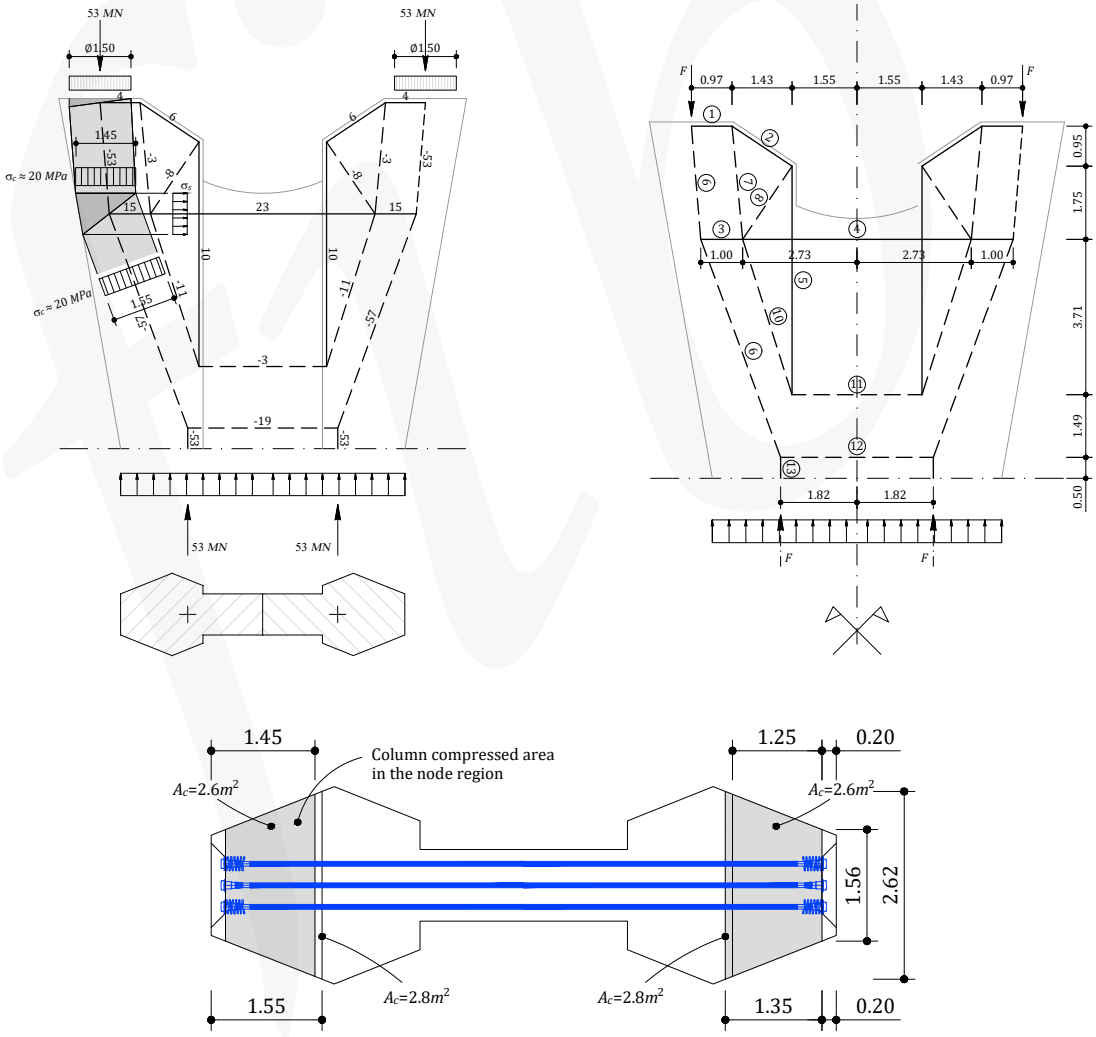


Fig. 6-16 a) Design strut-and-tie model; b) Model geometry and element numbering; c) Plan view of the compressed area.

This document is the intellectual property of the fib – International Federation for Structural Concrete. All rights reserved.
This PDF of fib Bulletin 100 is intended for use and/or distribution solely within fib National Member Groups.

The inclination of compressive force C_6 (Fig. 6-16b) was defined to limit the compressive stresses at the node region (CCT node of strut 6 and tie 3) to its design strength $\sigma_{c,Rd}$ for a compression-tension node given by 7.3.6.4 of MC2010[6-1]. Note that, the reinforcement is arranged in multiple layers and the angle between the strut and tie is greater than 45º; the design strength may thus be increased by 10% according to 7.3.6.2 of MC2010. The effect of the prestressed plates behind the node provides a state of pure compression, increasing the compressive strength at the node region, but it was not considered, leading to a safe-side design:

$$\sigma_{c,Rd} = 0.75 \cdot \left(\frac{30}{f_{ck}}\right)^{\frac{1}{3}} \cdot f_{cd} \cdot 1.1 = 0.75 \cdot \left(\frac{30}{40}\right)^{\frac{1}{3}} \cdot \frac{40}{1.5} \cdot 1.1 = 20 \text{ Mpa} \qquad 6\text{-}3$$

There is no other critical nodal region, nor high compressive stresses crossing areas of transversal tensile strains, and the check of the pier is, therefore, mainly based on the check of the ties as summarised in Table 6-1.

Table 6-1 Tension and provided reinforcement for LoA I model

Tension	Reinforcement	Steel area	Tensile strength	Check
T_1 = 4 *MN*	2 × 16Ø25	15'712 mm²	T_{Rd} = 6.8 *MN*	Ok
T_2 = 6 *MN*	2 × 16Ø25	15'712 mm²	T_{Rd} = 6.8 *MN*	Ok
T_5 = 10 *MN*	2 × 22Ø32	35'376 mm²	T_{Rd} = 15.4 *MN*	Ok
T_4 = 23 *MN*	2 × Ø16//0.15 (1.15m) + 4 × Ø12//0.15 (1.15m) + 9c × 9t (150 mm² each tendon)	6'547 mm² + 12'150 mm²	T_{Rd} = 20.5 *MN*	Not ok

6.4.3 LoA II Model

For the LoA II model for this case a full stress field model was defined as shown in Fig. 6-17. The model considers the provided horizontal web reinforcement in the pier, and in this way, reduces the force in the main tie from 23 *MN* to 20 *MN*. It is a statically-indeterminate model and the tensile force of 3 *MN* was set to a value slightly lower than the yielding force of the provided web reinforcement. The remaining ties have minor and not relevant reductions. With this model it is also possible to check all compressive stresses and check any critical regions, especially if important compressive stresses cross high-tensile strains, which in this case is not relevant, as mentioned before (see Table 6-2). Only the web and main reinforcement must be checked. The remaining are lower than in the previous analysis.

This document is the intellectual property of the fib – International Federation for Structural Concrete. All rights reserved.
This PDF of fib Bulletin 100 is intended for use and/or distribution solely within fib National Member Groups.

Table 6-2: Tension and provided reinforcement for LoA II model

Tension	Reinforcement	Steel area	Tensile strength	Check
$T = 20\ MN$	2 × Ø16//0.15 (1.15*m*) + 4 × Ø12//0.15 (1.15*m*) + 9c × 9t	6547 mm^2 + 12150 mm^2	$T_{Rd} = 20.5\ MN$	Ok
$T = 3\ MN$	6 × Ø12//0.15 (2.0 *m*)	9040 mm^2	$T_{Rd} = 3.9\ MN$	Ok

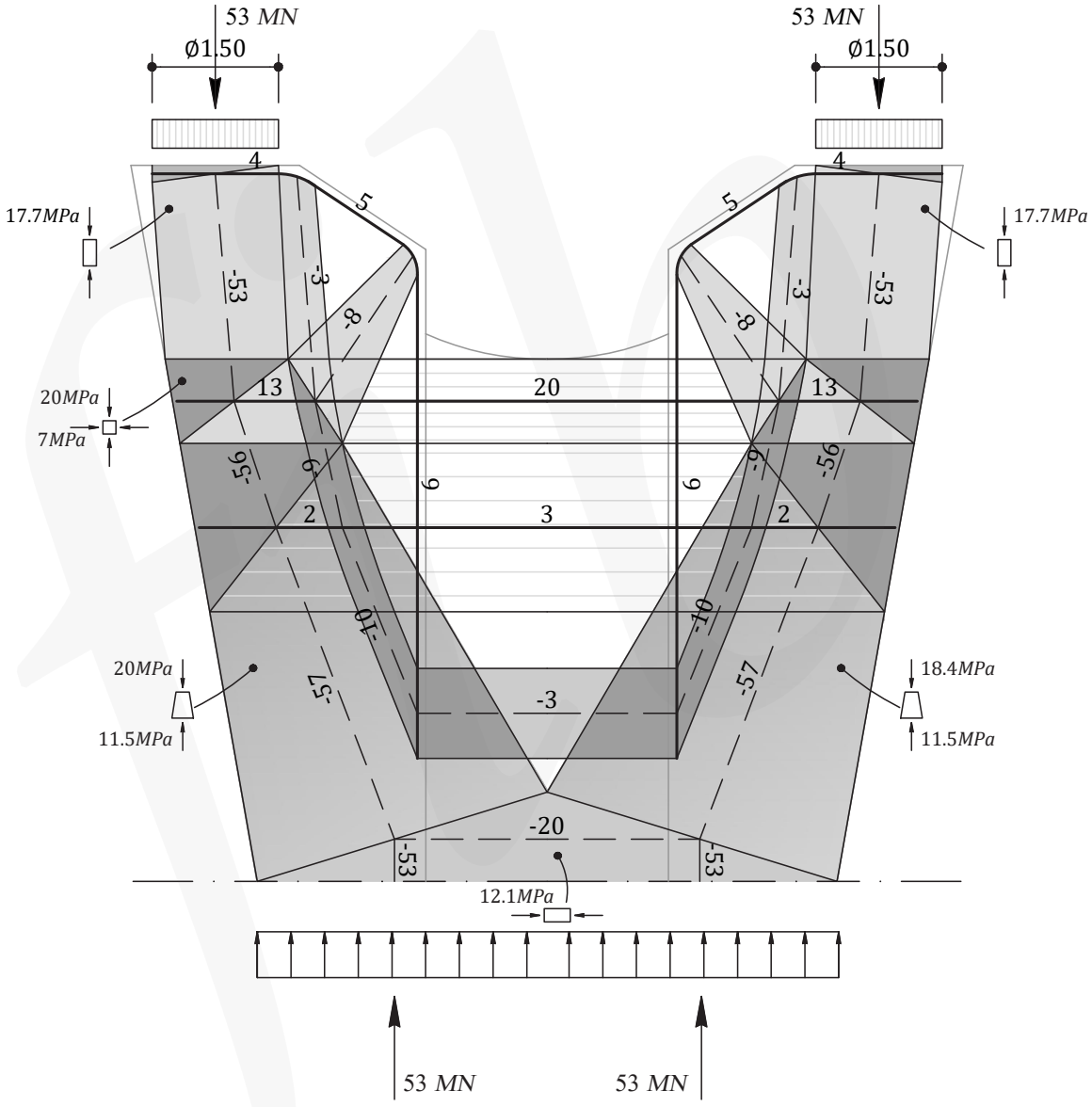


Fig. 6-17 Pier stress field model for vertical loads

6.4.4 LoA III Model

For this level of approximation, the finite element method is applied. The common parabolic constitutive relationship for the concrete without tensile resistance and an elastic-plastic σ_s-ε_s relationship for the steel is implemented. The compressive stresses in

This document is the intellectual property of the fib – International Federation for Structural Concrete. All rights reserved.
This PDF of fib Bulletin 100 is intended for use and/or distribution solely within fib National Member Groups.

the concrete and the tensile stresses in the reinforcement are presented in Fig. 6-18. The resultant tensile force in the main tie is less critical than in the previous analyses, with the main reason being the distribution of the vertical reactions at the base of the pier. In the previous LoAs, a uniform distribution of stresses at the base of the piers was assumed, since no compatibility of deformations was provided (see Fig. 6-16 and Fig. 6-17). However, the finite element analysis resulted in a non-uniform stress distribution at the bottom of the pier (see Fig. 6-18c), leading to a steeper inclination of the main compressive force (C_6) and, consequently, to a significant reduction at the main tie force from 20 MN to 14 *MN*. Similarly, the tension in the web reinforcement was also significantly reduced from 3 *MN* to 1.3 *MN*.

This analysis confirmed that concrete compression is not a critical issue and no significant compression softening occurs in regions with high compressive stresses. The only region where a significant reduction of concrete stresses occurs is near the re-entrant corner (see Fig. 6-18d), at the intersection of the vertical tie and main horizontal tie, but no compression crosses that region.

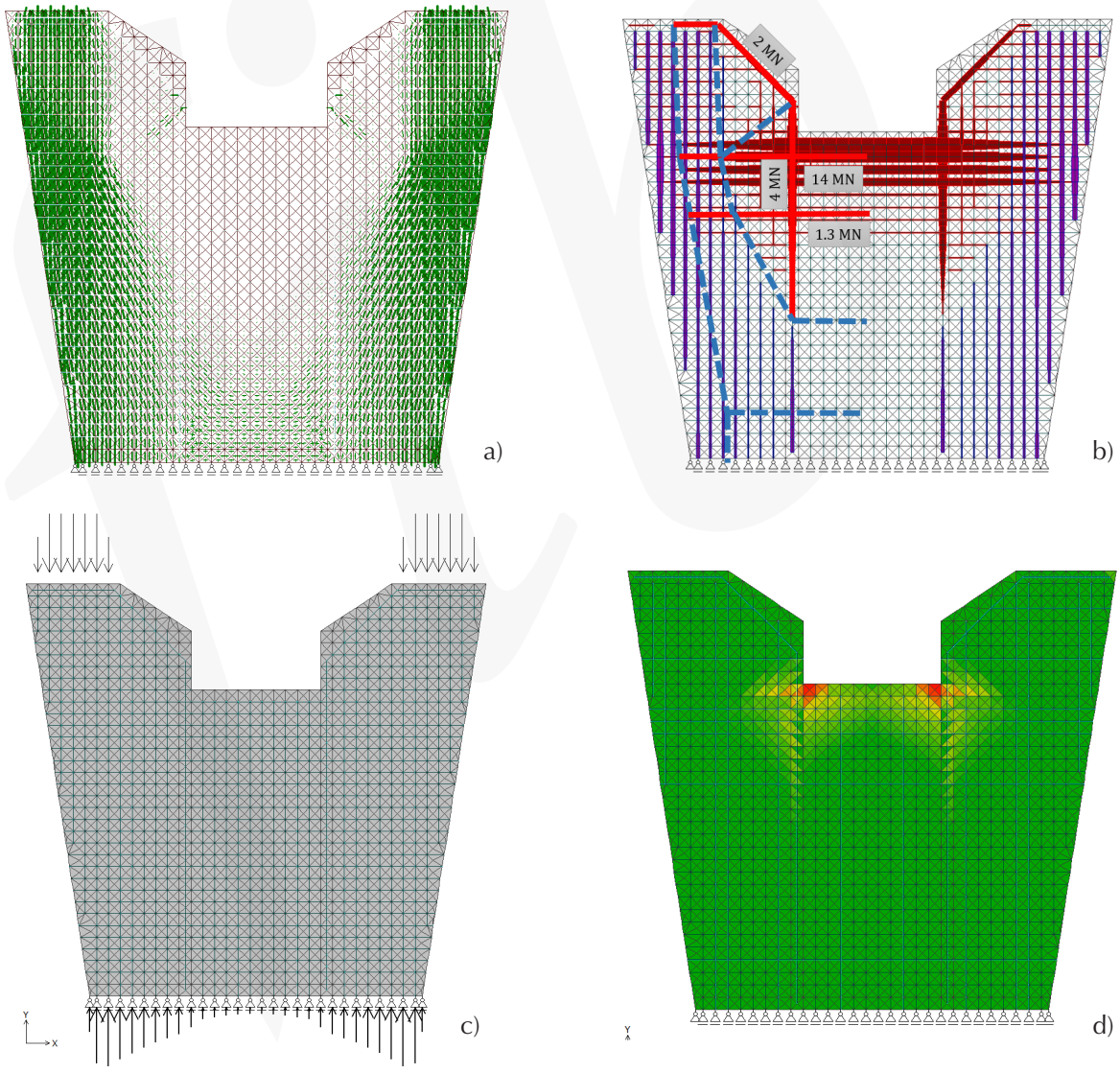


Fig. 6-18 a) Principal compressive stresses b) Reinforcement tensile stresses c) Reactions d) Compression softening

This document is the intellectual property of the fib – International Federation for Structural Concrete. All rights reserved.
This PDF of fib Bulletin 100 is intended for use and/or distribution solely within fib National Member Groups.

6.4.5 LoA IV Model

For this LoA finite element analysis was also performed, with the addition of a tension stiffening law for the steel. The results at ultimate load are identical to the previous analysis; however, the present analysis allows checking service behaviour, as well. The service load is 40 *MN* for each pot bearing and a prestress of 12.2 *MN* is introduced in the model to properly evaluate the steel stresses and the service behaviour.

Maximum steel stresses of about 170 MPa were obtained, leading to adequate service behaviour (see Fig. 6-19). Even in the absence of any prestressing, steel stresses were as low as 250 MPa, also leading to a satisfactory service behaviour. However, the solution with prestressing provides improved service behaviour and a global increase of the quality of the solution, since steel stresses of low value lead to limited crack width.

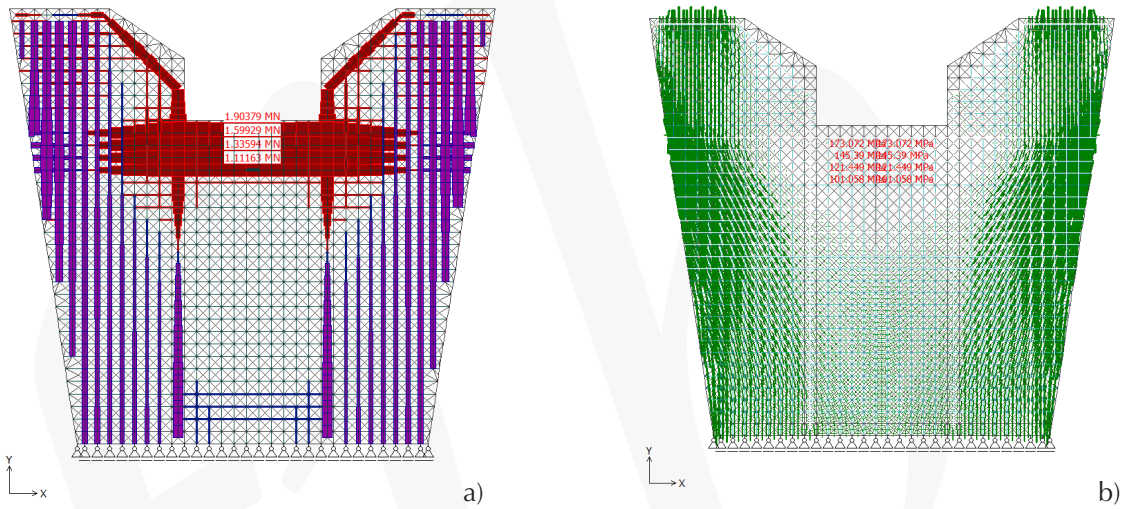


Fig. 6-19 a) Tensile forces for service loads b) Steel stresses for service loads

6.5 Assessment of a dapped-end beam at ultimate and serviceability limit states

Dapped-end beams are typical details used in the support regions of bridge construction leading to soffit continuity. The suitable performance of these regions shall be verified not only with respect to their structural resistance (at ultimate limit state, ULS), but also with respect to their cracking response (at serviceability limit state, SLS). The latter is particularly relevant in bridges to avoid corrosion issues. The Elastic-Plastic Stress Fields (EPSF) method has been shown to be a general and suitable tool to design or to assess these regions[6-7], [6-8], providing accurate estimates of the actual stresses and crack widths.

In this section, the EPSF method is used for an existing bridge built in Switzerland in 1974 (Fig. 6-20a) and presenting dapped-end supports. During inspections carried out in the structure, cracks were reported at the inner angle of joint with openings ranging between 0.1 and 0.3 mm Fig. 6-20b and c). Cracks of this size were considered by the owner to require a detailed assessment of the structural performance, comprising the response at SLS and ULS.

This document is the intellectual property of the fib – International Federation for Structural Concrete. All rights reserved.
This PDF of fib Bulletin 100 is intended for use and/or distribution solely within fib National Member Groups.

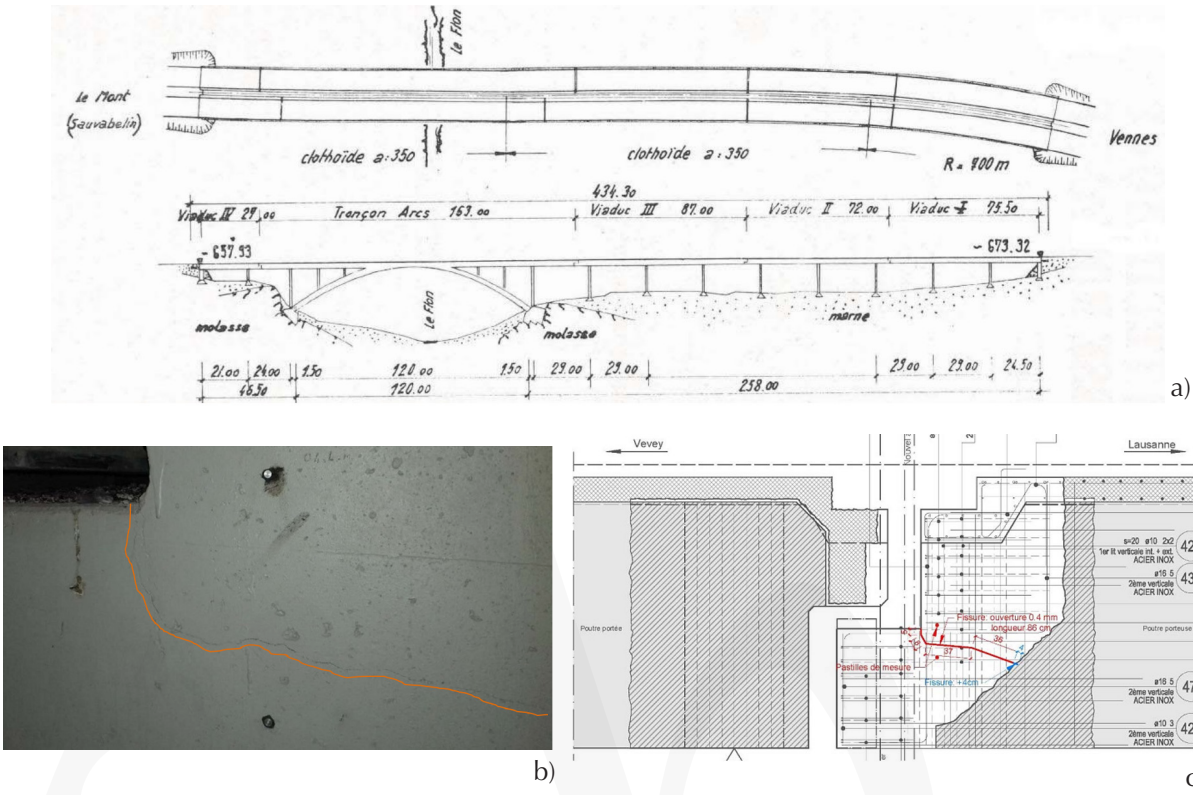


Fig. 6-20 Chocolatière Bridges (Switzerland): (a) plan view and side view of the bridges ; (b) picture of the crack developing at the inner angle of the dapped-end support; (c) position and opening of the identified crack

Due to the geometry and loading conditions of the region (leading to a non-linear strain distribution) a detailed analysis was performed by means of the EPSF method (refined analysis based on compatibility of deformations, lower-level LoAs not relevant for such analysis). The actual geometry of the structure was considered, as well as the reinforcement layout and its bond conditions (simplified LoA IV performed on the basis of a LoA III model). With respect to the latter, the considerations of Fig. 6-21 were taken into account to determine equivalent areas of reinforcement.

This document is the intellectual property of the fib – International Federation for Structural Concrete. All rights reserved.
This PDF of fib Bulletin 100 is intended for use and/or distribution solely within fib National Member Groups.

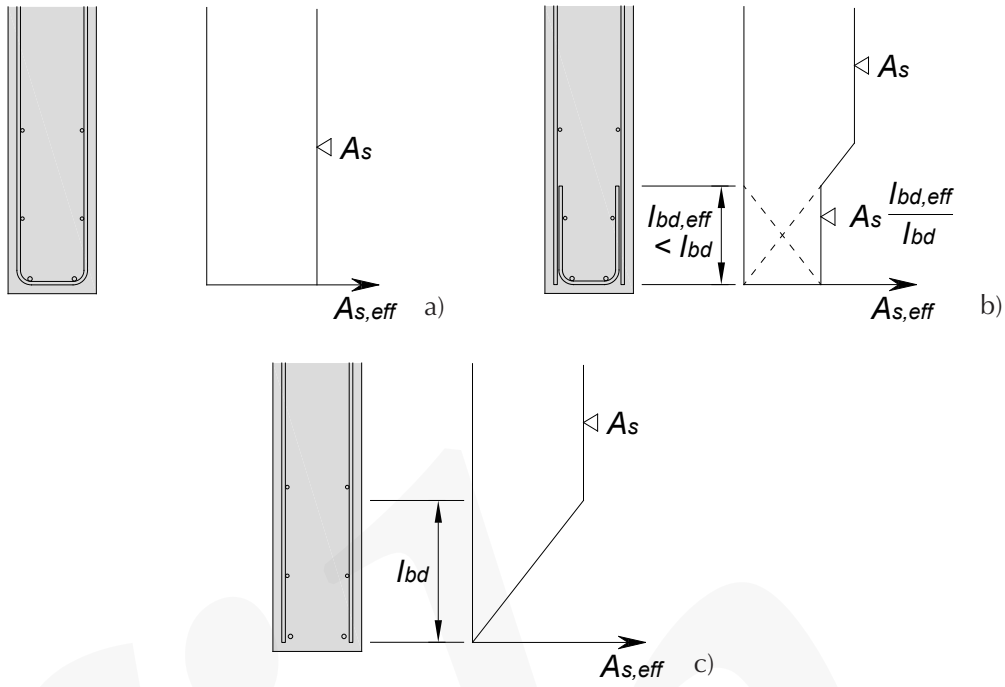


Fig. 6-21 Examples of stirrup anchorage conditions and corresponding modelled effective areas: (a) perfectly anchored stirrup ; (b) stirrup closed by a U-shaped bar of insufficient length and ; (c) open stirrup

6.5.1 Verification at ULS

Following these considerations, the stress field of the structure was determined under design loads (Fig. 6-22a) as well as the maximum failure load (Fig. 6-22b). On that basis, the compliance factor of the detail was determined, showing sufficient strength. It can be observed that in this case (Fig. 6-22b) failure is eventually governed by yielding of the reinforcement at the lap-splicing region.

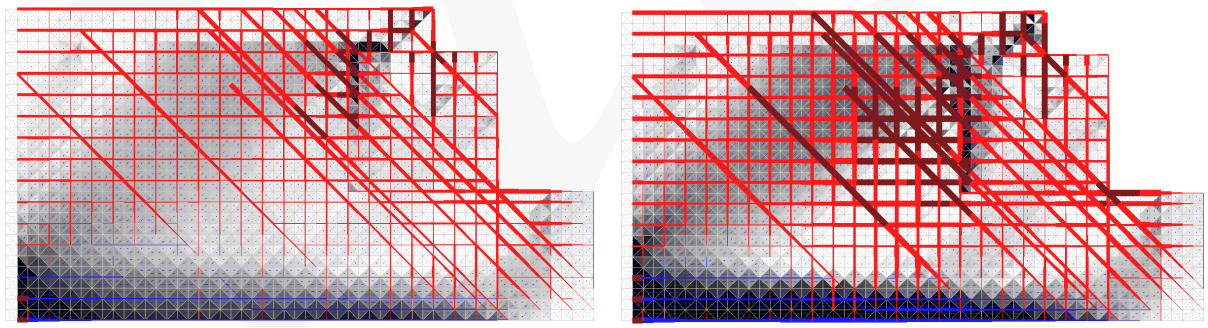


Fig. 6-22 Tensile stresses in reinforcement (in red, brown indicating yielding) and principal compressive stresses in concrete (in grey, black indicating yielding) obtained by the EPSF method for 2 different load levels: (a) design load E_d and ; (b) maximum failure load R_d ($n = R_d / E_d = 1.14$)

This document is the intellectual property of the fib – International Federation for Structural Concrete. All rights reserved.
This PDF of fib Bulletin 100 is intended for use and/or distribution solely within fib National Member Groups.

6.5.2 Verification at SLS

For structures such as bridges subjected to cyclic loads, crack opening depends strongly on the loading history, because of the nonlinear behaviour of bond and of the tensile response of concrete. As shown by Muttoni and Fernández Ruiz[6-9], after a complete process of loading and unloading, concrete still presents some residual cracks of non-negligible width, due to the effect known as negative tension-stiffening and because of the fact that crack lips are no longer perfectly aligned. This phenomenon requires that, even under permanent loading conditions, a realistic estimate of crack widths in bridges shall consider the potential unloading response of concrete ties (see Fig. 6-23a).

For simplification purposes, the analysis of the crack widths was performed in this case based on the EPSF analysis (level III) and by manually accounting for the tension-stiffening effects, leading to a level IV crack calculation. As the element under investigation presents a large amount of reinforcement, it was assumed that tension-stiffening had little influence on the results of level III. Following the approach of Mata Falcón[6-8], the stresses at crack location can be estimated by calculating the EPSF under service loads. Once this value is determined, the crack width can be estimated assuming that a perfectly-plastic bond law applies (see Fig. 6-23b) and that one crack localises the strains (see Fig. 6-20b,c and 6-24).

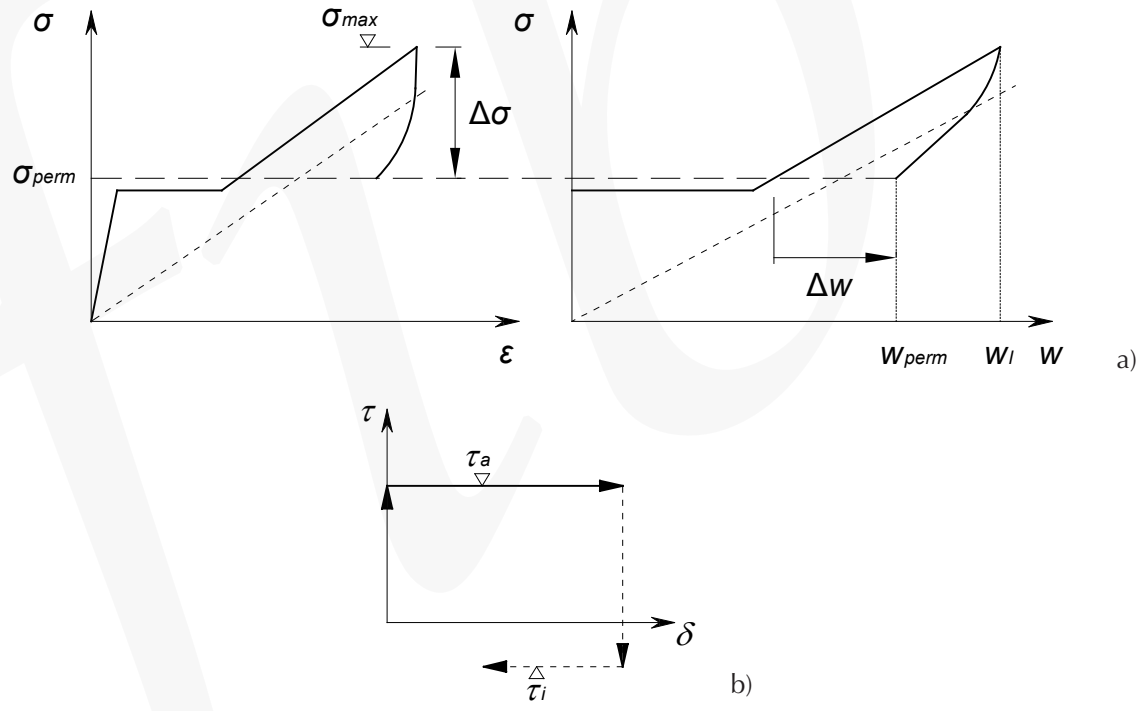


Fig. 6-23 (a) Stress-strain and stress-crack width relationship in reinforced concrete tie and ; (b) rigid-plastic bond law (taken from [Muttoni et al.[6-9]])

For the present case, it can be noted that such approach can be extended by considering the cyclic or long-term response of bond[6-9] (τ_a and $\tau_i = \tau_a/4$ under short-term conditions and $\tau_{a,\infty} = 0.70\tau_a$ and $\tau_i = \tau_a/8$ under long-term or repeated actions).

This document is the intellectual property of the fib – International Federation for Structural Concrete. All rights reserved.
This PDF of fib Bulletin 100 is intended for use and/or distribution solely within fib National Member Groups.

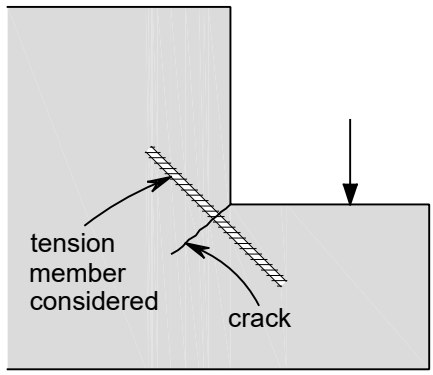


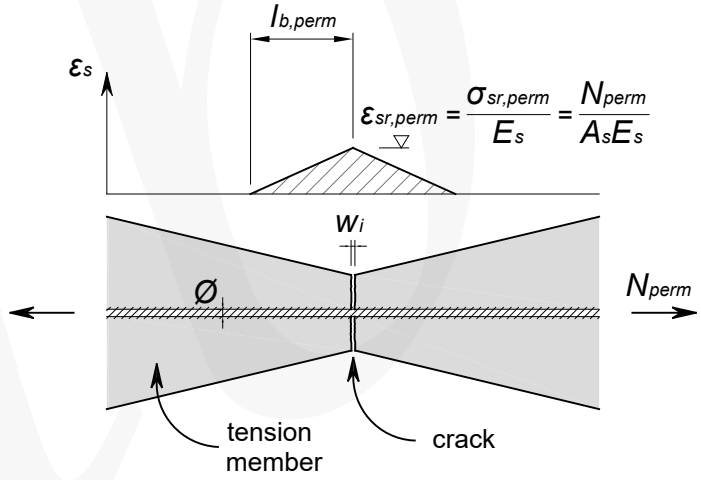
Fig. 6-24 Illustration of the crack localizing the strains in the inner angle and of the tension member considered in the analysis

On this basis, the crack width can be determined following a simple integration of strains, refer to Fig. 6-25a. This crack width is however a lower bound of the actual one. As shown in Fig. 6-23a, if a tie is loaded at levels higher than the service conditions, a residual opening remains, leading to a larger crack width than under a monotonic loading condition. In this case, referring to one crack, the different loading stages and associated crack widths can be formulated as shown in Fig. 6-25b,c.

(a) Monotonic loading up to N_{perm}: crack opening w_i

$$l_{b,perm} = \frac{\sigma_{sr,perm} \cdot \varnothing}{4\tau \cdot a}$$

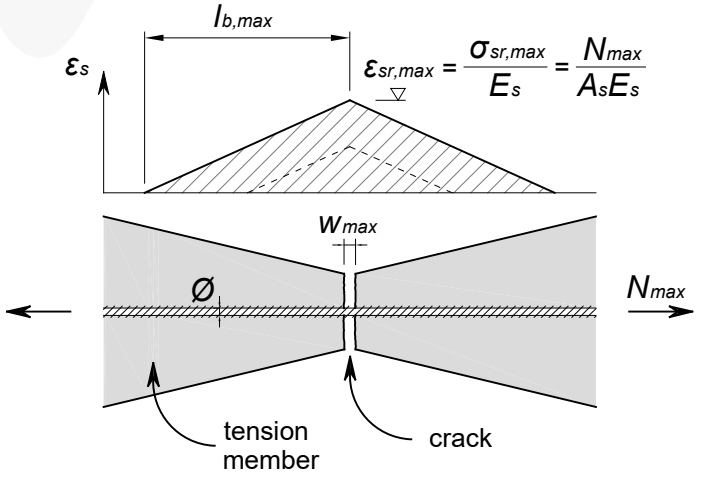
$$w_i = \frac{\sigma_{sr,perm}}{E_s} l_{b,perm}$$



(b) Monotonic loading for $N_{max} > N_{perm}$: crack opening w_{max}

$$l_{b,max} = \frac{\sigma_{sr,max} \cdot \varnothing}{4\tau \cdot a}$$

$$w_{max} = \frac{\sigma_{sr,max}}{E_s} l_{b,max}$$



This document is the intellectual property of the fib – International Federation for Structural Concrete. All rights reserved.
This PDF of fib Bulletin 100 is intended for use and/or distribution solely within fib National Member Groups.

(c) Unloading from N_{max} to N_{perm}: crack opening $w_{perm} > w_i$

$$w_{perm} = w_{max} - \frac{\left(\sigma_{sr,max} - \sigma_{sr,perm}\right)^2 \varnothing}{4E_s\left(\tau_i + \tau_a\right)}$$

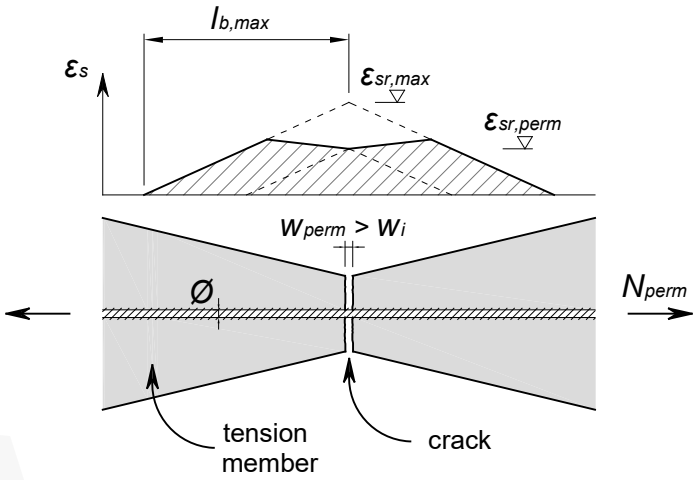


Fig. 6-25 Steel strain profile and calculation of the crack opening of an element with geometrical discontinuity for different load levels : (a) monotonic loading until N_{perm}; (b) monotonic loading until $N_{max} > N_{perm}$; and (c) unloading from N_{max} to N_{perm}

Following this methodology, the results of Fig. 6-26 are obtained. According to Muttoni et al.[6-9], the figure presents two calculations: one corresponding to the short-term response and another to the long-term one (including creep and repeated loading effects). As it can be noted, for a maximum stress $\sigma_{sr,max}$ ranging between quasi-permanent and rare values, calculated crack widths vary between 0.07 mm and 0.29 mm, in fair agreement to the in-situ observations on the bridge.

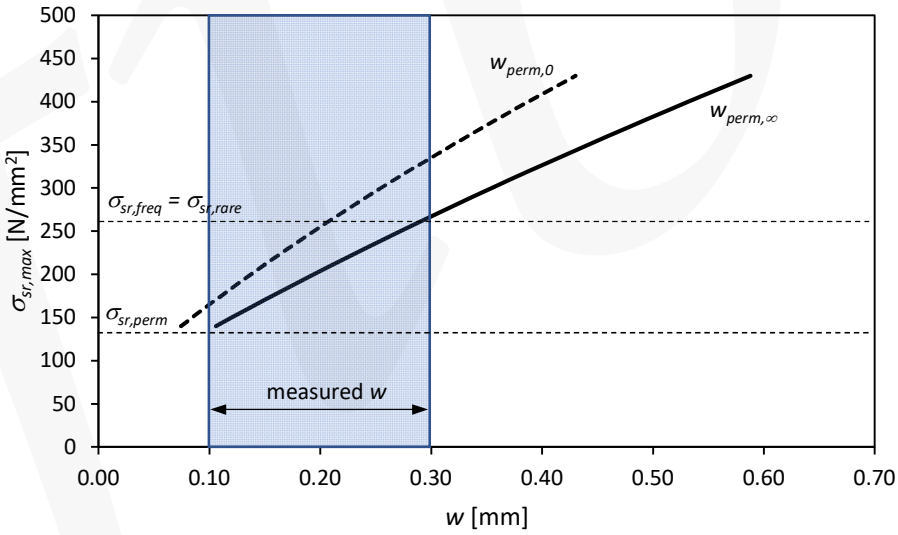


Fig. 6-26 Comparison between calculated crack opening values (dashed line for short term and continuous line for long term) and measured values on the structure (blue surface)

6.6 Detailed assessment of an existing element

6.6.1 Context and motivation

In this section, the detailed assessment of a shear-critical member is presented, combining simple and advanced analysis techniques with on-site testing. This example shows the

This document is the intellectual property of the fib – International Federation for Structural Concrete. All rights reserved.
This PDF of fib Bulletin 100 is intended for use and/or distribution solely within fib National Member Groups.

possibilities offered by strut-and-tie and stress field models to refine the level of accuracy where needed, a feature particularly suitable for existing structures.

6.6.2 Problem description

The assessment presented in this section was conducted on an existing reinforced concrete building, built in Lisbon in 1961 (see Fig. 6-27a). The building was originally designed to host manufacturing processes, but a change of use as residences was decided (Fig. 6-27b). The approach aimed at maintaining most of its structural elements, requiring large structural inspection to confirm their suitability (according to the "knowledge levels concept" from EN1998-3:2005[6-10]). This inspection revealed that, since the building was built before the Portuguese code for seismic design, the original design did not include any seismic consideration and retrofitting was required to ensure its performance.

The structure presented only a few internal columns and the slabs had large spans of approximately 14m×14m. For one part of the building, the structure consisted of simply supported beams, spaced at 2.9m, and with a span of 14m (Fig. 6-28). The beams had a rectangular section of 0.30m×0.65m with a top slab of 0.10m thickness (Fig. 6-29).



a) b)

Fig. 6-27 Building: a) state before recycle; b) future view of the building

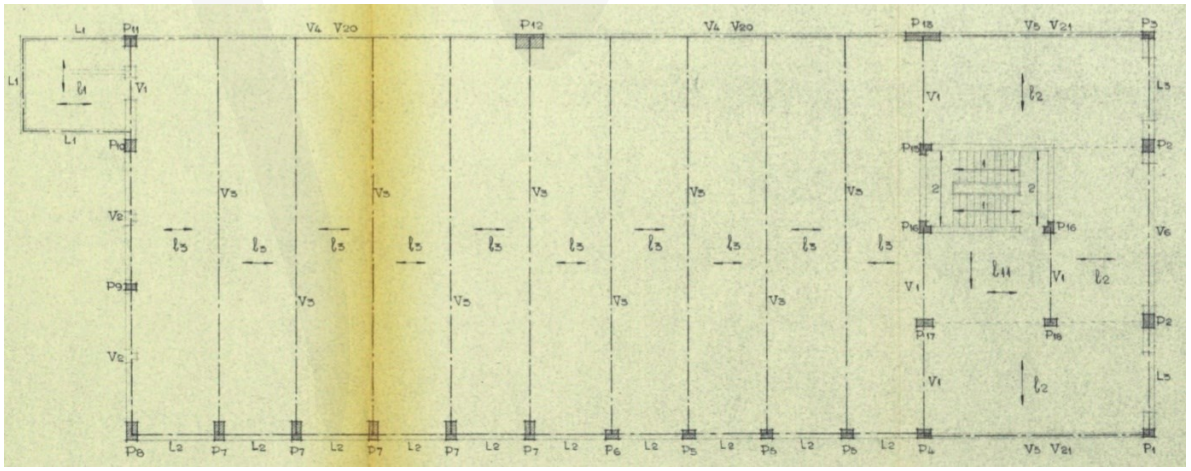


Fig. 6-28 Plan view of the structural solution for the 1st and 2nd levels.

This document is the intellectual property of the fib – International Federation for Structural Concrete. All rights reserved.
This PDF of fib Bulletin 100 is intended for use and/or distribution solely within fib National Member Groups.

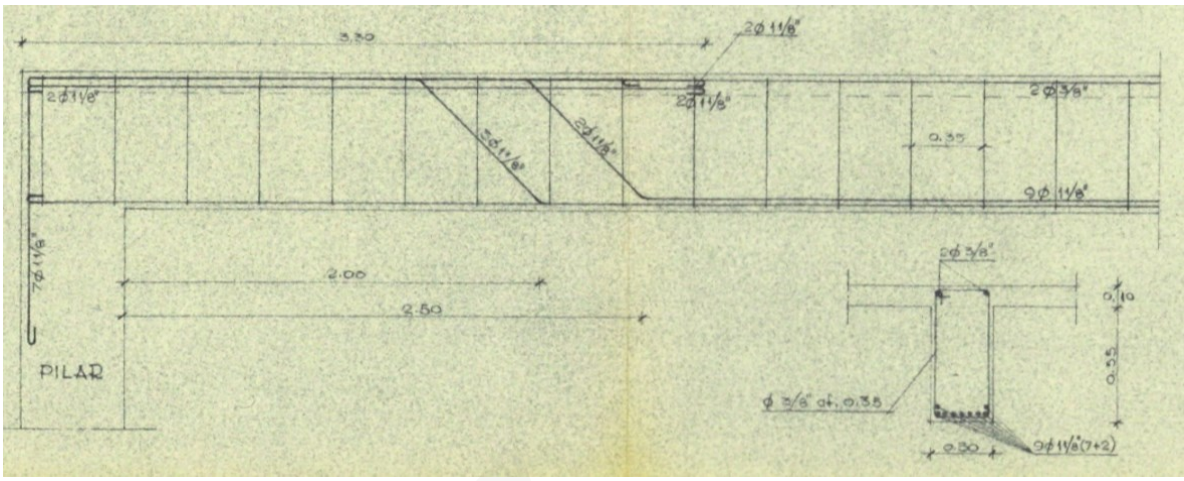


Fig. 6-29 V3 Beam detailing (dimensions for reinforcement in inches).

The original reinforcement drawings are shown in Fig. 6-29 (reinforcement dimensions in inches, equivalent dimensions in SI units are: stirrups Ø 3/8''→ Ø 10 mm; longitudinal reinforcement Ø 1+1/8'' → Ø 29 mm). During the inspection, 4 steel bars and 12 concrete samples were tested, yielding a characteristic yield strength of the steel f_{yk} = 290MPa (f_{yd} = 252MPa) and a characteristic concrete strength (measured in cylinder) f_{ck} = 19MPa.

According to the initial design and with respect to the minimum shear reinforcement, the stirrups provided are slightly higher than the minimum threshold prescribed by MC2010:

$$\rho_{w,\min} = \left(\frac{A_{sw}}{s \cdot b_w}\right)_{\min} = 0.08\frac{\sqrt{f_{ck}}}{f_{yk}} = 0.12\% \xrightarrow{b_w = 0.3m} \left(\frac{A_{sw}}{s}\right)_{\min} = 361\ \text{mm}^2/\text{m}$$

$$2\times\varnothing 10\,/\,/0.35 \rightarrow \left(\frac{A_{sw}}{s}\right)_{prov} = 449\ \text{mm}^2/\text{m} > 361\ \text{mm}^2/\text{m}$$

However, the in-situ inspection revealed that the beams were built with a width b_w = 0.50m and that the measured spacing of the stirrups was 0.3m (Ø10//0.30), leading to a transverse reinforcement amount lower than the one advised in MC2010:

$$\rho_{w,\min} = \left(\frac{A_{sw}}{s \cdot b_w}\right)_{\min} = 0.08\frac{\sqrt{f_{ck}}}{f_{yk}} = 0.12\% \xrightarrow{b_w = 0.5m} \left(\frac{A_{sw}}{s}\right)_{\min} = 601\ \text{mm}^2/\text{m}$$

$$2\times\varnothing 10\,/\,/0.30 \rightarrow \left(\frac{A_{sw}}{s}\right)_{prov} = 524\ \text{mm}^2/\text{m} > 601\ \text{mm}^2/\text{m}$$

In addition, detailing of the bent-up bars near the supports was shown with the bends located too far from the support, not allowing to consider them for the shear resistance when considering conventional angles for the inclination of the compression field, as shown in Fig. 6-30.

This document is the intellectual property of the fib – International Federation for Structural Concrete. All rights reserved.
This PDF of fib Bulletin 100 is intended for use and/or distribution solely within fib National Member Groups.

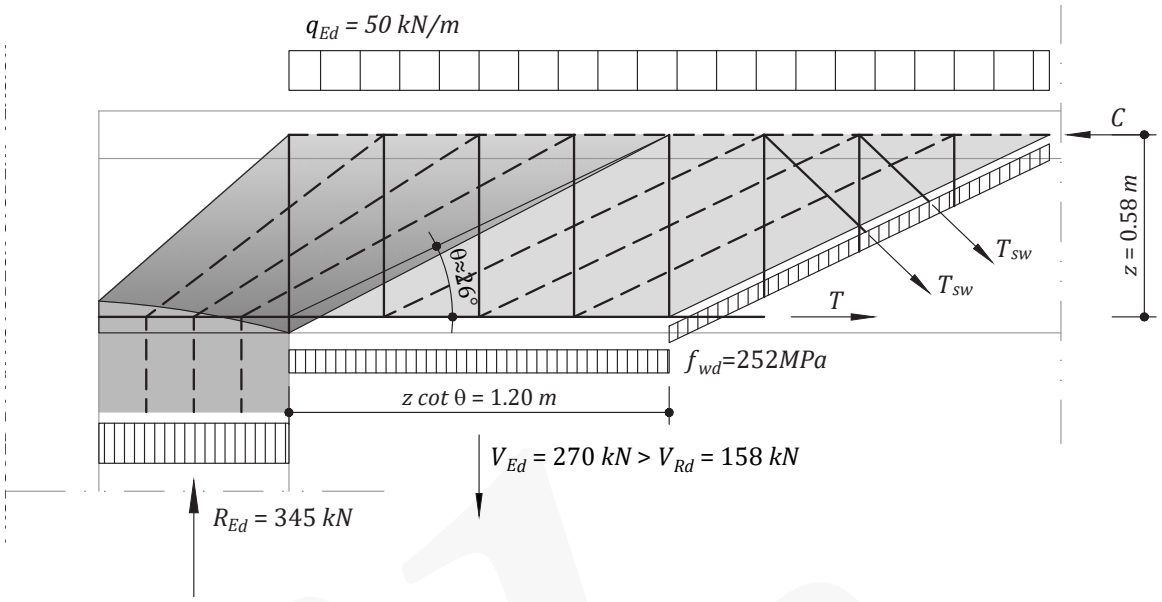


Fig. 6-30 Simple stress field model for the end region.

This assessment showed insufficient design shear resistance (for an angle of the compression field $\theta = 26°$):

$$V_{Rd} = 1.2 \cdot 524 \cdot 252 \cdot 10^{-3} = 158 \text{ kN} < V_{Ed} = 345 - 1.2 \cdot 50 = 270 \text{ kN}$$

According to this approach, the shear resistance is roughly one half of the design shear action. It cannot, thus, be excluded that the bent-up bars were actually accounted for in the initial shear design. However, taking such consideration is no longer possible when considering the minimum angles of the compression field suggested in current codes of practice (as in MC2010[6-1]). It should be noted, yet, that such values for the angle of the compression field are addressed mostly in design of new structures, but they can be adjusted to particular design cases (by developing specific strut-and-tie or stress field models). Such refined investigation was justified in the present case, as there were approximately 20 identical beams and the decision for a shear retrofitting would lead to a significant increase of the rehabilitation cost. To that aim, the application of the Level-of-Approximation concept to the strut-and-tie and stress field models was deemed particularly important and will be presented in the following sections.

The application of stress fields will be performed on a member with lower amount of shear reinforcement than that generally advised for such a structure. The relevance of the approaches will therefore be eventually verified by means of an in-situ test on the structure.

6.6.3 LoA I

The design model in this chapter considers that it is possible to have partial strutting of the load from the bent-up bar closest to the support (refer to the strut developing at 18° in Fig. 6-31). Some concerns can however be expressed on the applicability of such model, due to the rather flat angle resulting between the strut and the bottom tie (potentially reducing the concrete strength). In addition, the relatively low amount of transverse reinforcement may increase the possibility of having a brittle failure, thus limiting the applicability of design methods based on limit analysis.

This document is the intellectual property of the fib – International Federation for Structural Concrete. All rights reserved.
This PDF of fib Bulletin 100 is intended for use and/or distribution solely within fib National Member Groups.

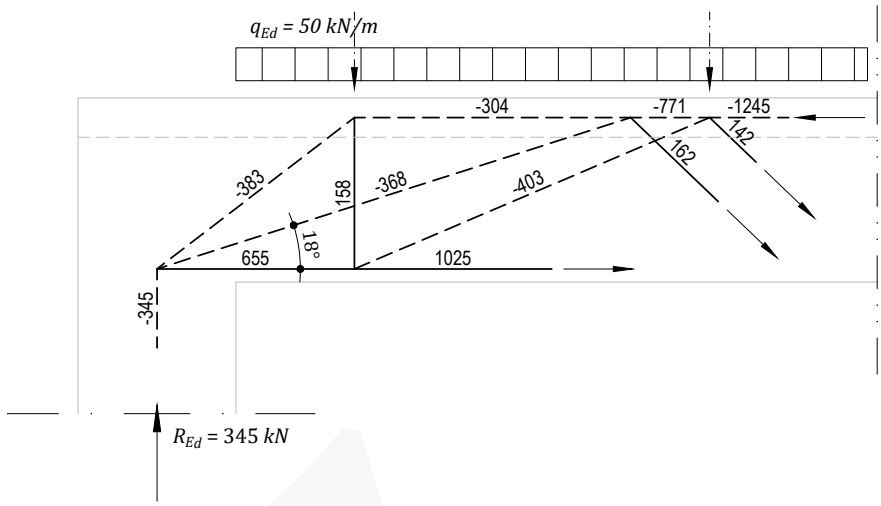


Fig. 6-31 Strut-and-tie model for the end support considering the inclined reinforcement.

6.6.4 LoA II

For LoA II, a detailed stress field model was developed as shown in Fig. 6-32, taking into consideration the width of the column to accurately evaluate the angle of the critical strut developing from the bent-up bar. Following this analysis, the angle of 18º of LoA I was slightly increased to 20º. In any case, the same concerns on the suitability and applicability of the design model remain.

With such a stress field, it is possible to check the compression softening in the diagonal strut. At design load, a compression stress $\sigma_{c,Ed}$ = 7 MPa results. The reduction in concrete compression capacity due to transverse strains can be evaluated according to the following equation (in discussion for pr EN 1992-1-1:2018[6-11]):

$$k_c = \frac{1}{1.28 + 0.16\left(\cot\theta\right)^2} = 0.36$$

Thus, the design concrete compression resistance, considering that the inspection undertaken secured a Knowledge Level 2 (KL2) leading to a partial factor for the concrete resistance γ_c=1.2, according to NP EN 1998-3 (2017), is determined as:

$$\sigma_{c,Rd} = 0.36\frac{19}{1.2} = 5.7 \text{ MPa} < \sigma_{c,Ed} = 7 \text{ MPa}$$

This document is the intellectual property of the fib – International Federation for Structural Concrete. All rights reserved.
This PDF of fib Bulletin 100 is intended for use and/or distribution solely within fib National Member Groups.

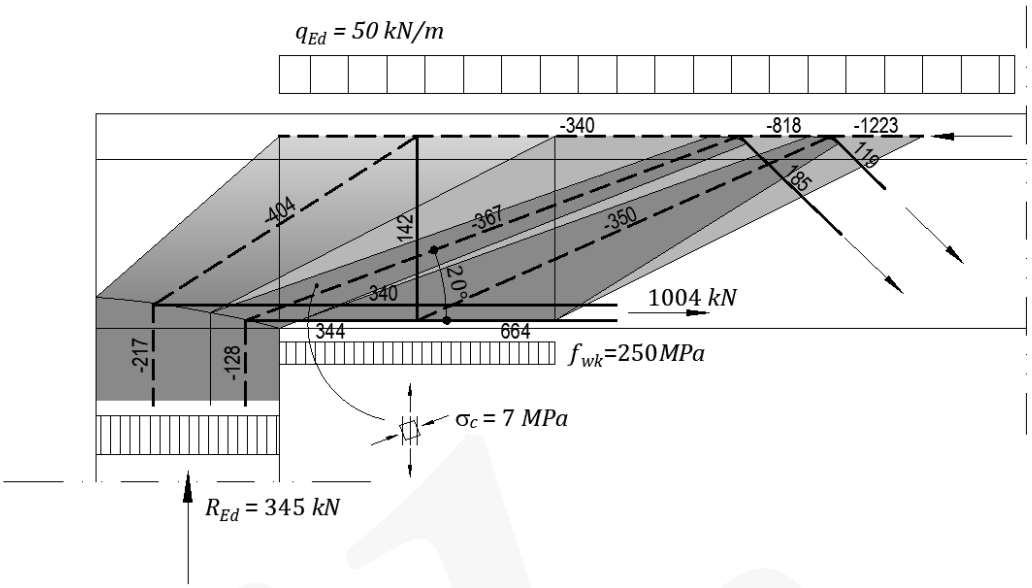


Fig. 6-32 Stress field model for the end support considering the inclined reinforcement

This leads to the conclusion that failure is governed by crushing of the concrete in the web of the beam when all the stirrups are yielding and that resistance is less than the design value (q_{Rd}=40.7 kN/m^2 < q_{Ed}=50 kN/m^2).

6.6.5 LoA III

For this LoA, an elastic-plastic stress field was developed, based on the finite element method and taking precisely into consideration beam reinforcement as well as its location and detailing. The design yield strength of the materials was considered in the analysis (f_{yd} = 252 MPa and f_{cd}=15.8 MPa).

The failure load calculated on this basis resulted q_{Rd} = 49 kN/m^2 (almost complying to the design specifications q_{Ed} = 50 kN/m^2). According to this analysis, stirrups near the support reached their yield strength (see Fig. 6-33a) and the compression stress field (see Fig. 6-33b) shows very flat angles which allow transfer of a fraction of the shear force directly to the support. Failure occurred (as for LoA II) by crushing of the concrete in the web (whose resistance was limited due to the wide cracks developing as shown in Fig. 6-33c).

This document is the intellectual property of the fib – International Federation for Structural Concrete. All rights reserved.
This PDF of fib Bulletin 100 is intended for use and/or distribution solely within fib National Member Groups.

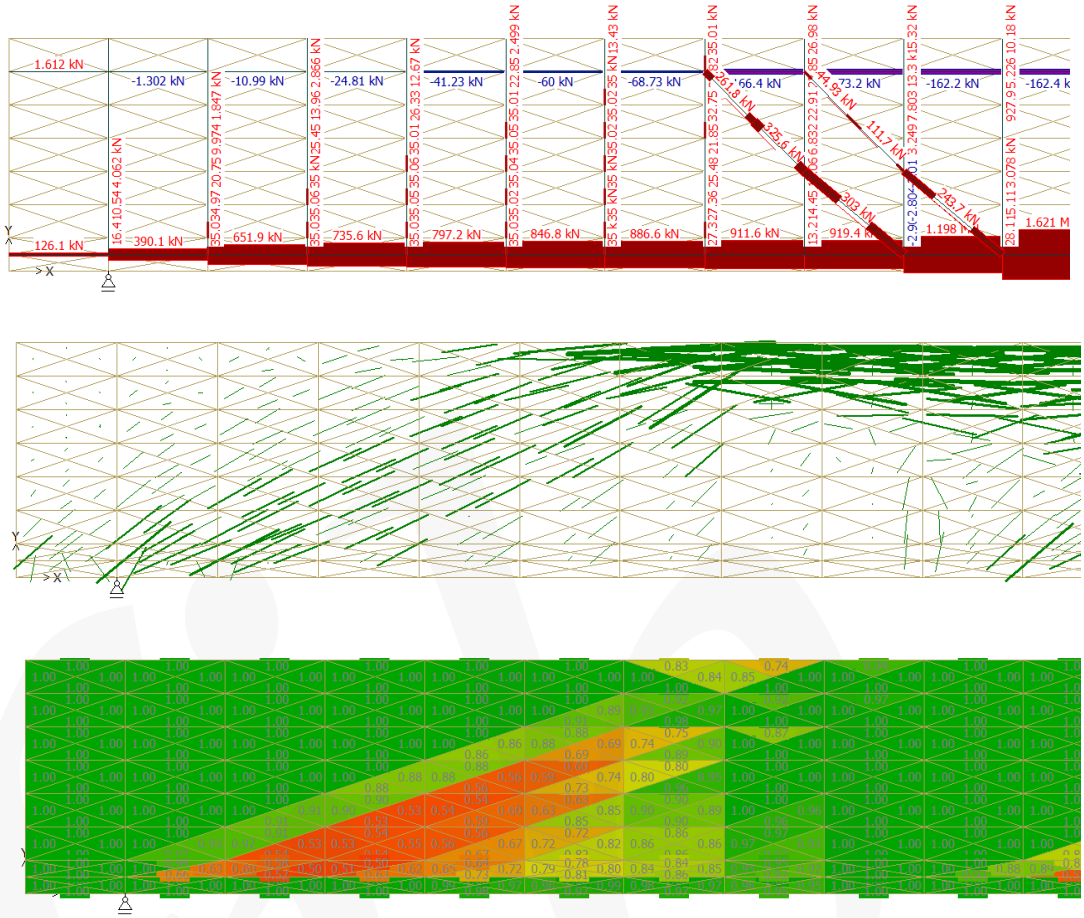


Fig. 6-33 Elastic-plastic analysis for the end support: a) Reinforcement forces; b) Concrete compression stress directions; c) Concrete softening due to transversal strains.

The failure mode of LoA III complies with the LoA II model, providing a higher value of failure load. This aspect is in accordance with the LoA concept: the lowest levels are simpler but also more conservative.

6.6.6 In-situ beam test

The refined analysis of LoA III led to the conclusion that the beams could be considered to be able to resist the design load. However, the fact that the shear reinforcement is less than the minimum advised by codes raises concerns on the applicability of equilibrium-based models, as localised cracking may govern the response of the member.

For that reason, it was decided to perform an in-situ test[6-13], to analyse the response of the elements. The main aim was to check if the beam had sufficient deformation capacity so that methods based on limit analysis (as in the stress field method) could be applied. A test was thus conducted according to Fig. 6-34a and b, where an actuator was placed near the inclined reinforcement. The loading frame was fixed to the existing column (left side in Fig. 6-34b) and to the beam (right side in Fig. 6-34b). A couple of external prestressing bars were also arranged vertically to preclude shear failure outside the region investigated Fig. 6-34c).

This document is the intellectual property of the fib – International Federation for Structural Concrete. All rights reserved.
This PDF of fib Bulletin 100 is intended for use and/or distribution solely within fib National Member Groups.

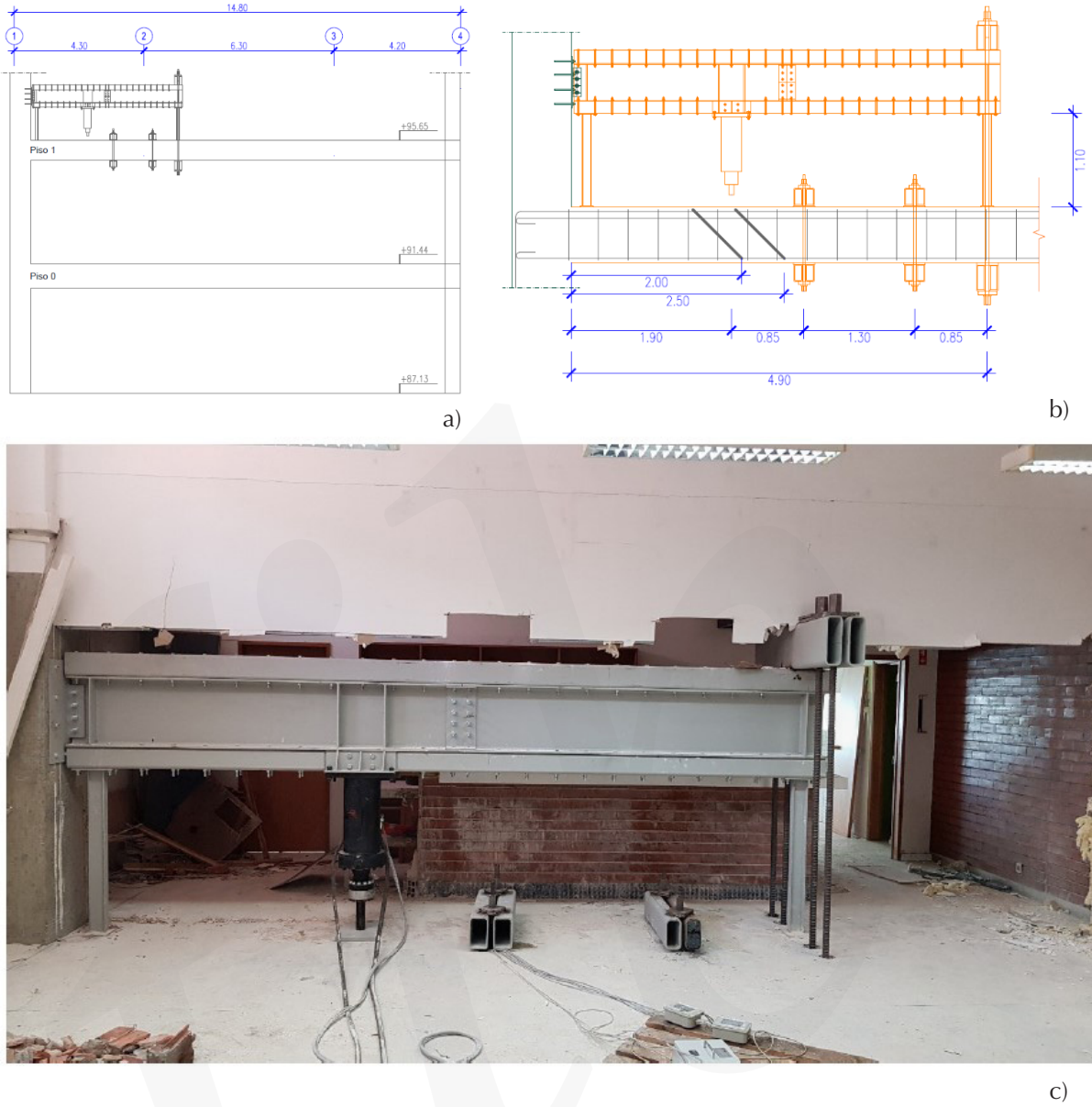


Fig. 6-34 In situ test structure and system: a) general view; b) detailed view with dimensions; c) Photo of the experimental system before the test.

Fig. 6-35 presents a photo of the crack pattern for the failure load of the beam. Smeared cracking developed, with failure eventually governed by a shear crack extending up to the support. Interestingly, after this crack appeared (at yielding of the stirrups), smaller cracks near the bottom face of the slab also started to open and the load introduced by the actuator could increase further. This response suggests that the beam experienced internal stress redistributions in a controlled manner, allowing for alternate load paths. By considering the failure load of the test F_u = 330 kN and taking into consideration the beam self-weight (leading to a shear at the support G = 177 kN), the reaction in the support results:

$R_u = 330 \cdot 3/4.9 + 177 = 379$ kN

The beam behaviour at ultimate load was in close agreement to the one predicted by means of the detailed stress field analysis presented before. In addition, the most important aspect of the test was the high deformation capacity observed, as presented in the load-displacement curve shown in Fig. 6-36. In fact, after development of the shear crack in the

This document is the intellectual property of the fib – International Federation for Structural Concrete. All rights reserved.
This PDF of fib Bulletin 100 is intended for use and/or distribution solely within fib National Member Groups.

web, the load was roughly maintained and even increased during a long plateau. Such response is in agreement to limit analysis assumptions, validating the applicability of plastic design models for this case despite the low amounts of transverse reinforcement (note that, the presence of flanges may however be considered as a favourable circumstance avoiding crack localization).



Fig. 6-35 Crack pattern of the beam at failure load.

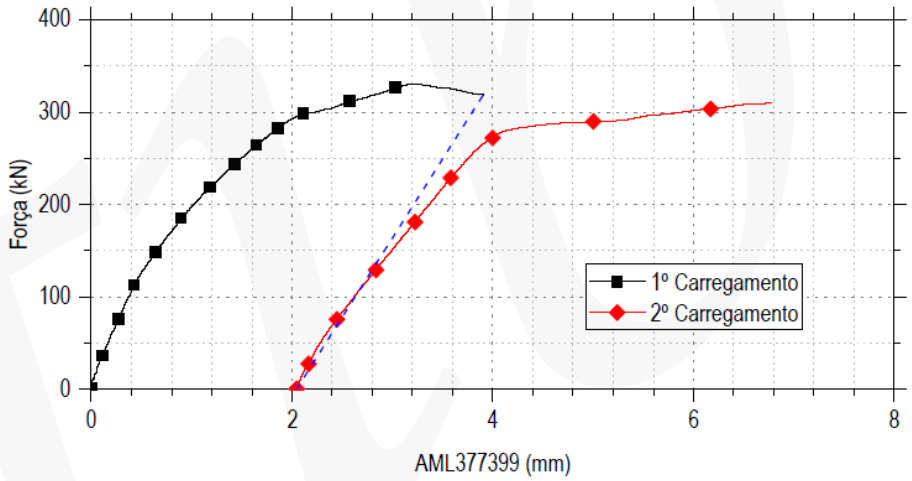


Fig. 6-36 Load in the actuator - displacement under the point load graphic.

6.6.7 Conclusion

This example shows that it is possible to use stress field modelling for elements with less than the minimum amount of reinforcement suggested by codes if sufficient deformation capacity is expected and redistributions of stresses can occur in a controlled manner. For this purpose, in-situ testing is a suitable tool validating the applicability of limit analysis. In the present case, such an approach allowed avoiding retrofitting and reduction of the costs of the intervention.

This document is the intellectual property of the fib – International Federation for Structural Concrete. All rights reserved.
This PDF of fib Bulletin 100 is intended for use and/or distribution solely within fib National Member Groups.

7. Special topics

7.1 Effect of load reversals

7.1.1 Load reversals

The strut-and-tie and stress-field methods for the design of disturbed concrete regions and members (D-regions, D-members) have been developed primarily for monotonic loading conditions, even though they are widely used in seismic design and other cases of cyclic loading. This has raised questions on whether the methods require modifications and special considerations when applied to cyclic load conditions, in particular when load reversals are expected. More specifically, the question is whether and to what extent load reversals modify the response of the compression fields in the concrete and reduce their load-bearing capacity: are the compression fields weakened, if compressive stresses need to be transferred across cracks caused by previous loading in the opposite direction? Are there other effects such as concrete spalling, bar buckling and bond degradation that require modifications of the strut-and-tie and stress-field design methods?

The goal of this section is to provide certain insight into these questions by focusing on two types of D-members, namely deep beams and short coupling beams. Due to their particular vulnerability to reversed cyclic loading, the discussion will further focus on short coupling beams with conventional shear reinforcement (stirrups) without diagonal bars.

Deep beams are commonly used as transfer girders in high-rise buildings and cap beams in bridge pier bents. As transfer girders carry predominantly vertical loads, they are typically not expected to undergo load reversals even in zones of high seismicity. This assumption however was proven wrong by the February 22, 2011 earthquake in Christchurch which devastated the third largest city of New Zealand. This earthquake produced extreme vertical peak ground accelerations of up to 2.0g and corresponding load reversals that damaged a number of heavily-loaded transfer structures.

While deep transfer girders are less likely to be subjected to load reversals, coupling beams in seismic zones are designed to sustain large inelastic load cycles, and in this way to provide ductility and energy dissipation capacity to the structure. As the longitudinal reinforcement of the coupling beams is expected to yield in the end sections, this results in the opening of wide cracks and weakening of the compression field that carries the shear forces in the web of the beam. Even though this problem is typically solved by providing heavy diagonal reinforcement[7-1], [7-2], there exist a large number of pre-1970s coupled-wall structures with conventional reinforcement which require proper strength/deformation capacity assessment.

To examine these issues, this subsection summarises experimental evidence for the effect of load reversals on the behaviour of deep beams and short coupling beams. The test results are compared to the predictions of strut-and-tie models (STM) based on the *fib* Model Code 2010[7-3] provisions to evaluate the adequacy of the models. The strut-and-tie approach is considered at level of approximation I (LoA I), while a kinematics-based approach (2PKT) will be used for LoA II. This latter approach predicts not only

https://doi.org/10.35789/fib.BULL.0100.Ch07

This document is the intellectual property of the fib – International Federation for Structural Concrete. All rights reserved.
This PDF of fib Bulletin 100 is intended for use and/or distribution solely within fib National Member Groups.

the load bearing capacity of the member, but also the deformations at failure which are important for the performance-based seismic evaluation of existing structures[7-4], [7-5], [7-6]. Comparisons to the predictions of a LoA IV approach, namely the Compatible Stress Field Method[7-7], [7-8], are also provided for the particular case of coupling beams with shear failures at high ductility ratios.

7.1.2 Models for deep girders and short coupling beams

Strut-and-tie models for deep beams and short coupling beams are presented in Fig. 7-1. It will be assumed that the member is deep (or short) when the shear-span-to-effective-depth ratio *a/d* is smaller than about 2.5. In such cases, a portion of the shear can be carried by a direct diagonal strut, while the rest is resisted by a truss mechanism involving the stirrups (two inclined struts and a vertical tie). As evident from Fig. 7-1a, the geometry of the model for deep beams is determined by the lever arm of the internal longitudinal forces *z* which is estimated at 0.9*d*. The size of the critical nodal zone at the support is defined by the width of the support l_b and by the distance c between the bottom edge of the beam and the bottom tie. In contrast, in the model for short coupling beams, the lever arm *z* is determined by the distance between the top and bottom longitudinal reinforcement, and the width of the critical nodal zones l_b is an open parameter (to be discussed later). As the nodal zones are inside the adjacent shear walls, their width is not limited by a clearly-defined loading element as in deep beams. In both models the vertical tie representing the stirrups is located in the middle of the clear span. Because stirrup deformations in the ends of the clear span are restrained, the area of the tie is assumed to be equal to one-half of the area of the stirrups in the clear span. The restraint comes from the clamping action of the load and support reaction in deep beams, and by the adjacent shear walls in coupling beams. As compared to test observations, the estimated area of the vertical tie is typically conservative, and therefore the tie is assumed to yield prior to the failure of the member. According to the models in Fig. 7-1, the failure of the member can occur with either crushing of the inclined struts (shear failure) or by yielding of the longitudinal ties (flexure).

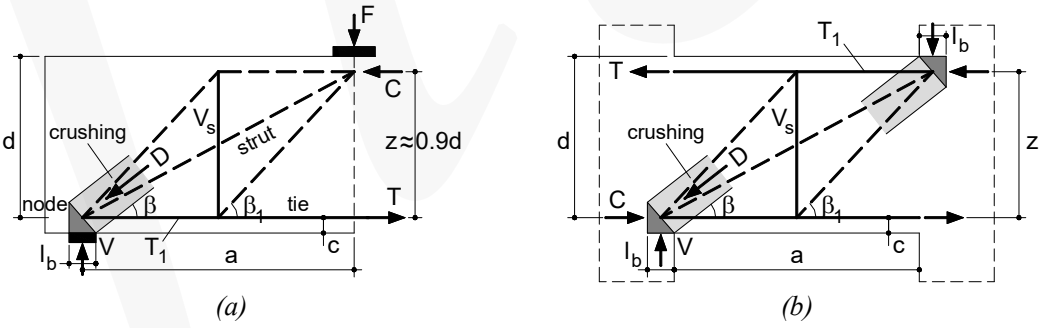


Fig. 7-1 Strut-and-tie models for: (a) deep beams; (b) short coupling beams with conventional shear reinforcement (stirrups)

To evaluate the shear force *V* corresponding to strut crushing, an iterative solution procedure needs to be employed. The solution can start by assuming a trial value of *V*. Next, the shear force carried by the stirrups V_s is calculated as the minimum of *V* and the yield resistance of the vertical tie. Knowing the values of *V* and V_s, the strut and tie model is statically determinate and the forces in the rest of the elements of the model can be calculated from equilibrium. More specifically, it is of interest to determine the resultant

This document is the intellectual property of the fib – International Federation for Structural Concrete. All rights reserved.
This PDF of fib Bulletin 100 is intended for use and/or distribution solely within fib National Member Groups.

compression force D of the two inclined struts in the vicinity of the critical nodal zone as it is this force that causes strut crushing. Force D and its angle of inclination β are calculated from:

$$D = \sqrt{V^2 + T_1^2} \qquad 7\text{-}1$$

$$\tan\beta = V/T_1 \qquad 7\text{-}2$$

where

$$T_1 = \frac{V_a}{z} - V_s \cot\beta_1 \text{ for deep beams} \qquad 7\text{-}3$$

$$T_1 = \frac{V\left(a + l_b\right)}{2z} - V_s \cot\beta_1 \text{ for short coupling beams} \qquad 7\text{-}4$$

In order to reach strut crushing, D must be equal to the strut capacity D_{max} evaluated on the basis of concrete strength equal to $0.55\min[(30/f_c)^{1/3},1]f_c$ (*fib* 2013[7-3]). If D is not equal to D_{max}, the value of V is adjusted and the calculations are repeated until convergence is achieved.

For coupling beams, this solution procedure is performed for a fixed value of the width of the nodal zone l_b. However, to determine the final strength prediction, l_b is optimised as illustrated in Fig. 7-2a. For each value of l_b, the model is used to calculate the shear corresponding to strut crushing (green line) and horizontal tie yielding (red line). The strength of the member for each lb is thus the minimum of the two shear forces. The final shear strength prediction corresponds to the l_b value that maximises the strength (lower bound approach).

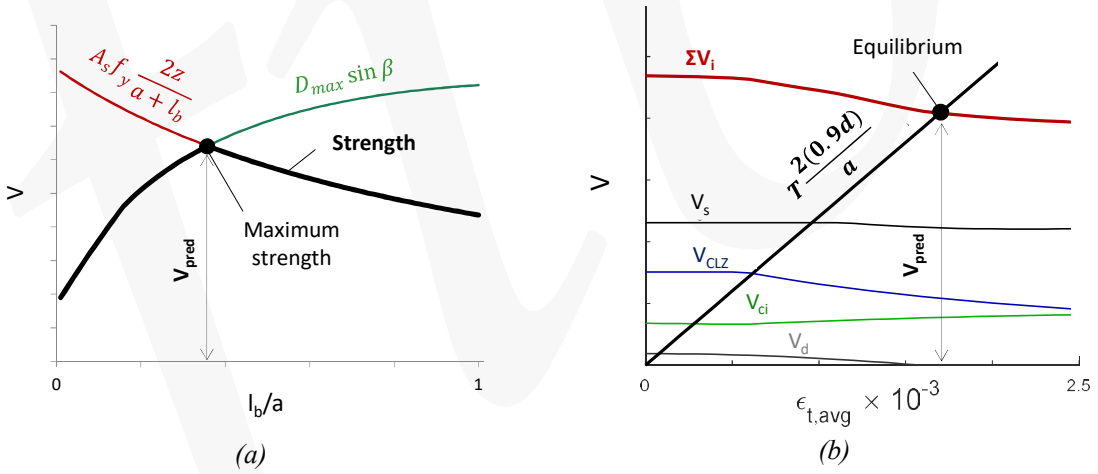


Fig. 7-2 Solution procedures for short coupling beams: (a) strut-and-tie model; (b) kinematics-based approach for diagonal tension failures

The kinematics-based approach used here for LoA II is illustrated in Fig. 7-3. It accounts for two failure modes: diagonal tension failures along a diagonal crack and sliding shear (or diagonal compression) failures in the end sections. The sliding shear failures occur when the member has a sufficient number of stirrups to supress the opening of the diagonal cracks,

This document is the intellectual property of the fib – International Federation for Structural Concrete. All rights reserved.
This PDF of fib Bulletin 100 is intended for use and/or distribution solely within fib National Member Groups.

and may develop prior to or after yielding of the longitudinal reinforcement. Therefore, the predicted strength of the member is obtained as the minimum of the shear forces obtained for each failure mode. Similarly to the strut-and-tie model, the kinematics-based approach does not account explicitly for the effects of load reversals. As this approach has been discussed in detail elsewhere[7-4], [7-5], [7-6], the following paragraphs present only a brief summary of its fundamentals.

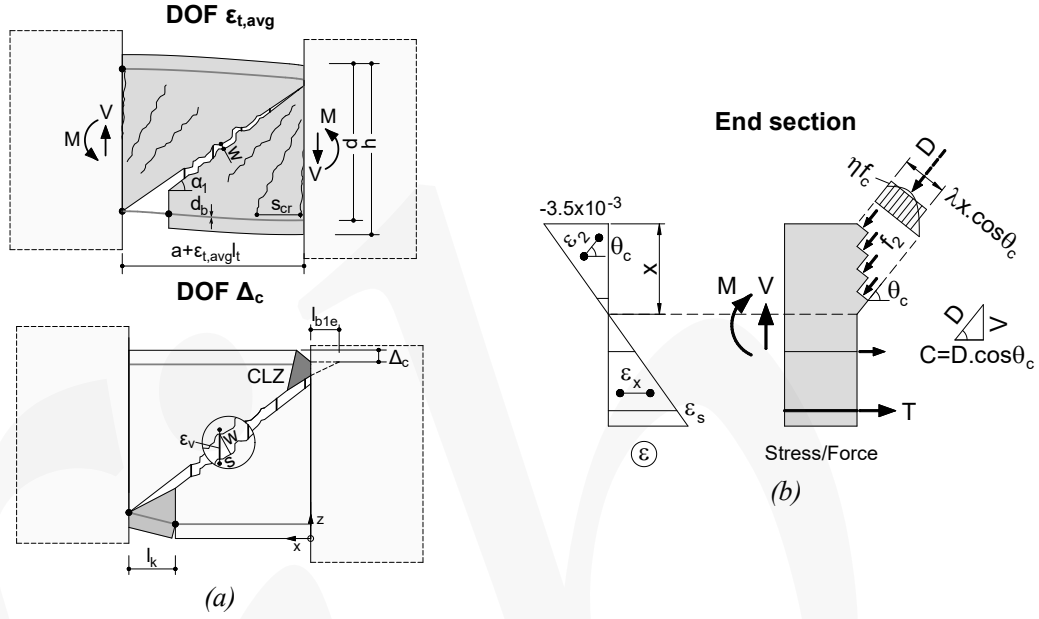


Fig. 7-3 Kinematics-based approach for coupling beams[7-4], [7-5], [7-6]: (a) diagonal tension failure (l_t is the cracked length along the longitudinal reinforcement); (b) sliding shear failure

The modelling of diagonal tension failures in coupling beams is based on a simple two-degrees-of-freedom (2DOFs) description of the deformation patterns of the member (Fig. 7-3a). These DOFs are the average strain in the longitudinal reinforcement $\varepsilon_{t,avg}$ and the transverse displacement Δ_c in the critical loading zone (*CLZ*) where the concrete crushes at failure. These two DOFs are also used to express the displacements in the critical diagonal crack, and therefore to express the mechanisms of shear resistance across the crack via appropriate constitutive relationships. The mechanisms accounted for in the kinematic approach include the shear carried in the *CLZ*, V_{CLZ}, aggregate interlock shear, V_{ci}, tension in the stirrups, V_s, and dowel action of the longitudinal reinforcement, V_d. DOF Δ_c is determined by assuming that the crushing of the *CLZ* triggers the failure of the beam, while $\varepsilon_{t,avg}$ is calculated from equilibrium as illustrated in Fig. 7-2b. As evident from the plot, the solution is obtained as the intersection of two curves: a shear capacity curve $\Sigma V_i = V_{CLZ} + V_{ci} + V_s + V_d$ and the shear derived from the tension force in the longitudinal reinforcement $T(\varepsilon_{t,avg})$. The equations of the kinematics-based approach for diagonal tension failures are summarised in Fig. 7-4. This approach has been developed to apply to members with short shear spans where the shear strength predicted by this method will exceed the shear strength predicted by sectional design procedures intended for longer spans. Therefore, in general, the final shear strength prediction is obtained as the maximum of the kinematics-based and sectional predictions.

This document is the intellectual property of the fib – International Federation for Structural Concrete. All rights reserved.
This PDF of fib Bulletin 100 is intended for use and/or distribution solely within fib National Member Groups.

a) Geometry

Effective size of critical loading zone

(5) $l_{b1e} = 0.11\sqrt{a^2 + h^2}$

Dowel length

(6) $l_k = l_0 + d(\cot\alpha - \cot\alpha_1)$

$l_0 = 1.5(h-d)\cot\alpha_1 \geq s_{\max}$

$s_{\max} = \frac{0.28 d_b}{\rho_l}\frac{2.5(h-d)}{d}$

Angle of critical crack

(7) $\alpha_1 = \alpha \geq \theta$

α – angle of the diagonal of the beam

θ – based on Simplified MCFT or 30°

Area of effective stirrups

(8) $A_v = \rho_v b(0.9d)\cot\alpha_1$

b) Degrees of Freedom

(9) $\varepsilon_{t,avg} = \frac{V \times 0.5a}{0.9d \times E_S A_S}$

(10) $\Delta_c = 0.0105 k_c l_{b1e}\cot\alpha$

$k_c = 1/(0.8 + 170\varepsilon_1) \leq 1$

$\varepsilon_1 = \left(1 + \cot^2\alpha\right)\varepsilon_{t,avg} \geq 0$

c) Compatibility

Crack width

(11) $w = \Delta_c \cos\alpha_1 + \frac{\varepsilon_{t,avg} l_k}{2\sin\alpha_1}$

Stirrup strain

(12) $\varepsilon_v = \frac{\Delta_c + 0.25\varepsilon_{t,avg} d\cot^2\alpha_1}{0.9d}$

d) Shear Strength

$V = V_{CLZ} + V_{ci} + V_d + V_s$

Critical loading zone

(13) $V_{CLZ} = 1.43 k_c f_c'^{0.8} l_{b1e} b \sin^2\alpha$

Dowel action

(14) $V_d = n_b f_{ye}\frac{d_b^3}{3l_k}$

$f_{ye} = f_y\left[1 - \left(\frac{\varepsilon_{t,avg}E_s}{f_y}\right)^2\right] \leq 500\,MPa$

≥ 0

Aggregate interlock

(15) $V_{ci} = \frac{0.18\sqrt{f_c'}}{0.31 + \frac{24w}{a_g + 16}} bd$

Stirrup resistance

(16) $V_s = E_s A_v \varepsilon_v \leq A_v f_{yv}$

Solution procedure: *Calculate geometry from* a) → *Choose* $V \approx 0.10 f_c' bd$ → b) ⇄ c) → d)

Notations: a = beam length; h = beam depth; d = effective depth; b = beam width; E_s = modulus of elasticity of steel; A_s = area of top/bottom longitudinal reinforcement; $\rho_l = A_s/bd$ = ratio of top/bottom reinforcement; ρ_v=stirrup ratio; d_b = diameter of top/bottom reinforcement; f_y = yield strength of top/bottom reinforcement; f_{yv} = yield strength of stirrups; f_c' = compressive strength of concrete; a_g = maximum size of course aggregate.

Fig. 7-4 Equations of the kinematics-based approach for diagonal tension strength of coupling beams [7-4], [7-6]

The sliding shear resistance in the kinematics-based approach is calculated based on the strain compatibility condition depicted in Fig. 7-3b. This condition resembles the classical plane-sections-remain-plane condition, except that the strains in the compression zone ε_2 are not horizontal but inclined at angle θ_c. The principal compressive stresses f_2 associated with ε_2 are also inclined at the same angle, where θ_c is determined in advance based on the equilibrium of the shear span ($\cot\theta_c \approx 0.5a/0.9d$). These assumptions result in a simple calculation procedure: the end sections are calculated as for pure bending, except that the width of the compression zone is reduced by a factor $\cos^2\theta_c$ to account for the high shear transferred across the compression zone[7-6]. As the compression zone is narrower, the flexural strength is reduced, and so is the corresponding shear force representing the sliding shear resistance.

Finally, it should be noted that the kinematics-based approach can be viewed as a more detailed way of calculating the strength of the struts of the strut-and-tie model. When diagonal tension failure is predicted, the shear contribution of the direct diagonal strut corresponds to the sum of shear components V_{CLZ}, V_{ci} and V_d, while the resistance of the truss mechanism involving the stirrups corresponds to V_s. Therefore, the kinematic approach accounts for the fact that the strut carries shear partly through uncracked concrete (V_{CLZ}), and partly through the rough cracks (V_{ci}) and bar-dowels (V_d) (Fig. 7-3a). In members with large amounts of transverse reinforcement, the strut-and-tie model will predict that the shear is carried entirely by the truss mechanism involving the stirrups, and sliding shear failure will occur with crushing of the struts in the end sections. In this failure mode, the strain compatibility condition used by the kinematic approach in the end sections provides means to evaluate the size and capacity of the struts (Fig. 7-3b).

This document is the intellectual property of the fib – International Federation for Structural Concrete. All rights reserved.
This PDF of fib Bulletin 100 is intended for use and/or distribution solely within fib National Member Groups.

In addition to the strut-and-tie and the kinematics-based approaches already introduced, the behaviour of coupling beams with shear failures at high ductility ratios will also be predicted by means of the Compatible Stress Field Method (CSFM)[7-7], [7-8]. The basic concepts of the CSFM are shown in Fig. 7-5 and were already introduced in Section 5.1. The CSFM consists of a simplified non-linear finite element-based continuous stress field analysis procedure that automatically computes the effective compressive strength of concrete. By considering equilibrium at stress-free cracks, simple uniaxial constitutive laws provided in standards for concrete and reinforcement are implemented without the need for the additional material properties required to perform nonlinear FE analyses. While concrete tensile strength is not considered in terms of strength (just as in standard structural concrete design), the CSFM accounts for its influence on members' stiffness (i.e., tension stiffening), and is therefore considered a LoA IV approach (refer to Section 3 and 5.2). By providing realistic stiffness to the elements, serviceability verifications and deformation capacity aspects (e.g., stirrup failures caused by insufficient ductility) are covered consistently. Tension stiffening is accounted for by modifying the input bilinear stress-strain relationship of the reinforcing bare bar in order to capture the average stiffness of the bars embedded in concrete ε_m (Fig. 7-5d). In the analysed coupling beams, the anchor blocks are modelled as linear elastic and the effect of reinforcement strain penetration into them (which has a large impact into the measured deformations) is not taken into account. Therefore, only the strength predictions provided by the CSFM are analysed in the following.

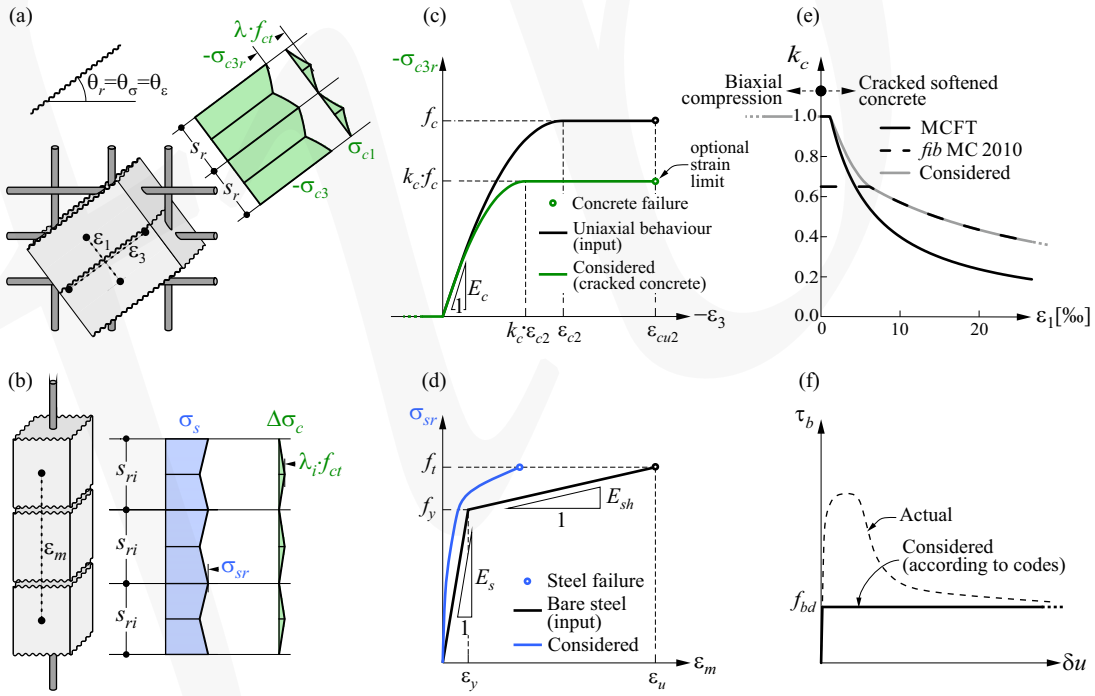


Fig. 7-5 Basic assumptions of the CSFM: (a) principal stresses in concrete; (b) stresses in the reinforcement direction; (c) stress-strain diagram of concrete in terms of maximum stresses and considering compression softening; (d) stress-strain diagram of reinforcement in terms of stresses at the cracks and average strains; (e) compression softening law; (f) bond shear stress-slip relationship for anchorage length verifications.

This document is the intellectual property of the fib – International Federation for Structural Concrete. All rights reserved.
This PDF of fib Bulletin 100 is intended for use and/or distribution solely within fib National Member Groups.

7.1.3 Shear failures at low ductility levels

The models discussed above will be employed to model tests of deep beams and short coupling beams subjected to monotonic and reversed cyclic loading. The discussion will focus first on specimens that failed without significant yielding of the longitudinal reinforcement and exhibited limited ductility. Such a test series consisting of eight deep beams was performed by Mihaylov et al.[7-9] to (in part) study the efficiency of strut action under seismic action. Even though the beams were tested before the 2011 Christchurch earthquake, half of them featured fully-reversed, large amplitude cyclic loading.

Fig. 7-6 depicts the crack patterns of the cyclically-loaded members at failure. All beams had a 1'200 mm by 400 mm rectangular section with a symmetric top and bottom longitudinal reinforcement with ratio $\rho_{l,bot} = \rho_{l,top} = 0.70\%$. The concrete strength was approximately 35 MPa, the a/d ratio was either 1.55 or 2.28, and the stirrup ratio was either 0 or 0.10%. Pairs of nominally identical specimens were tested under monotonic and fully-reversed cyclic loading. As evident from the crack diagrams in Fig. 7-6, the cyclically-loaded beams developed nearly symmetrical cracks under downwards and upwards loading resembling two fans centred at the loading points. The largest crack widths were measured along the diagonal cracks (up to 4.2 mm) together with significant slip displacements. This observation is explained by the second deformation pattern in Fig. 7-3a which shows that DOF Δ_c of the kinematic model is associated with additional opening as well as crack slip due to the deformations in the critical loading zone. It was the crushing of this zone that was observed to cause the shear failure of all eight test specimens. When the failure developed along the diagonal cracks, the flexural reinforcement was still in the elastic range.

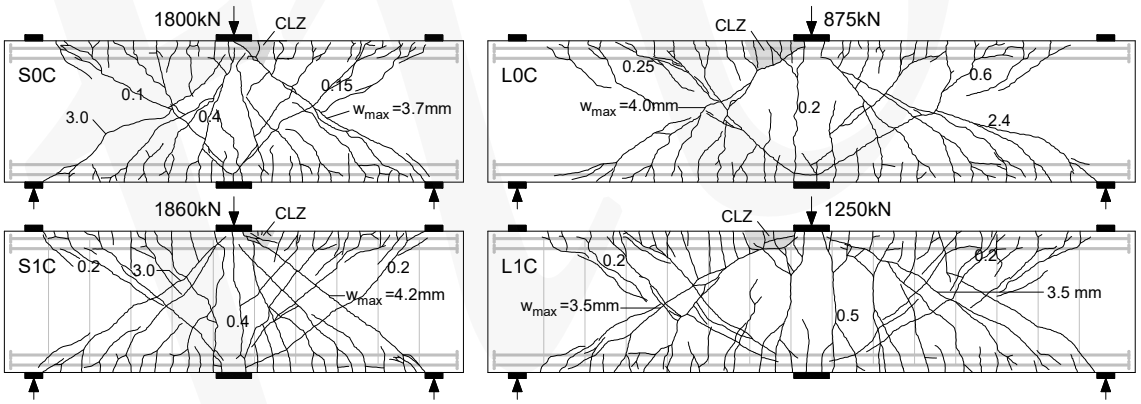


Fig. 7-6 Cyclic tests of deep beams – crack diagrams at failure (specimens S0C, S1C, L0C and L1C by Mihaylov et al.[7-9], where *S* corresponds to *a/d* = 1.55, *L* to *a/d* = 2.28, 0 to no stirrups, and 1 to a stirrup ratio of 0.1%)

The complete shear force vs. midspan deflection response of the specimens with stirrups is shown in Fig. 7-7. It can be immediately seen that, even though the cyclic tests were performed under full load reversals, this had nearly no effect on the shear strength as compared to the companion monotonic tests. For the specimens without stirrups, the cyclically-loaded beams were even stronger than the monotonically-loaded ones. In these cases, it was found

This document is the intellectual property of the fib – International Federation for Structural Concrete. All rights reserved.
This PDF of fib Bulletin 100 is intended for use and/or distribution solely within fib National Member Groups.

that, because the diagonal cracks were not controlled by web reinforcement, they exhibited significant variations in the vicinity of the applied load. As a result, the critical loading zones had variable dimensions, and therefore caused variations in the shear strength unrelated to the type of loading[7-9], [7-10]. Therefore, the eight deep beam tests showed that the direct struts that formed under downwards load were able to cross the cracks caused by upwards loading without loss of compression capacity. Similar results have also been reported by Alcocer and Uribe[7-11] who tested deep beams with larger stirrup ratios (ρ_v = 0.53%). In terms of strength predictions, the horizontal green lines in Fig. 7-7 show that both the strut-and-tie model (STM) and the kinematics-based approach (2PKT) provide excellent accuracy for the shorter beams, while the STM overestimates the shear strength of the longer specimens by about 20%. However, as in the latter case the angle of the critical strut β is only 24.6˚, specimens L1M/C can be considered outside the range of applicability of the strut-and-tie model.

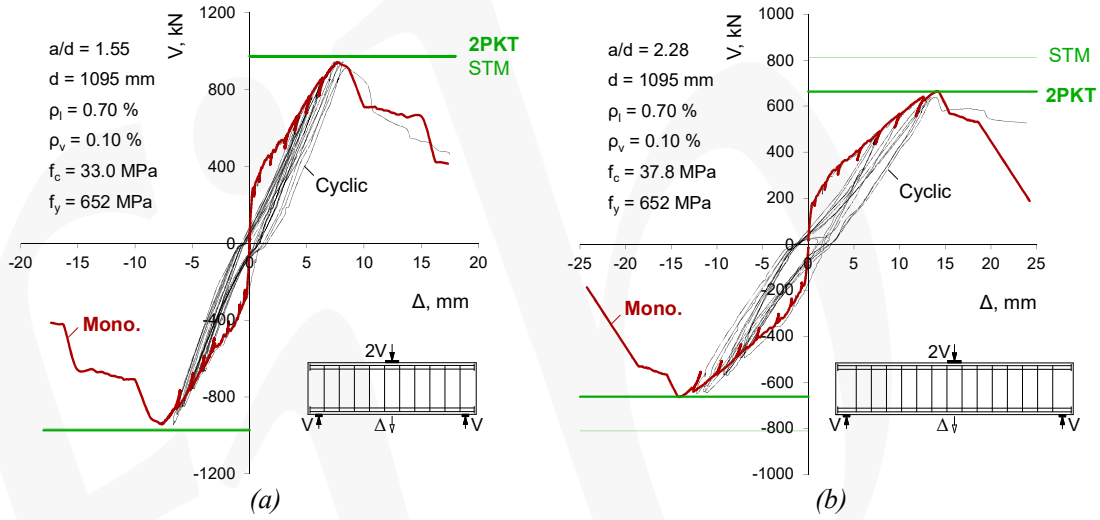


Fig. 7-7 Measured and predicted responses of deep beams with stirrups that exhibited diagonal tension failures (tests by Mihaylov et al.[7-9]): (a) tests S1M/C; (b) tests L1M/C

As the deep beam tests included a variety of measurements, it is also of interest to look at the effect of load reversals on important local deformations. Fig. 7-8a shows the vertical web strains measured in the shorter beams with transverse reinforcement. It can be seen that, while the load reversals resulted in residual deformations associated with DOF Δ_c of the kinematic model, they did not cause a significant increase of the peak deformations from one cycle to the next. This is likely because the other DOF of the kinematic model, $\varepsilon_{t,avg}$, returned to nearly zero upon unloading due to the elasticity of the longitudinal reinforcement (Fig. 7-8b). Under upwards load, DOF $\varepsilon_{t,avg}$ is associated with the opening of flexural cracks in the top critical loading zone. When the load is reversed however, these cracks close completely and the shear resistance of the CLZ appears unaffected. As shown in Fig. 7-8, the kinematics-based approach provides adequate estimates of both the vertical web strains and the strains in the longitudinal reinforcement at failure.

This document is the intellectual property of the fib – International Federation for Structural Concrete. All rights reserved.
This PDF of fib Bulletin 100 is intended for use and/or distribution solely within fib National Member Groups.

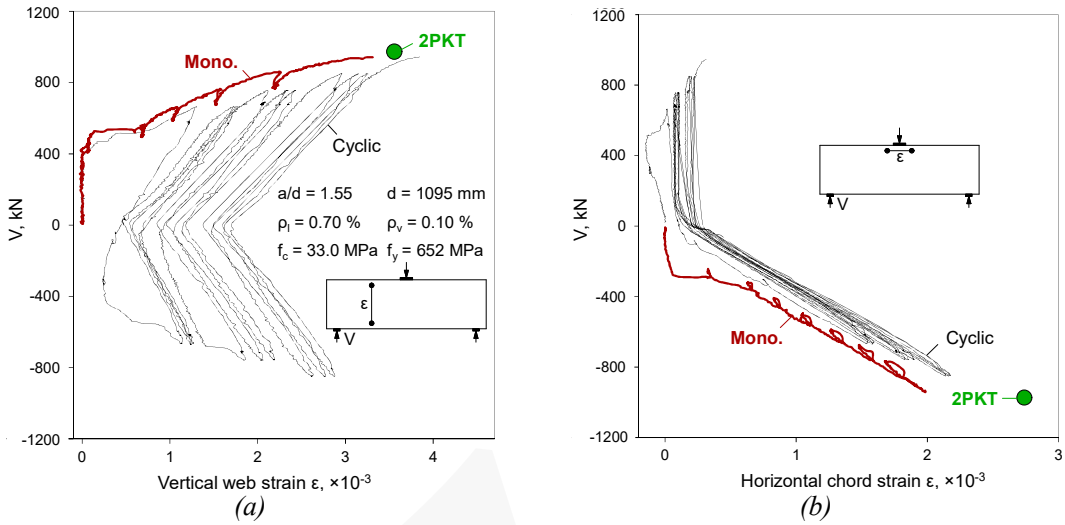


Fig. 7-8 Local cyclic deformations in deep beam specimens S1M/C (tests by Mihaylov et al.[7-9]): (a) Vertical web strains; (b) Longitudinal chord strains

In addition to deep beams, it is also of interest to verify whether similar conclusions can be reached from tests of short coupling beams with low ductility capacity. Fig. 7-9 shows the shear force vs. drift response of two pairs of nominally identical coupling beams subjected to monotonic and reversed cyclic loading[7-12]. The clear span of the beams was approximately 1'100 mm and the stirrup ratio was ρ_v = 0.88%. The main difference between the pairs of specimens was the aspect ratio: *a/d* of 1.11 vs. 2.27. As evident from the crack diagrams in Fig. 7-9, the shorter beams exhibited diagonal tension failures while the longer specimens failed due to sliding shear in the end sections. Only minor yielding of the longitudinal reinforcement was observed in the tests prior to failure. In the case of diagonal tension failures, the load reversals did not cause apparent strength degradation, even though it should be noted that the cyclically-tested beam had a stronger concrete (f_c = 38 MPa vs. 32 MPa). Inversely, in the case of sliding shear failure, the cyclically-loaded beam had 17% weaker concrete and was 6% weaker than its companion specimen subjected to monotonic loading. In terms of strength predictions, the strut-and-tie model is conservative and the kinematics-based approach improves the strength predictions as expected from a LoA II approach.

This document is the intellectual property of the fib – International Federation for Structural Concrete. All rights reserved.
This PDF of fib Bulletin 100 is intended for use and/or distribution solely within fib National Member Groups.

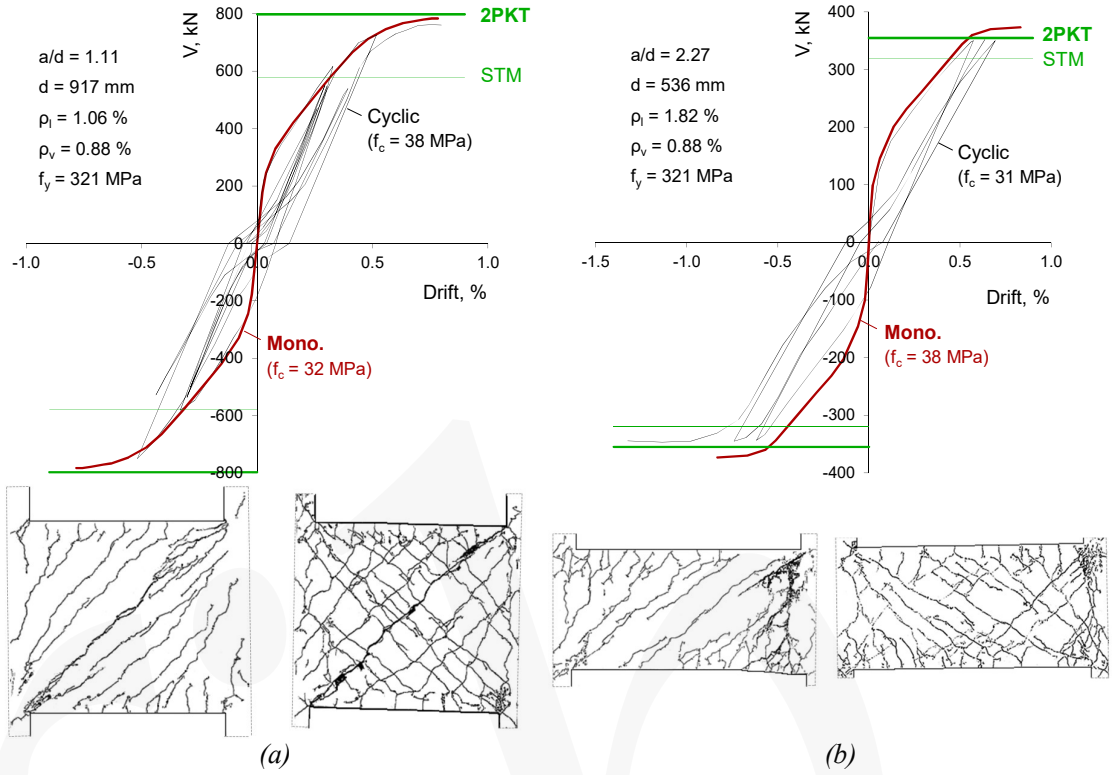


Fig. 7-9 Measured and predicted responses of coupling beams (tests by Paulay[7-12]): (a) Diagonal tension failure (specimens 391/392); (b) Sliding shear failure (specimens 242/243)

Fig. 7-10a shows the contribution of the stirrups to the shear resistance of the shorter coupling beams (a/d = 1.11) and how this contribution varied up to failure. The tension in the stirrups was evaluated from detailed strain measurements used together with the stress-strain curves of the reinforcement. Somewhat counterintuitively, the stirrups in the monotonic test carried more shear than those in the cyclic test prior to failure, even though load reversals are expected to weaken the concrete shear mechanisms. At failure, most of the stirrups yielded and provided about 63% of the shear strength in both tests, with the remaining 37% attributed to the concrete. The yielding of the stirrups is also evident from Fig. 7-10b where the vertical web strains exceed the yield strain of the steel. In the strut-and-tie model the concrete contribution is represented by the direct diagonal strut which carries 52% of the predicted failure load. In the kinematic-based approach the predicted concrete contribution of 44% is further subdivided into shear carried in the *CLZ* (25%) and by aggregate interlock (19%).

This document is the intellectual property of the fib – International Federation for Structural Concrete. All rights reserved.
This PDF of fib Bulletin 100 is intended for use and/or distribution solely within fib National Member Groups.

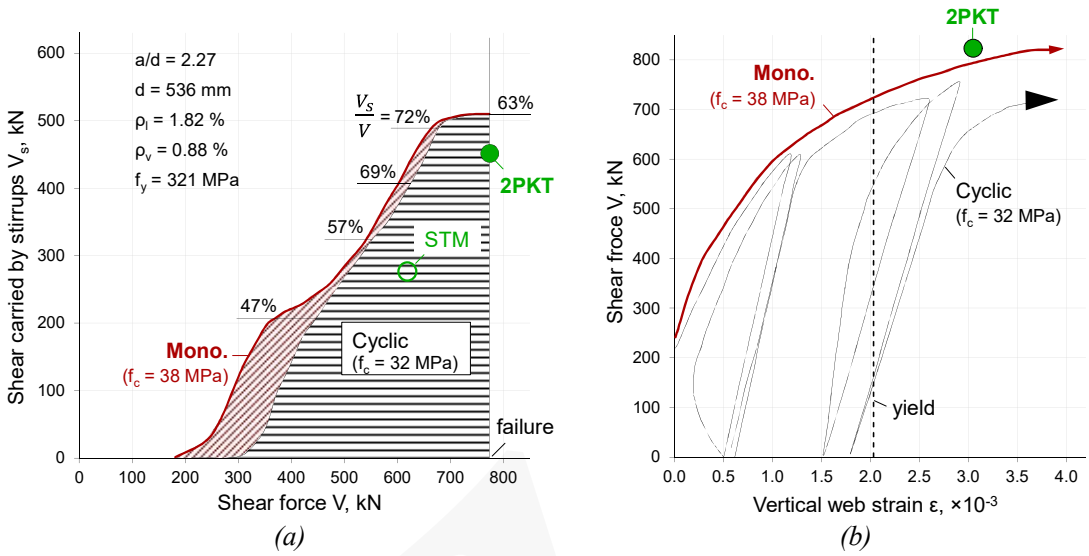


Fig. 7-10 Effect of cyclic loading by comparing coupling beam 391 (cyclic) to beam 392 (monotonic) (tests by Paulay 1969): (a) Mechanisms of shear resistance; (b) Vertical web strains

7.1.4 Shear failures at high ductility levels

A more severe cyclic degradation is expected when short coupling beams exhibit significant flexural yielding and ductility under monotonic loading. This is illustrated by the response of two pairs of specimens shown in Fig. 7-11[7-13], [7-14]. As in Fig. 7-9, the shorter beams with a/d = 1.25 failed in diagonal tension, while the longer specimens with a/d = 2.25 exhibited failures with crushing of the concrete in the end sections. In the former case the strength reduction due to load reversals was about 5%, while in the latter case it was 14%. Other two pairs of tests from the same series with a/d ratios of 1.52 and 1.94 showed no reduction and 14% reduction, respectively. While these values appear non-negligible, it is evident from Fig. 7-11 that both the strut-and-tie model and the kinematics-based approach provide conservative strength predictions of the cyclic shear strength. It should be noted however that these models do not predict the ductility of the members, while it is the ductility that is severely reduced by the load reversals. When using the Compatible Stress Field Model, which has a higher level of approximation, it can be seen that the predictions for monotonic tests are very accurate, but slightly unsafe for cyclic loads. This might indicate the necessity of accounting for the negative effect of cyclic loads when using models with the highest level of approximation. A first attempt in this direction was proposed by Kostic[7-15], who proposed reducing the compressive strength by a factor η_{LCF}. The suitability for coupling beams of the factor derived by Kostic for panel tests (η_{LCF} = 0.9), will be discussed in the following section.

To further understand the effect of cyclic loading on the strength and ductility of short coupling beams, Galano and Vignoli[7-16] performed tests under different loading protocols, see Fig. 7-12. From top to bottom the protocols are characterised by an increasing number of displacement levels and increasing number of cycles within each level. The beams had an a/d ratio of 1.61, d = 372 mm, ρ_v = 0.84%, and $f_c \approx$ 47 MPa. A benchmark monotonic test was also performed in the study. In this test the specimen failed in diagonal tension after flexural yielding, while failure due to yielding of the reinforcement and crushing of the concrete in the end sections was observed in the cyclically-tested beams. To compare the results, the shear resistance is normalised with respect to the monotonic strength and is plotted as a function of the cumulative ductility. It can be seen from the three curves that

This document is the intellectual property of the fib – International Federation for Structural Concrete. All rights reserved.
This PDF of fib Bulletin 100 is intended for use and/or distribution solely within fib National Member Groups.

all loading protocols resulted in negligible strength reduction (shear resistance at cumulative ductility of 1) and caused similar resistance degradation in the post-peak regime. As before, both the strut-and-tie model and the kinematics-based approach produced conservative strength predictions.

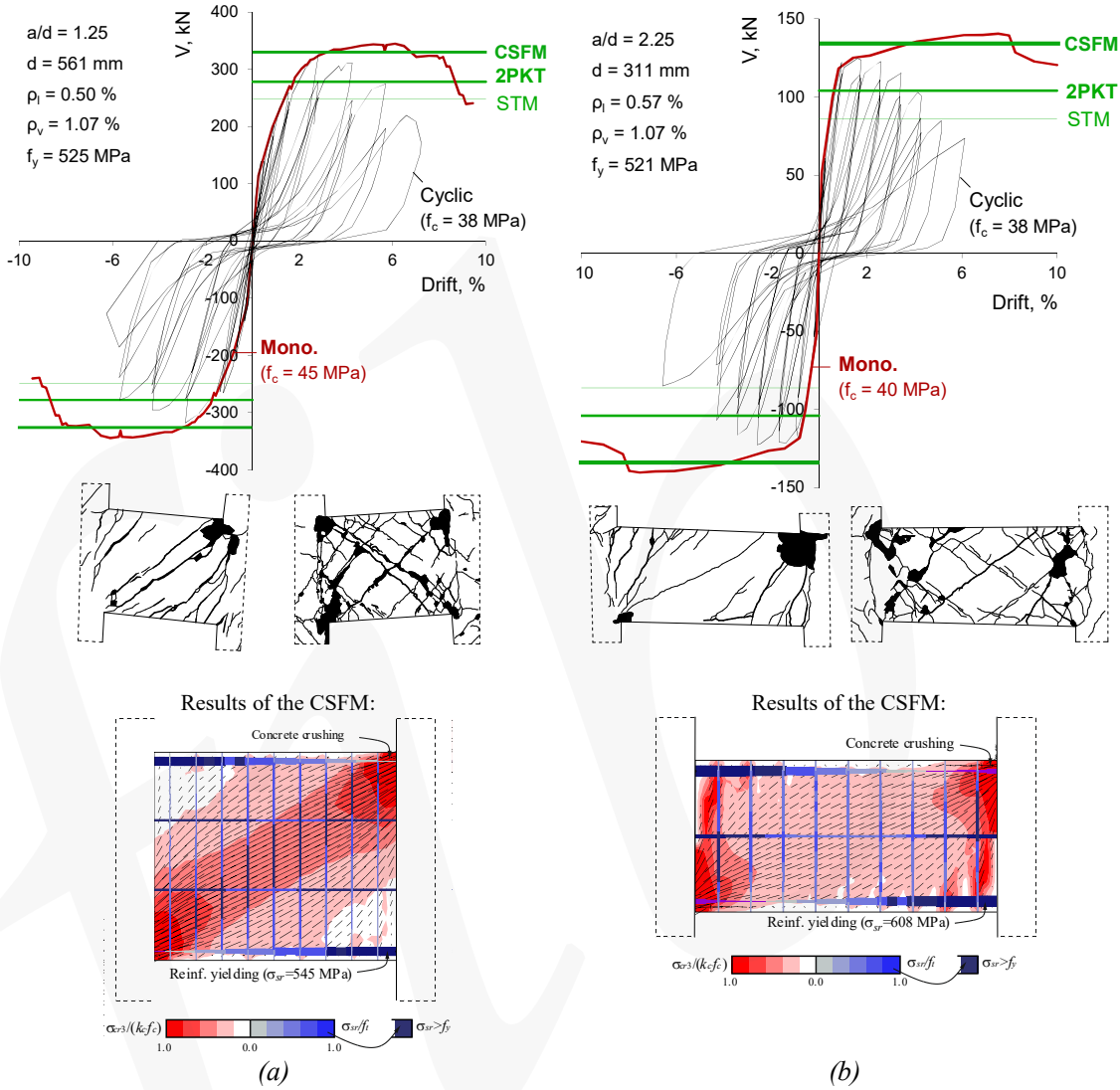


Fig. 7-11 Effect of cyclic loading on the response of coupling beams under large ductility demands (tests by Kwan and Zhao[7-13], [7-14]: (a) Diagonal tension failure (specimens MCB1 and CCB1); (b) Diagonal compression failure (specimens MCB4 and CCB4)

This document is the intellectual property of the fib – International Federation for Structural Concrete. All rights reserved.
This PDF of fib Bulletin 100 is intended for use and/or distribution solely within fib National Member Groups.

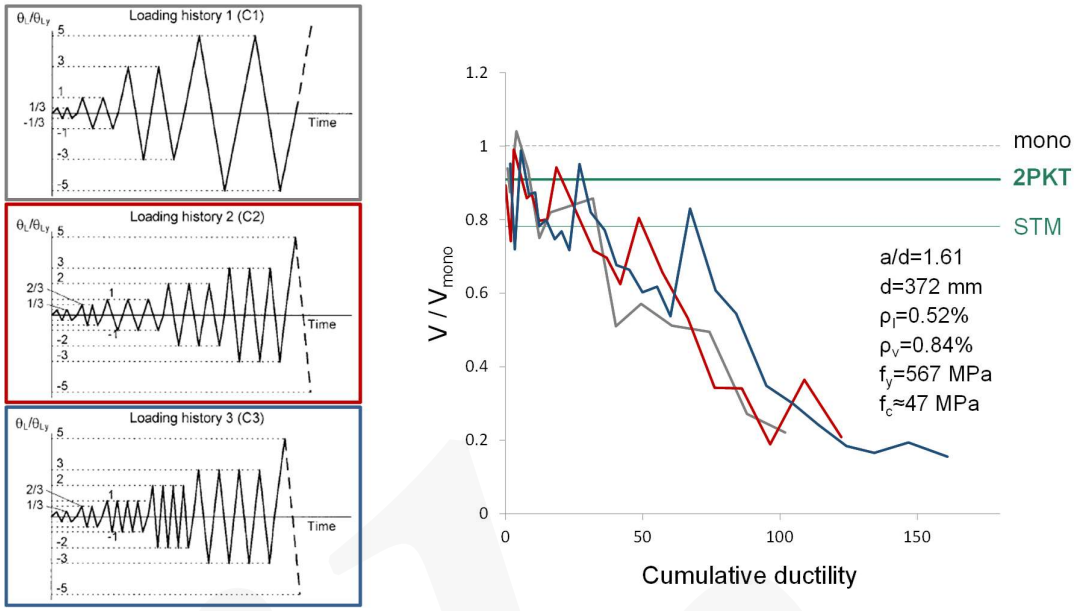


Fig. 7-12 Effect of cumulative ductility (adapted from Galano and Vignoli[7-16])

To understand whether these observations can be generalised, it is necessary to analyse the effect of flexural yielding with the help of the models considered in this study. According to the strut-and-tie model in Fig. 7-1b, the shear in the vicinity of the walls is carried by diagonal compressive stresses in the concrete. If yielding of the longitudinal reinforcement occurs in this zone due to earlier loading in the opposite direction, the stresses need to be transferred across open cracks via aggregate interlock. It follows that a substantial shear strength reduction can be expected if the plastic deformations in the reinforcement are large. A similar conclusion can be reached by considering the critical loading zone in Fig. 7-3a and the compression zone in Fig. 7-3b. However, the loading protocols in Fig. 7-12 as well as those typically used in tests consist of cycles with gradually increasing displacement magnitude. As a result, the peak load is reached at low ductility levels and is very close to the load associated with flexural yielding under monotonic loading. This explains the relatively small strength reduction in existing tests. It is expected that a more severe scenario can occur if the coupling beam is subjected to a large displacement pulse in one direction causing large plastic deformations, and consequently loaded to failure in the opposite direction. This scenario corresponds to near-fault ground motions and can cause very substantial strength reduction in the second loading direction. An indication for this effect has been provided by a test conducted by Paulay (specimen 393, Paulay[7-12]). Further research is therefore needed to investigate this issue and to evaluate the effect of such strength reduction on the global behaviour of coupled-wall structures. Additionally, it should be considered that the free elongation of the coupling beams is restrained by the stiff walls, and this can also affect the strength and ductility of the beams by introducing axial compressive forces.

7.1.5 Comparisons with test database

Comparisons similar to those shown above were performed with a database of 32 tests of short coupling beams collected from the literature[7-12], [7-13], [7-14], [7-16] [7-17], [7-18], [7-19]. It should be noted that the comparisons for the Compatible Stress Field Model were limited to the 10 tests of Kwan and Zhao[7-13], [7-14]. Fig. 7-13 summarises the results in terms of shear

This document is the intellectual property of the fib – International Federation for Structural Concrete. All rights reserved.
This PDF of fib Bulletin 100 is intended for use and/or distribution solely within fib National Member Groups.

strength experimental-to-predicted ratios obtained with the strut-and-tie model (LoA I), the kinematics-based approach (LoA II) and the Compatible Stress Field Model (LoA IV) without considering any reduction of the compressive strength due to cyclic loads. The two models with the lowest level of approximation provide consistently conservative predictions across the entire range of a/d ratios. By increasing the level of approximation from I to II, the average V_{exp}/V_{pred} ratio decreases from 1.37 to 1.10 and the coefficient of variation (CoV) from 8.9% to 7.1%. When the highest level of approximation is used, the average of V_{exp}/V_{pred} ratio is further decreased to 1.00 and the coefficient of variation to 5.7%. By comparing the blue and red data points in each plot, it can be seen that there is no substantial difference in the accuracy of the strength predictions for beams subjected to monotonic and reversed cyclic loading.

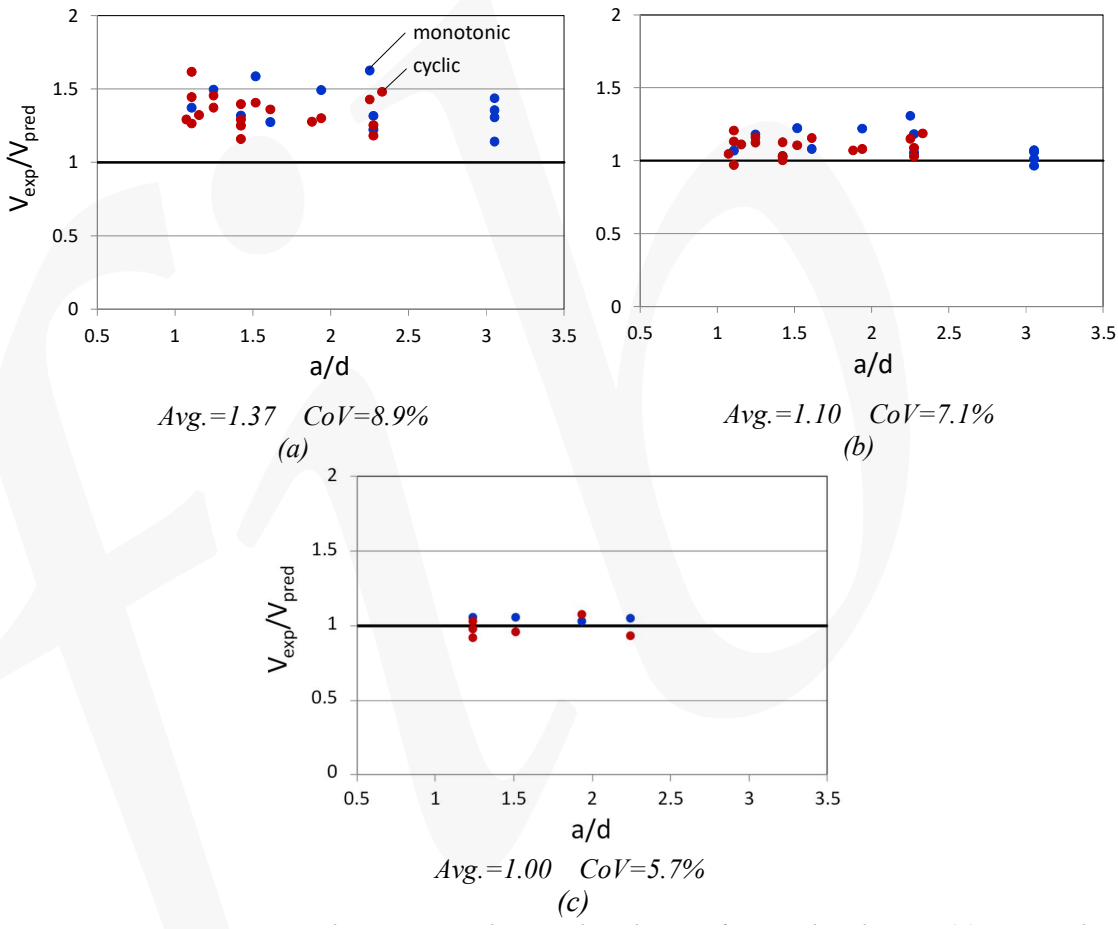


Fig. 7-13 Strength experimental-to-predicted ratios for coupling beams: (a) strut-and-tie model (LoA I); (b) kinematics-based approach (LoA II); (c) Compatible Stress Field Method (LoA IV) for specimens from Kwan and Zhao[7-13], [7-14] (η_{LCF} = 1.00).

When analysing in more detail the results obtained with the LoA IV, it can be seen that the predictions for the cyclic tests (Avg=0.98 and CoV=6.1%) are slightly unconservative, while for the monotonic tests are slightly conservative (Avg=1.04 and CoV=6.1%). To counteract this difference, the analysis for the cyclic test was repeated considering a reduced compressive strength, as proposed by Kostic[7-15]. A summary of the predictions of series CCB by Kwan and Zhao[7-13], [7-14] is provided in Table 7-1 for different values of the reduction factor of the compressive strength η_{LCF}. It can be seen that the strength predictions are not very sensitive to small changes in the compressive strength. Based

This document is the intellectual property of the fib – International Federation for Structural Concrete. All rights reserved.
This PDF of fib Bulletin 100 is intended for use and/or distribution solely within fib National Member Groups.

on the analysed data, a reduction of approximately 20% would be required in order to achieve the same level of conservatism as in the analogous monotonic tests, i.e., double than the value proposed by Kostic[7-15]. It should be noted however that this observation is based on a very limited amount of experimental data and failure modes. Therefore, further validation would be required to conclude about the general validity of this approach.

Table 7-1: Strength experimental-to-predicted ratios of compatible stress field model (LoA IV) for cyclic test of coupling beams of Kwan and Zhao[7-13], [7-14] for different values of the reduction factor of the compressive strength η_{LCF} accounting for the degradation due to cyclic loading.

	η_{LCF}				
	1.00	0.95	0.90	0.85	0.80
AVG	0.98	0.99	1.00	1.01	1.03
CoV	6.1%	6.0%	5.8%	5.7%	5.5%

7.1.6 Summary

The main results from the analysis of the test data from deep beams and short coupling beams with conventional reinforcement can be summarised as follows:

- Load reversals have negligible effect on the ultimate behaviour if the flexural reinforcement remains elastic up to failure.
- Flexural yielding results in a relatively modest reduction of peak resistance (0-14%) and a substantial reduction of ductility and displacement capacity.
- Single large inelastic cycles could cause significant shear strength reduction, even though further studies are necessary to confirm the extent of this effect.

When the test data is compared to the strength predictions of the strut-and-tie model (LoA I), the kinematics-based approach (LoA II) and the Compatible Stress Field Model (LoA IV), it is observed that:

- The strut-and-tie model is conservative even considering the cases of strength reduction of 14% due to load reversals.
- The kinematics-based approach reduces the conservatism and scatter of the strength predictions, while still providing conservative predictions for all 32 short coupling beams in the test database.
- The Compatible Stress Field Model provides predictions with very small conservatism and scatter for the 4 analysed monotonic tests of coupling beams, but slightly unconservative for the 6 cyclic tests. A 20% reduction of the compressive strength when modelling the cyclic tests leads to the same conservatism as in the analogous monotonic tests.
- As the kinematics-based approach and the Compatible Stress Field Model are built on deformations patterns and also includes constitutive relationships, they are suitable for predicting the strength as well as the displacement capacity of deep beams, short coupling beams, short walls, compact footings, and other shear-critical members.

This document is the intellectual property of the fib – International Federation for Structural Concrete. All rights reserved.
This PDF of fib Bulletin 100 is intended for use and/or distribution solely within fib National Member Groups.

7.2 3D models: general examples

7.2.1 Introduction

For simplicity and for practical reasons most concrete structures are treated as two-dimensional entities. This assumption is appropriate when forces and stresses in one of the spatial directions are negligible and is frequently applied in the analysis and design of discontinuity regions (D-regions). These are concrete elements (or parts of) characterised by complex stress fields and where the Bernoulli hypothesis is not valid. The strut-and-tie method[7-20] and the stress field method[7-21] are particularly suitable for the analysis and design of these critical elements and their application to elements with a predominantly planar behaviour is well covered in the literature and design codes, as previously shown in this Bulletin.

The response of some concrete structures and D-regions is three-dimensional. Examples of the latter are pile cap foundations, foundations of wind turbine towers, anchorage blocks and bridge diaphragms. A consistent and safe design of 3D D-regions is critical, especially considering that many of these elements cannot be inspected and/or repaired during their service life. 3D strut-and-tie models can be of great value for the design of such elements, but the reality is that they are hardly ever used by designers. The extension of the strut-and-tie and the stress field methods to 3D for the dimensioning and detailing of concrete structures has not seen significant progress since these methods were first proposed and little guidance can be found in the literature[7-22], [7-23]. This lack of guidance generally leads to excessively conservative solutions, which not only increase material requirements, construction time and costs, but may lead to construction problems, as it can be the case of excessively over-reinforced elements.

This section discusses the current state-of-the-art on the application of strut-and-tie and stress field models to the dimensioning of concrete members with three-dimensional behaviour. Since this is still an open topic, strong focus is placed on the difficulties in applying these models in 3D, as well as on those topics requiring additional research. The generalisation to 3D of compatibility-based stress fields generated by finite element analysis (discussed in Section 5.2 for the plane case) is presented as well. Two examples of application are provided: the first one, through which advantages and difficulties of 3D vs. 2D modelling are addressed, concerns the foundation of a wind tower turbine. The second example shows the application of the method to pile cap foundations considering different levels of approach (LoA).

General considerations on stress fields and strut-and-tie models were described in Chapter 2. Most provisions given there focus on 2D applications. While the same general principles apply for both 2D and 3D models, there are some differences observed in the 3D case. This section discusses the current state-of-the-art on the application of strut-and-tie and stress field models to the dimensioning of concrete members with three-dimensional behaviour and the differences with the 2D case. Since this is still an open topic, strong focus is placed on the difficulties in applying these models in 3D, as well as on those topics requiring additional research. The generalisation to 3D of compatibility-based stress fields generated by finite element analysis (discussed in Section 5.2 for the plane case) is presented as well. Two examples of application are provided: the first one, through which advantages and difficulties of 3D vs. 2D modelling are addressed, concerns

This document is the intellectual property of the fib – International Federation for Structural Concrete. All rights reserved.
This PDF of fib Bulletin 100 is intended for use and/or distribution solely within fib National Member Groups.

the foundation of a wind tower turbine. The second example shows the application of the method to pile cap foundations considering different levels of approach (LoA).

7.2.2 3D strut-and-tie models

7.2.2.1 Definition of the truss geometry and boundary conditions in 3D STM

The first step of strut-and-tie modelling is the development of a truss geometry consistent with the flow of forces inside the element. The visualisation of the flow of forces in 3D is more complex than in 2D and the use of linear-elastic stress fields does not always help in clarifying the flow of forces, as the stress fields become dispersed in large concrete volumes. Starting from simple 2D truss models for one of the principal planes of the element may be useful as shown in the example in section 7.2.3. It must be acknowledged though that additional resisting mechanisms that may appear in 3D are in some cases difficult to identify in simplified 2D models, which may limit the advantages of using spatial models.

Similarly to cases in 2D, the development of truss models is correlated with the definition of the boundary conditions because forces and support restraints are to be defined at the truss nodes. Loads need to be transformed into equivalent concentrated forces aiming for a balance between accuracy and simplicity of the resulting model. On the other hand, definition of support conditions may be an iterative process considering the obtained reaction forces (e.g. for the wind tower foundation shown in section 7.2.3, the ground reaction cannot be negative).

Once the truss geometry and boundary conditions are defined, the structural system can be solved. Resolution by hand calculations can be cumbersome depending on the number of elements, but almost any tool for analysis of 3D bar structures may be used. Many 3D models result in hyperstatic systems, which means that truss forces depend on the stiffness distribution; the practitioner needs to acknowledge the uncertainties in the obtained results and assess the influence of the element stiffnesses on the resulting truss forces.

7.2.2.2 Evaluation of the resistance of struts and ties

The strength of ties can be determined as for 2D models simply by multiplying the reinforcement cross sectional area times the design yielding stress of steel. Problems to determine the equivalent tie area from a given reinforcing bar distribution must be acknowledged for assessment. Moreover, there is not knowledge regarding the minimum amount of transverse reinforcement that provides sufficient deformation capacity to ensure a safe application of stress fields and strut-and-tie models in a 3D structure. Hence, experimental validation of 3D stress fields and strut-and-tie models is recommended particularly for members with an amount of transverse reinforcement below the provisions for shear reinforcement in beams (see Section 2.5.2).

Regarding the evaluation of the strength of struts and nodal zones, differences between 2D and 3D models must be accounted for. The resistance of these elements depends on the effective strength of concrete and the strut and node dimensions as commented next.

7.2.2.2.1 Evaluation of the effective strength of concrete

Two factors need to be considered for the evaluation of the effective strength of concrete (see section 2.3.1): (i) $\eta \cdot f_c$, which derives from material effects and, (ii) η_ε to consider structural effects. Material effects account for strength reduction to allow for plastic redistribution and no difference between 2D and 3D applications needs to be considered.

This document is the intellectual property of the fib – International Federation for Structural Concrete. All rights reserved.
This PDF of fib Bulletin 100 is intended for use and/or distribution solely within fib National Member Groups.

Structural effects account for the transverse strain state (cracking and confinement) and, therefore, the dimensionality of the model (2D or 3D) does have an effect on its evaluation. Factor η_ϵ is usually expressed as a function of the principal strain(s)/stress(es) transverse to the principal direction of compression, or simply based on the expected potential cracking state (see section 2.3.1). The evaluation of this factor in 3D becomes more complex than in 2D, because an additional strain component needs to be accounted for. Three strain states are of interest for the development of 3D strut-and-tie models:

(i) $\varepsilon_1 < 0, \varepsilon_2 < 0, \varepsilon_3 < 0$ (fully-confined state, C-C-C). 7-5

(ii) $\varepsilon_1 > 0, \varepsilon_2 < 0, \varepsilon_3 < 0$ (confined-cracked state, T-C-C). 7-6

(iii) $\varepsilon_1 > 0, \varepsilon_2 > 0, \varepsilon_3 < 0$ (cracked state, T-T-C). 7-7

Neglecting the concrete strength increment under confined states is a conservative, common practice in 2D. However, the extension of this principle to three-dimensionally confined states (C-C-C) can lead to excessively conservative results, as the presence of lateral stresses significantly increases the concrete strength (up to 4.1 times the magnitude of the lateral stresses according to some models). Different 3D concrete failure surfaces have been proposed in the literature which could be potentially considered[7-24], [7-25], [7-26], but the application of these formulae to strut-and-tie models needs to be explored further. In the absence of more precise data, MC2010 proposes the following strength increment for tri-axially compressed nodes with $\sigma_2 = \sigma_3$:

$$\frac{f_{ck,c}}{f_{ck}} = 1 + 3.5\left(\frac{\sigma_2}{f_{ck}}\right)^{3/4} \qquad 7\text{-}8$$

Some compression softening models for cases in which the compression field is subjected to transverse tension are presented in section 2.3.1 for 2D applications (T-C). A compressive or tensile intermediate principal strain (ε_2) will increase or reduce, respectively, the strength determined for a biaxial tension-compression, but quantification of this effect is difficult. Testing concrete specimens under tri-axial compression-tension states (T-C-C, T-T-C) has technical difficulties, especially for unreinforced concrete. Without specific 3D models, those proposed for 2D can be extended considering the following: (i) when $\varepsilon_2 < 0$ (T-C-C), the contribution of compressive stresses in the second principal direction can be neglected conservatively and (ii) when $\varepsilon_2 > 0$ the transverse tensile strain can be taken equal to $\varepsilon_1 + \varepsilon_2$ assuming they contribute equally to concrete softening[7-27]. This extension has at least two potential weaknesses: (i) as already noted in section 2.3.1, all compression softening relationships for 2D have been developed using data from biaxial experimental results and employing hypotheses which may not be applicable to 3D; and (ii) they were derived from tests on reinforced concrete panels; in 3D the existence of unreinforced compressive zones is common and the response of unreinforced concrete under tensile strain states can be very different. Therefore, further research is needed to better estimate concrete strength under tri-axial tension-compression states.

7.2.2.2.2 Determination of strut dimensions and nodal zones

Strut dimensions and nodal zones are generally determined considering: (i) restraining surfaces imposed by support devices, loading plates and reinforcement arrangement and, (ii) the truss geometry.

In 2D, strut dimensions are obtained by projecting the restraining surfaces onto planes perpendicular to the truss elements. For a planar truss model and for elements of constant

This document is the intellectual property of the fib – International Federation for Structural Concrete. All rights reserved.
This PDF of fib Bulletin 100 is intended for use and/or distribution solely within fib National Member Groups.

thickness, projected areas are of rectangular shape and, hence, the geometry of the strut is relatively simple. The same approach can be applied in 3D, but it must be considered that the geometrical shapes change (e.g. the projection of a circle is an ellipse and of a square a rhombus). For instance, in a pile cap foundation with circular piles of diameter ϕ_p and reinforcement cover c_b, the area of an inclined strut of angle θ_s^{3d} can be calculated as:

$$A_s = \pi/4\left(\phi_p \sin\theta_s^{3d} + 2c_b \cos\theta_s^{3d}\right)\phi_p \qquad 7\text{-}9$$

if it is assumed that the resultant of the tie forces at the reinforcement is aligned with the horizontal force component of the strut, which will always be the case if the horizontal reaction at the pile is assumed to be zero.

In 2D, nodal zones are defined to facilitate the calculation of the stress field inside the area. This generally leads to splitting nodal areas into triangles inside which the stress is constant and with stress continuity maintained at the boundaries. The stress check is then undertaken in principal stress components, i.e. without considering shear stresses. In 3D the definition of nodal zones generally involves non-planar surfaces on which the evaluation of stresses becomes complex. Application of the 2D approach to 3D would require splitting nodal volumes into constant stress tetrahedrons (equivalent geometry to triangle in 2D), which cannot be managed without resorting to computer methods. Alternatively, 3D nodal zones can be checked by taking a principal plane containing the line of action of the strut and applying the 2D methodology to this plane. However, this method can lead to excessively conservative results. This is shown through a simple nodal zone formed by the intersection of a vertical and an inclined strut of known areas and a horizontal tie (see Fig. 7-14). If $\tan\theta_s^{3d} \leq \phi_p \cdot a/2 \cdot c_b$, the maximum compressive stress in the 2D plane is σ_H, which can be calculated from the vertical stress σ_V and the normal and tangent stress components of the inclined strut σ, τ. If the nodal zone is treated as a 2D entity, any plane parallel to the direction of the inclined strut is under the same stress field. This implies that outside the central plane there are horizontal stresses acting in both directions which partially counteract themselves. As a result of the latter, in this example the calculated horizontal stress σ_H is 50% larger than the one that would have been obtained considering the horizontal component of the strut force and the projected area of the nodal zone ($0.75 c_b \pi \phi_p$).

This document is the intellectual property of the fib – International Federation for Structural Concrete. All rights reserved.
This PDF of fib Bulletin 100 is intended for use and/or distribution solely within fib National Member Groups.

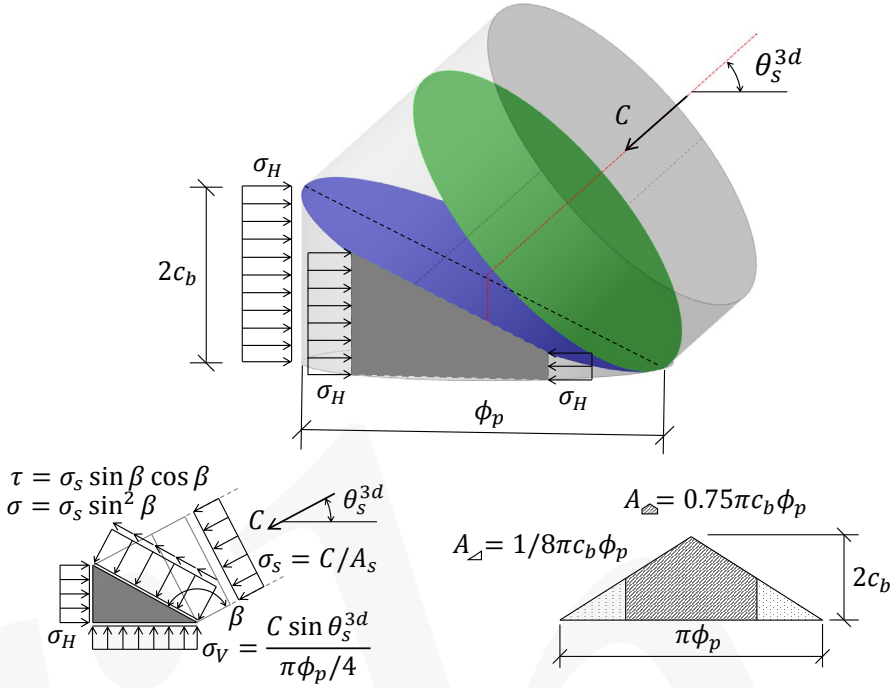
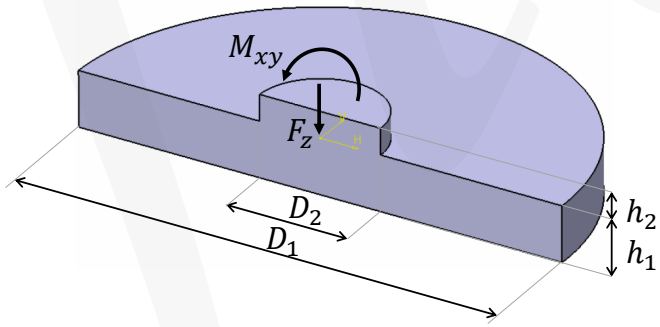


Fig. 7-14 Treatment of 3D nodal zone in plane stress.

7.2.3 Example of application of 3D strut-and-tie models: foundation of a wind tower turbine

The following example shows some of the benefits and difficulties of considering a 3D vs. a 2D strut-and-tie model. The foundation of a wind turbine tower has been chosen for this purpose. Different design configurations exist in practice; a solution formed by a circular slab (D_1) of constant depth (h_1) and pedestal (D_2 and h_2) in which the tower forces are transferred through a ring formed by vertical anchor bolts will be considered (see Fig. 7-15).



F_Z = 2'500 kN
M_{xy} = 80'000kNm
D_1 = 16 m, h_1 = 1.8 m
D_2 = 4 m, h_2 = 1.2 m
$\rho_{concrete} = \rho_{soil}$ = 25 kN/m^3

Fig. 7-15 Example of wind tower turbine foundation.

This document is the intellectual property of the fib – International Federation for Structural Concrete. All rights reserved.
This PDF of fib Bulletin 100 is intended for use and/or distribution solely within fib National Member Groups.

Fig. 7-16 shows a conceptual 2D strut-and-tie model that could be used for the analysis and design of the element. Two regions are distinguished: (i) one without contact to the ground (on the right of the image) and, (ii) one under compression (left side of the image). Two horizontal ties crossing the centre of the pedestal are needed for the equilibrium of forces, which in the 3D space represent the radial reinforcement. Crossing of multiple radial reinforcing bars necessarily leads to a congested reinforcement area at the centre of the pedestal. In order to reduce reinforcement density and avoid constructability problems, a discontinuity in radial reinforcement is desirable; but according to the 2D strut-and-tie model, continuity of the reinforcing bars is needed for the equilibrium of forces. A 3D strut-and-tie model can justify that the discontinuity in radial reinforcement is consistent with a rational flow of forces and, hence, be admissible.

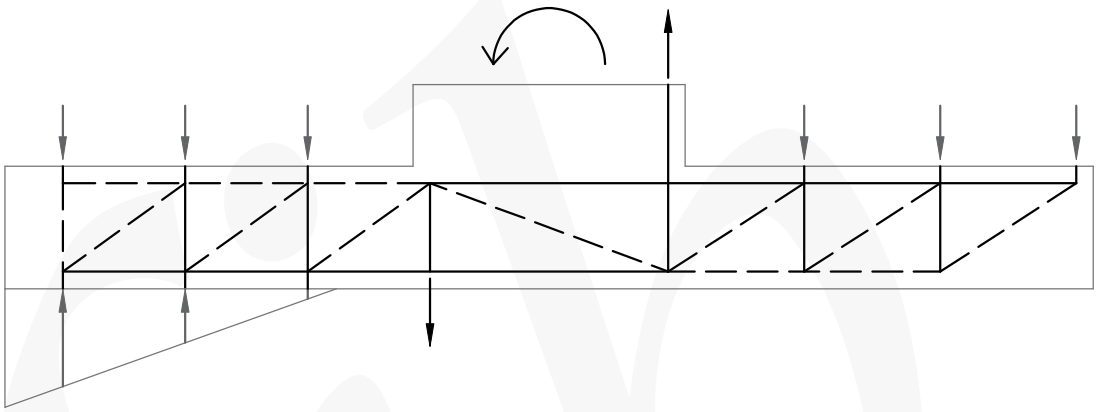


Fig. 7-16 2D strut-and-tie model for wind tower turbine foundation

To facilitate the development of the 3D model it is proposed to subdivide first the foundation into circular sectors θ_i - θ_j and radial segments R_i - R_j (see Fig. 7-17a). Only half of the foundation will be considered for clarity reasons. The acting loads can be transformed into equivalent concentrated forces considering this subdivision; three actions are distinguished: (i) the tower forces (F_z and M_{xy}), (ii) the weight of the foundation and the backfill soil, and (iii) the ground reaction.

Regarding the tower forces, the set of vertical loads $F_{v_i}^{\theta_i - \theta_j}$ and their position $S_{F_{v_i}}^{\theta_i - \theta_j}$ can be determined by integrating the force distribution $q_{M_{xy}}$ and q_{F_Z} along the ring as (see Fig. 7-17b):

$$F_{v_i}^{\theta_i-\theta_j} = \int_{\theta_i}^{\theta_j}\left(q_{M_{xy}} + q_{F_Z}\right)R\,d\alpha = \int_{\theta_i}^{\theta_j}\left(\frac{M_{xy}\cos\alpha}{\pi R^2} + \frac{F_z}{2\pi R}\right)R\,d\alpha = \frac{M_{xy}\left(\sin\theta_j - \sin\theta_i\right)}{\pi R} + \frac{F_z\left(\theta_j - \theta_i\right)}{2\pi} \qquad 7\text{-}10$$

$$s_{F_{v_i}}^{\theta_i-\theta_j} = \frac{\int_{\theta_i}^{\theta_j}\left(q_{M_{xy}} + q_{F_Z}\right)R^2\cdot\alpha\cdot d\alpha}{F_{v_i}^{\theta_i-\theta_j}} = \frac{M_{xy}\left(\theta_j\sin\theta_j + \cos\theta_j - \theta_i\sin\theta_i - \cos\theta_i\right)\Big/\pi + F_z\cdot R\left(\theta_j^2 - \theta_i^2\right)\Big/4\pi}{F_{v_i}^{\theta_i-\theta_j}} \qquad 7\text{-}11$$

This document is the intellectual property of the fib – International Federation for Structural Concrete. All rights reserved.
This PDF of fib Bulletin 100 is intended for use and/or distribution solely within fib National Member Groups.

Regarding the foundation and backfill soil weight, concentrated forces can be directly calculated from the material densities ($\rho_{concrete}$, ρ_{soil}), the element depths (h_1, h_2) and the area of each circular portion $A_{R_i-R_j}^{\theta_i-\theta_j}$, which can be calculated as:

$$A_{R_i-R_j}^{\theta_i-\theta_j} = \left(R_j^2 - R_i^2\right)\left(\theta_j - \theta_i\right)/2 \qquad 7\text{-}12$$

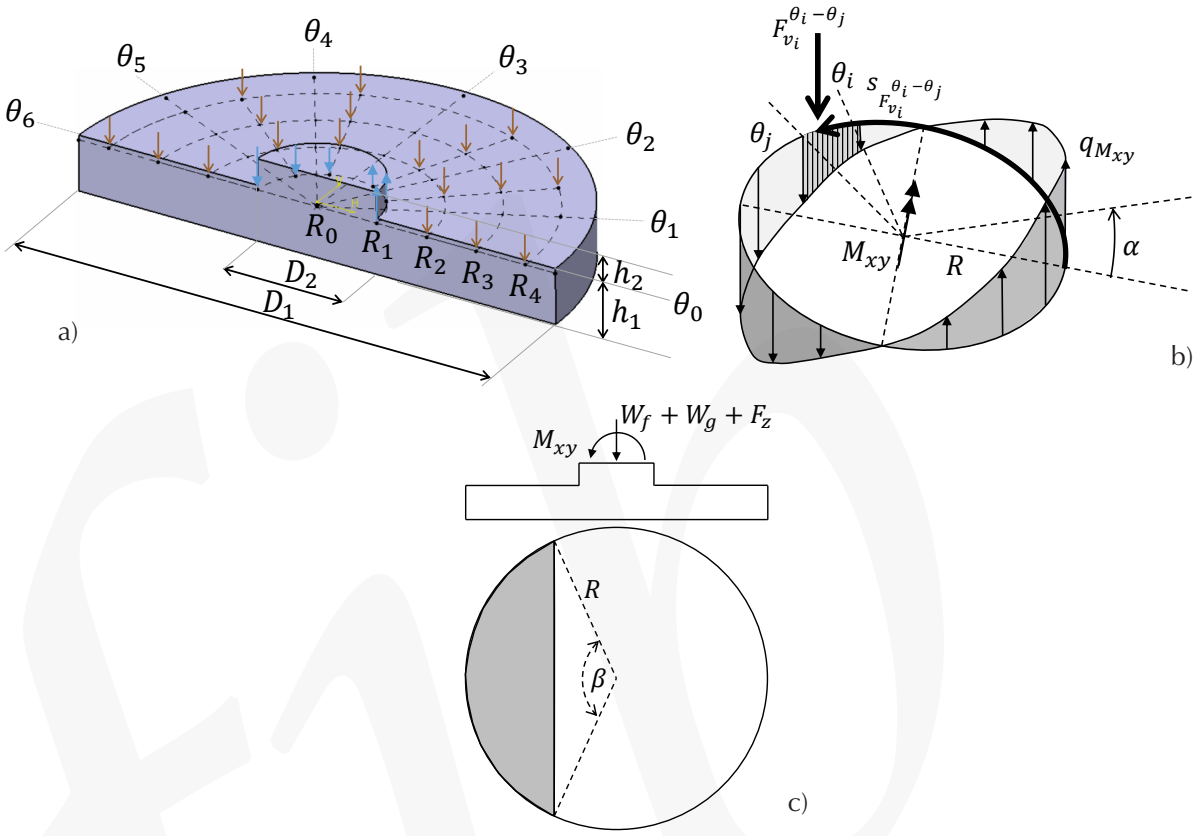


Fig. 7-17 Modelling of tower foundation: (a) Sectors and segments; (b) Integration of ring forces; (c) Ground reaction.

Regarding the ground reaction, a preliminary analysis can be undertaken to estimate the foundation area that will be in contact with the ground, which will be useful for the initial definition of the boundary conditions. For simplicity it can be assumed that the soil pressure is uniform, and the loaded area (see Fig. 7-17c) can be determined by solving the equation:

$$e = \frac{M}{\left(W_f + W_s + F_Z\right)} = \frac{4R\sin^3\frac{\beta}{2}}{3\left(\beta - \sin\beta\right)} \qquad 7\text{-}13$$

where e is the load eccentricity at the foundation base measured from its centre.

The subdivisions adopted (θ_i, R_j) determine the geometry of the 3D strut-and-tie model, as nodes need to be defined at the location of the concentrated loads. Six sectors θ_i (0º, 26º, 58º, 90º, 122º, 154º, 180º) and four segments in the radial direction R_j (0, 2.8, 4.5, 6.2, 8.0 m) have been adopted in this example; St. Venant's principle, which states that

This document is the intellectual property of the fib – International Federation for Structural Concrete. All rights reserved.
This PDF of fib Bulletin 100 is intended for use and/or distribution solely within fib National Member Groups.

the length of the dispersion zone is approximately equal to the depth of the element has been considered in the definition of these subdivisions. The obtained concentrated forces are shown in Table 7-2. For simplicity loads due to the foundation and backfill soil weight and ground reaction have been defined at mid distance of the radial segments R_i - R_j following the radial direction from the points of application of the tower forces.

Table 7-2 Equivalent concentrated forces for wind tower foundation example.

F_z(kN)		Ring	R_i - R_j (m)			
		R = 2	[0-2.8]	[2.8-4.5]	[4.5-6.2]	[6.2-8]
θ_i - θ_j	[0º-26º]	5'360	-103	-157	-228	-333
	[26º-58º]	5'024	-128	-195	-284	-415
	[58º-90º]	1'725	-128	-195	-284	-415
	[90º-122º]	-2'170	-128	-195	-284	-415
	[122º-154º]	-5'470	-128	-195	-284	-415
	[154º-180º]	-5'717	-103	-157	-228	-333
Action		$M_{xy} + F_z$	$(\rho_{concrete} + \rho_{soil})A_{ij}$			

Once the equivalent concentrated forces and their location are known, a truss model can be developed. More than one truss may be admissible. Two models are proposed here: (i) one in which radial reinforcement goes through the centre of the pedestal (model A, Fig. 7-18a) and (ii) one in which it does not (model B, Fig. 7-18b). Both truss models are hyperstatic, which implies that the magnitude of the forces at the elements depend on their relative stiffness. This is a common characteristic of many 3D strut-and-tie models because there is generally more than one admissible load path in the 3D space (in this example loads can be transferred in the radial and circumferential direction). In this case, and for simplicity reasons, it has been assumed that the area of all elements is the same and, hence, the stiffness of each element is inversely proportional to its length ($E \cdot A/L$). Alternatively, the 3D strut-and-tie model can be split into two isostatic models (one for each load path), distribute the load between the two models, and then obtain the truss forces by superposition. In this case the uncertainty is the estimation of the total load percentage which is carried by each system, which should be a function of its relative stiffness.

Once the system is solved, the model may be refined considering the obtained truss forces (change orientation of inclined struts, modify boundary conditions if inconsistent reactions are obtained, add additional elements…). The experience of the practitioner plays an important role in this process.

An in-depth description of the obtained results for model A and B would be extensive and is not the purpose of this example. Some aspects will be noted here to highlight the capability of a 3D strut-and-tie model to simulate the behaviour of such a complex element:

- In the radial direction the bending moment in models A and B is negative on the cantilever side and positive on the supported side, and they both increase towards the centre of the foundation. These results are consistent with the expected behaviour. It must be noted that at the very tip of the cantilever the bending moment is slightly positive due to the forces transferred by the outside circumferential elements.
- In the circumferential direction the bending moment for both models is negative on the cantilever side, reducing towards the supported side and becoming positive at an angle of around 45-50º. At the sections closer to the centre of the pedestal

This document is the intellectual property of the fib – International Federation for Structural Concrete. All rights reserved.
This PDF of fib Bulletin 100 is intended for use and/or distribution solely within fib National Member Groups.

(R = 2 m, R = 3.7 m), the circumferential moment is approximately constant around 0º and 180º. These results are consistent with those obtained from a 2D finite element model where the foundation is modelled with shell elements of thickness equal to the foundation depth. This type of 2D models are frequently used in practice, where sectional forces and moments determine the required reinforcement quantities.

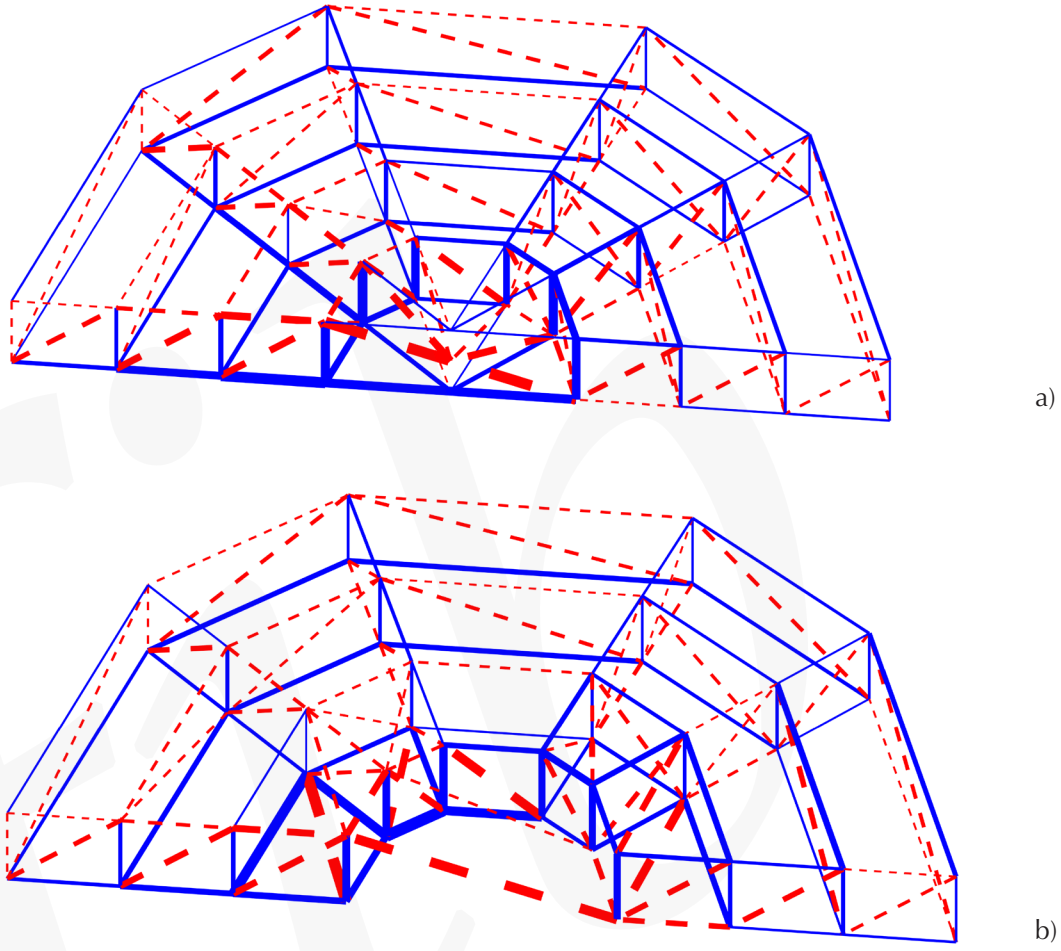


Fig. 7-18 3D strut-and-tie model for wind tower turbine: (a) Model A; (b) Model B.

Considering the obtained tie forces and a design yielding stress of steel equal to 400 MPa, the following reinforcement quantities are obtained:

- Radial direction, upper side: the total area of radial reinforcement for models A and B is 704 cm² and 1'030 cm², respectively. This area is determined by the tie forces acting outwards; the maximum tie force per unit length for model A requires 56 cm²/m of steel reinforcement while 82 cm²/m is the quantity required for model B. Towards the external perimeter of the foundation tie forces decrease and hence so does the required reinforcement area; nevertheless, radial reinforcement is generally extended up to the external perimeter. For model A with ties passing through the centre, the required reinforcement quantity inside the pedestal is approximately 10 cm²/m (total area 126 cm²), implying that it is not necessary that every radial reinforcing bar passes through the centre of the pedestal.

This document is the intellectual property of the fib – International Federation for Structural Concrete. All rights reserved.
This PDF of fib Bulletin 100 is intended for use and/or distribution solely within fib National Member Groups.

- Radial direction, lower side: 195 cm^2/m (total area 2'450 cm^2) for model A and 162 cm^2/m (total area 2'036 cm^2) for model B. These values are given by the forces at the ties over the compression side of the foundation, where point supports are considered in the model. A more accurate estimation of the required reinforcement can be obtained, provided that the reaction forces obtained are distributed in the radial direction for each sector and the bending moment diagram is determined afterwards.
- Circumferential direction, upper side: varies between 20-41 cm^2/m for model A and 40-64 cm^2/m for model B (lowest and largest reinforcement quantity required near the outside perimeter and around the pedestal ring, respectively).
- Circumferential direction, lower side: varies between: 27-32 cm^2/m for model A and 45-120 cm^2/m for model B (lowest and largest reinforcement quantity required near the outside perimeter and around the pedestal ring, respectively).
- Vertical direction, around the ring: 160 cm^2/m for both model A and B, leading to a total area 2010 cm^2. This reinforcement quantity determines the shear reinforcement at the pedestal.
- Vertical direction, foundation area outside the pedestal: is below 24 cm^2/m^2 in model A and below 25 cm^2/m^2 for model B. Near the outside perimeter the required reinforcement quantity is significantly lower than at the sections near the pedestal.

This example shows the potential of 3D strut-and-tie models to provide a better understanding of the behaviour of complex, reinforced concrete elements. Implications are noted of required reinforcement quantities with crossing or non–crossing radial reinforcement. However, difficulties must be acknowledged, such as the development of the 3D truss, the capacity check of nodal zones and the interpretation of results; this last point entails understanding of the flow of forces and is critical in reducing the likelihood of mistakes. The problem can become cumbersome when several load cases are considered. Computer models applying the simplified principles of the strut-and-tie and the stress field methods can be a promising alternative, as shown in the next section.

7.2.4 3D stress field models

The Elastic-Plastic Stress Field method proposed and implemented in a 2D FE environment by Fernández Ruiz and Muttoni[7-28] and introduced in Section 5.2 has shown the benefits of balancing the accuracy and adaptability of FE models with the simplicity of constitute models based on traditional engineering practice such as plasticity theory. Meléndez et al.[7-29] extended this approach to 3D in the tool FESCA 3D (Finite Elements for Simplified Concrete Analysis in 3D). Some of the main difficulties mentioned above in relation to 3D strut-and-tie models can be overcome with this simplified finite element-based approach. Regarding the capacity check of struts and nodal zones, finite elements allow assessment of the concrete stress at any integration point, which can then be compared against the maximum allowable value. Moreover, finite elements also allow for a better representation of the boundary conditions. Regarding the development of a 3D geometry, the assumption of neglecting the tensile strength of concrete and the use of traditional nonlinear resolution methods can lead to the automatic generation of clear 3D stress fields within a few iterations.

This document is the intellectual property of the fib – International Federation for Structural Concrete. All rights reserved.
This PDF of fib Bulletin 100 is intended for use and/or distribution solely within fib National Member Groups.

This section briefly describes the characteristics of FESCA 3D and some of its capabilities; a more detailed description of the tool can be found in Meléndez[7-30].

7.2.4.1 Concrete modelling

Concrete modelling in 3D can become very complex and parameter sensitive and requires a high level of expertise for model definition and interpretation of results. The concrete model proposed in FESCA 3D is a simplified one, where only one single input variable, the uniaxial compressive strength f_c, needs to be defined. A 3D orthotropic constitutive model is adopted, which permits decoupling of the 3D response into three quasi-independent uniaxial directions (see Fig. 7-19a). Material axes of orthotropy are defined through principal strain directions and rotate with them. The tangent shear modulus G_{ij} is determined to enforce coaxiality between principal strain and stress direction.

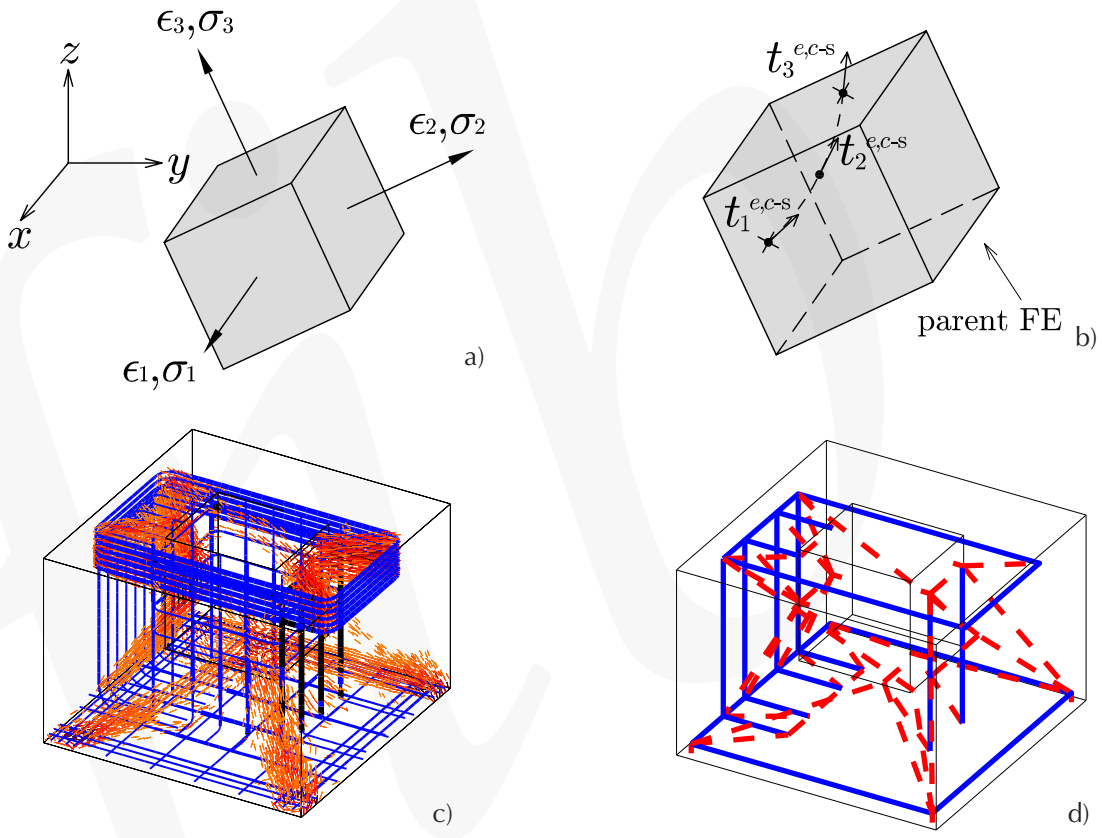


Fig. 7-19 FESCA 3D:(a) Orthotropic concrete model; (b) Embedded rebar model; (c) 3D stress field model; and (d) Strut-and-tie model

This document is the intellectual property of the fib – International Federation for Structural Concrete. All rights reserved.
This PDF of fib Bulletin 100 is intended for use and/or distribution solely within fib National Member Groups.

Interaction between principal directions is accounted for by considering the effect of transverse strains/stresses on the effective strength of concrete f_{ce}. For compression-compression interaction a Drucker-Prager yield surface is considered; for tension-compression interaction the proposed reduction factor is based on the Modified Compression Field Theory by Vecchio and Collins[7-31]:

$$\frac{f_{ce}}{f_{cp}} = \frac{1}{0.8+170\left(\varepsilon_1+\varepsilon_2\right)} \text{ if } \varepsilon_2 > 0 \qquad 7\text{-}14$$

$$\frac{f_{ce}}{f_{cp}} = \frac{1}{0.8+170\varepsilon_1} \text{ if } \varepsilon_2 < 0 \qquad 7\text{-}15$$

FESCA 3D allows the tensile strength of concrete to be neglected following the principles of the strut-and-tie and stress field methods (see Chapter 2). This assumption can lead to excessively conservative results for massive, lightly reinforced concrete elements. For more accurate results the user can define a tensile constitutive law to account for concrete contribution in tension. Meléndez[7-30] used the softening law proposed by Hordijk[7-32] in several practical applications, obtaining sound predictions.

7.2.4.2 Reinforcement modelling

Reinforcement definition in a 3D element can be tedious, unless a flexible approach is implemented. The discrete representation requires that reinforcement and concrete nodes are coincident. This may not be a very limiting factor in 2D because the mesh can be adapted to the reinforcing bar arrangement without much disturbance, but in 3D can lead to non-optimal meshes. The embedded approach permits definition of steel bars independently from the concrete mesh without adding additional nodes, using the concept of concrete parent element (Fig. 7-19b). This approach was implemented into FESCA 3D together with an algorithm which permits automatic generation of bar FEs from the intersection of the reinforcing bars and the concrete mesh.

7.2.4.3 Definition of boundary conditions

Boundary conditions due to loads and supports generally affect the stress field in the vicinity of the boundary surfaces, but, in the case of D-regions, the stress field inside the entire element and, hence its response, is also influenced. Therefore, the definition of the boundary conditions must be done with care when modelling D-regions. FESCA 3D incorporates special elements to consider the effect of loading and support devices in a simplified manner. These elements are based on the principles of finite element modelling and static condensation.

7.2.4.4 Automatic generation of 3D stress field models

The assumption of neglecting the tensile strength of concrete together with the use of the Newton-Raphson nonlinear solution algorithm leads to the automatic generation of 3D stress fields. The iterative process starts from the elastic solution. Residual forces appear at concrete elements under tension inducing the rotation of the principal directions. The concrete stress field is refined during each iteration until the residual forces vanish. A clear and consistent 3D stress field is generated after only a few iterations, from which the flow of forces can be identified. Fig. 7-19c shows the 3D stress field obtained for a socket-

This document is the intellectual property of the fib – International Federation for Structural Concrete. All rights reserved.
This PDF of fib Bulletin 100 is intended for use and/or distribution solely within fib National Member Groups.

based column-to-foundation connection subjected to a vertical load and a pair of opposite horizontal forces. The 3D strut-and-tie model associated with this reinforcement arrangement, which can be easily derived from the obtained stress field, is shown in Fig. 7-19d.

7.2.5 Design example of a four-pile cap

The Levels-of-Approximation (LoA) approach described in Chapter 3 is applied in this section for the design and assessment of a 3D D-region. Consider the four-pile cap foundation subjected to a central column load shown in Fig. 7-20. All checks and calculations will be based on *fib* Model Code for Concrete Structures 2010 (MC2010)[7-3] provisions.

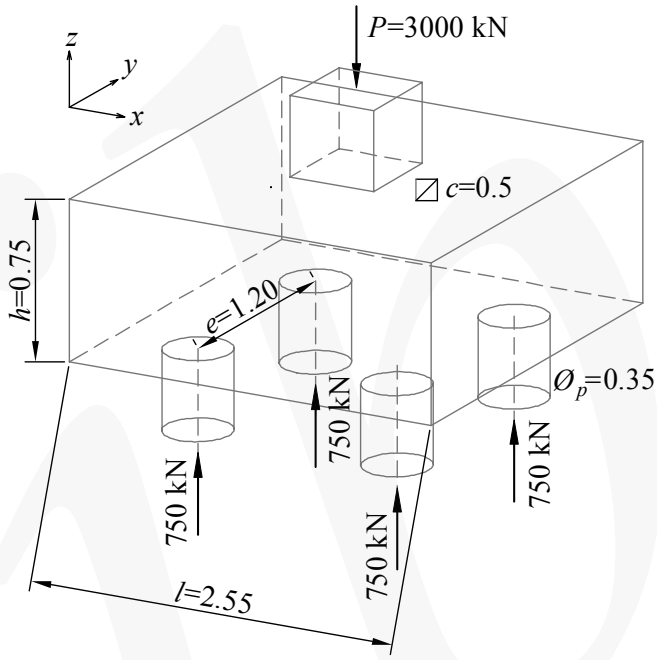


Fig. 7-20 Design example of a four-pile cap.

7.2.5.1 LoA I

Step 1: Define a simple strut-and-tie model to calculate location and area of the main reinforcement.

Two different truss geometries are proposed here to show the relevance of the adopted model: (i) in model A the column load is modelled by a single point force acting at the centre of the column; this option neglects the influence of the column dimensions (see Fig. 7-21a); (ii) in model B the column load is subdivided into four-point forces giving four upper nodes at the column quarter points (see Fig. 7-21b). In both cases the model is formed by four inclined struts that transfer the vertical load from the column to the piles and four horizontal ties which withstand the horizontal force components of the struts. The four lower nodes are fixed at the centre of the piles at the reinforcement level as is the general practice. The height of the upper nodes can be estimated from sectional analysis at the centre of the cap assuming the compressive block concentrates below the column, with z_n being the depth of the rectangular compressive block and c_b the cover of reinforcement (see Fig. 7-22).

This document is the intellectual property of the fib – International Federation for Structural Concrete. All rights reserved.
This PDF of fib Bulletin 100 is intended for use and/or distribution solely within fib National Member Groups.

Once the geometry of the model is defined, the forces at the struts and ties can be determined from equilibrium. These forces can be expressed as a function of the strut inclination θ_s^{3d} as follows:

$$F_c = \frac{P}{4\sin\theta_s^{3d}}, F_{t,x} = \frac{P\cos\varphi}{4\tan\theta_s^{3d}}, F_{t,y} = \frac{P\sin\varphi}{4\tan\theta_s^{3d}} \qquad 7\text{-}16$$

Note that in this case the reaction at the four piles is the same because the column only transfers a vertical load and this is centred. Pile reactions would not be equal if a bending moment is applied by the column or for eccentric vertical loads. In the latter case, reaction forces can be determined from static equilibrium assuming planar distribution. If the bending moment/load eccentricity is such that induces tensile stresses at the column base, a vertical tie should be considered in the strut-and-tie model to transfer the tensile stresses.

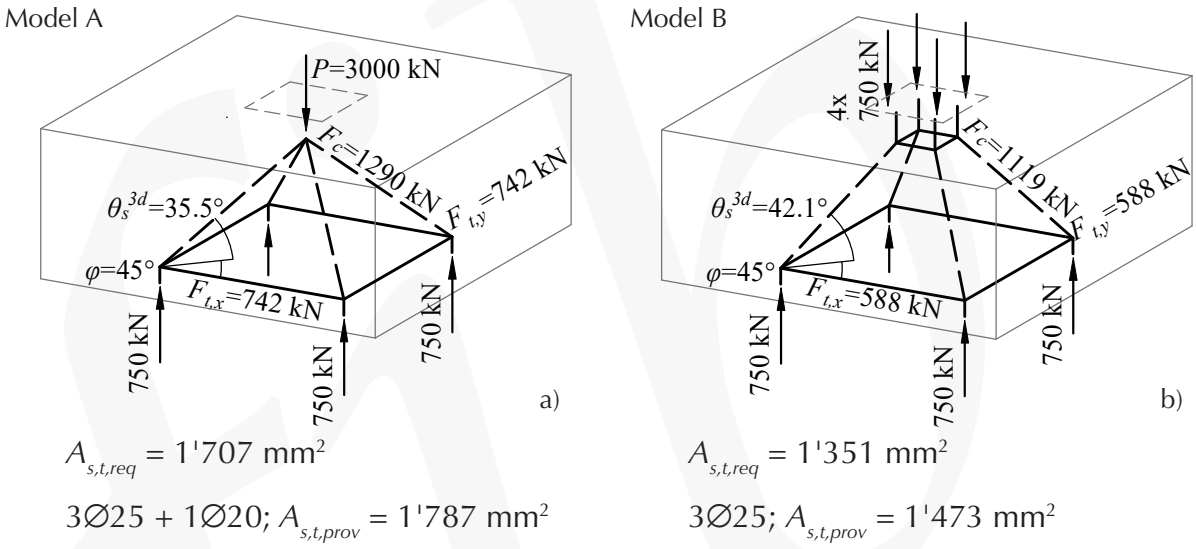


Fig. 7-21 Truss model for four-pile cap (Step 1, LoA I): (a) Model A, (b) Model B.

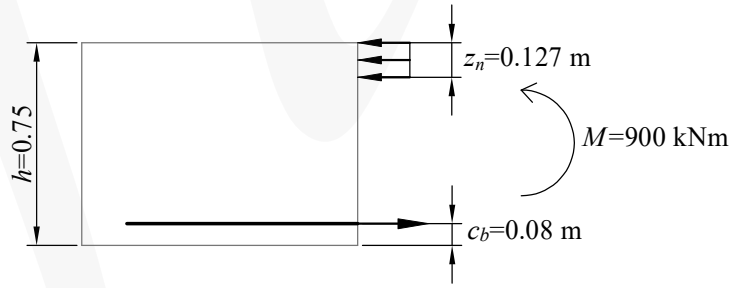


Fig. 7-22 Sectional analysis at central section of four-pile cap.

Step 2: Check diagonal compression field, nodal stresses and anchorage length of the bars.

The dimensions of the top section of the strut can be calculated by projecting one quarter of the column surface onto a plane perpendicular to the strut, giving the following expression for a square column:

$$A_{c,top} = \frac{1}{2}\alpha_2\frac{c\sqrt{2}}{2} = \frac{1}{2}\left(\frac{c\sqrt{2}}{2}\sin\theta_s^{3d} + z_n\cos\theta_s^{3d}\right)\frac{c\sqrt{2}}{2} \qquad 7\text{-}17$$

This document is the intellectual property of the fib – International Federation for Structural Concrete. All rights reserved.
This PDF of fib Bulletin 100 is intended for use and/or distribution solely within fib National Member Groups.

where c is the dimension of the square column and a_2 the strut width at the top section (see Fig. 7-23).

The dimensions of the bottom section of the strut can be obtained similarly by projecting the pile section onto a plane perpendicular to the strut. For circular piles of diameter ϕ_p this area can be calculated as:

$$A_{c,bot} = \frac{\pi}{4} a_3 \cdot \phi_p = \frac{\pi}{4}\left(\phi_p \sin\theta_s^{3d} + 2c_b \cos\theta_s^{3d}\right)\phi_p \qquad 7\text{-}18$$

where ϕ_p is the diameter of the pile and a_3 the strut width at the bottom section (see Fig. 7-23).

At the top section of the strut the increment in strength due to multiaxial compression can be considered. The formulation proposed for biaxial compression in MC2010 can be adopted conservatively ($\sigma_{c,Rd} = 1.1(30/f_{ck})^{1/3} f_{cd} = 24.4$ MPa). Stresses obtained from both model A and B fulfil this limit. At the bottom section the concrete strength needs to be reduced to account for the tensile stress field ($\sigma_{c,Rd} = 0.55(30/f_{ck})^{1/3} f_{cd} = 12.2$ MPa). The stress resulting from model A exceeds this limit, so had this model been considered, the design should be modified (by increasing the cap height, the concrete strength or the concrete cover, for instance).

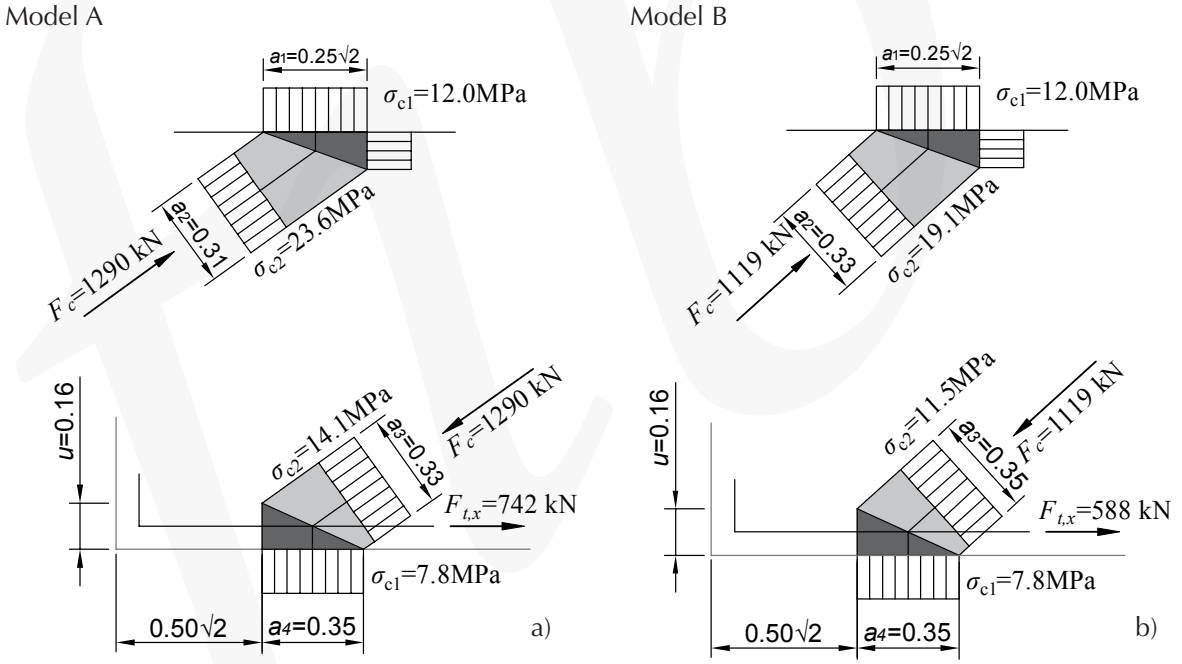


Fig. 7-23 Check of compressive field and nodal zones for four-pile cap (Step 2, LoA I): (a) Model A, (b) Model B.

Regarding the stress field at bottom nodal region, the maximum compressive stress can be determined as:

$$\sigma_{c,\max} = \frac{\sigma_{c2} \cos^2 \theta_s^{3d}}{1 - \sigma_{c2} \sin^2 \theta_s^{3d} / \sigma_{c1}} \qquad 7\text{-}19$$

Note that the principal compressive stress direction in the nodal region does not necessarily have to be aligned with the vertical or horizontal direction

This document is the intellectual property of the fib – International Federation for Structural Concrete. All rights reserved.
This PDF of fib Bulletin 100 is intended for use and/or distribution solely within fib National Member Groups.

and, therefore, the maximum compressive stress can be larger than σ_{c1} and σ_{c2}. The equation above results in a stress equal to 18.9 MPa in model B, which exceeds the strength of compression-tension nodes according to MC2010 ($\sigma_{c,Rd} = 0.75(30/f_{ck})^{1/3} f_{cd}$ = 16.6 MPa). As noted in Section 7.2.3, this approach of treating 3D nodal zones as 2D planes can lead to excessively conservative results. However this limitation can be overcome if it assumed that the reinforcing bars are anchored behind the node so that a state of pure compression exists in the node. To fulfil this, it must be checked that there is sufficient anchorage length behind the node. The minimum length required to anchor the reinforcing bars can be determined from:

$$F_t = n_{bars} \pi \phi \cdot l \cdot f_{bd} \qquad 7\text{-}20$$

According to MC2010, for ϕ20 with a concrete cover of 80 mm, f_{bd} = 2.76 MPa. The force that can be developed by 3ϕ25 in 0.42 m (available space behind the piles) is 390.2 kN. The tensile force calculated at the ties is almost two times larger than this value (742 kN). In order to fulfil the anchorage requirement, the arranged reinforcement should be increased to 6ϕ25. Had the nodal zone check being fulfilled, the available anchorage length would have been 0.77 m (0.35+0.42), the bond strength f_{bd} over the piles could have been increased to 5.92 MPa and the available anchorage length would have been sufficient to develop the tie force:

$$\sum F_b = 3 \cdot \pi \cdot 25 \left(350 \cdot 5.92 + 420 \cdot 2.76\right) = 761 \text{ kN} > 742 \text{ kN} = F_t$$

Step 3: Provide minimum reinforcement for the region.

The minimum reinforcement for crack control can be calculated as follows:

$$A_{s,\min} = k \cdot f_{ctm} A_{ct} \big/ f_{yd} \qquad 7\text{-}21$$

where k is a coefficient which allows for the effect of non-uniform self-equilibrating stresses, f_{ctm} is the average value of the tensile strength of concrete, A_{ct} the area of the concrete within the tensile force.

In this case the total arranged reinforcement (12ϕ25) is larger than the minimum required (A_{sT} = 5'890 > 2'571 = $A_{s,\min}$), but if this reinforcement is only arranged over the piles as inferred from the strut-and-tie model, the central part of the cap would stay unreinforced. For cracking control, it is advisable to arrange additional rebars at these areas fulfilling the required minimum reinforcement (958 mm^2/m).

This document is the intellectual property of the fib – International Federation for Structural Concrete. All rights reserved.
This PDF of fib Bulletin 100 is intended for use and/or distribution solely within fib National Member Groups.

$A_{s,\min} = k \cdot f_{ctm} \cdot A_{ct} / f_{yd}$
$k = 0.65 + 0.35/0.5 \cdot (0.8 - h) = 0.685$
$f_{ctm} = 3.2$ MPa
$A_{ct} = l \cdot h_{c,ef}$
$l = 2.55$
$h_{c,ef} = \min(2.5 \cdot r_c, (h - x)/3)$
$f_{yd} = 434.8$ MPa
$A_{s,\min} = 2'571$ mm^2

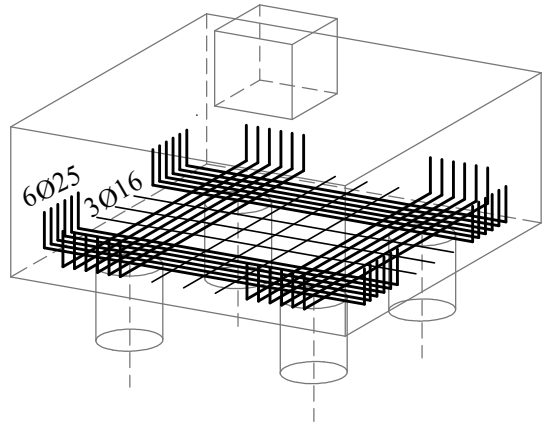


Fig. 7-24 Proposed reinforcement arrangement for four-pile cap (Step 3, LoA I).

7.2.5.2 LoA II

Step 1: Define the strut-and-tie model and include the necessary and relevant refinements within the model.

The use of more refined models derived from iteration of the truss geometry can lead to more accurate results. This approach was applied by Meléndez et al.[7-27] for the analysis and design of four-pile caps. In their model the strut inclination is not fixed from the geometry but determined by maximising the pile cap strength considering different failure conditions: (i) exceeding the reinforcement capacity, (ii) crushing of the diagonal strut at the base of the column and (iii) splitting of the strut due to transverse cracking. This refined model accounts for strain compatibility, reduction of the compressive strength for cracked concrete and reinforcement configuration (distribution and anchorage conditions).

For design, the strut angle maximising the strength of the pile cap is determined by limiting the force in the strut to its capacity at the top section at the intersection between the pile cap and the column, giving the following expression:

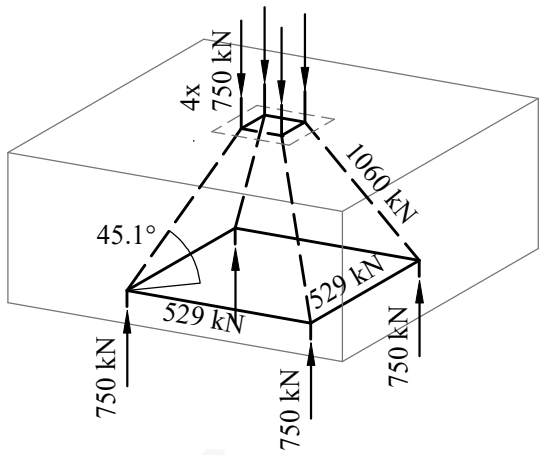
$$\cot\theta_s^{3d} = \frac{\lambda + \sqrt{\nu_u\left(1+\lambda^2\right) - \nu_u^2}}{1-\nu_u} \qquad 7\text{-}22$$

$$\lambda = \sqrt{2}\frac{e-c}{d}, \nu_u = \frac{P}{9f_{cp}} \qquad 7\text{-}23$$

where f_{cp} is the plastic strength of concrete ($f_{cp} = f_{cd}$ if $f_{cd} \leq 20$ MPa; $f_{cp} = 2.7 f_{cd}^{2/3}$ if $f_{cd} \geq 20$ MPa according to Muttoni et al.[7-21]).

Once the geometry of the strut-and-tie model is defined, forces at the truss elements and the required reinforcement can be determined from equilibrium as in LoA I.

This document is the intellectual property of the fib – International Federation for Structural Concrete. All rights reserved.
This PDF of fib Bulletin 100 is intended for use and/or distribution solely within fib National Member Groups.



$A_{s,t,req}$ = 1'217 mm²
4∅20; $A_{s,t,prov}$ = 1'257 mm²

Fig. 7-25 Truss model for four-pile cap (Step 1, LoA II).

Step 2: Check the compressive members of the element that may be critical.

According to Meléndez et al.[7-27], the maximum column load may be limited by splitting of the diagonal strut at the bottom section. The equation to determine this maximum load for circular piles is the following:

$$P \le \frac{\dfrac{\pi\phi_p \cdot f_{cp}\left(\phi_p + 2c_b \cot\theta_s^{3d}\right)}{1+\cot^2\theta_s^{3d}}}{0.8+170\left(\varepsilon_{tx}+\varepsilon_{ty}+\varepsilon_z-\varepsilon_s\right)} \qquad 7\text{-}24$$

with ε_{tx}, ε_{ty}, ε_z and ε_s being the reinforcement strain in *x*- and *y*-direction, the average concrete strain in z-direction over the piles and the average compressive strain of the concrete strut, respectively. These values can be obtained from forces in the struts and ties and their corresponding areas and elastic modulus and, hence, depend on the column load. For the example considered here with 4ϕ20, this equation results in a maximum allowable column load equal to 4'044 kN, which is larger than the considered design force.

7.2.6 Conclusions

For simplicity reasons concrete structures are generally treated as 2D elements. This is also the case in the analysis and design of D-Regions, although in some instances the response is clearly three-dimensional. This section has shown that considering this three-dimensionality and adopting 3D strut-and-tie and stress field models can bring some advantages for some elements and structures, leading to more efficient designs that may justify the increase in complexity.

The strut-and-tie and the stress field method emerged to shed some light and rationality on the design of D-Regions and today major design codes include provisions and guidelines for its application. However, these are limited to 2D. Further research on the use and limits of applicability of 3D strut-and-tie models and stress fields may lead to the

This document is the intellectual property of the fib – International Federation for Structural Concrete. All rights reserved.
This PDF of fib Bulletin 100 is intended for use and/or distribution solely within fib National Member Groups.

inclusion of new provisions in standards of practice to cover 3D elements, including the definition of the minimum amounts of reinforcement required to avoid brittle failures.

Partly due to the lack of provisions, but also due to apprehension of the unknown, practitioners are still reluctant to consider 3D strut-and-tie models. Publication of 3D examples of application that can be considered for reference could be of great help for overcoming the latter. Strut-and-tie modelling of a foundation for a wind tower turbine has been discussed in this section together with the frequently-found-in-literature pile cap foundation.

Even with the proper guidance strut-and-tie modelling of 3D D-regions can be complex and cumbersome and may require a relatively high level of expertise. Implementation of the hypotheses of compatibility-based stress fields in a 3D finite element environment can overcome these limitations avoiding the complexity of traditional nonlinear FE analysis. This approach does not only permit the capacity check of struts and nodal zones in an automatic manner after appropriate concrete strength limits have been defined, but also the derived 3D stress fields can provide a clear understanding of the internal resisting mechanism given a particular reinforcement arrangement, which ultimately can lead to more efficient designs of 3D D-regions.

This document is the intellectual property of the fib – International Federation for Structural Concrete. All rights reserved.
This PDF of fib Bulletin 100 is intended for use and/or distribution solely within fib National Member Groups.

8. Conclusions and outlook

8.1 Conclusions

This Bulletin has presented the recent advances in the application of stress fields and strut-and-tie models for structural concrete. These advances show that the methods are in constant evolution and allow the incorporation of state-of-the-art tools for design and verification in a consistent manner, as for instance the finite element method. Also, the consistency between simple (hand calculations) approaches and refined (computer-based) analyses is extensively shown in this Bulletin.

The stress field and strut-and-tie methods are in this sense an important tool for designers. They allow defining clear, equilibrium-based, load paths during the definition of a structure. The engineer thus has an active role in this process, taking decisions on the most suitable ways to reinforce a member. This provides engineers with a real understanding of the load-carrying actions of a structure and of its governing regions. As necessary, refinements or automated checks can be further implemented in a consistent manner, normally by accounting for the displacement and strain fields of the member. The results of such refined analyses, usually performed by numerical tools, can nevertheless still be checked by means of simple equilibrium-based models, enhancing the understanding of the structural response and optimising the design.

Such tools also provide a consistent and comprehensive framework for verifying existing structures. Simple (hand-made) analyses allow detection of critical members, whose response can be investigated in detail by performing refined analyses. Such an approach allows saving time during the process of a verification (only critical members or regions require to be investigated in detail) and allows obtaining precise and refined (computer-based) estimates of the strength for the critical elements.

The use of stress fields and strut-and-tie models as previously explained can be formulated in a consistent manner by following the philosophy of the Levels-of-Approximation (LoA) approach acknowledged in *fib*'s Model Code 2010. A potential manner for doing this (guidelines for this purpose were missing in MC2010) is presented within this Bulletin. Low-order LoAs (I and II) are devoted to simple (typically hand-made) models, that may incorporate some refinements on the governing load-carrying actions (LoA II). For refined analyses, a compatibility-based stress field can be determined. For example, by neglecting the tensile strength of concrete (at ultimate and for tension-stiffening effects), a refined analysis can be performed as suggested in the Elastic-Plastic Stress Fields (LoA III). This tool, extensively validated with test results, provides accurate estimates of the response and failure load, provided that a minimum deformation capacity in the response is ensured. More refined approaches, considering for instance tension-stiffening effects in the cracked response of concrete, are also introduced (LoA IV) as a way to obtain accurate representations of the response of a member both at serviceability and ultimate limit states, as well as to investigate in detail the deformation capacity in special cases.

Alternative approaches to derive suitable stress-fields are also presented in this Bulletin. These approaches refer to the optimisation of lower-bound solutions in the stress space

https://doi.org/10.35789/fib.BULL.0100.Ch08

This document is the intellectual property of the fib – International Federation for Structural Concrete. All rights reserved.
This PDF of fib Bulletin 100 is intended for use and/or distribution solely within fib National Member Groups.

(without any compatibility of deformations) or to the Stringer Panel Method (as a practical solution of a panel with a smeared compression field and distributed reinforcement bounded by compression and tension stringers).

8.2 Outlook

As presented in the Bulletin, the stress field and strut-and-tie methods are consistent tools that can be safely used and generalised, covering a wide range of cases concerning the design and assessment of structural concrete. These methods have significantly evolved in the last years to consistently incorporate state-of-the-art design tools (such as computer-based analysis).

Despite all these advances, further evolution of the strut-and-tie and stress field methods will still be required in the coming years to address the future needs of structural concrete. Some of the topics where potentially such attention will be required, are the following:

- The application of the methods for cement- or concrete-based materials with a relatively different response, such as fibre-reinforced concrete or ultra-high performance concrete;
- The applicability of the methods to materials with a potentially brittle response, such as the use of glass- or carbon-fibre reinforcement replacing ordinary reinforcing steel;
- To evaluate in a consistent manner the required deformation capacity, so that these methods can be safely applied (minimum reinforcement amount, ductility requirements of the materials, evaluation of the deformation demand);
- The consistency of safety formats across all levels-of-approximation from simple hand calculations to refined numerical modelling;
- Strengthening of existing structures.

These potential fields of application show that the techniques of stress fields and strut-and-tie models are far from being a static tool, but they constitute a consistent framework to model structural concrete and can follow its evolutions.

With respect to the relevance of these methods, another important aspect that will become increasingly significant in the design process will be automation in the design process. Such need will definitely be favoured by the potential to generate design models directly with Building Information Modelling (BIM) and to design and calculate them with numerical tools. In this respect, it is the belief of the authors of this Bulletin that the use of consistent physical theories that can be simplified, so that checking the results of complex (computer-based) results can be made with simple (hand calculations) analyses will be increasingly important. This will allow designers to have a real understanding of the structural response, to identify critical regions and to perform a critical review of automated results. In addition, good designs are, and will be, only possible on the premise that engineers have a clear understanding and representation of the governing load-carrying actions and load paths, and this is, after all, exactly the reason why stress fields and strut-and-tie models were developed more than a century ago.

This document is the intellectual property of the fib – International Federation for Structural Concrete. All rights reserved.
This PDF of fib Bulletin 100 is intended for use and/or distribution solely within fib National Member Groups.

9. References

Chapter 1

[1-1] Ritter, W. (1899), "The Hennebique construction method" (in German, "Die Bauweise Hennebique"), *Schweizerische Bauzeitung*, XXXIII, N° 7, pp. 41-61.

[1-2] Mörsch, E. (1908), "Reinforced concrete construction, theory and application" (in German, "Der Eisenbetonbau, seine Theorie und Anwendung"), 3rd edition, *Verlag von Konrad Wittwer*, 1908, 376 p.

[1-3] Leonhardt F. and Walther, R. (1966) "Deep beams" (in German, "Wandartige Träger"), *Deutscher Ausschuss für Stahlbeton*, Heft 178, Berlin, 159 pp.

[1-4] Schlaich, J. and Weischede, D. (1982), "A practical method for methodical design and building in reinforced concrete" (in German, "Ein praktisches Verfahren zum methodischen Bemessen und Konstruieren im Stahlbetonbau"), Bulletin d'Information n° 150, Comité Euro-International du Béton, 163 pp.

[1-5] Schlaich, J., Schäfer, K. and Jennewein, M. (1987), "Toward a consistent design of structural concrete", *Prestressed Concrete Institute Journal*, May-June, pp. 75-150.

[1-6] Gvozdev, A. A. (1938), "Opredelenie velichiny razrushayushchei nagruzki dlya staticheski neopredelimykh sistem, preterpevayushchikh plasticheskie deformatsii". Moscow/Leningrad, Akademia Nauk SSSR, 1938, pp. 19–38 (English translation: "The determination of the value of the collapse load for statically indeterminate systems undergoing plastic deformation". *Int. J. Mech. Sci.*, Vol. 1, 1960, pp. 322–333).

[1-7] Haythornthwaite, R.M. (1960) "The determination of the value of the collapse load for statically indeterminate systems undergoing plastic deformation". *Int. J. Mech. Sci.*, Vol. 1, pp. 322–333.

[1-8] Wagner, H. (1929). "Ebene Blechwandträger mit sehr dünnen Stegblech", *Zeitshrift für Flugtechnik und Motorluftschiffahrt*, Vol. 20, pp. 200-207, 227-233, 279-284, 306-314.

[1-9] Drucker, D.C. (1961), *On Structural Concrete and the Theorems of Limit Analysis, Publications*, International Association for Bridge and Structural Engineering, V.21, Zürich, Switzerland, pp. 49-59.

[1-10] Nielsen, M. P., and Hoang, L. C. (2016), *Limit Analysis and Concrete Plasticity*, 3rd edition, CRC Press, Boca Raton, FL, 2011, 796 pp.

[1-11] Thürlimann, B., Marti, P., Pralong, J., Ritz, P. and Zimmerli, B. (1983), "Application of the plasticity theory to reinforced concrete" (in German, "Anwendung der Plastizitätstheorie auf Stahlbeton"), Institut für Baustatik und Konstruction, ETH Zürich, 252 pp.

[1-12] Marti, P. (1985), Truss Models in Detailing, Concrete International 7 (12), pp 66–73.

[1-13] Muttoni, A.; Schwartz, J.; Thürlimann, B. (1997): *Design of concrete structures with stress fields*. Birkhäuser, Basel, Switzerland, 1997, 143 p.

[1-14] Blaauwendraad, J. (2018), *Stringer-Panel Models in Structural Concrete: Applied to D-region Design*, Springer Briefs in Applied Sciences and Technology, 99 pp.

This document is the intellectual property of the fib – International Federation for Structural Concrete. All rights reserved.
This PDF of fib Bulletin 100 is intended for use and/or distribution solely within fib National Member Groups.

[1-15] Fernández Ruiz M., Muttoni A. (2007), "On Development of Suitable Stress Fields for Structural Concrete", ACI, *Structural Journal*, Vol. 104 n°4, pp. 495-500.

[1-16] Lourenco, M. S., Almeida, J. F. (2013), "Adaptive Stress Field Models: Formulation and Validation", ACI, *Structural Journal*, Vol. 110, No. 1, pp. 71-81.

[1-17] Kaufmann, W., Mata-Falcón, J., Weber, M., Galkovski, T., Tran, Kabelac, J., Konecny, M., Navrátil, J, Cihal, M., Komarkova, P. (2020) *Compatible Stress Field Design of Structural Concrete: Principles and Validation*. ETH Zurich and IDEA StatiCa s.r.o, ISBN 978-3-906916-95-8, 2020, 158 pp.

[1-18] Hendriks, M.A.N., de Boer, A., Belletti, B., (2017). "Guidelines for Nonlinear Finite Element Analysis of Concrete Structures", Rijkswaterstaat Centre for Infrastructure, Report RTD:1016-1:2017, 2017.

[1-19] Mata-Falcón, J., Tran, D.T., Kaufmann, W., Navrátil, J., (2018), "Computer-aided stress field analysis of discontinuity concrete regions", *Proceedings of the Computational Modelling of Concrete and Concrete Structures Conference* (EURO-C 2018), Bad Hofgastein, Austria, 26 February – 1 March 2018, pp. 641-650.

[1-20] Muttoni, A., Fernández Ruiz, M., Niketić, F. (2015), "Design versus assessment of concrete structures using stress fields and strut-and-tie models", ACI, *Structural Journal*, Vol. 112, No. 5, pp. 605-615.

[1-21] Bairán, J. (2012), "Automatic generation of strut-and-tie schemes adjusted for constructability" (in Spanish: "Generación automática de esquemas de bielas y tirantes considerando criterios constructivos"). *Hormigón y acero*, Ed. ACHE, Spain, vol. 63, núm. 264, p. 67-79.

[1-22] Chai, Y.H., Priestley, M. J. and Seible, F. (1991) "Seismic retrofit of circular bridge columns for enhanced flexural performance", ACI *Structural Journal*, V. 88, No. 5, pp. 572-584.

[1-23] Xiao, Y., Priestley, M. J. and Seible, F. (1996) "Seismic assessment and retrofit of bridge column footings", ACI *Structural Journal*, V. 93, No. 1, pp. 79-94.

[1-24] Fernandes, B. C. (2015), "Stress field models for structural concrete – application to the strengthening of existing foundations", Report, Instituto Superior Tecnico, Lisbon.

[1-25] Menduiña Montero, R., Bairán García, J.M., Marí Bernat, A. (2014) "Refuerzo por recrecido de regiones 'D' en estructuras de hormigón: análisis experimental", Resúmenes de comunicaciones, *Congreso Internacional de Estructuras (Madrid)*, 2014, ISBN 978-84-89670-80-8, pp. 185-186.

[1-26] *fib* Bulletin 61 (2011): Design Examples for strut and tie models, *fib* Bulletin 61, Lausanne, pp.197-216.

[1-27] Panagiotou, M., Restrepo, J.I., Schoettler, M., and Geonwoo, K. (2012). "Nonlinear Truss Model for Reinforced Concrete Walls", ACI *Structural Journal*, Vol. 109, No. 2, pp. 205-214.

[1-28] Lu, Y., and Panagiotou, M. (2014). "Three-Dimensional Nonlinear Cyclic Beam-Truss Model for Reinforced Concrete Non-Planar Walls", *ASCE Journal of Struct. Eng.*, Vol. 140, No. 3, doi:10.1061/(ASCE)ST.1943-541X.0000852.

[1-29] Lu, Y., Panagiotou, M. and Koutromanos, I. (2016) "Three-dimensional beam-truss model for reinforced concrete walls and slabs – part 1: modeling approach, validation, and parametric study for individual reinforced concrete walls", *Earthquake Engng Struct. Dyn*. 2016; 45:1495–1513.

This document is the intellectual property of the fib – International Federation for Structural Concrete. All rights reserved.
This PDF of fib Bulletin 100 is intended for use and/or distribution solely within fib National Member Groups.

[1-30] Qazi, S., Michel, L., Ferrier, E. (2014) "Strut-and-tie model for a reinforced concrete wall strengthened with carbon fiber-reinforced polymers", 16th European Conference on Composite materials, Seville.

[1-31] Dhahir, M. (2018) "Strut and tie modeling of deep beams shear strengthened with FRP laminates", *Composite Structures*, 193, pp. 247-259.

[1-32] Mihaylov, B., Liu, J., Carretero Garcia, C. (2020) "A Mechanical Model for the Complete Shear Behavior of Short Coupling Beams with FRP Sheets", ASCE *Journal of Composites for Construction*, in press.

Chapter 2

[2-1] Chen, W.-F., and D.J. Han. (2007) *Plasticity for Structural Engineers*, Springer-Verlag. 606 p.

[2-2] Drucker, D.C. (1961), *On Structural Concrete and the Theorems of Limit Analysis*, Publications, International Association for Bridge and Structural Engineering, V.21, Zürich, Switzerland, pp. 49-59.

[2-3] Nielsen, M. P., and Hoang, L. C. (2016), *Limit Analysis and Concrete Plasticity*, 3rd edition, CRC Press, Boca Raton, FL, 2011, 796 pp.

[2-4] Thürlimann, B., Marti, P., Pralong, J., Ritz, P. and Zimmerli, B. (1983), "Application of the plasticity theory to reinforced concrete" (in German, "Anwendung der Plastizitätstheorie auf Stahlbeton"), Institut für Baustatik und Konstruction, ETH Zürich, 252 pp.

[2-5] Muttoni, A. (1990), "The applicability of plasticity theory to the design of reinforced concrete" (in German, "Die Anwendbarkeit der Plastizitätstheorie in der Bemessung von Stahlbeton"), IBK Bericht Nr. 176, Institut für Baustatik und Konstruktion, ETH Zürich, 158 pp.

[2-6] Sigrist, V. (1995), "Deformation capacity of reinforced concrete beams" (in German, "Zum Verformungsvermögen von Stahlbetonträgern"), IBK Bericht Nr. 210, Institut für Baustatik und Konstruktion, ETH Zürich, 159 pp.

[2-7] Kaufmann, W. (1998), "Strength and Deformations of Structural Concrete Subjected to In-Plane Shear and Normal Forces". IBK Report No. 234, Institute for Structural Engineering, Swiss Federal Institute of Technology ETH Zurich, 1998, 147 pp.

[2-8] Marti, P., Alvarez, M., Kaufmann, W., Sigrist, V. (1998). "Tension chord model for structural concrete". *Structural Engineering International*, 8(4), 1998, 287-298.

[2-9] Kaufmann, W., Mata-Falcón, J., and Beck, A. (2018). "Future directions for research on shear in structural concrete" *fib* Bulletin 85: *Towards a rational understanding of shear in beams and slabs*.

[2-10] Schlaich, J., Schäfer, K. and Jennewein, M. (1987), "Toward a consistent design of structural concrete", *Prestressed Concrete Institute Journal*, May-June, pp. 75-150.

[2-11] *fib* Bulletin 61 (2011): *Design Examples for strut and tie models*, *fib* Bulletin 61, Lausanne, pp.197-216.

[2-12] CEN 2004 EN1992-1-1:1992, Eurocode 2: Design of concrete structures Part 1-1: General rules and rules for buildings, 2004, 225 p.

This document is the intellectual property of the fib – International Federation for Structural Concrete. All rights reserved.
This PDF of fib Bulletin 100 is intended for use and/or distribution solely within fib National Member Groups.

[2-13] Muttoni, A., Fernández Ruiz, M., Niketić, F. (2015), "Design versus assessment of concrete structures using stress fields and strut-and-tie models", American Concrete Institute, *Structural Journal*, Vol. 112, No. 5, pp. 605-615.

[2-14] Kostic, N. (2009). "Topology of stress fields for the design of reinforced concrete structures" (in French "Topologie des champs de contraintes pour le dimensionnement des structures en beton arme"), (Doctoral dissertation), EPFL Lausanne.

[2-15] Meléndez, C. (2017), "A finite element-based approach for the analysis and design of 3D reinforced concrete elements and its application to D-regions", PhD Thesis, Universitat Politècnica de València, Valencia, Spain, 2017, 225 pp.

[2-16] Robinson, J. R., Demorieux, J. M. (1968),"Tension-compression test on model of reinforced concrete beams" (in French "Essais de traction-compression sur modèles d'âme de poutre en béton armé"), Institut de Recherches Appliquées du Béton Armé, Paris, France. 43 p.

[2-17] Vecchio F. J., Collins M. P. (1986) "The Modified Compression-Field theory for Reinforced Concrete Elements Subjected to Shear," *ACI Journal Proceedings*, Vol. 83, No. 2, pp. 219-231.

[2-18] Hars, E., Niketić, F., Fernández Ruiz, M. (2018). "Response of RC panels accounting for crack development and its interaction with rebars". Magazine of Concrete Research, V. 70, No. 8, 2018, pp. 410-432.

[2-19] Hognestad, E. (1951). *Study of combined bending and axial load in reinforced concrete members*. University of Illinois at Urbana Champaign, College of Engineering. Engineering Experiment Station.

[2-20] Vecchio, F.J.; Collins, M.P. (1993): "Compression response of cracked reinforced concrete. ASCE Journ. of Structural Engineering", V. 119, No.12, Dec. 1993, pp. 3590-3611.

[2-21] Popovics, S. (1973). A Numerical Approach to the Complete Stress-Strain Curve of Concrete. Cement and Concrete Research, Vol. 3, No.5, pp. 583-599.

[2-22] Zhang, Lixin (1995) "Constitutive laws of reinforced membrane elements with high strength concrete", PhD Thesis, University of Houston.

[2-23] Sigrist, V. (2011) "Generalized Stress Field Approach for Analysis of Beams in Shear", ACI *Structural Journal* 108 (4), 2011, pp. 479-487.

[2-24] *fib* 2013, *Model Code for Concrete Structures 2010*, Ernst & Sohn, Lausanne, Switzerland, 434 pp.

[2-25] ACI 318-14 (Full reference)

[2-26] Fernández Ruiz M., Muttoni A. (2007), "On Development of Suitable Stress Fields for Structural Concrete", ACI, *Structural Journal*, Vol. 104 n°4, pp. 495-500.

[2-27] Fernández Ruiz M., Muttoni A. (2008) "Shear strength of thin-webbed post-tensioned beams", ACI *Structural Journal*, Vol.105, No 3, USA, pp. 308-317.

[2-28] Dilger, W. (1966) *Veränderlichkeit der Biege- und Schubsteifigkeit bei Stahlbetontragwerken und ihr Einßuss auf Schnittkraftverteilung und Traglast bei statisch unbestimmter Lagerung*, Deutscher Ausschuss f.r Stahlbeton, Heft 179, Verlag Wilhelm Ernst & Sohn, Berlin, 101 pp.

This document is the intellectual property of the fib – International Federation for Structural Concrete. All rights reserved.
This PDF of fib Bulletin 100 is intended for use and/or distribution solely within fib National Member Groups.

[2-29] Shima, H., Chou, L.-L., and Okamura, H., "Micro and Macro Models for Bond in Reinforced Concrete", *Journal of the Faculty of Engineering*, Vol. XXXIX, No. 2, University of Tokyo, 1987, pp. 133-194.

[2-30] Cosenza, E., Greco, C. and Manfredi, G. (1993) *The Concept of Equivalent Steel*, Comit. Euro-International du Beton (CEB), Bulletin d'Information No. 218, Progress Report of Task Group 2.2 Ductility Requirements for Structural Concrete Reinforcement, Lausanne, pp. 163-183.

[2-31] Alvarez, M. (1998), "Einfluss des Verbundverhaltens auf das Verformungsvermögen von Stahlbeton". IBK Report No. 236, Institute for Structural Engineering, Swiss Federal Institute of Technology ETH Zurich, 1998, 182 pp.

[2-32] Seelhofer, H. (2009), "Ebener Spannungszustand im Betonbau: Grundlagen und Anwendungen", IBK Report No. 320, Institute for Structural Engineering, Swiss Federal Institute of Technology ETH Zurich, 2010, 147 pp.

[2-33] Mata-Falcón, J., Tran, D.T., Kaufmann, W., Navrátil, J., (2018), "Computer-aided stress field analysis of discontinuity concrete regions", *Proceedings of the Computational Modelling of Concrete and Concrete Structures Conference (EURO-C 2018),* Bad Hofgastein, Austria, 26 February – 1 March 2018, pp. 641-650.

[2-34] Kaufmann, W., Mata-Falcón, J., Weber, M., Galkovski, T., Tran, Kabelac, J., Konecny, M., Navrátil, J, Cihal, M., Komarkova, P. (2020) *Compatible Stress Field Design of Structural Concrete: Principles and Validation*. ETH Zurich and IDEA StatiCa s.r.o, ISBN 978-3-906916-95-8, 2020, 158 pp.

[2-35] Galkovski, T., Mata-Falcón, J., and Kaufmann, W. (2021), "Determination of the effective concrete area in tension relevant for modelling tension stiffening in SLS and ULS design", *fib Symposium 2021: Concrete Structures: New trends for Eco-Efficiency and Performance*, Lisbon, Portugal, pp.1598-1607.

[2-36] Ferreira M. (2020) "Studies of cyclic behaviour of concrete coupling beams" (in Portuguese: "Estudo de zonas de descontinuidade de betão estrutural sujeito a ações cíclicas através de modelos de campos de tensões"). PhD Thesis. University of Lisbon.

[2-37] Ferreira M., Almeida J.F., Lourenço M. (2019) "Modelling bond within elasto-plastic stress fields (EPSF) models"; *fib* Symposium, Innovations in Materials, design and Structures; Krakow.

[2-38] Muttoni, A., Fernández Ruiz, M., Niketic, F., & Backes, M. R. (2016). "Assessment of existing structures based on elastic-plastic stress fields-Modelling of critical details and investigation of the in-plane shear transverse bending interaction" (No. EPFL-REPORT-226731). Rapport OFROU.

Chapter 3

[3-1] *fib* 2013, *Model Code for Concrete Structures 2010*, Ernst & Sohn, Lausanne, Switzerland, 434 pp.

[3-2] CEN 2004 EN1992-1-1:1992, Eurocode 2: Design of concrete structures Part 1-1: General rules and rules for buildings, 2004, 225 p.

This document is the intellectual property of the fib – International Federation for Structural Concrete. All rights reserved.
This PDF of fib Bulletin 100 is intended for use and/or distribution solely within fib National Member Groups.

[3-3] FIP Recommendations (1999): *Practical Design of Structural Concrete*. FIP-Commission 3 "Practical Design", Sept. 1996. Publ.: SETO, London, Sept. 1999. (Distributed by: *fib*, Lausanne, email: administration@fib-international.org).

[3-4] CEB Bull. 195-196 (1990): *CEB-FIP Model Code 1990 - First Draft*. Bulletin d'Information No. 195-196, Comité Euro-International du Béton, Lausanne, 1990.

Chapter 4

[4-1] Schlaich, J., Schäfer, K. and Jennewein, M. (1987), "Toward a consistent design of structural concrete", *Prestressed Concrete Institute Journal*, May-June, pp. 75-150.

[4-2] Schlaich, J.; Schäfer, K. (1991): "Design and detailing of structural concrete using strut-and-tie models". *The Structural Engineer*, Vol 69, No. 6, 1991.

[4-3] FIP Recommendations (1999): *Practical Design of Structural Concrete*. FIP-Commission 3 "Practical Design", Sept. 1996. Publ.: SETO, London, Sept. 1999. (Distributed by: *fib*, Lausanne, email: administration@fib-international.org).

[4-4] CEN 2004 EN1992-1-1:1992, Eurocode 2: Design of concrete structures Part 1-1: General rules and rules for buildings, 2004, 225 p.

[4-5] *fib* Bulletin 61 (2011): *Design Examples for strut and tie models*, *fib* Bulletin 61, Lausanne, pp.197-216.

[4-6] Muttoni, A.; Schwartz, J.; Thürlimann, B. (1997): *Design of concrete structures with stress fields. Birkhäuser*, Basel, Switzerland, 1997, 143 p.

[4-7] Leonhardt F., and Walther, R. (1966) *Deep beams* (in German, *Wandartige Träger*), Deutscher Ausschuss für Stahlbeton, Heft 178, Berlin, 159 pp.

[4-8] *fib* Bulletins 1 to 3 (1999): *Structural concrete*. Textbook on behaviour, design and performance - updated knowledge of the CEB/FIP Model Code 1990.

Volume 1: *Introduction - design process - materials*. 244 pp., July 1999.

Volume 2: *Basis of design*. 305 pp., July 1999.

Volume 3: *Durability - design for fire resistance -member design - assessment, maintenance and repair - practical aspects*. *fib* Lausanne, July 1999.

Chapter 5

[5-1] Kaufmann, W., and Mata-Falcón, J. (2017). "Structural concrete design in the 21st century: are limit analysis methods obsolete?", Proceedings 24th Czech Concrete Days, Litomyšl, Czech Republic, 22-23 November 2017, 12 p.

[5-2] Vecchio F. J., Collins M. P. (1986) "The Modified Compression-Field theory for Reinforced Concrete Elements Subjected to Shear", *ACI Journal Proceedings*, Vol. 83, No. 2, pp. 219-231.

[5-3] Kaufmann, W., and Marti, P. (1998). "Structural concrete: cracked membrane model". *Journal of Structural Engineering*, V. 124, No. 12, 1998, pp. 1467-1475.

[5-4] Fernández Ruiz M., Muttoni A. (2007), "On Development of Suitable Stress Fields for Structural Concrete", ACI, *Structural Journal*, Vol. 104 n°4, pp. 495-500.

This document is the intellectual property of the fib – International Federation for Structural Concrete. All rights reserved.
This PDF of fib Bulletin 100 is intended for use and/or distribution solely within fib National Member Groups.

[5-5] Muttoni, A., Fernández Ruiz, M., Niketic, F., & Backes, M. R. (2016). "Assessment of existing structures based on elastic-plastic stress fields-Modelling of critical details and investigation of the in-plane shear transverse bending interaction" (No. EPFL-REPORT-226731). Rapport OFROU.

[5-6] Mata-Falcón, J., Tran, D.T., Kaufmann, W., Navrátil, J., (2018), "Computer-aided stress field analysis of discontinuity concrete regions", *Proceedings of the Computational Modelling of Concrete and Concrete Structures Conference (EURO-C 2018)*, Bad Hofgastein, Austria, 26 February – 1 March 2018, pp. 641-650.

[5-7] Kaufmann, W., Mata-Falcón, J., Weber, M., Galkovski, T., Tran, Kabelac, J., Konecny, M., Navrátil, J, Cihal, M., Komarkova, P. (2020) *Compatible Stress Field Design of Structural Concrete: Principles and Validation*. ETH Zurich and IDEA StatiCa s.r.o, ISBN 978-3-906916-95-8, 2020, 158 pp.

[5-8] Nadai, A, "Der Beginn des Fließvorganges in einem tordierten Stab", *Journal of Applied Mathematics and Mechanics/Zeitschrift für Angewandte Mathematik und Mechanik* 3.6 (1923), pp. 442–454.

[5-9] Hencky, H. Zur "Theorie plastischer Deformationen und der hierdurch im Material hervorgerufenen Nachspannungen". *Journal of Applied Mathematics and Mechanics/ Zeitschrift für Angewandte Mathematik und Mechanik* 4.4 (1924), pp. 323–334.

[5-10] Handelman, G H, Lin, C C, Prager, W. "On the mechanical behaviour of metals in the strain-hardening range", *Quarterly of Applied Mathematics* 4.4 (1947), pp. 397–407.

[5-11] De Saint-Venant, B., "Mémoire sur l'établissement des équations différentielles des mouvements intérieurs opérés dans les corps solides ductiles au-delà des limites où l'élasticité pourrait les ramener á leur premier état", Compt. Rend 70 (1870), pp. 473–480.

[5-12] Lévy, M., "Mémoire sur les équations générales des mouvements intérieurs des corps solides ductiles au delà des limites où l'élasticité pourrait les ramener à leur premier état", CR Acad. Sci. Paris 70 (1870), pp. 1323–1325.

[5-13] Prager, W. (1948), "The theory of plastic flow versus theory of plastic deformation, *Journal of Applied Physics*, Vol. 19, pp. 540-543

[5-14] Garbelini, C., "Advances in the Soil-Structure Interaction Analysis – from Surface Footings to Thermoactive Deep Foundations", PhD thesis, École Polytechnique Fédérale de Lausanne, 2020, 303 p.

[5-15] Wagner, H. (1929). Ebene Blechwandträger mit sehr dünnen Stegblech, Z. für Flugtechnik und Motorluftschiffahrt, Vol. 20, pp. 200-207, 227-233, 279-284, 306-314.

[5-16] Hendriks, M.A.N., de Boer, A., Belletti, B., (2017). "Guidelines for Nonlinear Finite Element Analysis of Concrete Structures", Rijkswaterstaat Centre for Infrastructure, Report RTD:1016-1:2017, 2017.

[5-17] Costa, R., Providencia, P. and Ferreira, M. (2017). Influence of joint modelling on the pushover analysis of a RC frame. Structural Engineering and Mechanics, 64(5), 641-652.

[5-18] Ferreira M., Almeida J.F., Lourenço M. (2019) "Modelling bond within elasto-plastic stress fields (EPSF) models"; *fib Symposium, Innovations in Materials, design and Structures*; Krakow.

This document is the intellectual property of the fib – International Federation for Structural Concrete. All rights reserved.
This PDF of fib Bulletin 100 is intended for use and/or distribution solely within fib National Member Groups.

[5-19] *fib* 2013, *Model Code for Concrete Structures 2010*, Ernst & Sohn, Lausanne, Switzerland, 434 pp.

[5-20] Oñate, E., (1995), *Cálculo de Estructuras por el Método de los Elementos Finitos - Análisis Estático Lineal*, CIMNE, Spain, 807 p

[5-21] Frey F., Jirousek J. (2001) *Méthode des éléments finis (TGC volume 6) Analyse des structures et milieu continues*, Presses Polytechnique et Universitaires Romandes, 298 p., Lausanne.

[5-22] Mata-Falcón, J. (2015), "Serviceability and Ultimate Behaviour of Dapped-end Beams" (In Spanish: "Estudio del comportamiento en servicio y rotura de los apoyos a media madera"), PhD Thesis, Universitat Politècnica de València, Valencia, Spain, 2015, 719 pp.

[5-23] Meléndez, C. (2017), "A finite element-based approach for the analysis and design of 3D reinforced concrete elements and its application to D-regions", PhD Thesis, Universitat Politècnica de València, Valencia, Spain, 2017, 225 pp.

[5-24] Gvozdev, A. A. (1938), "Opredelenie velichiny razrushayushchei nagruzki dlya staticheski neopredelimykh sistem, preterpevayushchikh plasticheskie deformatsii". Moscow/Leningrad, Akademia Nauk SSSR, 1938, pp. 19–38 (English translation: "The determination of the value of the collapse load for statically indeterminate systems undergoing plastic deformation". *Int. J. Mech. Sci.*, Vol. 1, 1960, pp. 322–333).

[5-25] Prager, W (1952): The general theory of limit design. Proc. 8th Int. Congr. Theor. Appl. Mech., Istanbul, Vol. II, 1952, pp. 65–72.

[5-26] Drucker, DC; Greenberg, HJ; Prager, W (1952), Extended limit design theorems for continuous media. Q. Appl. Math., V. 9, 1952, pp. 381–389.

[5-27] Braestrup, MW (2019), "Concrete plasticity – a historical perspective". Keynote lecture, *Proceeding of the fib symposium*, Krakow, May 2019.

[5-28] Johansen, KW (1943): *Brudlinieteorier* (*Yield line theories*). Copenhagen, Gjellerup, 1943, 189 pp.

[5-29] Hillerborg, A (1974): *Strimlemetoden* (*The strip method*). Stockholm, Almqvist & Wiksell, 1974.

[5-30] Nielsen, M. P., and Hoang, L. C. (2011), *Limit Analysis and Concrete Plasticity*, 3rd edition, CRC Press, Boca Raton, FL, 2011, 796 pp.

[5-31] Grierson, DE; Gladwell, GML (1971), "Collapse load analysis using linear programming". *Journal of Structural Division*, ASCE, V. 97, 1971, pp. 1561-1573.

[5-32] Anderheggen, E; Knöpfel, H (1972): "Finite element limit analysis using linear programming". *International Journal of Solids and Structures*, V. 8, 1972, pp. 1413-1431.

[5-33] Makrodimopoulos, A; Martin, CM (2006): "Lower bound limit analysis of cohesive-frictional materials using second-order cone programming". *Int. J. for Num. Meth. In Eng*. 66(4): 604-634, 2006.

[5-34] Bispos, C; Pardalos, P (2007), "Second-order cone and semi-definite representation of material failure criteria". *Journal of Optimization Theory and Applications*, V. 134, No. 2, 2007, pp. 275-301.

[5-35] Krabbenhøft, K; Lyamin, AV; Sloan, SW (2007): "Formulation and solution of some plasticity problems as conic programs". *Int. J. solids and struct.*, 44, 1533-1549, 2007.

This document is the intellectual property of the fib – International Federation for Structural Concrete. All rights reserved.
This PDF of fib Bulletin 100 is intended for use and/or distribution solely within fib National Member Groups.

[5-36] Larsen, KP (2010): Numerical Limit Analysis of Reinforced Concrete Structures. Ph.D. thesis, DTU, Dept. of Civil Eng., 2010.

[5-37] Herfelt, M.A., Poulsen P.N., Hoang, L.C., Jensen, J.F. (2017) "Lower bound plane stress element for modelling 3D structures", *Proceedings of the Institution of Civil Engineers - Engineering and Computational Mechanics*, V. 170, No. 3, 2017, pp. 107-117.

[5-38] Herfelt MA (2017), "Numerical limit analysis of precast concrete structures". PhD thesis, DTU, Dept. of Civil Eng., 2017.

[5-39] Krenk, S; Damkilde, L; Høyer, O (1994): "Limit analysis and optimal design of plates with equilibrium elements". *J. Engng. Mech*. 120, 1237-1254, 1994.

[5-40] Damkilde, L; Høyer, O (1993), "An efficient implementation of limit state calculations based on lowerbound solutions". *Computers & Structures*, V. 49, 1993, pp. 953-962.

[5-41] Damkilde, L; Poulsen, PN; Olesen, JF (1994), "A program for limit state analysis of plane, reinforced concrete plates by the stringer method". *Bygningsstatiske Meddelelser*, V. 65, 1994, pp. 1-26.

[5-42] Poulsen, PN; Damkilde, L (2000): "Limit analysis of reinforced concrete plates subjected to in-plane forces". *International Journal of solids and structures*, V. 37, 2000, pp. 6011-6029.

[5-43] Larsen, KP; Poulsen, PN; Nielsen, LO (2009): "Limit Analysis of Solid Reinforced Concrete Structures". in: 1st *Int. Conf. on Computational Technologies in Concrete Structures (CTCS '09)*, May, 2009, Jeju, Korea.

[5-44] Jensen, TW; Poulsen, PN; Hoang, LC (2019): "Layer model for finite element limit analysis of concrete slabs with shear reinforcement". *Engineering Structures*, to be published, 2019.

[5-45] Nielsen, LO (2012): "On computational limit analysis for structural plasticity by second order cone programming, Part 1". Lecture note U090, DTU, Dept. of Civil Eng., 2012.

[5-46] Poulsen, PN; Olesen, JF; Andersen, S: *Computational Structural Modelling – Non linear Finite Element Method*. Text book, DTU, Dept. of Civil Eng., 2018.

[5-47] MOSEK ApS (2019): MOSEK optimization toolbox for MATLAB. Release 9.0.95, June 2019.

[5-48] Schlaich, J., Schäfer, K. and Jennewein, M. (1987), "Toward a consistent design of structural concrete", *Prestressed Concrete Institute Journal*, May-June, pp. 75-150.

[5-49] Muttoni, A., Fernández Ruiz, M., Niketić, F. (2015), "Design versus assessment of concrete structures using stress fields and strut-and-tie models", American Concrete Institute, *Structural Journal*, Vol. 112, No. 5, pp. 605-615.

[5-50] Niketic, F (2017): "Development of a consistent approach for design and assessment of structural concrete members using stress fields and strut-and-tie models". PhD thesis No. 7911, École Polytechnique Fédérale De Lausanne, 2017.

[5-51] Herfelt, MA; Poulsen, PN; Hoang, LC (2018), "Closed-form adaptive effectiveness factor for numerical models". 5th International *fib*-congress, Melbourne, Oct. 2018.

[5-52] Lourenco, M. S., Almeida, J. F. (2013), "Adaptive Stress Field Models: Formulation and Validation", ACI *Structural Journal*, Vol. 110, No. 1, pp. 71-81.

This document is the intellectual property of the fib – International Federation for Structural Concrete. All rights reserved.
This PDF of fib Bulletin 100 is intended for use and/or distribution solely within fib National Member Groups.

[5-53] Schlaich, J.; Schäfer, K. (1983): *Zur Druck-Querzug-Festigkeit des Stahlbetons*. BuStb 78 (1983), H.3, 73-78.

[5-54] Schäfer, K.; Schelling, G.; Kuchler, T. (1990): *Druck- und Querzug in bewehrten Betonelementen*. DAfStb H.408, Beuth Verlag, Berlin, 1990.

[5-55] Eibl, J.; Neuroth, U. (1988): *Untersuchungen zur Druckfestigkeit von bewehrtem Beton bei gleichzeitig wirkendem Querzug*. Institut für Massivbau und Baustofftechnologie, Univ. Karlsruhe, 1988.

[5-56] Kollegger, J.: Mehlhorn, G. (1990): *Experimentelle Untersuchungen zur Bestimmung der Druckfestigkeit des gerissenen Stahlbetons bei einer Querzugbeanspruchung*. DAfStb H.413, Beuth Verlag, Berlin, 1990.

[5-57] Vecchio, F.J.; Collins, M.P. (1993): "Compression response of cracked reinforced concrete." ASCE *Journ. of Structural Engineering*, V. 119, No.12, Dec. 1993, 3590-3611.

[5-58] Marti, P., Alvarez, M., Kaufmann, W., Sigrist, V. (1998). Tension chord model for structural concrete. Structural Engineering International, 8(4), 1998, 287-298.

[5-59] Leonhardt F., and Walther, R. (1966) "Deep beams" (in German, "Wandartige Träger"), Deutscher Ausschuss für Stahlbeton, Heft 178, Berlin, 159 pp.

[5-60] M.P. Nielsen and Hoang, L. C. (1998). *Limit Analysis and Concrete Plasticity*, CRC Press LLC, 2nd edition 1999.

[5-61] Hoogenboom. P.C.J. (1998), "Discrete elements and nonlinearity in design of structural concrete walls", Doctoral thesis, Delft University of Technology, Netherlands.

[5-62] Heinzmann, D. (2012), "Stringer-Tafelmodelle für Stahlbeton", Doctoral thesis, ETH Zürich, Switzerland.

Chapter 6

[6-1] *fib* 2013, *Model Code for Concrete Structures 2010*, Ernst & Sohn, Lausanne, Switzerland, 434 pp.

[6-2] CEN 2004 EN1992-1-1:1992, Eurocode 2: Design of concrete structures Part 1-1: General rules and rules for buildings, 2004, 225 p.

[6-3] Fernández Ruiz M., Muttoni A. (2007), "On Development of Suitable Stress Fields for Structural Concrete", ACI, *Structural Journal*, Vol. 104 n°4, pp. 495-500.

[6-4] Muttoni A., Burdet O., Hars E. (2006) "Effect of Duct Type on the Shear Strength of Thin Webs", ACI, *Structural Journal*, Vol.103, No 5, pp. 729-735.

[6-5] Fernández Ruiz M., Muttoni A. (2008) "Shear strength of thin-webbed post-tensioned beams", ACI, *Structural Journal*, Vol.105, No 3, USA, pp. 308-317.

[6-6] Rupf M., Fernández Ruiz M., Muttoni A. (2013) "Post-tensioned girders with lowamounts of shear reinforcement: Shear strength and influence of flanges", *Engineering structures*, Vol. 56, pp. 357-371.

[6-7] Muttoni, A., Fernández Ruiz, M., Niketic, F., & Backes, M. R. (2016). "Assessment of existing structures based on elastic-plastic stress fields-Modelling of critical details and investigation of the in-plane shear transverse bending interaction" (No. EPFL-REPORT-226731). Rapport OFROU.

This document is the intellectual property of the fib – International Federation for Structural Concrete. All rights reserved.
This PDF of fib Bulletin 100 is intended for use and/or distribution solely within fib National Member Groups.

[6-8] Mata-Falcón, J. (2015), "Serviceability and Ultimate Behaviour of Dapped-end Beams" (In Spanish: "Estudio del comportamiento en servicio y rotura de los apoyos a media madera"), PhD Thesis, Universitat Politècnica de València, Valencia, Spain, 2015, 719 pp.

[6-9] Muttoni A., Fernández Ruiz (2007), M., "Concrete cracking in tension members and application to deck slabs of bridges", ASCE *Journal of Bridge Engineering*, 12, USA, 2007, pp. 646-653.

[6-10] CEN 2005. European Standard EN 1998-3: 2005 Eurocode 8: Design of structures for earthquake resistance. Part 3: Assessment and retrofitting of buildings. European Committee for Standardization, Brussels, Belgium.

[6-11] CEN (2018), prEN 1992-1-1:2018 Eurocode 2: Design of concrete structures –

Part 1-1: General rules, rules for buildings, bridges and civil engineering structures, draft of April 2018 by the Project Team SC2.T1 working on Phase 1 of the CEN/TC 250 work programme, D3, 293 p.

[6-12] NP EN 1998-3 (2017).

[6-13] Costa, I.G.; Barros, J.A.O., "Ensaio de carga em vigas de betão armado", Relatório CVT19015, 23 pags. 2 August 2019.

Chapter 7

[7-1] Paulay, T., & Binney, J. R. (1974). *Diagonally reinforced coupling beams of shear walls*. ACI Special Publication, 42, 579-598.

[7-2] CEN 2005. European Standard EN 1998-3: 2005 Eurocode 8: Design of structures for earthquake resistance. Part 3: Assessment and retrofitting of buildings. European Committee for Standardization, Brussels, Belgium.

[7-3] *fib* 2013, *Model Code for Concrete Structures 2010*, Ernst & Sohn, Lausanne, Switzerland, 434 pp.

[7-4] Mihaylov, B. I., Bentz, E. C., & Collins, M. P. (2013). "Two-Parameter Kinematic Theory for Shear Behavior of Deep Beams". *ACI Structural Journal*, 110(3).

[7-5] Mihaylov, B. I., & Franssen, R. (2017). "Shear-flexure interaction in the critical sections of short coupling beams". *Engineering Structures*, 152, 370-380.

[7-6] Kaufmann, W., Mata-Falcón, J., and Beck, A. (2018). "Future directions for research on shear in structural concrete." *fib* Bulletin 85: *Towards a rational understanding of shear in beams and slabs*.

[7-7] Mata-Falcón, J., Tran, D.T., Kaufmann, W., Navrátil, J., (2018), "Computer-aided stress field analysis of discontinuity concrete regions", P*roceedings of the Computational Modelling of Concrete and Concrete Structures Conference (EURO-C 2018)*, Bad Hofgastein, Austria, 26 February – 1 March 2018, pp. 641-650.

[7-8] Kaufmann, W., Mata-Falcón, J., Weber, M., Galkovski, T., Tran, Kabelac, J., Konecny, M., Navrátil, J, Cihal, M., Komarkova, P. (2020) *Compatible Stress Field Design of Structural Concrete: Principles and Validation*. ETH Zurich and IDEA StatiCa s.r.o, ISBN 978-3-906916-95-8, 2020, 158 pp.

[7-9] Mihaylov, B. I., Bentz, E. C., & Collins, M. P. (2010). "Behavior of Large Deep Beams Subjected to Monotonic and Reversed Cyclic Shear". *ACI Structural Journal*, 107(6).

This document is the intellectual property of the fib – International Federation for Structural Concrete. All rights reserved.
This PDF of fib Bulletin 100 is intended for use and/or distribution solely within fib National Member Groups.

[7-10] Mihaylov, B. (2015). "Five-spring model for complete shear behaviour of deep beams". *Structural Concrete*, 16(1), 71-83.

[7-11] Alcocer, S. M., & Uribe, C. M. (2008), "Monolithic and cyclic behavior of deep beams designed using strut-and-tie models", ACI, *Structural Journal*, 105(3), 327.

[7-12] Paulay, T. (1969). *The coupling of shear walls*. University of Canterbury Christchurch (New Zealand).

[7-13] Kwan, A. K. H., & Zhao, Z. Z. (2002). "Testing of coupling beams with equal end rotations maintained and local joint deformation allowed". *Proceedings of the Institution of Civil Engineers: Structures and Buildings*.

[7-14] Kwan, A. K. H., & Zhao, Z. Z. (2002). "Cyclic behaviour of deep reinforced concrete coupling beams". Proceedings of the Institution of Civil Engineers: Structures and Buildings.

[7-15] Kostic, N. (2009). "Topology of stress fields for the design of reinforced concrete structures" (in French "Topologie des champs de contraintes pour le dimensionnement des structures en beton arme"), (Doctoral dissertation), EPFL Lausanne.

[7-16] Galano, L., & Vignoli, A. (2000). "Seismic behavior of short coupling beams with different reinforcement layouts". *Structural Journal*, 97(6), 876-885.

[7-17] Tassios, T. P., Moretti, M., & Bezas, A. (1996). "On the behavior and ductility of reinforced concrete coupling beams of shear walls". ACI, *Structural Journal*, 93(6), 711-720.

[7-18] Fisher, A. W. (2016). *Shear performance of heavily reinforced high-strength concrete coupling beams*. University of Toronto (Canada).

[7-19] Lim, E., Hwang, S. J., Wang, T. W., & Chang, Y. H. (2016). "An investigation on the seismic behavior of deep reinforced concrete coupling beams". ACI, *Structural Journal*, 113(2), 217.

[7-20] Schlaich, J., Schäfer, K. and Jennewein, M. (1987), "Toward a consistent design of structural concrete", *Prestressed Concrete Institute Journal*, May-June, pp. 75-150.

[7-21] Muttoni, A., Schwartz, J., Thürlimann, B. (1997): *Design of concrete structures with stress fields*. Birkhäuser, Basel, Switzerland, 1997, 143 p.

[7-22] Foster, S. J., Marti, P., & Mojsilovic, N. (2003), "Design of reinforced concrete solids using stress analysis". ACI, *Structural Journal*, 100(6), 2003, pp. 758-764.

[7-23] Reineck K., Lourenço M.S., Almeida J.F., Haugerud S.A. (2011), "Gaining experience with strut and tie models for the design of concrete structures", *fib* bulletin 61, *Design Examples for Strut-and-Tie Models*, pp. 197-216.

[7-24] Hannant D. J. (1974), "Nomograms for the failure of plain concrete axial stresses", *The Structural Engineer* 5(52), pp. 151-165.

[7-25] Kotsovos, M. and Pavlovic, M. (1995), *Structural concrete. Finite-element analysis for limit-state design*. London, Thomas Telford, pp. 550.

[7-26] Menetrey P., Willam K.J. (1995), "Triaxial Failure Criterion for Concrete and its Generalization", ACI, *Structural Journal* 92(3), pp. 311-318.

[7-27] Meléndez, C., Sagaseta, J., Miguel Sosa, P.F., Pallarés Rubio, L. (2019), "Refined 3D Strut-and-Tie Model for Analysis and Design of four-pile Caps", ACI, *Structural Journal* 116(4), pp. 15-29.

This document is the intellectual property of the fib – International Federation for Structural Concrete. All rights reserved.
This PDF of fib Bulletin 100 is intended for use and/or distribution solely within fib National Member Groups.

[7-28] Fernández Ruiz M., Muttoni A. (2007), "On Development of Suitable Stress Fields for Structural Concrete", ACI, *Structural Journal*, Vol. 104 n°4, pp. 495-500.

[7-29] Meléndez C., Miguel P.F., Pallarés L. (2016), "A simplified approach for the ultimate limit state analysis of three-dimensional reinforced concrete elements", *Engineering Structures* 123, pp. 330–340.

[7-30] Meléndez, C. (2017), "A finite element-based approach for the analysis and design of 3D reinforced concrete elements and its application to D-regions", PhD Thesis, Universitat Politècnica de València, Valencia, Spain, 2017, 225 pp.

[7-31] Vecchio F. J., Collins M. P. (1986) "The Modified Compression-Field theory for Reinforced Concrete Elements Subjected to Shear", *ACI Journal Proceedings*, Vol. 83, No. 2, pp. 219-231.

[7-32] Hordijk D. (1991), "Local approach to fatigue of concrete", Doctoral thesis, Delft University of Technology, pp. 210.

This document is the intellectual property of the fib – International Federation for Structural Concrete. All rights reserved.
This PDF of fib Bulletin 100 is intended for use and/or distribution solely within fib National Member Groups.

10. Notations

A_s	cross-section area of the reinforcement
a	shear span, distance between load and reaction resultant
$A_{s,\min}$	minimum amount of reinforcement
A_v	area of effective stirrups
C	compression force
C_d	design value of a compression force
D	diagonal strut force
E_s	modulus of elasticity of steel
E_h	hardening modulus of reinforcement
F_d	design value of a force
F	force
F_w	web force
M	bending moment
N	axial load
T	tension force
T_d	design value of a tension force
V	shear force
V_d	design value of the shear force
V_{Rd}	design value of the shear strength
V_s	shear carried by stirrups
V_{CLZ}	shear carried by critical loading zone
V_{ci}	shear carried by aggregate interlock
V_d	shear carried by dowel action
a	shear span
a_g	maximum aggregate size
b_w	web thickness
d	effective depth pf section
d_b	bar diameter
f_{bd}	concrete design bond strength
f_c	concrete strength measured in cylinder
f_{cd}	design value of the uniaxial compressive strength of concrete
f_{ct}	axial tensile strength of concrete

https://doi.org/10.35789/fib.BULL.0100.Ch10

This document is the intellectual property of the fib – International Federation for Structural Concrete. All rights reserved.
This PDF of fib Bulletin 100 is intended for use and/or distribution solely within fib National Member Groups.

f_{ctm}	mean value of axial tensile strength of concrete
f_{ck}	characteristic compressive cylinder strength of concrete (at 28 days)
f_t	tensile strength of reinforcement
f_y	yield strength
f_{yd}	design value of the yield strength of the reinforcement
f_{ye}	effective yield strength of bar-dowels
f_{yv}	yield strength of stirrups
f_{yk}	characteristic yield strength of reinforcement
h	total depth of section
l_b	width of bearing area parallel to the axis of the member
$l_{bd,net}$	net anchorage design length
l_{b1e}	effective width of loading plate
l_k	length of dowels
l_t	cracked length along flexural reinforcement
$l_{\varepsilon,avg}$	assumed distance between fictitious cracks in the pull-out tension stiffening model
n	modular ratio ($=E_s/E_c$)
n_b	number of bars
q_d	design value of a distributed load
s	crack slip
s_{cr}, s_r	crack spacing
$s_{\max}$	maximum crack spacing
s_{r0}	theoretical maximum value of the crack spacing
t	thickness of a member
w	crack width
x	depth of compression zone
z	lever arm
z_n	neutral depth
$\varnothing$	bar diameter
α	angle of compression field
α_1	angle of critical crack
β	strut inclination angle
Δ_c	transverse displacement in the critical loading zone
ε_1	principal tensile strain in section
ε_2	principal compressive strain in section

This document is the intellectual property of the fib – International Federation for Structural Concrete. All rights reserved.
This PDF of fib Bulletin 100 is intended for use and/or distribution solely within fib National Member Groups.

ε_c	compressive strain at strength peak in the concrete
ε_{cu}	ultimate compressive strain in the concrete
ε_m	average strain of reinforcement
ε_{my}	average strain of reinforcement at yielding
ε_{mu}	average strain of reinforcement at maximum load
ε_p	strain at maximum strength in the concrete model
ε_s	reinforcement strain
$\varepsilon_{s,x}, \varepsilon_{s,y}$	reinforcement strain at direction x and y
$\varepsilon_{t,avg}$	average strain along flexural reinforcement
ε_u, ε_{su}	reinforcement strain at maximum load
ε_v	stirrup strain
ε_x	longitudinal strain in section
ε_y, ε_{sy}	reinforcement strain at yielding
ηf_c	strength reduction factor accounting for the brittleness of higher strength concrete
η_ε	strength reduction factor accounting for transverse concrete cracking
ν_d	unitary shear force
θ_c	angle of ε_2
θ_b	orientation of the reinforcing bar
θ_r	crack orientation with respect to horizontal / longitudinal axis
λ, η	stress block factors
λ	crack spacing coefficient ($=s_r/s_{r0}$)
ρ	geometric reinforcement ratio
ρ_l	ratio of flexural reinforcement
ρ_v	stirrup ratio
ρ_{cr}	minimum reinforcement ratio in uniaxial tension
ρ_{eff}	effective reinforcement ratio
$\rho_{\min}$	minimum shear reinforcement specified by structural concrete codes
σ_c	concrete stress
$\Delta\sigma_c$	concrete stress variation
σ_{cd}	design value of a concrete stress
σ_s	steel stress
σ_{sr}	reinforcing steel stress at the cracks
τ_b	bond shear stress
τ_{b0}	bond shear stress before yielding
τ_{b1}	bond shear stress after yielding

This document is the intellectual property of the fib – International Federation for Structural Concrete. All rights reserved.
This PDF of fib Bulletin 100 is intended for use and/or distribution solely within fib National Member Groups.

11. Definitions

Chord	Compression or tension part of a member idealised as having a narrow width and which interacts with adjacent membrane elements through longitudinal shear.
Compatibility-based stress field	Stress field in which the compatibility of deformations are satisfied.
Compression field	Region of a stress field where concrete is subjected to uniaxial compressive stresses.
Concrete cover	Distance between the surface of a reinforcement bar or tendon (including links and stirrups and surface reinforcement where relevant) and the nearest concrete surface.
Deformation capacity	Ability of a member or part of it or a structure to deform while maintaining its resistance.
Crack formation phase	Phase of the cracking process which occurs when forces are close to the cracking forces and in which the full crack pattern is not yet developed. It is typical of the type of cracking due to imposed deformations with large crack spacings. An increase in the imposed strain will not increase cracks width. Instead it will form new cracks.
Effective tension area	Concrete area in tension around reinforcement within which the crack opening is effectively controlled by the reinforcement (area of concrete that needs to be tensioned up to the tensile resistance of concrete to produce a new crack).
Effective depth	In a cross section, distance from the extreme compression fibre to geometrical centroid of longitudinal tension reinforcement.
Elastic-Plastic stress field	Compatibility-based stress field resulting from an elastic-plastic material behaviour.
Exact solution	The kinematically admissible mechanism whose internal stress state does not violate the yield condition.
Headed bar	Reinforcing bar with head attached at one or both ends.
Hook	End stretch of a reinforcement bar, bent at not less than 150°.
Internal forces	Resultant of stresses in cross section of a member (axial force, shear force, bending moment, torsion).
Lightweight aggregate concrete	Concrete having a closed structure and a density of not more than 2'200 kg/m^3, consisting of or containing a proportion of artificial or natural lightweight aggregates having a particle dry density of less than 2'000 kg/m^3.
Linear member	Structural element, straight or curved, with one dimension significantly larger than the others (such as beams and columns).
Link	Reinforcement bent to form single or multiple legs that surrounds longitudinal reinforcement. Links may be closed or open with sufficient anchorage at their ends.

https://doi.org/10.35789/fib.BULL.0100.Ch11

This document is the intellectual property of the fib – International Federation for Structural Concrete. All rights reserved.
This PDF of fib Bulletin 100 is intended for use and/or distribution solely within fib National Member Groups.

Loop	U-shaped reinforcement bar where both legs transmit their forces to other reinforcement or to concrete through bond.
Lower-bound solution	Any statically admissible stress state that does not violate the yield condition (i.e. a solution satisfying the lower-bound or static theorem of limit analysis). A lower-bound solution allows determining a failure load lower or equal than the one corresponding to the exact solution according to limit analysis.
Minimum reinforcement	Reinforcement that avoids brittle failure after cracking, provides good serviceability behaviour and ensures sufficiently deformation capacity in order to conduct a design based on the theory of plasticity.
Nodal regions	Region of a stress field where the force is transferred amongst concurrent compression fields and/or ties.
Node	Point of intersection of struts and/or ties transferring forces amongst them.
Ordinary reinforcement	Reinforcement which is not prestressed. Where not specified otherwise, it is made of reinforcement steel.
Plain reinforcement	Reinforcement with a smooth surface.
Plain or lightly reinforced concrete members	Structural concrete members having no reinforcement (plain concrete) or less reinforcement than the minimum amounts prescribed.
Prestressed reinforcement	Reinforcement made of strands, wires or bars subjected to a prestressing process. Where not specified otherwise, it is made of prestressing steel.
Reinforcement	Assembly of bars and/or tendons, prestressed (prestressed reinforcement) or not (ordinary reinforcement), embedded in or connected to concrete members. Where not specified otherwise, it is made of steel and is bonded to the concrete.
Rigid-Plastic stress field	Stress field resulting from a rigid-perfectly plastic material behaviour with no tensile strength for concrete.
Shear reinforcement	Stirrups, links, headed bars or bent-up bars specifically placed to resist action effects caused by shear and torsion.
Stabilised cracking	Phase of the cracking process in which the crack pattern is fully developed. An increase in the actions will normally result in an increase in the crack opening. This type of cracking is typically associated with applied external loads, when such loads are sensibly above the cracking loads.
Stirrup	Reinforcement bent to form double or multiple legs that surrounds longitudinal reinforcement. Stirrups may be closed or open with sufficient anchorage at their ends.
Stress field	Stress state in a structure equilibrating the external actions.
Strut	Resultant of a compression field, part of a Strut-and-tie model.
Strut-and-tie model	Model composed of the resultant forces of a stress field with struts for the compression fields and ties for the tension reinforcement.

This document is the intellectual property of the fib – International Federation for Structural Concrete. All rights reserved.
This PDF of fib Bulletin 100 is intended for use and/or distribution solely within fib National Member Groups.

Tendon	In post-tensioned applications, the tendon is a complete assembly consisting of anchorages, prestressing steel, and sheathing with coating for unbonded applications or ducts with grout for bonded applications. In pre-tensioned applications, the tendon is an individual element of prestressed reinforcement.
Tension stiffening	Influence of the concrete tensile strength between two cracks on member stiffness, which is typically relevant for serviceability, load-deformation and deformation capacity aspects.
Tie	Concentrated or distributed reinforcement carrying tension forces.
Transverse reinforcement	Reinforcement arranged perpendicular to the bar considered. In linear members, it can consist of stirrups, links or hoops enclosing the longitudinal reinforcement considered.
Upper-bound solution	Any kinematically admissible deformation state for which the rate of work of the external loads exceeds the rate of internal dissipation (i.e. a solution satisfying the upper-bound or kinematic theorem of limit analysis). Also formulated as: Any kinematically admissible mechanism which satisfies the kinematic condition of limit analysis (action equals the strength in the plastic regions). An upper-bound solution allows determining a failure load higher or equal than the one corresponding to the exact solution according to limit analysis.
Wall	Planar member (plane, curved or segmented) with a length not more than 4 times its thickness carrying mainly in-plane forces (see also Diaphragm).

This document is the intellectual property of the fib – International Federation for Structural Concrete. All rights reserved.
This PDF of fib Bulletin 100 is intended for use and/or distribution solely within fib National Member Groups.

The *fib* (International Federation for Structural Concrete - Fédération internationale du béton) is grateful for the invaluable support of the following national member groups and sponsoring members, which contributes to the publication of *fib* technical bulletins, the *Structural Concrete* journal and *fib*-news.

National member groups

UNNOBA - Universidad Nacional del Nor Oeste de la Provincia de Buenos Aires, Argentina
CIA - Concrete Institute of Australia
ÖBV - Österreichische Bautechnik Vereinigung, Austria
GBB-BBG - Groupement Belge du Béton, Belgium
ABCIC - Associação Brasileira da Construção Industrializada de Concreto, Brazil
ABECE - Associação Brasileira de Engenharia e Consultoria Estrutural, Brazil
IBRACON - Instituto Brasileiro do Concreto, Brazil
CPCI (Canadian Precast Prestressed Concrete Institute)
Université Laval, Canada
CCES - China Civil Engineering Society
Cyprus University of Technology
Cyprus Association of Civil Engineers
Česká Betonářská Společnost, Czech Republic
DBF - Dansk Betonforening, Denmark
SB - Suomen Betoniyhdistys, Finland
AFGC - Association Française de Génie Civil, France
DAfStb - Deutscher Ausschuss für Stahlbeton, Germany
Technical Chamber of Greece
University of Patras, Department of Civil Engineering, Greece
Hungarian Group of the *fib*
The Institution of Engineers, India
fib-Indonesia
University of Amirkabir, Iran
IACIE - Israeli Association of Construction and Infrastructure Engineers
AICAP - Associazione Italiana Calcestruzzo, Armato e Precompresso, Italy
CTE - Collegio dei tecnici della industrializzazione edilizia, Italy
ITC - CNR, Istituto per le Tecnologie della Costruzione, Italy
ReLUIS, Italy
JCI - Japan Concrete Institute
JPCI - Japan Prestressed Concrete Institute
Administration des Ponts et Chaussées, Luxembourg
fib Netherlands
NZCS - New Zealand Concrete Society
NB - Norsk Betongforening / Norwegian Concrete Association
Polish Academy of Sciences, Committee for Civil Engineering, Poland
GPBE - Grupo Português de Betão Estrutural, Portugal
Polytechnic University of Timisoara, Romania
Technical University of Civil Engineering, Romania

This document is the intellectual property of the fib – International Federation for Structural Concrete. All rights reserved.
This PDF of fib Bulletin 100 is intended for use and/or distribution solely within fib National Member Groups.

University of Transylvania Brasov, Faculty of Civil Engineering, Romania
Association for Structural Concrete, Russia
SNK *fib*, Slovakia
Slovenian Society of Structural Engineers, Slovenia
The Concrete Institute, South Africa
KCI - Korean Concrete Institute, South Korea
ACHE - Asociación Cientifico-Técnica del Hormigon Estructural, Spain
SB - Svenska Betongföreningen, Sweden
Délégation nationale suisse de la *fib*, Switzerland
ITU - Istanbul Technical University, Turkey
NIISK - Research Institute of Building Constructions, Ukraine
Society of Engineers, United Arab Emirates
fib UK, United Kingdom
ASBI - American Segmental Bridge Institute, United States of America
PCI - Precast/Prestressed Concrete Institute, United States of America
PTI - Post-Tensioning Institute, United States of America

Sponsoring members

Strong Force-MGC W.L.L., Bahrain
Liuzhou OVM Machinery Company, China
Shenzhen University, China
Peikko Group Corp., Finland
Consolis, France
ECS - European Engineered Construction Systems Association, Germany
FBF - Betondienst, Germany
ISB - Institut für Stahlbetonbewehrung, Germany
MKT - Metall-Kunststoff-Technik, Germany
Progress Group GmbH, Germany
Larsen & Toubro Ltd, ECC Division, India
FUJI P. S. Corporation, Japan
IHI Construction Service Company, Japan
Oriental Shiraishi Corporation, Japan
P. S. Mitsubishi Construction Company, Japan
SE Corporation, Japan
Sumitomo Mitsui Construction Company, Civil Engineering Division, Japan
Cimenterie Nationale S.A.L., Lebanon
Hilti, Liechtenstein
BBR VT International, Switzerland
Sika Schweiz, Switzerland
VSL International, Switzerland
PBL Group, Thailand
CEG – The Consulting Engineers Group, United States of America

This document is the intellectual property of the fib – International Federation for Structural Concrete. All rights reserved.
This PDF of fib Bulletin 100 is intended for use and/or distribution solely within fib National Member Groups.

fib Bulletins published since 1998

1 *Structural Concrete – Textbook on Behaviour, Design and Performance*; Vol. 1: *Introduction, Design Process, Materials*
Manual - textbook (244 pages, ISBN 978-2-88394-041-3, July 1999)

2 *Structural Concrete – Textbook on Behaviour, Design and Performance*; Vol. 2: *Basis of Design*
Manual - textbook (324 pages, ISBN 978-2-88394-042-0, July 1999)

3 *Structural Concrete – Textbook on Behaviour, Design and Performance*; Vol. 3: *Durability, Design for Fire Resistance; Member Design, Maintenance; Assessment and Repair, Practical aspects*
Manual - textbook (292 pages, ISBN 978-2-88394-043-7, December 1999)

4 *Lightweight aggregate concrete: Extracts from codes and standards*
State-of-the-art report (46 pages, ISBN 978-2-88394-044-4, August 1999)

5 *Protective systems against hazards: Nature and extent of the problem*
Technical report (64 pages, ISBN 978-2-88394-045-1, October 1999)

6 *Special design considerations for precast prestressed hollow core floors*
Guide to good practice (180 pages, ISBN 978-2-88394-046-8, January 2000)

7 *Corrugated plastic ducts for internal bonded post-tensioning*
Technical report (50 pages, ISBN 978-2-88394-047-5, January 2000)

8 *Lightweight aggregate concrete*: Part 1 (guide) – *Recommended extensions to Model Code 90*; Part 2 (technical report) – *Identification of research needs*; Part 3 (state-of-art report) – *Application of lightweight aggregate concrete* (118 pages, ISBN 978-2-88394-048-2, May 2000)

9 *Guidance for good bridge design*: Part 1 – Introduction, Part 2 – *Design and construction aspects*
Guide to good practice (190 pages, ISBN 978-2-88394-049-9, July 2000)

10 *Bond of reinforcement in concrete*
State-of-art report (434 pages, ISBN 978-2-88394-050-5, August 2000)

11 *Factory applied corrosion protection of prestressing steel*
State-of-art report (20 pages, ISBN 978-2-88394-051-2, January 2001)

12 *Punching of structural concrete slabs*
Technical report (314 pages, ISBN 978-2-88394-052-9, August 2001)

13 *Nuclear containments*
State-of-art report (130 pages, 1 CD, ISBN 978-2-88394-053-6, September 2001)

14 *Externally bonded FRP reinforcement for RC structures*
Technical report (138 pages, ISBN 978-2-88394-054-3, October 2001)

15 *Durability of post-tensioning tendons*
Technical report (284 pages, ISBN 978-2-88394-055-0, November 2001)

16 *Design Examples for the 1996 FIP recommendations Practical design of structural concrete*
Technical report (198 pages, ISBN 978-2-88394-056-7, January 2002)

17 *Management, maintenance and strengthening of concrete structures*
Technical report (180 pages, ISBN 978-2-88394-057-4, April 2002)

18 *Recycling of offshore concrete structures*
State-of-art report (33 pages, ISBN 978-2-88394-058-1, April 2002)

19 *Precast concrete in mixed construction*
State-of-art report (68 pages, ISBN 978-2-88394-059-8, April 2002)

This document is the intellectual property of the fib – International Federation for Structural Concrete. All rights reserved.
This PDF of fib Bulletin 100 is intended for use and/or distribution solely within fib National Member Groups.

20 *Grouting of tendons in prestressed concrete*
Guide to good practice (52 pages, ISBN 978-2-88394-060-4, July 2002)

21 *Environmental issues in prefabrication*
State-of-art report (56 pages, ISBN 978-2-88394-061-1, March 2003)

22 *Monitoring and safety evaluation of existing concrete structures*
State-of-art report (304 pages, ISBN 978-2-88394-062-8, May 2003)

23 *Environmental effects of concrete*
State-of-art report (68 pages, ISBN 978-2-88394-063-5, June 2003)

24 *Seismic assessment and retrofit of reinforced concrete buildings*
State-of-art report (312 pages, ISBN 978-2-88394-064-2, August 2003)

25 *Displacement-based seismic design of reinforced concrete buildings*
State-of-art report (196 pages, ISBN 978-2-88394-065-9, August 2003)

26 *Influence of material and processing on stress corrosion cracking of prestressing steel – case studies*
Technical report (44 pages, ISBN 978-2-88394-066-6, October 2003)

27 *Seismic design of precast concrete building structures*
State-of-art report (262 pages, ISBN 978-2-88394-067-3, October 2003)

28 *Environmental design*
State-of-art report (86 pages, ISBN 978-2-88394-068-0, February 2004)

29 *Precast concrete bridges*
State-of-art report (83 pages, ISBN 978-2-88394-069-7, November 2004)

30 *Acceptance of stay cable systems using prestressing steels*
Recommendation (80 pages, ISBN 978-2-88394-070-3, January 2005)

31 *Post-tensioning in buildings*
Technical report (116 pages, ISBN 978-2-88394-071-0, February 2005)

32 *Guidelines for the design of footbridges*
Guide to good practice (160 pages, ISBN 978-2-88394-072-7, November 2005)

33 *Durability of post-tensioning tendons*
Recommendation (74 pages, ISBN 978-2-88394-073-4, December 2005)

34 *Model Code for Service Life Design*
Model Code (116 pages, ISBN 978-2-88394-074-1, February 2006)

35 *Retrofitting of concrete structures by externally bonded FRPs*
Technical Report (224 pages, ISBN 978-2-88394-075-8, April 2006)

36 *2006 fib Awards for Outstanding Concrete Structures*
Bulletin (40 pages, ISBN 978-2-88394-076-5, May 2006)

37 *Precast concrete railway track systems*
State-of-art report (38 pages, ISBN 978-2-88394-077-2, September 2006)

38 *Fire design of concrete structures – materials, structures and modelling*
State-of-art report (106 pages, ISBN 978-2-88394-078-9, April 2007)

39 *Seismic bridge design and retrofit – structural solutions*
State-of-art report (300 pages, ISBN 978-2-88394-079-6, May 2007)

40 *FRP reinforcement in RC structures*
Technical report (160 pages, ISBN 978-2-88394-080-2, September 2007)

41 *Treatment of imperfections in precast structural elements*
State-of-art report (74 pages, ISBN 978-2-88394-081-9, November 2007)

42 *Constitutive modelling of high strength / high performance concrete*
State-of-art report (130 pages, ISBN 978-2-88394-082-6, January 2008)

This document is the intellectual property of the fib – International Federation for Structural Concrete. All rights reserved.
This PDF of fib Bulletin 100 is intended for use and/or distribution solely within fib National Member Groups.

43 *Structural connections for precast concrete buildings*
Guide to good practice (370 pages, ISBN 978-2-88394-083-3, February 2008)

44 *Concrete structure management: Guide to ownership and good practice*
Guide to good practice (208 pages, ISBN 978-2-88394-084-0, February 2008)

45 *Practitioners' guide to finite element modelling of reinforced concrete structures*
State-of-art report (344 pages, ISBN 978-2-88394-085-7, June 2008)

46 *Fire design of concrete structures —structural behaviour and assessment*
State-of-art report (214 pages, ISBN 978-2-88394-086-4, July 2008)

47 *Environmental design of concrete structures – general principles*
Technical report (48 pages, ISBN 978-2-88394-087-1, August 2008)

48 *Formwork and falsework for heavy construction*
Guide to good practice (96 pages, ISBN 978-2-88394-088-8, January 2009)

49 *Corrosion protection for reinforcing steels*
Technical report (122 pages, ISBN 978-2-88394-089-5, February 2009)

50 *Concrete structures for oil and gas fields in hostile marine environments*
State-of-art report (36 pages, IBSN 978-2-88394-090-1, October 2009)

51 *Structural Concrete – Textbook on behaviour, design and performance*, Vol. 1
Manual – textbook (304 pages, ISBN 978-2-88394-091-8, November 2009)

52 *Structural Concrete – Textbook on behaviour, design and performance*, Vol. 2
Manual – textbook (350 pages, ISBN 978-2-88394-092-5, January 2010)

53 *Structural Concrete – Textbook on behaviour, design and performance*, Vol. 3
Manual – textbook (390 pages, ISBN 978-2-88394-093-2, December 2009)

54 *Structural Concrete – Textbook on behaviour, design and performance*, Vol. 4
Manual – textbook (196 pages, ISBN 978-2-88394-094-9, October 2010)

55 *fib Model Code 2010, First complete draft* – Volume 1
Draft Model Code (318 pages, ISBN 978-2-88394-095-6, March 2010)

56 *fib Model Code 2010, First complete draft* – Volume 2
Draft Model Code (312 pages, ISBN 978-2-88394-096-3, April 2010)

57 *Shear and punching shear in RC and FRC elements - Workshop proceedings*
Technical report (268 pages, ISBN 978-2-88394-097-0, October 2010)

58 *Design of anchorages in concrete*
Guide to good practice (282 pages, ISBN 978-2-88394-098-7, July 2011)

59 *Condition control and assessment of reinforced concrete structures exposed to corrosive environments (carbonation/chlorides)*
State-of-art report (80 pages, ISBN 978-2-88394-099-4, May 2011)

60 *Prefabrication for affordable housing*
State-of-art report (130 pages, ISBN 978-2-88394-100-7, August 2011)

61 *Design examples for strut-and-tie models*
Technical report (220 pages, ISBN 978-2-88394-101-4, September 2011)

62 *Structural Concrete – Textbook on behaviour, design and performance*, Vol. 5
Manual – textbook (476 pages, ISBN 978-2-88394-102-1, January 2012)

63 *Design of precast concrete structures against accidental actions*
Guide to good practice (78 pages, ISBN 978-2-88394-103-8, January 2012)

64 *Effect of zinc on prestressing steel*
Technical report (22 pages, ISBN 978-2-88394-104-5, February 2012)

65 *fib Model Code 2010*, Final draft – Volume 1
Model Code (350 pages, ISBN 978-2-88394-105-2, March 2012)

This document is the intellectual property of the fib – International Federation for Structural Concrete. All rights reserved.
This PDF of fib Bulletin 100 is intended for use and/or distribution solely within fib National Member Groups.

66 *fib Model Code 2010*, Final draft – Volume 2
Model Code (370 pages, ISBN 978-2-88394-106-9, April 2012)

67 *Guidelines for green concrete structures*
Guide to good practice (56 pages, ISBN 978-2-88394-107-6, May 2012)

68 *Probabilistic performance-based seismic design*
Technical report (118 pages, ISBN 978-2-88394-108-3, July 2012)

69 *Critical comparison of major seismic codes for buildings*
Technical report (216 pages, ISBN 978-2-88394-109-0, August 2013)

70 *Code-type models for structural behaviour of concrete*
State-of-art report (196 pages, ISBN 978-2-88394-110-6, November 2013)

71 *Integrated life cycle assessment of concrete structures*
State-of-art report (62 pages, ISBN 978-2-88394-111-3, December 2013)

72 *Bond and anchorage of embedded reinforcement: Background to the fib Model Code for Concrete Structures 2010*
Technical report (170 pages, ISBN 978-2-88394-112-0, May 2014)

73 *Tall buildings: Structural design of concrete buildings up to 300m tall*
State-of-the-art report (158) pages, ISBN 978-2-88394-113-7, August 2014)

74 *Planning and design handbook on precast building structures*
Manual – textbook (313 pages, ISBN 978-2-88394-114-4, September 2014)

75 *Polymer-duct systems for internal bonded post-tensioning*
Recommendation (172 pages, ISBN 978-2-88394-115-1, December 2014)

76 *Benchmarking of deemed-to-satisfy provisions in standards: Durability of Reinforced Concrete Structures Exposed to Chlorides*
State-of-the-art-report (191 pages, ISBN 978-2-88394-116-8, May 2015)

77 *Corrugated-steel-web bridges*
State-of-the-art-report (110 pages, ISBN 978-2-88394-117-5, December 2015)

78 *Precast-concrete buildings in seismic areas*
State-of-the-art-report (273 pages, ISBN 978-2-88394-118-2, March 2016)

79 *Fibre-reinforced concrete - From design to structural applications*
ACI-*fib* workshop proceedings (480 pages, ISBN 978-2-88394-119-9, May 2016)

80 *Partial factor methods for existing concrete structures*
Recommendation (129 pages, ISBN 978-2-88394-120-5, December 2016)

81 *Punching of structural concrete slabs: Honoring Neil M. Hawkins*
ACI SP-315, ACI-*fib* symposium proceedings (378 pages, ISBN 978-2-88394-121-2, April 2017)

82 *Precast segmental bridges*
Guide to good practice (183 pages, ISBN 978-2-88394-122-9, August 2017)

83 *Precast Tunnel Segments in Fibre-Reinforced Concrete*
State-of-the-art report (162 pages, ISBN 978-2-88394-123-6, November 2017)

84 *Precast insulated sandwich panels*
State-of-the-art report (129 pages, ISBN 978-2-88394-124-3, December 2017)

85 *Towards a rational understanding of shear in beams and slabs*
Technical Report (338 pages, ISBN 978-2-88394-125-0, May 2018)

86 *Safety and performance concepts*
Guide to good practice (357 pages, ISBN 978-2-88394-126-7, August 2018)

87 *2018 fib Awards for Outstanding Concrete Structures*
Bulletin (39 pages, ISBN 978-2-88394-127-4, October 2018)

This document is the intellectual property of the fib – International Federation for Structural Concrete. All rights reserved.
This PDF of fib Bulletin 100 is intended for use and/or distribution solely within fib National Member Groups.

88 *Sustainability of precast structures*
State-of-the-art report (153 pages, ISBN 978-2-88394-128-1, December 2018)

89 *Acceptance of cable systems using prestressing steels*
Recommendation (153 pages, ISBN 978-2-88394-129-8, March 2019)

90 *Externally applied FRP reinforcement for concrete structures*
Technical report (229 pages, ISBN 978-2-88394-131-1, May 2019)

91 *Floating concrete structures*
State-of-the-art report (100 pages, ISBN 978-2-88394-133-5, August 2019)

92 *Serviceability Limit State of Concrete Structures*
Technical report (209 pages, ISBN 978-2-88394-135-9, September 2019)

93 *Birth Certificate and Through-Life Management Documentation*
Technical report (90 pages, ISBN 978-2-88394-137-3, June 2020)

94 *Precast concrete bridge continuity over piers*
Technical report (44 pages, ISBN 978-2-88394-140-3, July 2020)

95 *Fibre Reinforced Concrete: From Design to Structural Applications*
ACI SP-343, ACI-*fib* workshop proceedings (539 pages, ISBN 978-2-88394-141-0, August 2020)

96 *Guidelines for Submerged Floating Tube Bridges*
Guide to good practice (119 pages, ISBN 978-2-88394-143-4, October 2020)

97 *External Tendons for Bridges*
State-of-the-art report (108 pages, ISBN 978-2-88394-145-8, December 2020)

98 *Acceptance of post-tensioning systems for cryogenic applications*
Recommendation (106 pages, ISBN 978-2-88394-148-9, April 2021)

99 *Conceptual Design of Precast Concrete Bridge Superstructures*
Technical report (276 pages, ISBN 978-2-88394-149-6, August 2021)

Abstracts for *fib* Bulletins and lists of available CEB Bulletins and FIP Reports are available on the *fib* website at www.fib-international.org/publications.

This document is the intellectual property of the fib – International Federation for Structural Concrete. All rights reserved.
This PDF of fib Bulletin 100 is intended for use and/or distribution solely within fib National Member Groups.

fib
CEB-FIP

Design and assessment with strut-and-tie models and stress fields: from simple calculations to detailed numerical analysis

Contents

Scope
1 Introduction
2 General considerations on stress fields and strut-and-tie models
3 Use of the Levels-of-Approximation approach to design with stress fields and strut-and-tie models
4 Equilibrium-based models
5 Principles of computer modelling
6 Practical examples
7 Special topics
8 Conclusions and outlook
9 References
10 Notations
11 Definitions

ISBN 978-2-88394-152-6
ISSN: 1562-3610

International Federation for Structural Concrete
Fédération internationale du béton
www.fib-international.org